

Angui Li

Attachment Ventilation Theory

OPEN ACCESS

 Springer

Attachment Ventilation Theory

Angui Li

Attachment Ventilation Theory

 Springer

Angui Li 
School of Building Services Science
and Engineering
Xi'an University of Architecture
and Technology
Xi'an, Shaanxi, China



ISBN 978-981-19-9258-2 ISBN 978-981-19-9259-9 (eBook)
<https://doi.org/10.1007/978-981-19-9259-9>

© The Editor(s) (if applicable) and The Author(s) 2023. This book is an open access publication.

Open Access This book is licensed under the terms of the Creative Commons Attribution-NonCommercial-NoDerivatives 4.0 International License (<http://creativecommons.org/licenses/by-nc-nd/4.0/>), which permits any noncommercial use, sharing, distribution and reproduction in any medium or format, as long as you give appropriate credit to the original author(s) and the source, provide a link to the Creative Commons license and indicate if you modified the licensed material. You do not have permission under this license to share adapted material derived from this book or parts of it.

The images or other third party material in this book are included in the book's Creative Commons license, unless indicated otherwise in a credit line to the material. If material is not included in the book's Creative Commons license and your intended use is not permitted by statutory regulation or exceeds the permitted use, you will need to obtain permission directly from the copyright holder.

This work is subject to copyright. All commercial rights are reserved by the author(s), whether the whole or part of the material is concerned, specifically the rights of translation, reprinting, reuse of illustrations, recitation, broadcasting, reproduction on microfilms or in any other physical way, and transmission or information storage and retrieval, electronic adaptation, computer software, or by similar or dissimilar methodology now known or hereafter developed. Regarding these commercial rights a non-exclusive license has been granted to the publisher.

The use of general descriptive names, registered names, trademarks, service marks, etc. in this publication does not imply, even in the absence of a specific statement, that such names are exempt from the relevant protective laws and regulations and therefore free for general use.

The publisher, the authors, and the editors are safe to assume that the advice and information in this book are believed to be true and accurate at the date of publication. Neither the publisher nor the authors or the editors give a warranty, expressed or implied, with respect to the material contained herein or for any errors or omissions that may have been made. The publisher remains neutral with regard to jurisdictional claims in published maps and institutional affiliations.

This Springer imprint is published by the registered company Springer Nature Singapore Pte Ltd.
The registered company address is: 152 Beach Road, #21-01/04 Gateway East, Singapore 189721, Singapore

Foreword by Risto Kosonen

The primary goal of ventilation is to provide occupants with clean air for breathing. Also, ventilation is used quite often as a major source for space cooling and heating, and then especially in the cooling mode, it is important to guarantee local thermal conditions. In this process, the distribution of the supplied air in spaces is of significant importance that has not often been recognized.

At present, total volume air distribution and fully mixing ventilation is most commonly applied in practice. This ventilation is also known as ventilation by dilution. The goal is to mix as well as possible the supplied air with the most often warm room air and to obtain uniform temperature and contaminant distribution in the occupied zone of rooms. However, the strategy of mixing ventilation is inefficient. Clean and cool air is supplied far from occupants, typically from room terminal units located on the ceiling level, and is mixed with room air. The supply air becomes warm and polluted and possibly contains contaminants before it reaches the occupants.

The stated disadvantages of mixing ventilation call for the need to develop new air distribution methods able to provide a better indoor climate for occupants in an energy-efficient manner. At the same time, the methods should provide efficient and smart control and flexibility in space use. However, at the moment, novel ventilation solutions have still not been planned for spaces where it could give great benefits compared to mixing ventilation. For that, there are two main reasons: Firstly, there is still a lack of knowledge of the suitable applications of novel solutions, and secondly, consultants do not know how to design the system. Air distribution is a complex combination of processes and technologies which requires an in-depth understanding of thermodynamics, fluid mechanics, jet theory, ventilation systems, thermal comfort, and indoor air quality. Workplaces are multifaceted indoor spaces contained within various types of buildings, which are required to be ventilated effectively to make them safe and comfortable for occupants who have to work in these spaces for several hours on a daily basis. This diversity has always been a challenge for HVAC engineers to design and select effective and energy-efficient air distribution methods for their projects.

Attachment ventilation (vertical wall and column attachment ventilation, etc.) is a high-performance ventilation that was firstly proposed by Prof. Angui Li. Over

the past 20 years, he has been incessantly devoted to developing attachment ventilation theory, design methods, and engineering applications. Attached ventilation has achieved a new breakthrough in ventilation theory.

This book, *Attachment Ventilation Theory*, systematically summarizes the current research progress on attachment ventilation. This book comprises chapters covering airflow patterns, possible applications, and design methods of the attachment ventilation system, aiming to help HVAC engineers to design attachment ventilation. The performance of attached ventilation is detailed and presented in this book.

I am deeply impressed by the outstanding research and dedication of Prof. Angui Li for writing this *Attachment Ventilation Theory* book. It is an invaluable resource for engineers as well as for students who wish to specialize in air distribution. I am sure that you will find this book useful when you design or develop new ventilation solutions.



June 2022

Risto Kosonen
Professor, Aalto University
Espoo, Finland

Foreword by Thomas Olofsson

The quality of the indoor air environment is of importance in our everyday life. The level and efficiency of the exchange of indoor air will influence the personal health, the comfort as well as the productivity, the costs for operation, maintenance, and construction, and the use of energy and resources that are related to climate change. Recently, based on learnings from the COVID-19 pandemic, the collected evidence shows how the spread of viruses is depending on the strategies for supply and exchange of indoor air.

In order to provide an indoor air environment that is comfortable, healthy, economical, and sustainable, a careful selection of ventilation technology is required. Traditionally, ventilation techniques are based on two major modes, mixing ventilation and displacement ventilation. Mixing ventilation is characterized by a high inlet velocity driven by mechanical momentum aiming to generate fully mixing air volume. Displacement ventilation is characterized by introducing air at a low level in space, at a lower air temperature than the room air, which mainly aims to eliminate the cooling load of the occupied zone. The mixing, as well as the displacement ventilation mode, is the basis for various ventilation techniques, characterized by their pros and cons.

Attachment ventilation is a novel ventilation technology that combines the advantages of the modes of traditional mixing ventilation and displacement ventilation. Attachment ventilation is eliminating the occupied zone's cooling/heating load and provides an intended environment for the conditioned zone. It has the merit of both traditional mixing ventilation and displacement ventilation by offering a lowering cooling or heating load on the demand side. It overcomes the inherent defect that displacement ventilation is normally used for occasions where there is a cooling load. It delivers better air to the occupied zone and saves valuable workspace or occupied space.

Attachment ventilation was invented by Prof. Angui Li about 20 years ago. Over the years, the technology has been theoretically and experimentally validated. Prof. Angui Li has proved to be the foremost excellent scholar and leading international expert in his field. Lately, the practical use of attachment ventilation is demonstrated great success in various spaces, from office spaces to large spaces such as subway stations, high-speed railway stations, and international airport terminals. Based on documented findings from the demonstrations in practice as well as experimental and theoretical studies, attachment ventilation shows promising features as a new breakthrough as a ventilation theory and technology to meet future sustainability, economical, comfortable, and safety issues. COVID-19 has presented challenges to the control of the indoor environment. Attachment ventilation applied to the respiratory infectious disease isolation wards has been found to significantly improve the removal efficiency of contaminants.

In this book, Prof. Angui Li, for the first time, provides a comprehensive demonstration of attachment ventilation for an international audience. As the leading expert in this field, he presents the necessary theory for understanding the fundamentals, the design conditions, a set of novel air distribution theories, and design methods for built environments needed for applying the technique and function. Further, references to applications in practice for the demonstration of the usability of attachment ventilation are appended. Additionally, the book contains an overview of the significant breakthrough that has been made by Prof. Angui Li in the research of ventilation and indoor air science. Based on the presented demonstration projects, attachment ventilation has shown evidence to solve many critical technical challenges of environment control for many mega-projects, which is promoting the development of ventilation theory and technology in the world. The book also introduces a selection of findings from these references.

In this unique book, Prof. Angui Li shows a good balance between theory and practice. The book contains a comprehensive presentation of attachment ventilation theory and is, for the first time, introduced to a larger audience worldwide. The book also helps in understanding the basic principles. The latest new principles and systems are illustrated in the book. The book is suitable not only as a textbook for universities and technical colleges but also as a handbook for professionals who like to keep their knowledge updated. Clear illustrations make it easy to read and assist in the understanding of the complex systems and principles described. The illustrations are beneficial to those not so familiar with the basic sciences. This means, the book can also be used in the education of various disciplines, such as architects and other professionals involved in building design and construction.

Finally, for the emergent task of the ventilation discipline to meet the future challenges of providing a healthy and safe indoor environment using global resources in a sustainable way, this book can provide valuable knowledge and guidance on using attachment ventilation.



September 2022

Thomas Olofsson
Professor, Umeå University
Umeå, Sweden

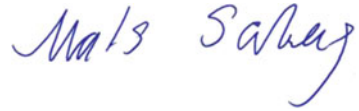
Foreword by Mats Sandberg

Supply of clean air is important for people's well-being. The supply must be carried out such that people's sensation of thermal comfort is satisfied. Supplying large amounts of air to rooms without causing discomfort due to draft is a challenge. For more than 20 years, Prof. Angui Li and his team have been developing an air distribution system called "attachment ventilation". The characteristic feature of this novel air distribution system is that the ventilation air is supplied at the ceiling level and from there passes along vertical surfaces in the room when propagating toward the occupied zone. The surfaces may be walls and columns. The air is attached to surfaces the whole time. By this arrangement, the air is forced to travel a long distance before it arrives at the occupied zone. This allows the supplied air to attain the conditions necessary to meet the conditions for thermal comfort upon arrival at the occupied zone. This property allows supply of air with high velocities without causing discomfort.

In buildings with no heating systems, there may at times be a need to heat the building. A common solution is to heat the supply air and occasionally convert the ventilation system into a warm air system. Now, penetration of air downward is counteracted by the buoyancy force that will lift the air upward. The challenge now is to make it possible for the air to penetrate down into the occupied zone. With attachment ventilation, air can be supplied with a large momentum which overcomes the tendency to lift the air. Attachment ventilation is thus a flexible air distribution system that can cope with many difficult situations and with both heating and cooling loads. The system has been successfully installed in both ordinary offices and large spaces such as railway stations and airports. This is a great benefit to promote ventilation efficiency.

The book by Prof. Angui Li is very comprehensive. It covers both the theory on which the air distribution principle is based and practical design procedures. A multitude of research methods have been used to collect the information necessary for establishing practical design procedures. The research methods are also described in the book, making it a unique text.

The book, *Attachment Ventilation Theory*, can be used both as a manual by designers of air distribution systems and as a textbook for teaching. Those interested in the behavior of ventilation jets passing along surfaces and deflected by 90° bends will find useful information in the book.



July 2022

Mats Sandberg
Professor, University of Gävle
Gävle, Sweden

Preface

From the perspective of indoor environment control, the building envelope divides the “world” into two parts: internal and external spaces. The outdoor climate is dominated by nature, while the indoor environment control is mainly the tasks and missions of building designers, especially heating, ventilation, and air-conditioning (HVAC) engineers. The purpose of ventilation is to maintain a prescribed condition and cleanliness of the air in a control zone, in other words, the temperature, air velocity, concentrations, etc. Ventilation is essentially the science that studies the interaction relationship between natural currents caused by thermal convection over human bodies or production processes and organized air currents of ventilation.

The attachment ventilation (attached ventilation) theory is introduced here to present a unique view of the mechanics that air jets, consisting of air similar to that of its surroundings, develop and move along the wall surface, then impinge on the floor, and spread over the floor surface, forming a horizontal air reservoir or air lake in the occupied zone to maintain the permissible temperatures or concentrations within rooms.

Any room, workshop, or any given space can be referred to as “air-filled zone”. The air currents induced by heated objects or production processes in the zone are diverse and usually invisible. One purpose of ventilation is to maintain the state of air (such as temperature t and velocity u) within a space to meet the requirements of hygiene and human comfort through the interaction of supplied jets and the natural air currents that arise owing to various technical processes of manufacture in the conditioned zone. In other words, ventilation aims scientifically to control the environmental parameters and air movements in a given space to create a comfortable, healthy, and energy-efficient built environment suitable for work and life. It involves living or production environments in all walks of life, from civil and industrial buildings to aeronautics and astronautics fields, and so forth.

To date, traditional air distributions can mainly be classified into two modes: mixing ventilation and displacement ventilation.

- Mixing ventilation indicates that the air is supplied to a room with a high inlet velocity, which aims to eliminate the cooling load of the whole room. The airflow

is driven by mechanical momentum. The high turbulence intensity generates fully mixing and uniform temperature and pollution distribution in the occupied zone. Its ventilation efficiency or temperature efficiency is lower compared to displacement ventilation.

- Displacement ventilation creates room air distribution by introducing air at a low level in space at a lower air temperature than the room air, which mainly aims to eliminate the occupied zone's cooling load to meet the requirements for human comfort or production processes. Therefore, there is less supply air and ambient air mixing and high temperature efficiency. However, displacement ventilation is costly and has the disadvantage of occupying the lower room area (with a supply plenum typically, the height of the raised floor is 0.30~0.45 m). Wall-mounted diffusers often require significant wall space and reduce occupied zone. It requires a higher airflow rate for the same cooling load than mixing ventilation.

To solve the problems of present ventilation modes, a novel ventilation mode, attachment ventilation based on wall/column, has been proposed. Attachment ventilation combines the strengths of traditional mixing ventilation and displacement ventilation. Its ventilation efficiency is higher compared to mixing ventilation. Furthermore, it overcomes the inherent defect that displacement ventilation is only used for occasions where there is a cooling load and saves valuable workspace and occupied zone.

Over 20 years since the concept of attachment ventilation based on vertical wall/column was proposed, the author has been devoted to developing the attachment ventilation theory, design method, and engineering applications. The correlation equations of the characteristic parameters of attachment ventilation have been established, and the design method of the attachment ventilation system has been presented.

This book comprises six chapters covering a range of airflow patterns, mechanisms, and design methods of attachment ventilation, written to help HVAC engineers design and use attachment ventilation described in this book. Chapter 1 introduces traditional air distributions and indoor environment evaluation indexes. Chapter 2 mainly presents the patterns of air movement and the principle of vertical wall and column-attached jets. Then, Chaps. 3 and 4 establish characteristic parameter correlations of the vertical region and horizontal air reservoir region for the isothermal and non-isothermal wall/column-attached jets. Additionally, adaptive attachment ventilation mode is analyzed in Chap. 5. Finally, Chap. 6 expounds on design methods and case studies for attachment ventilation.

In the recent years, attachment ventilation theory and technology have been included in the *Industrial Ventilation Design Guidebook*, *Practical Heating Ventilation and Air Conditioning Design Handbook*, etc. “Knowledge begins with practice (scientific experiments), and theoretical knowledge which is acquired through practice must then return to practice”. The theory and technique of attachment ventilation have been successfully used in industrial and civil construction, such as subway stations, high-speed railway stations, underground hydropower projects, facility agriculture, and office buildings.

Time flies like an arrow. In the past 20 years, the research work has been supported by the National Natural Science Foundation of China (NSFC) and the National Key Technology R&D Program of the 12th Five-Year Plan. The author is grateful to the reviewers, Prof. Mats Sandberg, Prof. Arsen Melikov, Prof. Risto Kosonen, Prof. Thomas Olofsson, and Professors of engineering Yungang Pan, Xiangyang Rong, Min Zhou.

The author would also like to thank my former graduate students or present colleagues, including but not limited to H. G. Yin, C. Q. Yang, G. J. Song, W. D. Zhang, R. C. Zhang, Y. P. Liu, S. H. Qiu, G. D. Wang, W. F. Cui, X. Wang, H. Zhang, X. W. Wang, Z. Y. Liu, Y. R. Cao, Y. X. Sun, C. C. Yao, J. Yang, T. Chen, R. Wu, J. X. Li, etc. Supervised by the author, they have completed the dissertation topics related to attachment ventilation, and some contents have been incorporated into this book. The author also thanks O. Han, X. J. He, W. Q. Zhang, Y. Q. Ma, and H. N. Yang for their help in preparing this manuscript.

October 2021

Angui Li
Professor, Xi'an University
of Architecture and Technology
Xi'an, China

Contents

1	Air Distribution and Indoor Environment Evaluation	1
1.1	Ventilation and Air Distribution	2
1.2	Objective Evaluation of the Indoor Air Environment	7
	References	17
2	Air Movement and Airflow Patterns of Attachment Ventilation	21
2.1	Coanda Effect and Ventilation	21
2.1.1	Coanda Effect	21
2.1.2	Extended Coanda Effect and Air Movement	25
2.2	Vertical Wall-Attached Jet and Airflow Pattern	25
2.3	Column Attachment Ventilation Airflow Pattern	39
2.4	Comparison of the Attachment, Mixing and Displacement Ventilation	45
	References	50
3	Isothermal Attachment Ventilation Mechanisms	53
3.1	Wall-Attached Jet Parameters	54
3.2	Jet Impinging Region	56
3.3	Isothermal Vertical Wall Attachment Ventilation Parameter Correlations	59
3.3.1	Centerline Velocity in Vertical Attachment Region	60
3.3.2	Centerline Velocity in Horizontal Air Reservoir Region	65
3.3.3	Cross-Sectional Velocity Profile	68
3.3.4	Characteristic Thickness of a Wall-Attached Jet	70
3.3.5	Cross-Sectional Flow Rate	73
3.4	Airflow of Column Attachment Ventilation	74
3.4.1	Rectangular Column-Attached Jet	74
3.4.2	Circular Column-Attached Jet	77
3.5	Velocity Distributions with Different Attachment Ventilation Modes	80
3.5.1	Comparison of Centerline Velocity in Vertical Attachment Region	81

- 3.5.2 Comparison of Centerline Velocity in Horizontal Air Reservoir Region 81
 - References 84
- 4 Nonisothermal Attachment Ventilation Mechanisms 85**
 - 4.1 Nonisothermal Vertical Wall Attachment Ventilation 85
 - 4.2 Nonisothermal Column Attachment Ventilation 91
 - 4.3 Characteristic Parameter Correlations of Nonisothermal Attachment Ventilation 93
 - 4.3.1 Vertical Attachment Region 93
 - 4.3.2 Horizontal Air Reservoir Region 97
 - 4.4 Air Opening and Control Zone in Rooms 101
 - 4.4.1 Influence of Air Opening Types 101
 - 4.4.2 Control Zone and Column Spacing 106
 - 4.4.3 Airflow at the Exhaust Outlet 111
 - 4.5 Effect of Heat Sources on Indoor Airflow 112
 - 4.5.1 Evenly Distributed Heat Sources on the Floor 112
 - 4.5.2 Concentrated Plane Heat Sources 114
 - 4.5.3 Volumetric Heat Sources 116
 - 4.6 Human Movement Effect on Airflow Field of Attachment Ventilation 119
 - 4.7 Effect of Wall Temperature 122
 - 4.8 Effect of Wall Roughness 124
 - References 131
- 5 Adaptive Attachment Ventilation with Deflectors 133**
 - 5.1 Adaptive Attachment Ventilation for Breathing Zone 134
 - 5.1.1 Deflector Forms 135
 - 5.1.2 Installation Height of Deflectors 139
 - 5.1.3 Deflector Application 140
 - 5.2 Curved Surface Attachment Ventilation 142
 - 5.2.1 Isothermal Curved Surface Attachment Ventilation 143
 - 5.2.2 Nonisothermal Curved Surface Attachment Ventilation 145
 - 5.3 Some Applications of Attachment Ventilation 150
 - 5.3.1 Tiny Interior Spaces 150
 - 5.3.2 Some Applications to Particular Spaces 154
 - References 157
- 6 Design Methods of Attachment Ventilation Systems 159**
 - 6.1 Scope of Application of Attachment Ventilation Systems 160
 - 6.1.1 Distinguishing Features of Attachment Ventilation Systems 160
 - 6.1.2 Occupied Zone 160
 - 6.1.3 Airflow Parameters and Diffusers in the Occupied Zone 161

- 6.2 Attachment Ventilation Design Procedure 163
- 6.3 Adaptive Attachment Ventilation Design Procedure 167
- 6.4 Comparison of Design Methods of Attachment, Mixing
and Displacement Ventilation 169
- 6.5 Case Study and Design of Attachment Ventilation Systems 174
 - 6.5.1 Office Room 174
 - 6.5.2 Exhibition Hall 176
 - 6.5.3 Subway Station 179
 - 6.5.4 Waiting Hall of High-Speed Railway Station 180
- References 184

Nomenclature

a	1. Side length of a square column, m; 2. thermal conductivity, W/(m·K)
Ar	Archimedes number
b	Slot width, m
b_0	Deflector width, m
c	Indicator or pollutant concentration, mg/kg
c_p	Specific heat at constant pressure, kJ/(kg °C)
c_s	Indicators of air supply or pollutant concentration, mg/kg
C	Shape factor
C_v	Empirical coefficient
d	Column diameter, m
Δt_g	Indoor vertical temperature gradient, °C/m
Δt	Temperature difference between supply air and occupied zone, $\Delta t = t_0 - t_n$, °C
Δt_{oz}	Temperature difference between supply and exhaust air, °C
E_T	Ventilation effectiveness
f	Projected area of heat source, m ²
F	Floor area, m ²
g	Acceleration of gravity, m/s ²
h	Installation height of slots or openings, m
h_0	Deflector installation height, m
H	Room height, m
k	Wall absolute roughness, mm
K_h	Height correction factor
k_v	Empirical coefficient
q	Heat flux, W/m ²
Q	1. Cross-sectional flow rate of a wall-attached jet, m ³ /s; 2. indoor excessive heat, W
Q_0	Discharge flow rate of a wall-attached jet, i.e., air supply rate, m ³ /s
Q_n	Excessive heat in the occupied zone, W
$L \times W \times H$	Room dimension length \times width \times height, m \times m \times m
m	Indoor heat distribution factor, generally $m = 0.50\sim 0.85$

n	Number of measuring points
N	1. Air change rate (h^{-1}); 2. number of air openings
s	Interval between the center of the slot and the jet-attached wall surface, m
S	Distance in the direction normal to the vertical wall from a slot's inner edge or surface adjacent to the wall, m
S_{max}	Maximum attachment distance
t	Air temperature, $^{\circ}\text{C}$
t_0	Supply air temperature, $^{\circ}\text{C}$
t_e	Exhaust air temperature, $^{\circ}\text{C}$
t_i	Air temperature of measuring point i , $^{\circ}\text{C}$
\bar{t}	Averaged air temperature of measuring point, $^{\circ}\text{C}$
t_n	Indoor air temperature, $^{\circ}\text{C}$
t_w	Wall temperature, $^{\circ}\text{C}$
t_x	Indoor air temperature at a given point x , $^{\circ}\text{C}$
u	Air velocity, m/s
u_0	Supply air velocity, m/s
u_i	Air velocity at measuring point i , m/s
\bar{u}	Averaged air velocity at the measuring point, m/s
$u_{m, x}$	Jet centerline velocity, m/s
$u_{m, 1.0}$	Air velocity in the control boundary, i.e., the airflow centerline velocity in the air reservoir region at a distance of 1.0 m from the vertical attached wall, m/s
$u_m(y^*_{\text{max}})$	Centerline velocity at the separation point of a wall-attached jet, m/s
u_p	Air jet averaged velocity, m/s
u_s	Air velocity at the deflector, m/s
u_x	Indoor air velocity at a given point x , m/s
V	Room volume, m^3
x	x -axis coordinate, m
y	y -axis coordinate, m
y^*	Distance from a given point along the wall to the jet entrance (air inlet), $y^* = h - y$
y_1	y -coordinate of the attachment point, m
y_2	y -coordinate of the separation point, m
z	z -axis coordinate, m
α	Air opening turbulence coefficient
β	Slope surface angle, $^{\circ}$
δ_m	Normal distance between the wall and the point where the attached jet velocity is equal to u_m , m
$\delta_{0.5}(\delta)$	Characteristic thickness of a wall-attached jet, $\delta_{0.5}$ is the normal distance between the wall and the point where the attached jet velocity is equal to $0.5u_m$ in the outer layer of a wall-attached jet, m
η	Dimensionless distance, $x/\delta_{0.5}$ or $y/\delta_{0.5}$
θ_{ed}	Effective draft temperature, $^{\circ}\text{C}$
τ	1. Shear stress, Pa; 2. time, s

τ_t	Turbulent shear stress, Pa
κ	Dimensionless temperature rise near the floor (0.1 m above the floor)
μ	Viscosity, Pa·s
ν	Kinetic viscosity, m ² /s
ρ	Air density, kg/m ³
σ	Volume expansion coefficient, 1/K

Note: For the above symbols, when there are any other annotations on the figure or text, the nearest one shall prevail.

Chapter 1

Air Distribution and Indoor Environment Evaluation



Abstract This book comprises six chapters covering a range of air movement patterns, mechanisms, parameter correlations, and design methods of attachment ventilation, written to help HVAC engineers design and use attachment ventilation described in this book. This chapter introduces the traditional air distribution methods and the indexes to evaluate ventilation performance. The traditionally used ventilation modes comprise mixed and displaced ventilation. The mixed ventilation is based on the dilution principle, supplying a high momentum flow from the ceiling/upper sidewall to the room, while the displaced ventilation is based on the displacement principle, supplying a low momentum flow from the floor/lower wall area to the occupied zone. This chapter briefly presents their pros and cons. Following this, a novel ventilation mode has been proposed, i.e., vertical wall attachment and column attachment ventilation. The ventilation evaluation indexes, such as vertical temperature gradient, effective draft temperature, air diffusion performance index, ventilation efficiency, and thermal stratification height, are presented.

Keyword Air distribution · Mixing ventilation · Displacement ventilation · Attachment ventilation · Attached ventilation · Ventilation efficiency

Air distribution affects air quality, thermal environment, and work efficiency. The goal of ventilation is to provide occupants with clean air for breathing and thermal comfort. In essence, ventilation means controlling air movement in rooms or built environments. It is the science of studying the interaction of natural convection and organized currents of ventilation air. Ventilation affects not only indoor air quality and thermal comfort, but also energy consumption over the building's life. The air distribution is a result of the complex interaction of different flows. Therefore, room air distribution in space and in time domains should be carefully considered in order to avoid regions of high velocity and low temperature as well as regions of polluted air, which may affect occupants' comfort and well-being. This book introduces the principle and methods of applying fluid mechanics to predict the air movement along various wall surfaces in a ventilated room. Attachment ventilation (attached ventilation) theory and design methods are put forward.

The air currents induced by production processes or heated objects are diverse in any room, industrial workshop, or any given space. The purpose of ventilation

is to meet the required air parameters (such as temperature t , velocity u , and relative humidity RH , etc.) in a given space and guarantee the environmental condition of people's lives or industrial production. It is essential to control those natural air currents by jets of air supplied, as a result of interaction, eventually achieving specified parameters of the built environment.

The ventilation task is to regulate the air change in a confined enclosure to create the intended temperature, velocity, concentration field, etc. For mechanical ventilation, the air is supplied to given spaces in the form of jets by air diffusers or openings of the air passage. The ventilation jets can dilute or blow thermal air (excessive heat and moisture) or hazardous pollutants to a specific area and then remove them in an ordered manner.

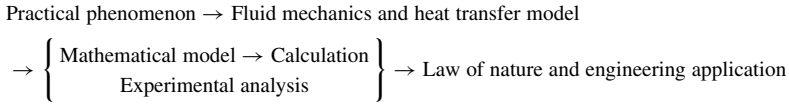
A wide variety of definitions exist in literature for air distribution. ASHRAE defines air distribution as "room air distribution systems are intended to provide thermal comfort and ventilation for space occupants and processes" (ASHRAE 2017). In a broad sense, air distribution is a rationalized and organized air flow process in any given space to meet the requirements of air temperature, velocity, humidity, airflow rate, and human comfort (CIBSE 2016). The "given spaces" comprise ordinary industrial and civil buildings, enclosed and semi-enclosed zones involved in aeronautic and astronautic, transportation, facility agriculture environment, etc.

Up to date, there have mainly been traditionally two kinds of ventilation modes, mixing and displacement ventilation, since the invention of central air-conditioning systems. The former is based on the dilution principle, supplying a high momentum flow from the ceiling or upper sidewall to the room, while the latter is based on the displacement principle, supplying a low momentum flow from the floor or lower wall area into the occupied zone. This chapter briefly presents their pros and cons. Following this, a novel ventilation mode has been proposed, i.e., vertical wall attachment (VWAV) and column attachment ventilation (CAV). The ventilation evaluation indexes are presented, such as vertical temperature gradient, effective draft temperature, air diffusion performance index, ventilation efficiency, and thermal stratification height.

1.1 Ventilation and Air Distribution

Tracing back to history, creating an intended living environment is closely related to the development and progress of human civilization. As a necessary means of indoor environment control, ventilation has been widely paid attention to. Since ancient times, people have come to realize that a favorable indoor environment can be achieved by rational air movement. That is to say, ventilation always has been a historic and vital topic in the field of heating, ventilation and air conditioning (HVAC) (Cao et al. 2014; Li et al. 2014; Melikov 2004; Lin et al. 2011; Han et al. 2019). Before the development of the electric power industry in the late nineteenth century, natural ventilation through operable windows was the only means of ventilating buildings. It was not until electric power became generally available early in the twentieth century

that the desired living environment could be achieved by mechanical ventilation. Even in contemporary society, ventilation is still the primary means of controlling residential and industrial pollutants. So far, there has been a well-accepted research paradigm (Chen 2009; Baturin 1965; Bakhalev and Troyanovski 1965; Li et al. 2010):



In view of the essence of ventilation's complexity of turbulent motion and the diversity of boundary conditions in engineering applications, it is foreseeable that ventilation theory and technology will remain hotspots and challenges in the future.

Creating a healthy and comfortable environment in low energy or nearly zero energy consumption is challenging. In other words, the indoor environment control of intended temperature and humidity, good air quality, and low energy consumption is related to a rational cooling and heating source system and directly to air distribution (Zhang et al. 2011; Karimipناه et al. 2007).

The room air distribution is the ultimate manifestation of a series of air handling processes (such as heating or cooling processes) of the environment control system, and it is also the most direct terminal technique for creating a comfortable indoor environment. On the one hand, it is directly related to the ventilation effectiveness of the conditioned zone; on the other hand, it closely influences the required cooling and heating loads of the buildings, i.e., the total energy consumption of ventilation or air-conditioning systems. For instance, traditional mixing ventilation is required to bear the total cooling/heating loads of the entire space, whereas displacement ventilation only needs to remove the local cooling loads of the occupied space.

Ventilation is a complex combination of theory and technology based on the requirement. From the perspective of indoor environment control, when designing ventilation systems, we should comprehensively apply theoretical methods such as mechanics, heat transfer, etc., to the design of airflow paths, air diffuser forms, and locations, forming intended parameters distribution for given spaces (Lu 2007; GB/T 50155-2015; REHVA 2013).

Generally, ventilation involves two broad categories of issues:

Air movement in a confined space—the confined jet movement mechanisms in spaces with or without obstacles, in other words, the airflow velocity variations with time and space.

Heat exchange (or pollutants dilution) of a ventilated room—from the consideration of conservation of the convective heat and mass transfer in the jet, the equality of the increments of momentum, buoyancy force, or the temperature (concentration) distribution, that is, airflow temperature (concentration) variations with time and location.

From the perspective of force decomposition, the essence of air distribution is to control the mutual effects of mechanical momentum and thermal buoyancy in ventilation processes. The influencing factors include but are not limited to air supply rate, temperature, air inlet structure, and jet throw. For example, the air supply velocity of the underfloor air distribution (UFAD) system can affect indoor air interacting dynamic characteristics. The air distribution performance is closely related to ventilation efficiency or temperature efficiency.

Since the invention of air conditioners in the early twentieth century, two main indoor air distribution methods have been developed: mixing and displacement ventilation (Li 2000; Awbi 2008; Cao et al. 2014). The simplified diagrams of various air distributions and vertical temperature distributions are demonstrated in Fig. 1.1.

As is well known, the mixing ventilation theory is based on the dilution principle. Mechanical momentum is the source power to drive the interaction between supplied jets and ambient air, to meet the requirements of designed parameters. The mechanical momentum is generally “opposite” to the thermal plume arising from the buoyancy forces created by temperature differences. The supplied air will incessantly mix with ambient air, and the indoor air temperature of the entire space is uniformly

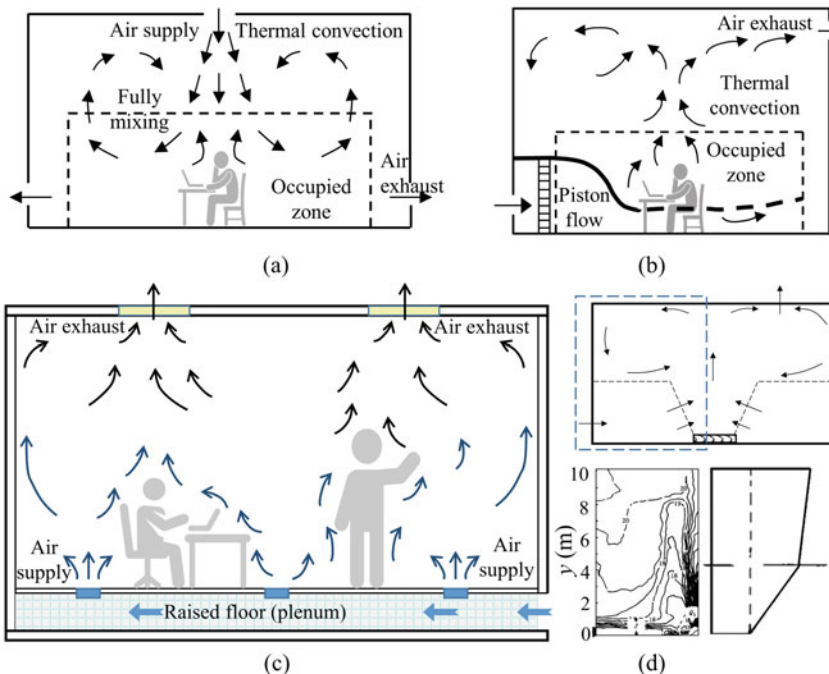


Fig. 1.1 Simplified diagram of various air distributions. **a** Mixing ventilation, **b** displacement ventilation (sidewall air supply), **c** underfloor air distribution (UFAD), **d** temperature distribution of displacement ventilation with concentrated heat sources on the floor (Zhao and Li 1998)

distributed (CIBSE 2016; Rock et al. 1995). Thus, there is no thermal stratification, as shown in Fig. 1.1a. The mixing ventilation mainly aims to remove all of the heating/cooling load of the entire space. The principle behind completely mixing is to dilute the contaminants or “excessive” heat with the supplied air. This goal can be achieved by creating air recirculation, resulting in the same concentrations in occupied zones as the exhaust air. To date, there has been convincing evidence that the mixing air distribution spreads out “flooding-like irrigation” features, and the ventilation efficiency is relatively low (Li 2000; Zhao and Li 1998; Rock et al. 1995; Awbi 2008; Croome and Roberts 1981; Zhao 2008; Ma and Yao 2015). Nevertheless, its advantage lies in that the air supply plenums and duct systems are installed in the upper room zone; accordingly, it saves the occupied zone.

For displacement ventilation, indoor polluted air (excessive heat) is replaced by sidewall or underfloor-supplied air. Starting from the perspective of “acting force”, the synergized effects of thermal buoyancy and mechanical momentum are taken into account in displacement ventilation. There is consistency between the mechanical momentum of supplied air and thermal buoyancy for their direction and magnitude, so seldom or rarely mixing occurs between supplied air and ambient air (ASHRAE 2017), as shown in Fig. 1.1b–d. Better air quality can be obtained under this displacement ventilation mode, and excessive heat in the conditioned zone can be removed effectively, which meets the requirements of the living or production process. The thermal stratification phenomenon occurs in the room accordingly. The interface height of thermal stratification in the vertical direction depends on the relationship among air supply position, total air supply rate, heat load, etc. (Li 2000; Zhao and Li 1998; Rock et al. 1995; Awbi 2008; Croome and Roberts 1981; Zhao 2008; Ma and Yao 2015; Griefahn et al. 2001; Lau and Chen 2006).

For displacement ventilation, a slight temperature difference (2.0–4.0 °C) exists between the jets and surroundings, and so does the supply air velocity (0.1–0.5 m/s). Therefore, displacement ventilation needs a more significant airflow rate under the same cooling load than mixing ventilation. Accordingly, more terminal energy will be consumed; meanwhile, it also occupies the lower room zone for installing plenums and duct systems (Zhao 2010). In addition, there is a risk of draft sensation with the improper design of air distributions (Seppänen 2008). Displacement ventilation is only used for cooling.¹ It can also be used as a fresh air supply system combined with a radiant heating system in rooms (Awbi 2008). In addition, the plenum duct systems for displacement ventilation are mostly installed beneath the interlayer of floors, as shown in Fig. 1.1c, which suggests that it needs to raise the floor (up to 30–50 cm). Compared to mixing ventilation, its initial investment is relatively higher; therefore, its engineering application is much restricted (Fred 2003, 2006; Yuan et al. 1998).

Over the years, Angui Li and his team have been devoted to developing the theory and design methods for the vertical wall (VWAV) and column attachment ventilation (CAV) (Li 2019; Li et al. 2008, 2015). Figure 1.2 shows the schematic

¹ Awbi HB (2007) Ventilation systems—Design and performance. Taylor & Francis, P291.

diagram of attachment ventilation. It combines the advantages of both mixing ventilation and displacement ventilation and avoids a series of shortcomings, such as low-temperature efficiency of mixing ventilation and occupying workspaces of displacement ventilation. Attachment ventilation aims to focus on the environmental control of the occupied zone or conditioned zone. A vertical air temperature gradient exists in conditioned spaces, so it only bears the partial cooling load and has higher temperature efficiency than mixing ventilation. Attachment ventilation system is used to supply cool/thermal air or remove contaminants, which has been widely used in various scenarios, such as Xiong'an high-speed railway stations (Li et al. 2021), Zhengzhou subway stations (Sun et al. 2021), hospital wards (Li et al. 2020; Zhang et al. 2022), office buildings (Zheng et al. 2019), etc.

Normally, for the interior layout of buildings, the duct systems of attachment ventilation are laid in the upper room space. The supply air moves along the vertical wall or column, impinges the floor, then turns horizontal, creating a thin layer of the air reservoir or air lake. That is to say, thin-layer air spreads evenly over the floor with low velocity and slight temperature differences. The attachment ventilation delivers high-quality fresh air to the occupied zone through the Coanda effect (CE) and extended Coanda effect (ECE) (Li 2019). It meets the requirements of the air temperature, velocity, and concentration field, etc. for the occupied zone. Attachment

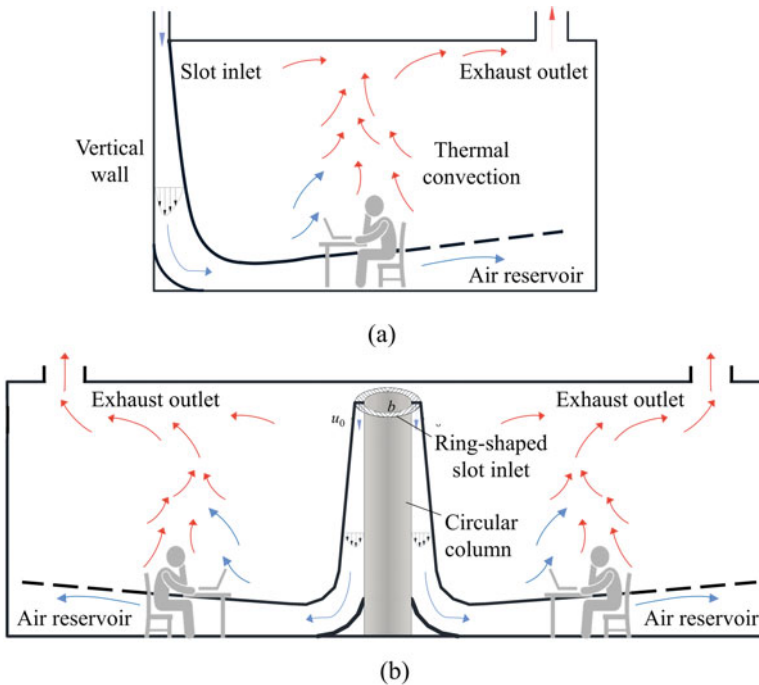


Fig. 1.2 Schematic diagram of the air distribution of attachment ventilation. **a** Vertical wall attachment ventilation (VWAV), **b** column attachment ventilation (CAV)

ventilation mode can be applied to all kinds of spaces with little or large cooling load, especially suitable for large space environmental control. More importantly, attachment ventilation can be applied to solve the problem that thermal air is difficult to deliver to the occupied zone for large spaces in the winter time.

Compared to mixing ventilation, the temperature efficiency of attachment ventilation has been dramatically enhanced. Taking a standardized subway station as an example, under the premise to ensure indoor comfort requirements, the CAV can reduce the airflow rate by 20%, and the cooling capacity by 31%, compared with traditional mixing ventilation. The synthetical coefficient of performance (SCOP) of the air conditioning system has increased by 17%, demonstrating that attachment ventilation can significantly reduce the initial investment and operating energy consumption for the ventilation and air conditioning system (Liu 2018).

This book systematically summarizes the current research progress on attachment ventilation, covering vertical wall (VWAV), column (CAV), and adaptive attachment ventilations (AAV), etc. The parameter correlations of air distribution and case studies are presented. It provides a set of novel air distribution theories and design methods for the building environment.

1.2 Objective Evaluation of the Indoor Air Environment

A series of evaluation indexes can be used to evaluate the ventilation effect. The objective evaluation indexes for the indoor environment mainly comprise the vertical temperature gradient, effective draft temperature θ_{ed} , ventilation efficiency (temperature efficiency) E_T , thermal stratification interface height, air diffusion performance index (ADPI), velocity non-uniformity coefficient K_V , temperature non-uniformity coefficient K_T , air age τ_A , air exchange efficiency η_A , etc. The primary air parameters include jet centerline velocity, excess temperature, averaged air temperature, averaged velocity, mean radiant temperature, operative temperature, radiant temperature asymmetry, etc.

1. Vertical temperature gradient

For air distribution modes, there is usually a vertical air temperature difference in the vertical direction, i.e., vertical temperature gradient, which is generally caused by the air temperature difference between supply air and the conditioned zone, internal heat sources, etc. Attachment ventilation aims to provide occupants with clean air for breathing more effectively. With attachment ventilation, it is possible to utilize buoyancy flows that transfer contaminant from the occupied zone towards the upper room zone and improve the air quality inhaled by occupants. Simultaneously, with better air quality, attachment ventilation creates a vertical temperature gradient in the room, with a higher temperature near the ceiling. Additionally, the vertical temperature gradient is a function of flow rate and load.

Also, the high vertical air temperature difference between the head and ankles can cause discomfort. From the perspective of hygiene and human comfort, it is

necessary to keep the vertical air temperature difference within a specific range. For instance, ISO (International Organization for Standardization) (BS EN ISO 7730-2005) specifies allowable differences between the air temperature at head level and ankle level, using categories of Class A, B, and C as follows:

- Class A < 2.0 °C,
- Class B < 3.0 °C,
- Class C < 4.0 °C.

The ANSI/ASHRAE standard (ANSI/ASHRAE Standard 55-2017) states that the vertical air temperature difference between the head and ankles should be less than 3.0 °C (sedentary occupants) or 4.0 °C (standing occupants). It should be noted that the above two standards do not specifically emphasize the ventilation modes, i.e., displacement ventilation or mixing ventilation. Chinese standard *Design Code for Heating, Ventilation, and Air Conditioning of Civil Buildings* (GB50736-2012) stipulates that for displacement ventilation, the vertical air temperature difference between 0.1 and 1.1 m above the floor should not be greater than 3.0 °C.

REHVA defines the representative measurement heights for air temperature gradient between the head and ankles as: 0.1 and 1.1 m above the floor for a sedentary person; 0.1 and 1.7 m above the floor for a standing person (REHVA 2002; GB/T50785-2012).

If the vertical temperature difference between the head and ankles is less than 8.0 °C, the local percentage dissatisfied (*LPD*) caused by the vertical temperature gradient can be determined using Eq. (1.1) (GB/T50785-2012).

$$LPD = \frac{100}{1 + \exp(5.76 - 0.856\Delta t_{a,v})} \quad (1.1)$$

where

LPD local percentage dissatisfied, %;

$\Delta t_{a,v}$ vertical air temperature difference between head and ankles, °C.

2. Effective draft temperature θ_{ed}

The effective draft temperature provides a quantifiable comprehensive comfort index at a discrete point in space by combining the physiological effects of air temperature and air movement on the human body. The effective draft temperature θ_{ed} (a calculated temperature difference that combines air temperature difference and measured air speed at each test point) can be calculated using Eq. (1.2) for cooling conditions (Fanger et al. 1988).

$$\theta_{ed} = t_x - t_n - 8(u_x - 0.15) \quad (1.2)$$

where

θ_{ed} effective draft temperature, °C;

- t_x local airstream dry-bulb temperature, °C;
 t_n averaged (control) room dry-bulb temperature, °C;
 u_x local airstream centerline velocity, m/s.

When the effective draft temperature falls within the range of $-1.5 < \theta_{ed} < +1.0$ (ASHRAE Handbook) (ASHRAE 2017) or $-1.7 < \theta_{ed} < +1.1$ (Zhu 2010), and the air velocity $u_x < 0.35$ m/s, most people feel thermal comfort for sedentary occupants.

3. Air diffusion performance index

The air diffusion performance index (*ADPI*) has been developed as an indicator to quantify the comfort level in heating or cooling for a given space conditioned by a mixed air system. *ADPI* employs the effective draft temperature collected at an array of points taken within the occupied zone to predict comfort. *ADPI* is the percentage of points in a given space where the effective draft temperature is between -1.7 and $+1.1$ K for cooling and -2.2 and $+2$ K for heating. The acceptable air velocity is less than 0.35 m/s for heating and cooling. In addition, the acceptable vertical temperature gradient should be less than 3 K/m (ASHRAE 2017). In other words, *ADPI* is defined as the percent of test points in the room where the effective draft temperature and mean velocity (speed) meet the criteria in Eqs. (1.3a, 1.3b). *ADPI* can also be used to evaluate the air diffusion performance of the occupied zone of displacement and attachment ventilation.

For cooling

$$ADPI = \frac{\text{Number of measuring points that meet } (-1.7 < \theta_{ed} < +1.1)}{\text{Total number of measuring points}} \times 100\% \quad (1.3a)$$

For heating

$$ADPI = \frac{\text{Number of measuring points that meet } (-2.2 < \theta_{ed} < +2)}{\text{Total number of measuring points}} \times 100\% \quad (1.3b)$$

Acceptable air velocity ≤ 0.35 m/s for heating and cooling. For temporary staying zone, such as subway stations, the acceptable air velocity is ≤ 0.5 m/s.

High *ADPI* values generally correlate to high space thermal comfort levels with the maximum obtainable value of 100%. Selecting inlets/outlets to provide a minimum *ADPI* value of 80% generally results in a well-mixed space (ASHRAE 2017; Zhao 2008).

4. Ventilation efficiency (temperature efficiency) E_T

Ventilation efficiency (temperature efficiency) can be used to evaluate the ventilation effectiveness of air distribution modes (Zhao 2010; Sandberg 1981). Ventilation efficiency refers to the system's ability to remove excessive heat or pollutants from sources in a given space. It can be understood as the ratio of the supply airflow rate

utilized to dilute the pollutants effectively to the total supply airflow rate in the space. It can be further subdivided into transient ventilation efficiency and steady-state ventilation efficiency.

When the indoor excessive heat load remains stable, the steady-state ventilation efficiency can be used to evaluate the air distribution effectiveness to eliminate the heat load in the occupied zone. In terms of this view, the ventilation efficiency can also be called temperature efficiency (dimensionless excess temperature), which is reciprocal to the heat distribution factor m . It can be determined using Eqs. (1.4a, 1.4b)

$$E_T = \frac{t_e - t_0}{t_n - t_0} \quad (1.4a)$$

or

$$m = \frac{t_n - t_0}{t_e - t_0} \quad (1.4b)$$

where

t_e temperature in the exhaust air terminal, °C;

t_0 temperature in the supply air terminal, °C;

t_n averaged air temperature of the occupied zone (conditioned zone), °C.

The evaluation indexes for ventilation effectiveness cover many factors, such as building space types, heat source forms, ventilation modes, etc. It is always challenging to carry out a systematic quantitative analysis of each factor. As a solution, a comprehensive analysis of multiple factors can be performed based on experiments. Zhao (2010) randomly selected experimental data of air supplied downwards and exhausted upwards air distribution. For ventilated spaces of civil and industrial buildings with low-intensity discrete heat sources ($q_v < 50 \text{ W/m}^3$), Fig. 1.3 shows the relationship between $\lg Ar$ and E_T . The experimental conditions are summarized in Table 1.1. E_T can be calculated by Eq. (1.5)

$$E_T = 0.31 \lg Ar - 0.01 \quad (r = 0.898) \quad (1.5)$$

where Ar is Archimedes number, which is defined as $Ar = \frac{gH}{u_0^2} \frac{\Delta t}{T_0}$.

For typical room spaces, the averaged velocity of air distribution with underfloor air supply can be approximated by the ratio of the supply airflow rate G to the room cross-sectional area F_n , that is

$$u_0 = G/F_n \quad (1.6a)$$

$$\Delta t = Q/\rho c_p G \quad (1.6b)$$

Therefore, for nonisothermal rooms

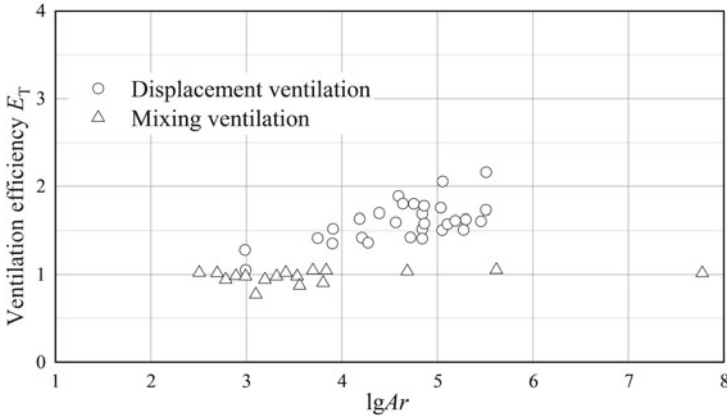


Fig. 1.3 Ventilation efficiency of different ventilation modes (Zhao 2010)

$$Ar = \frac{gQH F_n^2}{\rho c_p T_0 G^3} = \frac{B_0 H F_n^2}{G^3}$$

where B_0 is buoyancy flux, $B_0 = \frac{gQ}{\rho c_p T_0}$.

For ordinary offices or residential buildings, the ventilation temperature range is 15–40 °C, and thus $B_0 \approx 0.000028Q$.

For displacement ventilation with low-intensity heat sources, the relationship between the seven parameters of Q , G , H , F_n , t_0 , t_e , t_w in the ventilated room can be determined according to $E_T = f(Ar)$.

It can be observed from Fig. 1.3 that the E_T of mixing ventilation is about 1, while the E_T of displacement ventilation is 1–2. This indicates that the supply air of mixing ventilation and indoor air are intensively mixed, resulting in the temperature of the occupied zone and the exhaust temperature being almost the same, yet displacement ventilation shows a significant temperature gradient $t_e > t_n$.

5. Thermal stratification interface height

In ventilated or air-conditioned rooms, the temperature increases with height in the lower and upper layers. The air enters the room at a low temperature, and is mixed slightly with the room air and heated by convection from the occupied zone, thus making the air temperature at the floor level higher than the supply temperature. The air temperature increases from the floor level to the ceiling, more or less linearly, because the thermal plume rises to the ceiling due to its buoyancy, while the outer, cooler parts of the plume layer according to their temperature. If the thermal plume flow rate G_H at the exhaust opening exceeds the ventilation air flow rate G , part of the excessive thermal flow will be forced to move downward in the reverse direction, as shown in Fig. 1.4.

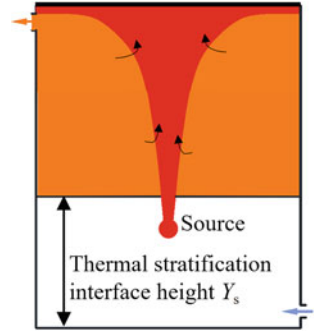
When the ventilation air flow rate G is equal to the flow G_Y of the buoyant plume at a particular height Y section of the room, $G = G_Y$, the thermal stratification is formed,

Table 1.1 Experimental conditions of different ventilation modes²

Ventilation mode	Location of supply-exhaust	No. of cases	F (m ²)	h (m)	q (W/m ³)	G (m ³ /s)	E_T	lg Ar
Mixing ventilation	Lower sidewall-ceiling	Civil—16	15–150	2.4–3.9	6.3–26.6	0.045–0.48	1.4–2.1	4.4–5.5
	Lower sidewall-ceiling	Industrial—16	270–960	3–10	8.2–43.1	1.38–18.3	1.1–2.2	3–4.5
	Floor-ceiling	Civil—1	15	2.65	17.1	0.06	1.4	4.7
	Lower sidewall-higher sidewall	Industrial—5	270	6	40	3.57–9.4	1–1.4	3–4.2
Displacement ventilation	Ceiling-floor	Civil—9	20	3.6	5.6–28	0.01–0.38	0.96–1.0	2.5–7.8
	Ceiling-floor	Industrial—6	270	6	40	6.1–10.6	0.91–0.95	2.8–3.5
	Higher sidewall-lower sidewall	Industrial—3	270	6	4.0	5.3–8.7	0.71–0.85	3.1–3.8

² Note from Zhao HZ (2010) Indoor heat convection and ventilation, China Architecture & Building Press, Beijing, Table 1–3.

Fig. 1.4 Thermal stratification interface of a ventilated room



and the height Y is defined as the thermal stratification interface height Y_s (Zhao 2010). In this scenario, the velocity component in the vertical direction of the airflow at the thermal stratification interface outside the main plume section is 0. Above the thermal stratification interface, the thermal airflow is a vortex turbulent recirculation mixed flow. The negative pressure gradient affects the airflow in the lower zone and shows a low-speed irrotational flow. The vertical temperature distribution outside the main plume is simplified to the model shown in Fig. 1.5.

If the velocity u in the vertical direction is proportional to the distance from the thermal stratification interface height Y_s , that is

$$u = -k(y - Y_s) = -k\tilde{y} \tag{1.7}$$

where \tilde{y} is the height from the thermal stratification interface, $\tilde{y} = y - Y_s \geq 0$.

Based on the one-dimensional steady-state energy equation in a room, the vertical temperature distribution of thermal stratification at any height is derived (Zhao 2010)

$$(t - t_0)/(t_e - t_0) = 0.5(1 + erf H^*) \tag{1.8}$$

where

Fig. 1.5 Simplified model of buoyancy plume diffusion

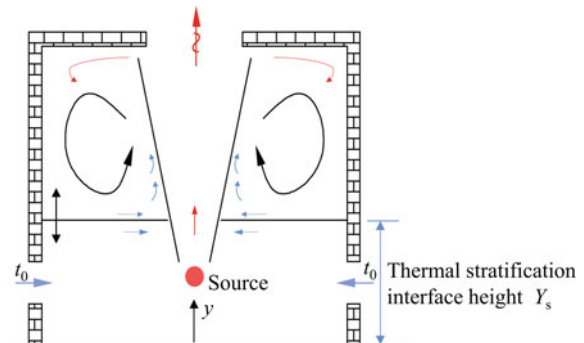
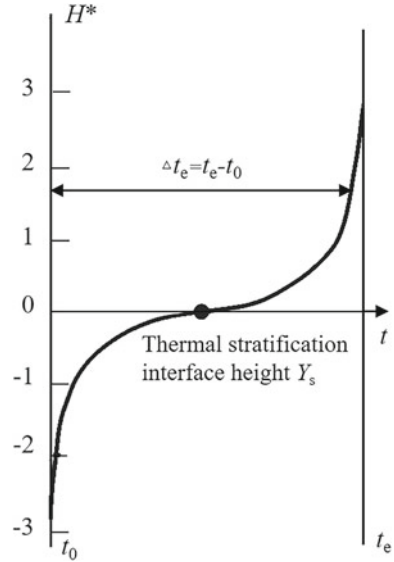


Fig. 1.6 Vertical temperature distribution of thermal stratification



$erfH^*$ Gaussian error function, $erfH^* = \frac{2}{\sqrt{\pi}} \int_0^{H^*} e^{-\eta^2} d\eta$, $H^* = \left(\frac{k\bar{y}^2}{2a}\right)^{0.5}$;
 a thermal conductivity, W/m·K;
 t_0 air supply temperature, °C;
 t_e air exhaust temperature, °C.

The vertical temperature curve in Fig. 1.6 represents a symmetrical nonlinear distribution (Zhao 2010), with the thermal stratification interface height Y_s as the origin. For $y = Y_s$, $t = (t_0 + t_e)/2$, that is, the temperature of the thermal stratification interface is just the averaged value of the supply and exhaust air temperature.

Thermal stratification interface height is an essential characteristic parameter that describes thermal stratification flow features. It is related to factors such as indoor vertical temperature distribution, indoor-outdoor temperature differences, geometric forms, locations, number of heat sources, ventilation modes, and even wall heat transfer. For the thermal stratification interface height of the indoor space with an isolated heat source, substituting ventilation airflow rate G into plume flow rates G_Y of various heat sources to obtain the thermal stratification interface height expression. For heat sources with different shapes or multiple heat sources, the corresponding thermal stratification interface height can be obtained by correcting a single heat source (Zhao 2010).

6. Velocity and temperature non-uniformity coefficient

Differences in air velocity and temperature exist in different room space positions. This difference can be evaluated by the non-uniformity coefficient. The velocity non-uniformity coefficient K_v and temperature non-uniformity coefficient K_t are defined as

$$K_v = \frac{\sqrt{\frac{1}{n} \sum_{i=1}^n (u_i - \bar{u})^2}}{\bar{u}} \quad (1.9a)$$

$$K_t = \frac{\sqrt{\frac{1}{n} \sum_{i=1}^n (t_i - \bar{t})^2}}{\bar{t}} \quad (1.9b)$$

where

n number of sampling points;

u_i, t_i velocity, and temperature of each sampling point, respectively;

\bar{u}, \bar{t} arithmetic averaged of velocity and temperature of each sampling point.

7. Air age

The concept of air age in indoor air distribution is derived from the experience of the reaction time of chemical kinetics (Wang 1992), which initially refers to the time from the start of the reaction of the material in the reactor to the time when the required conversion rate is reached, that is, the reaction duration. In a continuous flow reactor, the time the material particles enter the reactor until departure is the residence time.

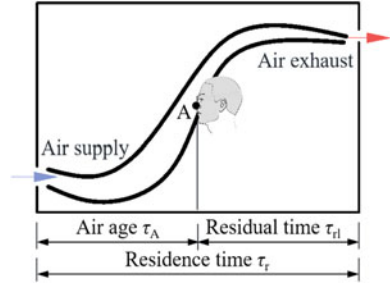
When comparing the air movement process of the indoor air distribution to the flow of materials in the reactor, the concepts of the air age τ_A and air residence time τ_r can be obtained (Fanger et al. 1988; Li et al. 2003; Sandberg and Sjoberg 1983; ASHRAE 2017). The “youngest” air is at the point where outdoor air enters a room by mechanical or natural ventilation, or through infiltration. The “oldest” air may be at some location in the room or in the exhaust air. When the air distribution system’s characteristics are varied, air age is inversely correlated with the quality of outdoor air delivery (ASHRAE 2017).

Obviously, the air age τ_A refers to the time it takes for the air to enter the room until it reaches a certain point A in the room, which is illustrated in Fig. 1.7. The air residence time, τ_r is the time it takes for the air from the entrance until departure. The residual time τ_{rl} (or life expectancy) is defined as the time required for the air to leave the exit from the current position (Fig. 1.7). For the gas micro-cluster, which are groups of air molecules at a specific location in the room, the relationship between air age, residence time, and residual time is as follows

$$\tau_A + \tau_{rl} = \tau_r \quad (1.10)$$

Essentially, air age reflects the ability of different air distributions to remove pollutants (including thermal pollution), and it can be obtained by experiments. When using the step-down (decay) tracer gas method, fill the room with tracer gas and then supply air (tracer gas concentration is 0) to the room. The initial concentration at point A (any point) in the room is $c(0)$. The time-dependent data of tracer gas concentration $c(\tau)$ are available by measuring tracer gas concentration at point A at every certain time. The time-averaged air age is defined as

Fig. 1.7 Air age, residual time, and residence time at room point A



$$\tau = \frac{\int_0^{\infty} c(\tau) d\tau}{c(0)} \quad (1.11)$$

The time-averaged air age in the room is defined as the average of the local averaged air age at each point, that is

$$\bar{\tau} = \frac{1}{V} \int_V \tau dV \quad (1.12)$$

where V is the room volume, m^3 .

The averaged air age of the whole room is 1/2 of the residence time τ_r , that is

$$\bar{\tau} = 1/2\tau_r \quad (1.13)$$

If the ventilation airflow pattern in the room is taking the shape of ideal piston flow, the air residence time is the shortest, which is equal to the nominal time constant, i.e., the room volume to the ventilation volume, $\tau_n = V/G$, that is

$$\tau_r = \tau_n = V/G \quad (1.14)$$

Generally, it refers to the airflow inside a room in the concept of air age, and the air age at the room's entrance is regarded as 0. If the influence of the air handling equipment and the flow process in air supply ducts are taken into account, the concept of air age should be modified. The time that the gas micro-cluster enters the ventilation system from outdoor to a certain point A in the room, can be defined as the modified air age (or total air age), which reflects the air freshness of different ventilation or air conditioning systems.

8. Air exchange efficiency

Air exchange efficiency, η_a , is an index used to evaluate ventilation effect: how efficiently room air is replaced by supply air. It is one of the characteristic parameters of air distribution and has nothing to do with pollutants (Zhu 2010). The air exchange efficiency is defined as the ratio between the shortest possible time needed for replacing the air in a room (τ_n) and the average time for whole room air exchange (τ_r). It is a dimensionless number expressing the effectiveness of renewal of the internal air population by the supply air.

$$\eta_a = \frac{\tau_n}{\tau_r} = \frac{\tau_n}{2\bar{\tau}} \quad (1.15)$$

According to the relation (1.15), the upper limit for this efficiency is 100%, which occurs for idea flow.

The air exchange efficiency η_a is $\leq 100\%$. The greater the air exchange efficiency, the better the ventilation performance. The air exchange efficiency of some typical ventilation modes is as follows:

- $\eta_a = 100\%$ for piston flow;
- $\eta_a \approx 100\%$ for perforated ceiling air supply;
- $\eta_a = 50\text{--}100\%$ for lower-supply and upper-exhaust with single air vents.

It should be pointed out, when defining the air exchange efficiency of mechanical ventilation, the influence of envelope airtightness on air age is not considered. A building's envelope airtightness can be measured with a blower-door test or pressure pulse method (JGJ/T 177-2009). Here, the blower-door test is mentioned by the way. The airflow rate is generally measured at 50 and -50 Pa pressure differences. The envelope airtightness is quantified by Eq. (1.16) by calculating the air change rate.

$$N_{50}^{\pm} = G/V \quad (1.16)$$

where N_{50}^+ , N_{50}^- is the air change rate at pressure differences of 50 and -50 Pa, h^{-1} .

References

- ANSI/ASHRAE Standard 55-2017 (2017) Thermal environmental conditions for human occupancy. American Society of Heating, Refrigeration and Air-Conditioning Engineers Inc., Atlanta
- ASHRAE (2017) ASHRAE handbook: fundamentals. American Society of Heating, Refrigeration and Air-Conditioning Engineers Inc., Atlanta
- Awbi HB (2008) Ventilation systems: design and performance. Taylor and Francis, USA
- Baturin VV (1965) Fundamentals of industrial ventilation (trans: Liu YN). China Industry Press, Beijing (in Chinese)
- Bakhalev BA, Troyanovski BH (1965) Design and calculation principle of central air supply heating and ventilation (trans: Song DP). China Industry Press, Beijing (in Chinese)

- Bauman FS (2003) Underfloor air distribution (UFAD) design guide. American Society of Heating Refrigerating and Air-Conditioning Engineers Inc., Atlanta
- Bauman FS (2006) Underfloor air distribution (UFAD) design guide (trans: Yang GR, Fang W, Reng YW, Hu YQ). China Architecture & Building Press, Beijing (in Chinese)
- BS EN ISO 7730-2005 (2005) Ergonomics of the thermal environment—analytical determination and interpretation of thermal comfort using calculation of the PMV and PPD indices and local thermal comfort criteria. British Standards
- Cao GY, Awbi H, Yao RM, Fan YQ, Sirén K, Kosonen R, Zhang JS (2014) A review of the performance of different ventilation and airflow distribution systems in buildings. *Build Environ* 73:171–186
- Chen QY (2009) Ventilation performance prediction for buildings: a method overview and recent applications. *Build Environ* 44(4):848–858
- CIBSE (2016) Heating, ventilation, air conditioning and refrigeration-CIBSE Guide B. CIBSE Publications, Norwich
- Croome DJ, Roberts BM (1981) Air conditioning and ventilation of buildings, vol 10. Pergamon Press, New York
- Fanger PO, Melikov AK, Hanzawa H, Ring J (1988) Air turbulence and sensation of draught. *Energ Build* 12(1):21–39
- GB 50736-2012 (2012) Design code for heating ventilation and air conditioning of civil buildings. China Architecture & Building Press, Beijing (in Chinese)
- GB/T 50785-2012 (2012) Evaluation standard for indoor thermal environment in civil buildings. China Architecture & Building Press, Beijing (in Chinese)
- GB/T 50155-2015 (2015) Standard for terminology of heating, ventilation and air conditioning. China Architecture & Building Press, Beijing (in Chinese)
- Griefahn B, Künemund C, Gehring U (2001) The impact of draught related to air velocity, air temperature and workload. *Appl Ergon* 32(4):407–417
- Han O, Li AG, Kosonen R (2019) Hood performance and capture efficiency of kitchens: a review. *Build Environ* 161:106221
- JGJ/T 177-2009 (2009) Standard for energy efficiency test of public buildings. China Architecture & Building Press, Beijing (in Chinese)
- Karimipناه T, Awbi HB, Sandberg M, Blomqvist C (2007) Investigation of air quality, comfort parameters and effectiveness for two floor-level air supply systems in classrooms. *Build Environ* 42(2):647–655
- Lau J, Chen QY (2006) Energy analysis for workshops with floor-supply displacement ventilation under the U.S. climates. *Energ Build* 38(10):1212–1219
- Li AG, Qin E, Bao X, Wang GD, Wang JM (2010) Experimental analysis on the air distribution of powerhouse of Hohhot hydropower station with 2D-PIV. *Energ Convers Manag* 51(1):33–41
- Li AG, Qiu SH, Wang GD (2008) Vertical wall attached airflow and air lake mode ventilation system. Chinese patent ZL 200810017349.0 (in Chinese)
- Li AG, Zhu YX, Li YG (2014) Proceedings of the 8th international symposium on heating, ventilation and air conditioning. Springer, Singapore
- Li AG, Yang CQ, Ren T (2015) An attached ventilation with double side devices to form air reservoir distribution. Chinese patent ZL201510548195.8 (in Chinese)
- Li AG (2019) Extended coanda effect and attachment ventilation. *Indoor Built Environ* 28(4):437–442
- Li AG, Zhang Y, Han O, Hou LA, Chen YH, Li ZX, Ma YC, Xiang WZ (2020) Effectiveness of air distribution and pollutant control in isolation wards. *J HV&AC* 50:26–34
- Li GP, Wang TC, Sun ZJ, Dong YW, Guo XH (2021) Air distribution optimizing design of air conditioning system for first-floor waiting hall of Xiongan station. *J HV&AC* 51(9):24–29,35
- Li QM (2000) Displacement ventilation: principles, design and applications. *J HV & AC* 30(5):41–46 (in Chinese)
- Li XT, Li DN, Yang XD, Yang JR (2003) Total air age: an extension of the air age concept. *Build Environ* 38(11):1263–1269

- Lin Z, Yao T, Chow TT, Fong KF, Chan LS (2011) Performance evaluation and design guidelines for stratum ventilation. *Build Environ* 46(11):2267–2279
- Liu ZM (2018) Application of a novel air distribution mode to ventilation and air conditioning system of underground railway stations. *J HV&AV* 48(9):41–44+62 (in Chinese)
- Lu YQ (2007) Practical heating ventilation and air conditioning design handbook, 2nd edn. China Architecture & Building Press, Beijing (in Chinese)
- Ma ZL, Yao Y (2015) Air conditioning design of civil buildings. Chemical Industry Press, Beijing (in Chinese)
- Melikov A K (2004) Personalized ventilation. *Indoor Air* 14:157–167
- REHVA (2013) Mixing ventilation-Guide on mixing ventilation air distribution design-REHVA Guidebook No. 19. Federation of European Heating, Ventilation and Air Conditioning Associations, Finland
- REHVA (2002) Displacement ventilation-REHVA Guidebook No. 23. Federation of European Heating, Ventilation and Air Conditioning Associations, Finland
- Rock BA, Brandemuehl MJ, Anderson R (1995) Toward a simplified design method for determining the air change effectiveness. *ASHRAE Trans* 101(1):217–227
- Sandberg M (1981) What is ventilation efficiency? *Build Environ* 16(2):123–135
- Sandberg M, Sjoberg M (1983) The use of moments for assessing air quality in ventilation rooms. *Build Environ* 18(4):181–197
- Seppänen O (2008) Ventilation strategies for good indoor air quality and energy efficiency. *Int J Vent* 6(4):297–306
- Sun XM, Lan J, Yu WZ (2021) Innovative application of column-attached ventilation in the ventilation and air conditioning system in public area of subway station. *Railway Standard Des* 65(1):122–127
- Wang DJ (1992) Fundamentals of chemical engineering. Higher Education Press, Beijing (in Chinese)
- Yuan XX, Chen QY, Glicksman LR (1998) A critical review of displacement ventilation. *ASHRAE Trans* 104:78
- Zhang YP, Mo JH, Li YG, Sundell J, Wargoeki P, Zhang J, Little JC, Corsi R, Deng QH, Leung M, Fang L, Chen WH, Li JG, Sun YX (2011) Can commonly-used fan-driven air cleaning technologies improve indoor air quality? A literature review. *Atmospheric Environ* 45(26):4329–4343
- Zhao RY (2008) Air conditioning, 4th edn. China Architecture & Building Press, Beijing (in Chinese)
- Zhao HZ, Li AG (1998) Prediction of vertical temperature distribution in rooms with upward air supply. *J HV&AC* 28(5):74–77 (in Chinese)
- Zhao HZ (2010) Indoor heat convection and ventilation. China Architecture & Building Press, Beijing (in Chinese)
- Zheng K, Han WS, Pan YG, Zhang J, Jin CH, Guo R, Zhao G, Guo SY, Wang WL (2019) Analysis on key energy-saving technologies of HVAC of a government office building in Beijing. *Constr Sci Technol* 379:75–80 (in Chinese)
- Zhang Y, Han O, Li A, Hou LA, Olofsson T, Zhang LH, Lei WJ (2022) Adaptive wall-based attachment ventilation: a comparative study on its effectiveness in airborne infection isolation rooms with negative pressure. *Engineering* 8:130–137
- Zhu YX (2010) Built environment, 3rd edn. China Architecture & Building Press, Beijing (in Chinese)

Open Access This chapter is licensed under the terms of the Creative Commons Attribution-NonCommercial-NoDerivatives 4.0 International License (<http://creativecommons.org/licenses/by-nc-nd/4.0/>), which permits any noncommercial use, sharing, distribution and reproduction in any medium or format, as long as you give appropriate credit to the original author(s) and the source, provide a link to the Creative Commons license and indicate if you modified the licensed material. You do not have permission under this license to share adapted material derived from this chapter or parts of it.

The images or other third party material in this chapter are included in the chapter’s Creative Commons license, unless indicated otherwise in a credit line to the material. If material is not included in the chapter’s Creative Commons license and your intended use is not permitted by statutory regulation or exceeds the permitted use, you will need to obtain permission directly from the copyright holder.



Chapter 2

Air Movement and Airflow Patterns of Attachment Ventilation



Abstract This chapter presents the principle of attachment ventilation (attached ventilation) and airflow patterns. Attachment ventilation is based on the extended Coanda effect, which refers to the phenomenon that the jet flows along the wall surface and attaches to the adjacent walls, maintains continuous flow until it reaches the floor, and continues to adhere to the floor for extending flow to produce air reservoir or air lake. The airflow patterns of vertical wall attachment and column attachment ventilation are fully illustrated and compared by 2D-PIV and trajectory experiments.

Keywords Attachment ventilation · Attached ventilation · Coanda effect · Extended Coanda effect · Airflow pattern · Air movement · Flow visualization

The goal of ventilation is to control air movement as required in a room or given space to provide a comfortable and healthy indoor air environment. The indoor airflow is invisible, and the visualization technique makes the airflow pattern visible and observable macroscopically. The airflow pattern visualization by 2D-PIV and trajectory experiments depicts the fundamental interaction between the forced jet delivered from diffusers and the heat convection. This chapter provides the airflow pattern of vertical wall attachment and column attachment ventilation, and clarifies the significant factors affecting attachment ventilation performance.

2.1 Coanda Effect and Ventilation

2.1.1 *Coanda Effect*

The Coanda effect simply refers to the tendency of a fluid jet to stay attached to an adjacent solid surface. The principle of the Coanda effect is that when fluid 1 flows into another fluid 2 (or environmental fluid) from an orifice with a certain initial velocity, fluid entrainment will be formed in the surrounding environment, as shown in Fig. 2.1a. The jet will deflect towards the side with greater flow resistance when

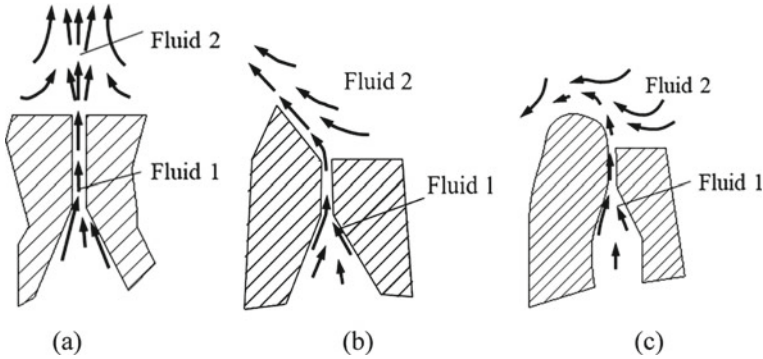


Fig. 2.1 Coanda effect of jet flow. **a** Free jet, **b** wall-attached jet, **c** curved surface-attached jet

the entrainment effect of the jet on ambient air is unbalanced (Fig. 2.1b, c) (Coanda 1936). The airflow direction of a jet can be altered by appropriately adjusting the boundary conditions of the jet. If the boundary conditions of the flow near the wall are continuously changed, the jet can be formed into a streamlined flow in any desired direction theoretically (Coanda 1964, 1938; Panitz and Wasan 1972).

There is an inertial movement of fluid flowing out of an orifice; the entrainment effect of surrounding fluid will lead to a low-pressure region near the wall surface. Consequently, a wall-attached flow is formed. The process of the Coanda effect driving the jet toward the wall can be further shown in Fig. 2.2. The jet is initially flowing in a straight line from an orifice, gradually driving the surrounding air with decreasing velocity, as illustrated in Fig. 2.2a. With the further extension of the jet, the pressure distribution between the upper and lower sides of the jet is different. The jet's pressure in the lower side is equal to the atmosphere pressure, attributed to the jet being filled with sufficient surrounding air to maintain the atmospheric pressure.

On the contrary, the supplementary airflow near the wall can only enter the low-pressure zone through the gap between the upper side of the jet and the wall. The jet deflects to the wall due to the pressure difference between the upper and lower sides, as shown in Fig. 2.2b. As the jet continues to deflect upward, the replenishment channel of airflow becomes narrower, and the pressure of the jet's upper side is further decreased so that the jet finally adheres to the wall surface. Eventually, a jet that is fully attached to the wall surface is formed and pushed forward, as depicted in Fig. 2.2c.

Some studies have shown that if there is no Coanda effect, almost all the jet throw of supply air will be reduced by about 30% (ASHRAE 2008). The following factors have a dominant influence on the Coanda effect (Awbi 2003, 2011; Wen 1982; Zhu 1984):

- Normal distance between the slot and the attached wall surface S ;
- Width of the slot inlet b , also called slot outlet (ASHRAE 2017);
- Slot jet velocity u ;
- Wall obstacles and other influencing factors;
- Temperature difference between jet and ambient air Δt .

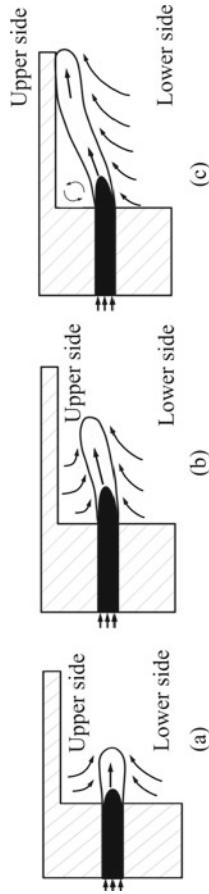


Fig. 2.2 Formation process of the Coanda effect. **a** Jet discharge, **b** jet deflection, **c** wall attachment

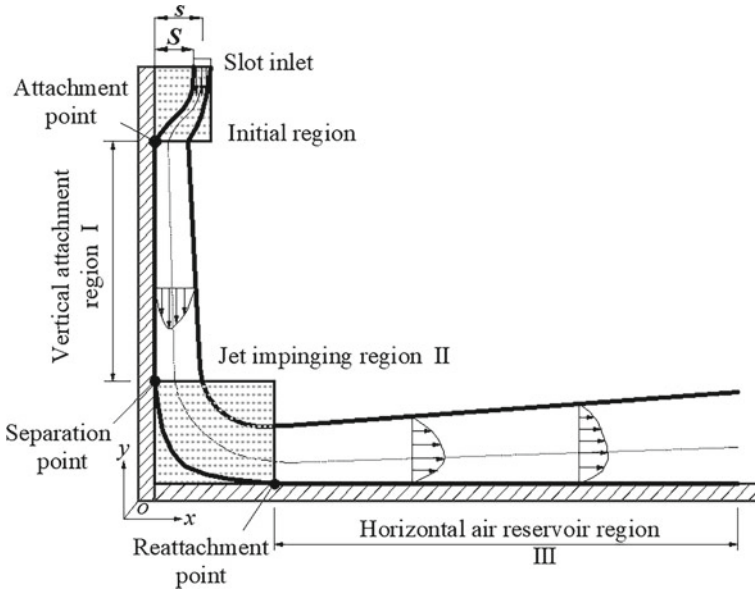


Fig. 2.3 Airflow structure of attachment ventilation by extended Coanda effect (ECE)

In point of fact, the air jet can be affected by the Coanda effect when the distance between the supply air jet and the wall surface is less than the maximum attachment distance S_{\max} (see Sect. 2.2), and a confined wall-attached jet is formed finally. The airflow pattern is closely related to the location of the air jet inlet (see Fig. 2.3). When the air inlet is close to a wall surface, it is more likely to form a wall-attached jet. The axis direction of the jet is inclined to the wall surface. With the jet throw extending, the entrained airflow rate increases, and the jet velocity decays, resulting in the attenuation of the Coanda effect (ASHRAE 2008).

It should be noted that the buoyancy effect resulting from the temperature difference between a jet and the ambient air will directly affect the flow feature of a wall-attached jet. The flow field details will be explored in the subsequent chapters. For office rooms with a temperature difference of 8–12 °C when supplying cold air, the distance between the air inlet and wall surface should be kept within 300 mm, and 0 mm is preferred. Furthermore, the obstacles may also cause jet separation, making the Coanda effect no longer valid. When obstacles' thickness is smaller than the attached boundary layer, the jet could remain attached to the wall. This phenomenon is related to jet velocity, obstacle height, obstacle position, etc. (ASHRAE 2017; JGJ/T 177-2009 2009), which are discussed in detail in Chap. 4, Sect. 4.8.

2.1.2 Extended Coanda Effect and Air Movement

The extended Coanda effect (ECE) (Li 2019) refers to the phenomenon that the jet flows along the wall surface, forming the Coanda effect and maintains continuous flow until it impinges on the floor, and continues to adhere to the floor for extending flow. The difference between the ECE and the Coanda effect lies in the presence of an impinging region. The principle of the ECE is as follows: when the jet exits from the adjacent solid surface, the jet will deflect and be inclined to attach to the wall surface (that is, forming the Coanda effect in the traditional sense, see Region I in Fig. 2.3). Because of the influence of inertia momentum, it moves along the original direction, reaches a separation point, and causes a stagnation phenomenon after impinging the ground. With the recovered dynamic pressure, the jet moves further forward along the floor and entrains the surrounding air above the floor. As shown in Fig. 2.3, there are two key points worth noting: jet separation point and floor reattachment point. The jet separation point refers to the location where $\partial u_y / \partial x|_{x=0} = 0$ and the Coanda effect fails, or it resembles the jet “perceives” the occurrence of the impinging effect, and then separates from the vertical wall. On the contrary, the floor reattachment point refers to the position where the airflow re-attaches to the floor under the ECE, and here $\partial u_x / \partial y|_{y=0} = 0$. The pressure of the stagnation zone between the separation point and the reattachment point (Region II) is close to the ambient pressure (the pressure distribution is related to the air jet parameters). In the downstream of Region II of the stagnation point, the dynamic pressure gradually increases and reaches a maximum value. With the recovered dynamic pressure, fluid can overcome the floor resistance and move along a horizontal floor surface, forming horizontal air reservoir region (Region III), as illustrated in Fig. 3.4.

2.2 Vertical Wall-Attached Jet and Airflow Pattern

As mentioned above, mixing ventilation has the characteristic of high supply air velocity (momentum). The air openings are often arranged in a room’s upper space, and the room’s lower spaces are saved. For mixing ventilation, the entire room is conditioned so that the ventilation efficiency or temperature efficiency is relatively low (Yin and Li 2015).

The features of displacement ventilation lie in that air is supplied at floor level with a very low velocity (0.1–0.3 m/s), and the supply air momentum is so low that it does not substantially impact the dominant thermal plume. The supply air temperature is usually 2–4 °C lower than the occupied zone temperature. The cool air is denser and sinks to the floor, and spreads throughout the room, creating a piston-like flow or air reservoir in the occupied zone. The indoor air slowly rises due to the rising thermal plume’s entrainment effect and the exhaust opening’s suction effect. Indoor pollutants (including thermal pollution) are removed from the upper exhaust openings. The exhaust air temperature is higher than the indoor occupied zone air temperature.

Correspondingly, the ventilation efficiency or temperature efficiency is relatively high (Li 2000). However, wall-mounted diffusers of displacement ventilation often require significant spaces and occupied zones, which greatly limits the applications of displacement ventilation.

Attachment ventilation combines the advantages of the above two types of ventilation modes. Attachment ventilation mainly consists of the following modes (Song 2005; Li et al. 2012a, b; Yin and Li 2012):

- Vertical wall attachment ventilation (VWAV);
- Rectangular column attachment ventilation (RCAV);
- Circular column attachment ventilation (CCAV);
- Adaptive attachment ventilation (AAV).

1. Principle of VWAV

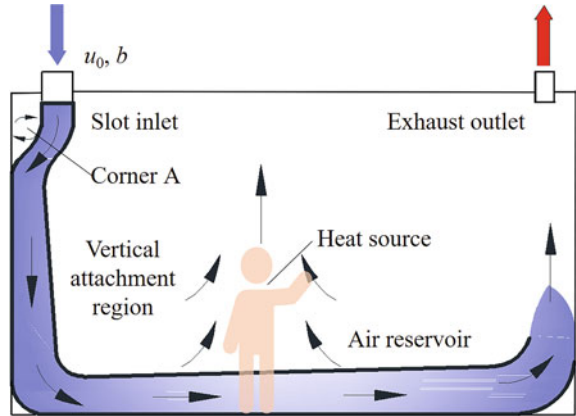
Essentially, attachment ventilation is to create appropriately air environment parameters for the occupied zone by designing the air supply temperature, velocity, air supply volume, air terminal types, locations, etc. For VWAV, the supply air moves along the vertical wall to close to the ground, an “downstream air reservoir” is formed due to impinging, and the dynamic pressure is transformed into static pressure, and momentum is transformed into the impulse, which consumes a small percentage of the kinetic energy.

The theory of vertical wall-attached jets and air reservoir airflow is the basis for the design of attachment ventilation. The air distribution design of VWAV aims to determine the physical parameters of the supply air jet appropriately, to deliver the maximum amount of fresh air or conditioned air to the occupied zone, and to ensure that the air temperature and velocity in the occupied zone meet the comfort requirements (Yin and Li 2014; Zhang 2005; Zheng et al. 2019).

Figure 2.4 shows a diagram of the airflow pattern of VWAV mode. After the jet is discharged from the linear slot inlet (if $l/b \geq 10:1$, jets can be regarded as two-dimensional plane jets), it keeps the momentum conservation and continuously entrains the ambient air. The entrained air near the wall is far less than that on the other side, and a low-pressure zone is formed at the upper corner A of the vertical wall (see Fig. 2.4). The pressure difference between the two sides of the supply air jet drives it to deflect toward the vertical wall and attach to the surface. The airflow continues to flow downward along the wall and extends to the floor level, the adverse pressure gradient increases, and the air supply jet will separate from the vertical wall. After impinging the floor, it extends forward along the floor to form an air reservoir. Then, the load in the control zone (occupied zone) is “taken away”, forming a kind of air temperature, velocity, and humidity fields that are similar to displacement ventilation mode (Yin and Li 2015). This air reservoir is created by the attached jet flow from the upper part of the room after impinging, which is different from the airflow mechanism of traditional displacement ventilation.

From the perspective of jet mechanics, the VWAV can be regarded essentially as a combination of a vertical wall-attached jet and a horizontal floor-attached airflow (Wang 2009).

Fig. 2.4 Indoor airflow pattern of VWAV



According to the distance between the air inlet and the wall surface, the VWAV can be divided into two modes, complete attachment (i.e., tangential attachment) and deflected attachment, as shown in Fig. 2.5. For the theoretical analysis, the slot width b , which has a more significant influence on the air supply characteristics, is selected as the characteristic size. s is the normal distance between the opening center and the attached wall surface, and $S = s - b/2$ is defined as the distance between the slot's inner side and the attached wall surface, called the deflection distance. When $S/b > 0$, i.e., $s/b > 0.5$, the air supply jet deflection will occur, and the full attachment ventilation will turn into partially attached or deflected attachment ventilation. The difference between S/b and s/b is noted in Fig. 2.5.

For indoor air movement of VWAV, three regions can be distinguished (see Fig. 2.3) (Wang 2009).

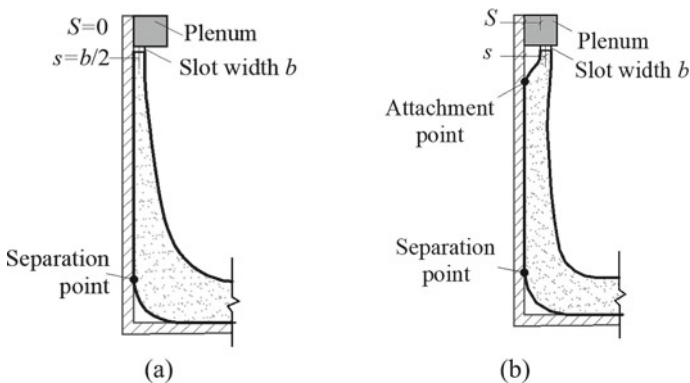


Fig. 2.5 Complete and deflected attachment ventilations. **a** Complete attachment, **b** deflected attachment

Region I, Vertical attachment region

For the deflected attachment ventilation, there is $S > 0$. The discharge jet is a free turbulent jet within a short distance from the air inlet (Cho et al. 2008). After that, the jet deflects toward the vertical wall and attaches to its adjacent surface due to Coanda Effect. It is found that the initial region zone has a crucial influence on the confined attachment jet, which will be analyzed in detail in the subsequent chapters. For deflected attachment, there is usually a vortex flow at corner A (see Fig. 2.4). The possible reason is that the adverse pressure gradient increases gradually in the jet direction, which hinders the jet flow, and the fluid micro cluster near the wall will be more strongly blocked. When their kinetic energy is depleted, they are forced to turn back, forming a vortex flow phenomenon (Cui 2010).

The air supply jet attaches to the vertical wall under the action of the pressure difference between the two sides of the supply jet, and moves downward along the wall, realizing the effective transport of the jet along the vertical wall, and the centerline velocity of the air supply jet decays very slowly. With the decrease of s , the range of the initial region becomes smaller. When s equals $b/2$, the deflected attachment is converted into a complete attachment.

Region II, Jet impinging region

When the discharge jet approaches the ground along the vertical wall, the air supply jet separates from the vertical wall due to the influence of the adverse pressure gradient of the ground, impinges the ground, and turns into a horizontal flow. The jet flow direction deflects by 90° (the jet deflection angle is related to the wall structure), the jet mixes with the ambient air in a large amount, and the centerline velocity decays rapidly in this region.

Region III, Horizontal air reservoir region

A long region of major engineering importance that is often called horizontal air reservoir region, i.e., fully established turbulent floor-attached flow and its distance is depends on the air supply velocity (initial velocity), the shape and area of the slot inlet, and the dimensions of the space into which the slot inlet discharges.

In region III, the air supply jet spreads along the floor, forming a forward piston flow and presenting air reservoir distribution over the floor. It is the control zone for the air distribution of VWAV. It resembles a displacement ventilation mode in the flow pattern, meets the thermal comfort of the human body, and achieves high ventilation efficiency.

The essence of the design method of the air distribution of the attachment ventilation is how to calculate and determine the appropriate air supply parameters, to ensure the velocity field, temperature field, etc., in the air reservoir region.

2. Airflow pattern of VWAV

Air movement in a room is a rather complex process. Airflow pattern visualization is helpful in deeply understanding the air movement mechanism and then effectively optimizing air distribution.

Airflow pattern visualization can be performed by many methods. It is a common way to display (e.g., visually inspect, detecting and photographing, etc.) the movement and state of the airflow through the tracer gas.

The following assumptions are made about the tracer particles in the visualization tests.

- (a) The concentration of particles in the airflow is low and will not interfere with the flow field.
- (b) The particles are spherical with a small diameter. Their flow is in the low Reynolds number region, and there is no interaction between particles. The gravity and buoyancy are ignored.
- (c) The tracer particles are completely and uniformly mixed with the airflow.
- (d) The temperature of the tracer particle is the same as that of the airflow. According to our experience, the smoke generator can be connected with a 2–5 m hose to reduce the smoke generation temperature and ensure that the temperature of the tracer particle is the same as that of the airflow.

The movement of smoke tracer particles can be described by Eq. (2.1)

$$M_p \frac{du_p}{d\tau} = C_d \frac{1}{2} \rho_f A_p (u_f - u_p)^2 \quad (2.1)$$

where

M_p tracer particle mass, kg;

C_d resistance coefficient;

ρ_f airflow density, kg/m³;

A_p cross-sectional area of tracer particle, m²;

u_f airflow velocity, m/s;

u_p tracer particle velocity, m/s;

τ time of tracer particle moving together with the airflow.

If u_p is a constant (i.e., does not change with time), C_d is related to the Re number and is only a function of $u_f - u_p$. When the time τ is equal to 0, the tracer particles enter the airflow, and the initial velocity u_p is equal to 0, and then Eq. (2.1) can be simplified as Eq. (2.2).

$$u_p = u_f \left[1 - \exp\left(-\frac{18\mu_f}{\rho_p d_p^2} \tau\right) \right] \quad (2.2)$$

where

μ_f dynamic viscosity of airflow, Pa·s;

ρ_p tracer particle density, kg/m³;

d_p tracer particle diameter, m.

The above equation indicates that when u_f , d_p , ρ_p are determined, the tracer particle velocity u_p is a function of time. Once the tracer particles enter the flow field, u_p can immediately converge to the airflow velocity u_f (i.e., $u_f = u_p$).

It is a common visualization method to trace the flow field with ethylene glycol (less than $1.0 \mu\text{m}$ in diameter), which has good light reflection performance and particle tracking performance, and it is easy for CCD high-speed digital camera to photograph the experimental process (Song 2005).

The test model and geometric parameters for the ethylene glycol visual test are shown in Fig. 2.6. During the test, either a CCD high-speed digital camera or an ordinary digital video system can be used to take pictures of the airflow patterns of the air supply jet. The CCD digital camera system is labeled in the figure, which is used to record the changing air jet pattern qualitatively. The lens of the camera system is kept in a horizontal fixed state to eliminate the influence of image distortion on the test data, and the horizontal direction of the lens is perpendicular to the plane where the central axis of the jet flow is located. In fact, ordinary digital video can also better qualitatively record the airflow process and change the filming position according to actual needs (Qiu 2008; Song 2005; Zhang 2005). Figures 2.7 and 2.8 show the visualization results and airflow patterns of VWAV under different scenarios.

To understand the air movement mechanism of VWAV and investigate the influence of parameters u_0 and s on the ventilation performance, a series of visualization tests were conducted on VWAV in a three-dimensional real-size test chamber (Yin 2012). Figure 2.9 shows the test chamber used, with dimensions of $5.4 \text{ m} \times 7.0 \text{ m} \times 3.16 \text{ m}$. A plenum chamber with a dimension of $2.5 \text{ m} \times 0.5 \text{ m} \times 0.5 \text{ m}$ was used to realize the uniform air supply of the slot inlet, whose area is $2.0 \text{ m} \times 0.05 \text{ m}$ and the installation height is 2.5 m away from the floor. A flexible connection hose between the air supply duct and plenum chamber is adopted to realize the adjustment of the

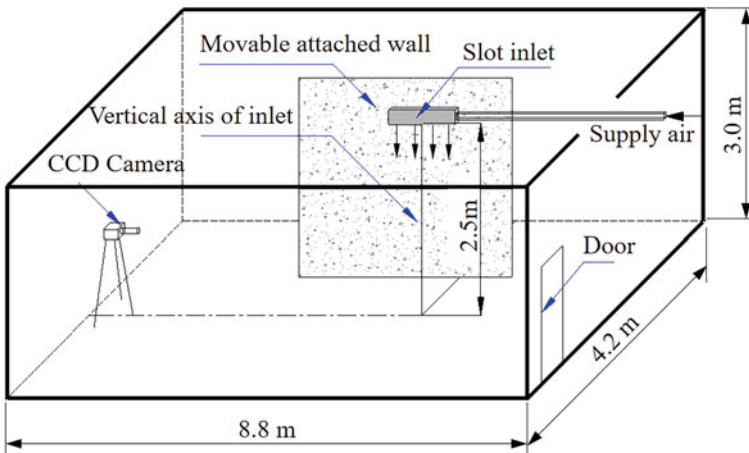


Fig. 2.6 Visualization test system

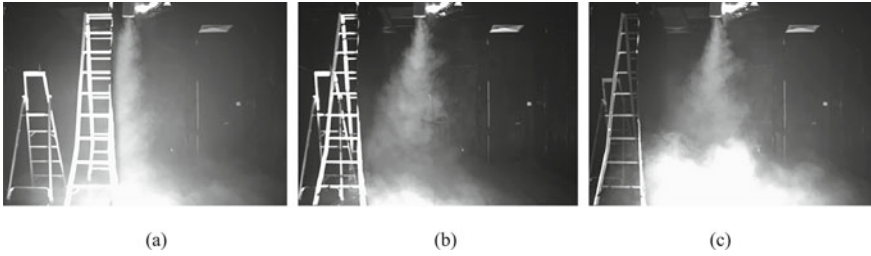


Fig. 2.7 Visualization of air supply flow patterns at different distances from the vertical wall ($u_0 = 5.15 \text{ m/s}$, $t_0 = 22.0 \text{ }^\circ\text{C}$, $t_n = 24.5 \text{ }^\circ\text{C}$), a vertical baffle is set on the right side of the folding ladder to form a movable vertical wall in the visualization test. **a** $s = 0.13 \text{ m}$, **b** $s = 0.60 \text{ m}$, **c** $s = 0.78 \text{ m}$

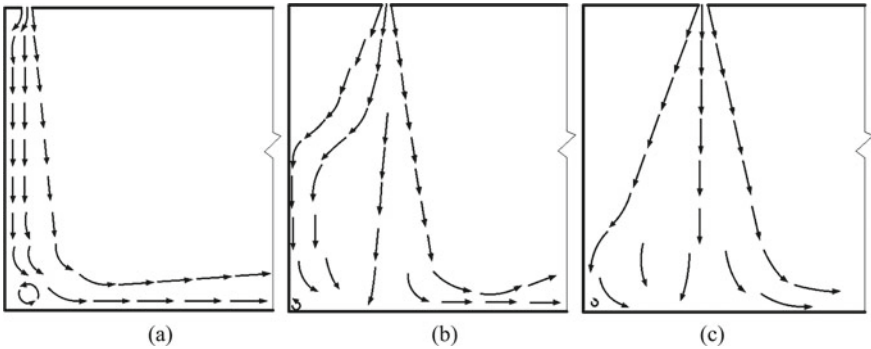


Fig. 2.8 Airflow patterns in rooms of different distances from the vertical wall ($Re = 17,098$, $t_0 = 22.0 \text{ }^\circ\text{C}$, $t_n = 24.5 \text{ }^\circ\text{C}$). **a** $s = 0.13 \text{ m}$, **b** $s = 0.60 \text{ m}$, **c** $s = 0.78 \text{ m}$

vertical distance between the slot inlet and vertical wall, which can also eliminate the impact of vibration from air supply plenum chamber on air supply airflow.

The visualization results and airflow patterns of VWAV under different u_0 and s are shown in Figs. 2.10 and 2.11, respectively. The slot inlet locations s/b are equal to 2, 5, 8, and 10, respectively, and the air supply velocity is varied from 1.0 to 2.0 m/s. The airflow pattern at different slot inlet locations is analyzed below.

- (a) When s/b is equal to 2, the air supply velocity changes from 1.0 to 2.0 m/s, and the supply air can form an effective attachment with the wall surface. It can be clearly seen from the figure that when the tracer gas approaches the ground along the vertical wall, the direction turns to the horizontal diffusion flow process after impinging (see Figs. 2.10 and 2.11a–c). In other words, the 0.07 m gap between the slot inlet and the vertical wall does not influence the attachment effect, almost forming a complete attachment ventilation air movement.
- (b) When s/b is equal to 5, the air supply inlet is further away from the attached wall surface. Under the cases of different air supply velocities, after the jet is discharged from the slot inlet, the pressure difference between the two sides of the supply jet drives it to deflect toward the vertical wall gradually. Influenced

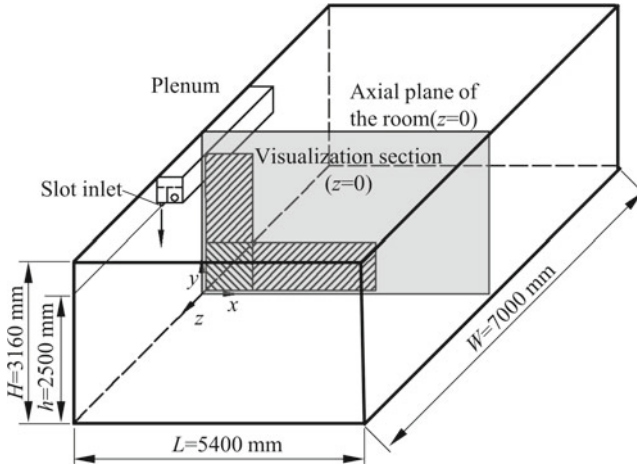


Fig. 2.9 Three-dimensional real-size test chamber

by the adverse pressure gradient, a vortex is generated at the upper left corner of the room (corresponding to Fig. 2.4). However, once the attachment is formed, the airflow movement is similar to cases of $s/b = 2$ (Figs. 2.10 and 2.11d–f).

- (c) When s/b is equal to 8, the air supply inlet further deviates from the attached wall surface, and the included angle between the inlet jet and the wall increases significantly. Compared to the case of $s/b = 5$, in addition to the increase in the included angle of the air supply jet, the distance of the upper deflection zone is also increased, approaching $1/3$ of the room height (see Figs. 2.10 and 2.11g–i). It is noted that there is a small amount of air diffusing along the direction of the room height, which will cause a decrease in the effectiveness of attachment ventilation in the occupied zone.
- (d) When the air inlet is far away from the adjacent wall, that is, s/b is equal to 10, it is difficult to form an attachment airflow, see Figs. 2.10 and 2.11j–l, there is an apparent gap between the air supply jet and the vertical wall.

In summary, the slot inlet location s has a crucial influence on the air distribution of VWAV. With the slot location gradually away from the wall, the attachment effect gradually weakened, and the mixing of air supply jet with indoor air intensified. When s is small, the air supply jet deflects toward the wall, almost forming a complete attachment jet, and the flow field distribution in the floor region can be obtained similarly to that of displacement ventilation. With the s/b increase to 10, the air supply jet almost leaves the vertical wall and turns to mixing ventilation, and the VWAV mode fails (Qiu 2008). The test results show that within the design velocity range of the ventilation and air conditioning system, the maximum attachment distance should be maintained within 0.25–0.40 m (i.e., s/b is approximately equal to 5 ~ 8).

When s is determined, increasing air supply velocity is conducive to strengthening the attachment effect and reducing the mixing of the air supply jet with the ambient

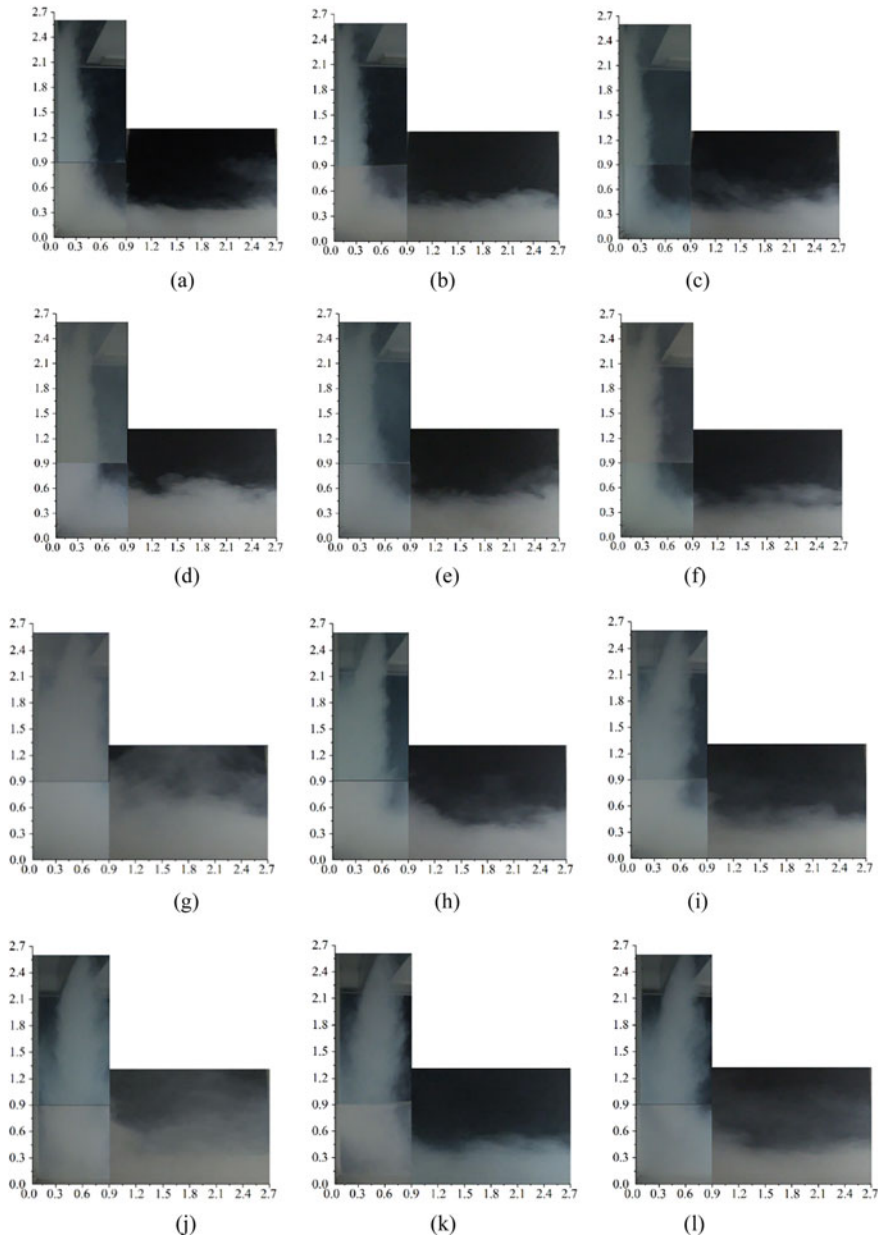


Fig. 2.10 Visualization of airflow patterns of VWAV. **a** $s/b = 2$, $u_0 = 1.0$ m/s, **b** $s/b = 2$, $u_0 = 1.5$ m/s, **c** $s/b = 2$, $u_0 = 2.0$ m/s, **d** $s/b = 5$, $u_0 = 1.0$ m/s, **e** $s/b = 5$, $u_0 = 1.5$ m/s, **f** $s/b = 5$, $u_0 = 2.0$ m/s, **g** $s/b = 8$, $u_0 = 1.0$ m/s, **h** $s/b = 8$, $u_0 = 1.5$ m/s, **i** $s/b = 8$, $u_0 = 2.0$ m/s, **j** $s/b = 10$, $u_0 = 1.0$ m/s, **k** $s/b = 10$, $u_0 = 1.5$ m/s, **l** $s/b = 10$, $u_0 = 2.0$ m/s

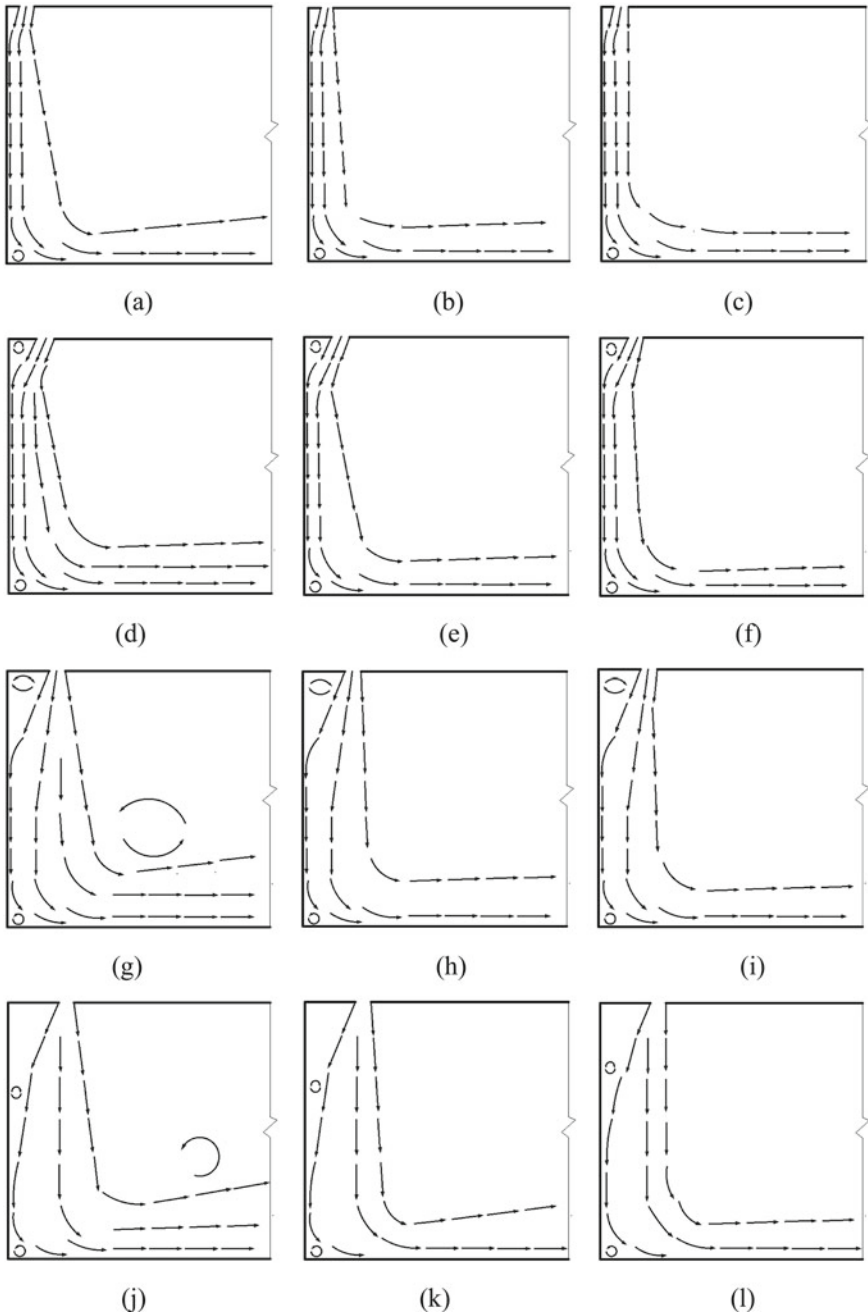


Fig. 2.11 Airflow patterns of VWAV. **a** $s/b = 2$, $Re = 3320$, **b** $s/b = 2$, $Re = 4980$, **c** $s/b = 2$, $Re = 6640$, **d** $s/b = 5$, $Re = 3320$, **e** $s/b = 5$, $Re = 4980$, **f** $s/b = 5$, $Re = 6640$, **g** $s/b = 8$, $Re = 3320$, **h** $s/b = 8$, $Re = 4980$, **i** $s/b = 8$, $Re = 6640$, **j** $s/b = 10$, $Re = 3320$, **k** $s/b = 10$, $Re = 4980$, **l** $s/b = 10$, $Re = 6640$

air. With a further increase of air supply velocity, the jet thickness of the vertical wall and horizontal air reservoir becomes thinner. Thus, it is essential to select the appropriate air supply velocity to ensure the effectiveness of attachment ventilation.

3. 2D-PIV flow field test

Another technique for airflow visualization is particle image velocimetry (PIV), which has become a well-established technique for velocity field measurement in fluid mechanics, power engineering, and other fields (Cao et al. 2014; Wang 2010). It is a non-invasive (indirect) measurement technology for flow field profiles with high spatial resolution, clear flow field observation, and the ability to obtain quantitative flow field velocity from its images (Hosni and Jones 2002).

The 2D-PIV technique can be used to measure the displacement of the tracer particles in a short time interval through the flow trace of the tracer particles, to obtain the transient velocity distribution of the flow field. The methods for testing the flow field are mainly divided into two categories. One is to expose the particle on the flow field cross-section of the sheet light source twice or more times to establish the PIV flow field picture, and use Young’s stripe method or related algorithm to read the PIV picture point by point to obtain the flow field on the cross-section of the sheet light source. The other is to use a high-speed CCD camera to directly input the flow field image on the cross-section of the sheet light source to the computer for image processing, and use related software to obtain the flow field velocity.

The essence of the 2D-PIV velocity field test is to obtain the ratio of displacement to time. Let the position of the tracer particle at time t_1 be (x_1, y_1) , the position at time t_2 be (x_2, y_2) , and the time interval is Δt . The velocity calculation is shown in Fig. 2.12.

The velocity component of the tracer particle is shown in Eq. (2.3a, 2.3b).

$$v_x = \lim_{t_2 \rightarrow t_1} \frac{x_2 - x_1}{t_2 - t_1} = \frac{dx}{dt} \tag{2.3a}$$

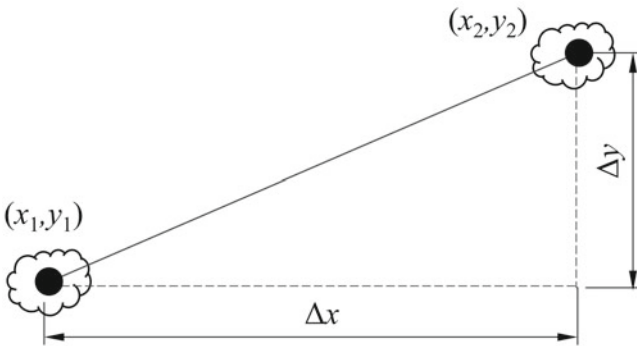


Fig. 2.12 2D-PIV velocity field measurement

$$v_y = \lim_{t_2 \rightarrow t_1} \frac{y_2 - y_1}{t_2 - t_1} = \frac{dy}{dt} \quad (2.3b)$$

2D-PIV technology can measure 3500 to 14400 instantaneous velocity vector points in a cross-section with an error range of only 0.1–1% (Fan 2002). For ventilated flow fields, it is generally recommended to use smoke or oil mist particles (Zhao 2004) as tracer particles. In particular, the time difference between the two laser pulses plays a vital role in the PIV tests, and setting a correct value is the key to the success of the PIV tests. Our research shows that the time difference between the two laser pulses (Δt , μs) and the maximum velocity (u_{max} , m/s) in the photographed area vary inversely, and there is the linear logarithm function, that is, $\ln(\Delta t) = 5.52 - \ln(u_{max})$, i.e., $\Delta t \cdot u_{max} = 250$. The flow field in the near-wall region can be photographed using a cylindrical lens to obtain a more realistic and clear velocity vector. For the experimental study of the flow field in the near-wall region, the above method can be referred to Qin et al. (2009).

The experimental results of using 2D-PIV to study VWAV (ambient air temperature 24 °C) with different influencing factors (u_0 , s) are presented (Qiu 2008). A high-velocity CCD camera is used to capture the flow field images to obtain the velocity field. The dimension of the PIV test chamber is 600 mm \times 300 mm \times 340 mm, the slot inlet size is 300 mm \times 10 mm, and the distance of the slot inlet from the attached wall is adjustable, as shown in Fig. 2.13 (the shooting area is x from 10 to 250 mm, and y from 12 to 330 mm). During the test, a special fixed low turbulence fan is used to supply air to the chamber. To ensure the uniformity and stability of the air supply jet, a plenum chamber and a rectification section need to be set in front of the slot inlet. The tracer particle smoke generator and tracer particle are set in the front section of the fan, to ensure the uniformity of tracer particle concentration and improve the accuracy of the PIV test.

The results of 2D-PIV tests are given below to analyze the relationship between the air supply velocity u_0 , s , and the flow field of the VWAV (Qiu and Li 2010).

1. The effect of air supply velocity (u_0)

Observe changes of the centerline velocity of the attached ventilation by changing the air supply velocity (u_0). See Table 2.1 for the test conditions.

Fig. 2.13 Diagram of 2D-PIV test chamber with attachment ventilation

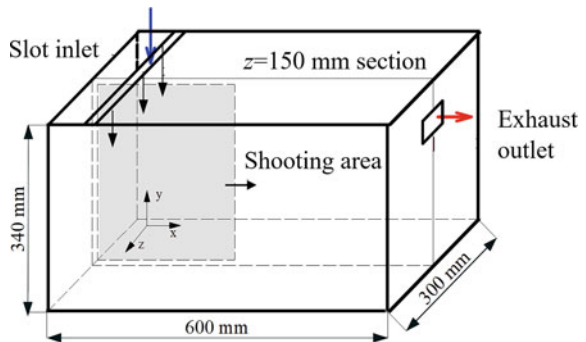


Table 2.1 Test conditions for different u_0

Slot inlet width b (m)	Distance of slot inlet from the wall s/b	Air supply velocity u_0 (m/s)	Air supply temperature t_0 (°C)	Roughness of wall surface k (mm)
0.01	5	0.3	24	0 (smooth wall surface)
		1.0		
		1.5		

The flow field distribution of the attachment ventilation is shown in Fig. 2.14. For different u_0 , the jet's centerline velocity decreases with the flow path's increase. When u_0 gradually increases from 0.3 to 1.5 m/s, the centerline velocity gradually increases, and the effective attachment distance along the vertical wall is extended accordingly.

2. The influence of the distance between the air supply inlet and the vertical wall

Experimental results have shown that the distance between the air supply inlet and the adjacent vertical wall (s), the installation height (h), has a crucial influence on the centerline velocity of the air supply jet (Li 1993).

Table 2.2 shows the test conditions for the variation of s . The 2D-PIV velocity field test results are shown in Fig. 2.15. As s increases from 50 to 100 mm (i.e., $s/b = 5-10$), the vortex region formed between the jet inlet and the attached vertical wall (see the upper left corner in Fig. 2.15) gradually expanded downwards, hence the location of the attachment point accordingly moved downward. It can be clearly seen that when s/b exceeds a certain threshold value (i.e., $s/b = 5-8$), the jet attachment phenomenon disappears and finally turns to the ceiling air supply mode (mixing ventilation).

In practical ventilation engineering applications, in some cases, there may be a gap between the slot inlet and the attached wall. What will happen to the attached jet? The airflow visualization presents air movement patterns. After leaving the slot inlet for a certain distance, the discharge jet gradually tends to attach to the adjacent wall surface (or column surface) due to the Coanda effect, forming the deflected attachment, see Fig. 2.11. The effect of air inlet location (the distance from the slot inlet to the attached wall) on room air movement is significant. This section analyzes the features of the deflected attached jets ($S/b > 0$). Here, S is the distance in the direction normal to the vertical wall from a slot's inner edge or surface adjacent to the wall.

In the jet mainstream section, both the deflected and the complete attachment jet have the same cross-sectional velocity distribution and similar velocity profiles. However, in the initial region, the significant difference between deflected and fully attached jets exists for $0 < S/b \leq S_{\max}$, where S_{\max} is the maximum attachment distance (see initial region in Fig. 2.16b). The location of the attachment point on the attached wall surface will be altered for different distances S . Particularly, as the

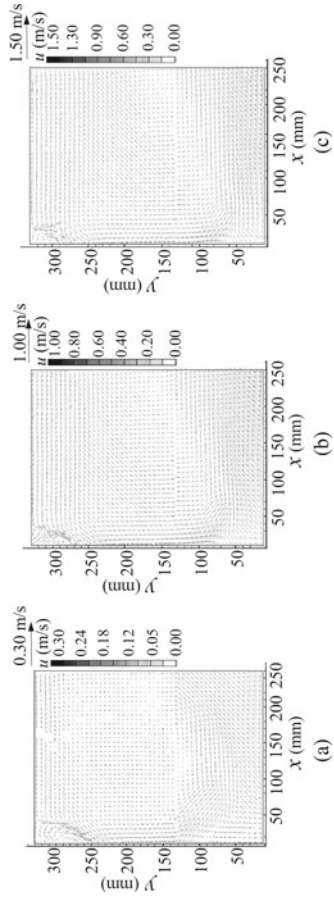


Fig. 2.14 Velocity field vector of attachment ventilation with different u_0 ($s/b = 5$, $k = 0$, $t_0 = 24$ °C). **a** $u_0 = 0.3$ m/s, **b** $u_0 = 1.0$ m/s, **c** $u_0 = 1.5$ m/s

Table 2.2 Test conditions for different s

Slot inlet width b (m)	Relative distance of slot inlet from the wall s/b	Air supply velocity u_0 (m/s)	Air supply temperature t_0 (°C)	Roughness of wall surface k (mm)	Slot inlet width b (m)
0.01	5	0.5	24	24	0
	8				
	10				

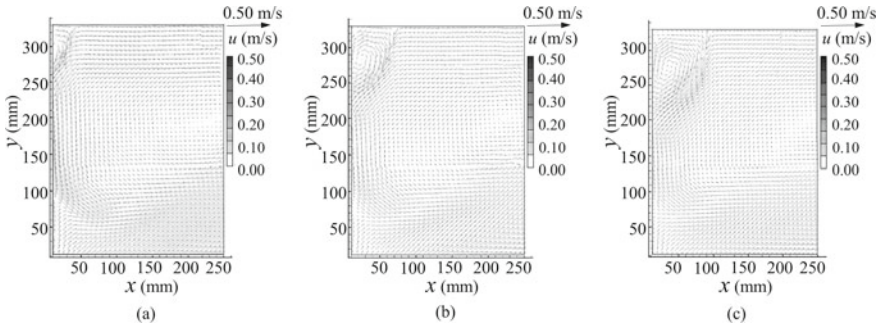


Fig. 2.15 Velocity field vector of attachment ventilation with different s ($u_0 = 0.5$ m/s, $k = 0$, $t_0 = 24$ °C). **a** $s/b = 5$, **b** $s/b = 8$, **c** $s/b = 10$

distance S gradually increases, the airflow in the upper corner shows a larger vortex and further extended entrainment range. When $S/b > S_{max}$, the Coanda effect is no longer valid, and the air jet fails to stick to the wall surface, which finally turns out to become the traditional mixing ventilation. According to the experimental results, for ordinary office rooms, the S_{max}/b is in the range of 4.5–6.5. For attachment ventilation design, the critical value of $S_{max}/b = 4.5$ is recommended. In addition, a larger air supply velocity enables the jet to better withstand the adverse pressure gradient, resulting in the attachment point moving upstream (see top-left region, Fig. 2.14).

2.3 Column Attachment Ventilation Airflow Pattern

1. Analysis of CAV

The rectangular column attachment ventilation (RCAV) mode belongs to a kind of attachment ventilation (Liu 2016; Liu et al. 2017; Yin et al. 2015; Li et al. 2012a, b; Yin et al. 2016a, b, c), where the air movement along the column is similar to VWAV, but the flow field is not exactly the same because of the column’s arris effect. Figure 2.17 gives a schematic diagram of the air distribution of RCAV. After the air supply jet is discharged from the ambulatory-shaped slot inlet installed on the upper part of the rectangular column, it creates a column

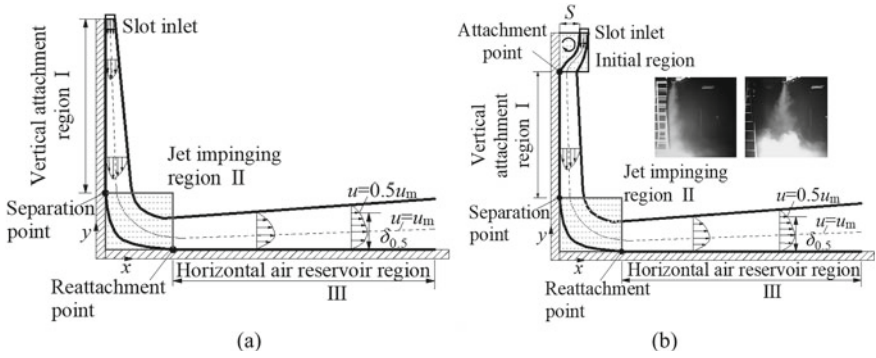


Fig. 2.16 Schematic diagram of wall-attached jets. **a** Complete attached jet ($S/b = 0$), **b** deflected attached jet ($S/b > 0$)

attachment ventilation similar to VWAV. When the air supply jet moves downwards along the column approaching the ground, then the jet separates from the rectangular column surface and turns to a horizontal airflow (see Fig. 2.17). Different from VWAV, due to the arris effect of the column, while entering the occupied zone, the air supply jets from two adjacent surfaces of the rectangular column can result in the airflow intersection and superposition, further consuming the fluid momentum. As a result, the airflow velocity in the horizontal air reservoir region formed by CAV decays faster than that of WAV (Yin et al. 2016c).

CAV is particularly suitable for places with existing columns, such as subway stations, airport terminals, exhibition centers, shopping malls, supermarkets, etc. Making full use of various columns in those buildings can realize the CAV mode (Yin et al. 2016a, b, c).

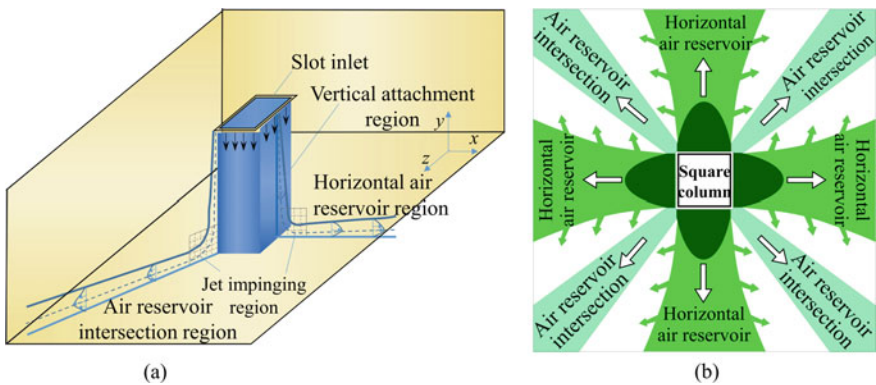


Fig. 2.17 Air movements of RCAV. **a** Principle of RCAV, **b** air distribution in horizontal air reservoir region

Four regions can be distinguished for a indoor air movement of RCAV (see Fig. 2.17).

Region I, vertical attachment region

The air supply jet is discharged from a slot inlet with “I”, “L”, or “ \square ” shapes, and then attached to the column surface and delivered to the control zone. The centerline velocity of jet flow is kept equal to u_0 , nearly 10 times s/b . The inlet velocity distribution is one of the major factors in determining the airflow pattern.

The supply air jet vortex motion, affected by the velocity difference between the internal and external fluids, induces a secondary velocity field in the ambient fluid, which draws the non-turbulent ambient fluid into the jet flow. As the vertical jet moves downstream along the column, it is observed from the airflow visualization that local and temporary ejections of low-momentum fluid from the wall outward, inrush movements towards the wall accompanied by sweep movements almost parallel to the column, and alternating with the generation locally of unstable instantaneous velocity-distributions, resulting in turbulence fluctuations, see Fig. 2.20. However, statistically speaking, both in time and in space, there is still a similarity of the time-averaged velocity distributions. Consequently, the centerline and the cross-section velocity can be expressed.

Region II, jet impinging region

When the momentum of the vertical jet flow is not sufficient to overcome the inverse pressure gradient, the jet flow will separate from the column surface and turn into the horizontal flow after impinging on the floor. There exists a sharp change in the turbulence intensity of the jet flow at a horizontal distance of 0.5–1.0 m away from the column surface, and more information can be found in Sect. 2.2.

Region III, horizontal air reservoir region

After impinging the floor, the jet is converted to horizontal flow; it spreads along the floor and carries out more heat exchange in the occupied zone. The air volume and jet thickness increase continuously with the airflow moving forward. This region is the main target zone for the indoor airflow control of RCAV.

Region IV, air reservoir intersection region

As shown in Fig. 2.17, the arris effect of the rectangular column is significant in this intersection region. The momentum of the main flow could be partially depleted by the superimposed mixing of two adjacent flows at the corner or intersection region. Compared to the VWAV, the airflow velocity in this region of RCAV decays more rapidly.

The difference between circular column attachment ventilation (CCAV) and RCAV mainly lies in the curvature effect. For the air supply from the top annular slot, there is a similarity between circular column attachment ventilation (CCAV) and RCAV in the vertical attachment region.

However, in horizontal air reservoir region, the airflow pattern of the jet is slightly different from that of RCAV, showing a 360° radially expanding airflow along the

circumference over the floor (Li et al. 2010; Li et al. 2012a, b; Sun 2017). Figure 2.18 illustrates a diagram of the air distribution of CCAV mode.

The flow patterns of CCAV can also be divided into the vertical attachment region I, jet impinging region II and horizontal air reservoir region III, as shown in Fig. 2.18 (Sun 2017). Among them, region I, and II are consistent with the RCAV. It is noted that in horizontal air reservoir region III, due to the cylindrical geometric symmetric characteristics of the column, the flow rate and thickness of the jet are increased with the jet radial throw; meanwhile, the centerline velocity is decreased more rapidly.

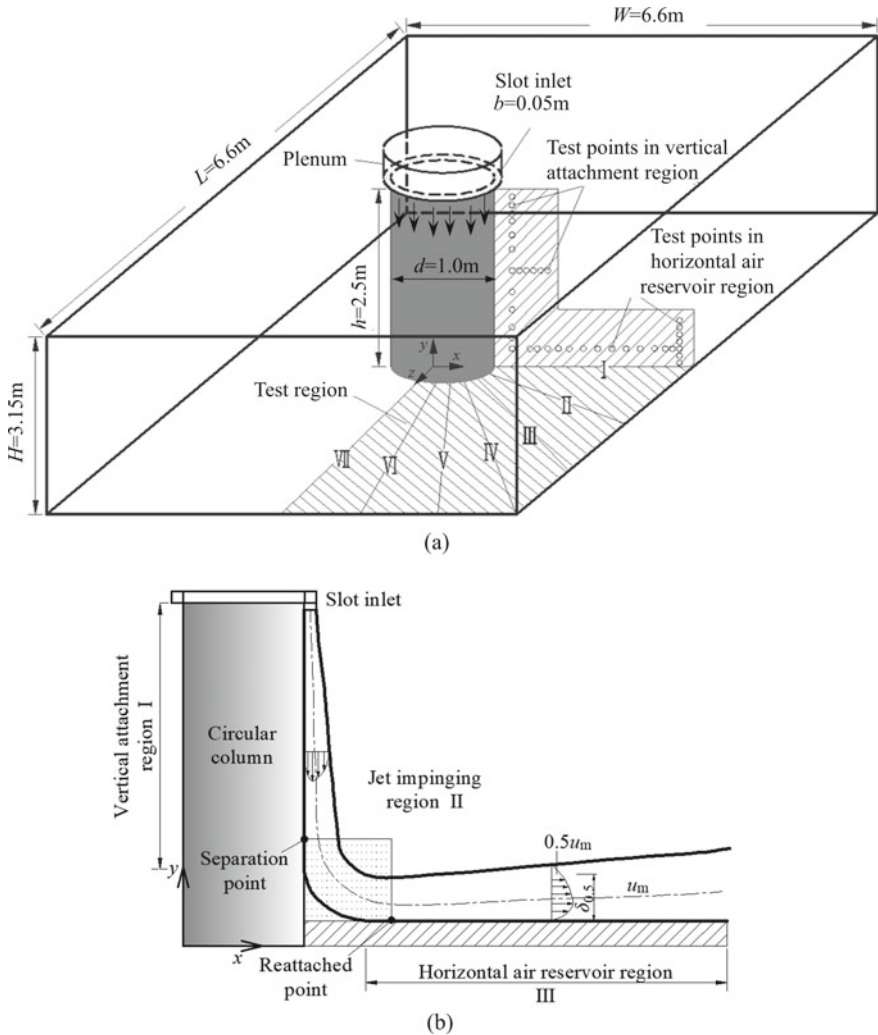


Fig. 2.18 Principle of CCAV. **a** Configuration of the test chamber, **b** schematic representation of column attached-jet

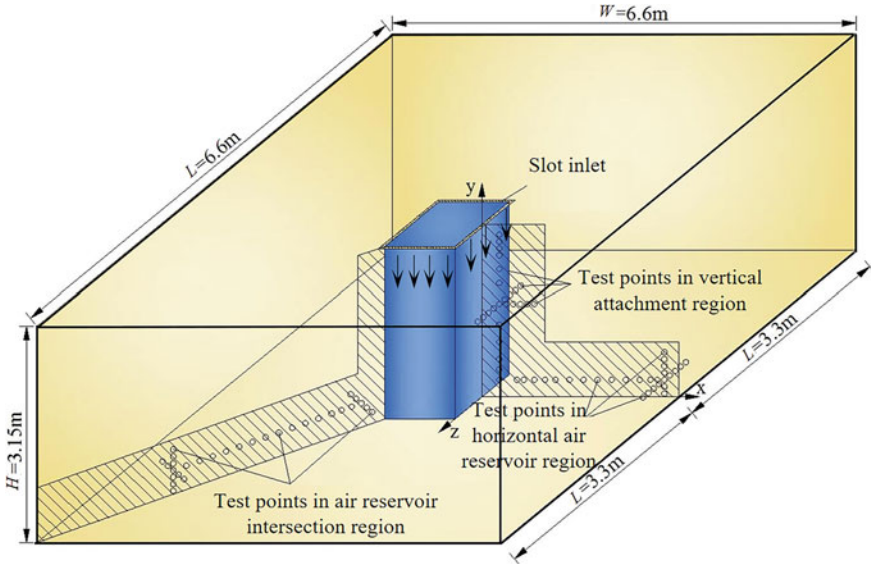


Fig. 2.19 Flow field visualization test of RCAV

2. Airflow pattern of RCAV

The full-size visualization test of RCAV is shown in Fig. 2.19. The test room dimensions are 6.6 m × 6.6 m × 3.15 m with a rectangular column of 1.0 m × 1.0 m × 2.5 m (length × width × height). The slot inlet of 0.05 m in width is attached to the column surface, and the installment height of the slot is 2.5 m from the floor. The air supply temperature is identical to the room temperature.

The smoke tracing visualization can be used for a better understanding of the flow process of RCAV qualitatively. The visualization results are shown in Fig. 2.20, and the corresponding airflow patterns are presented in Fig. 2.21. The visualization results demonstrate that an air reservoir flow field similar to displacement ventilation is created in the room RCAV.

It can be seen from the vertical attachment region in Fig. 2.20 that when increasing the air velocity from 1.0 to 2.0 m/s, the thickness in the jet extension δ_m becomes thinner, indicating less mixing of the jet with the surrounding air. The three visualized airflow patterns at the floor level show that, after the jet impinges the floor, the airflow diverges at the column’s plinth, almost creating a symmetrically radial flow pattern in the horizontal air-reservoir region.

3. Airflow pattern of CCAV

Similar with the principle of CCAV, the visualization test rigs are shown in Fig. 2.18. A comprehensive series of tests are conducted in a 6.6 m × 6.6 m × 3.15 m chamber. The circular column with a diameter of 1.0 m is set in the center of the room. The air is supplied through a column’s annular slot located 2.5 m above the floor, which is 0.05 m in width. In the vertical attachment region,

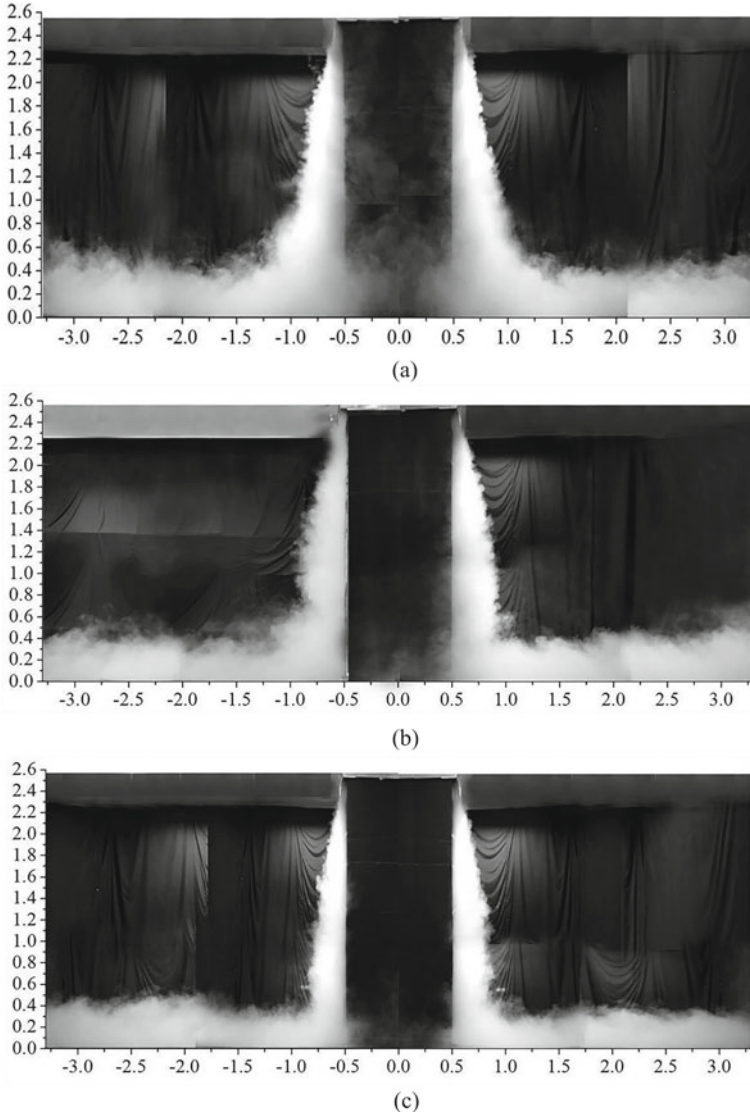


Fig. 2.20 Visualization of airflow patterns of RCAV with different u_0 . **a** $u_0 = 1.0$ m/s, **b** $u_0 = 1.5$ m/s, **c** $u_0 = 2$ m/s

the CCAV airflow patterns are similar to that of RCAV, as shown in Figs. 2.22 and 2.23. As u_0 increases from 1 to 2 m/s, the thickness of the air reservoir region decreases progressively, whereas the horizontal jet throw further extends accordingly.

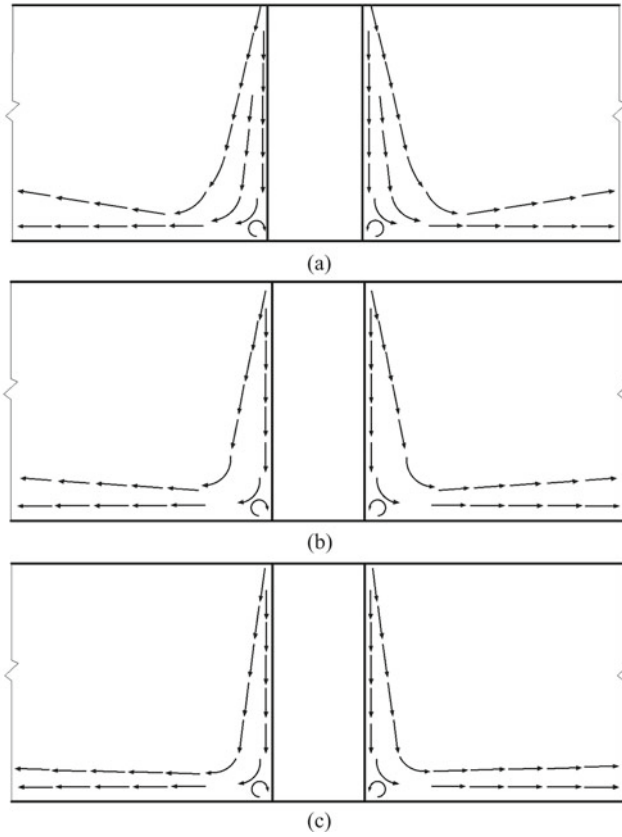


Fig. 2.21 Airflow patterns of RCAV with different Re numbers. **a** $Re = 3320$, **b** $Re = 4980$, **c** $Re = 6640$

2.4 Comparison of the Attachment, Mixing and Displacement Ventilation

As described in Sect. 1.1, the essence of air distribution is to control indoor air temperature, velocity, humidity, and pollutant concentration, etc. Scientific design of air distribution can create an indoor environment with low energy consumption and high indoor air quality (Awbi 2003, 2008; Bauman 2003; Li 2000; Ma 1997; Yin and Li 2013). A comparison of the characteristics of different ventilation modes is shown in Table 2.3. It can be seen that attachment ventilation, a new type of air distribution, combines the advantages of mixing ventilation and displacement ventilation. It not only has the advantage of mixing ventilation mode without occupying space (Etheridge and Sandberg 1996), but also has the advantages of displacement ventilation mode with good indoor air quality and high temperature efficiency.

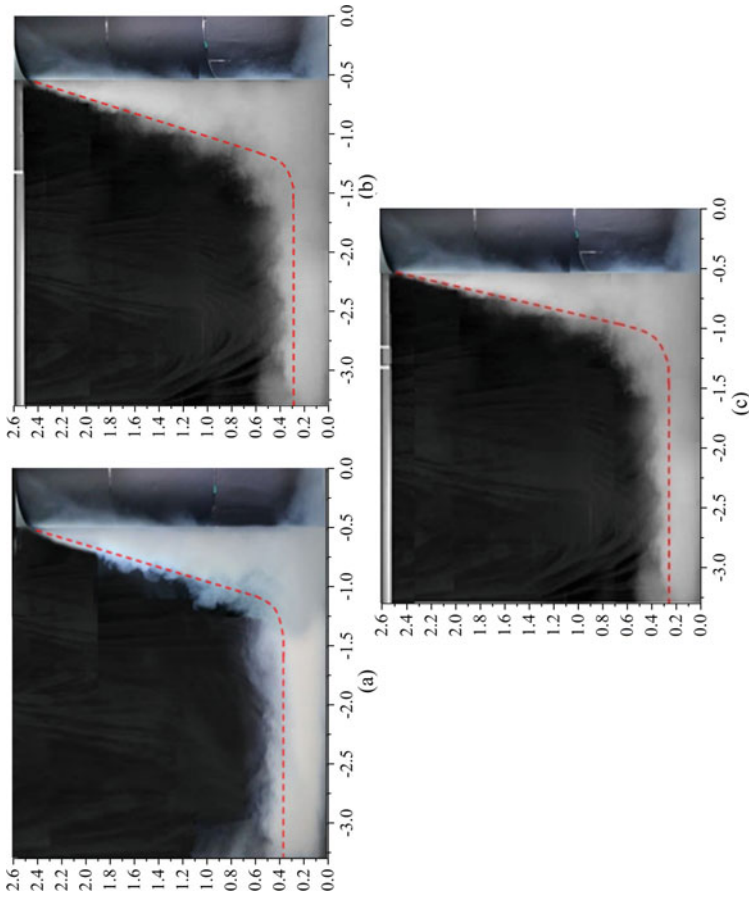


Fig. 2.22 Visualization of airflow patterns of CCAV with different u_0 . **a** $u_0 = 1.0$ m/s, **b** $u_0 = 1.5$ m/s, **c** $u_0 = 2.0$ m/s

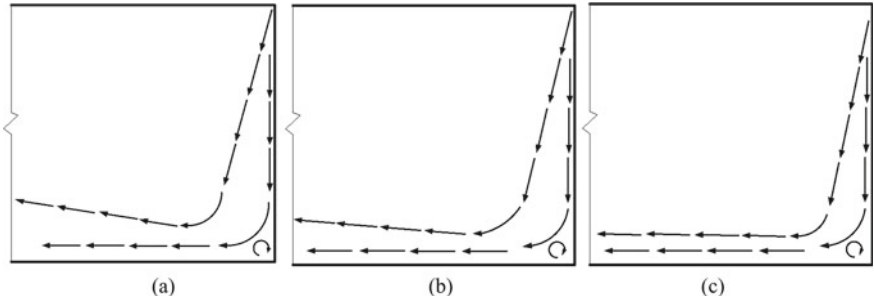
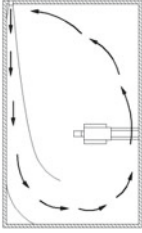
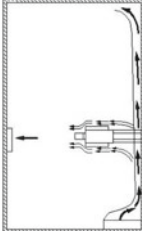
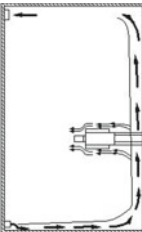
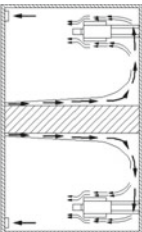


Fig. 2.23 Airflow patterns of CCAV with different Re numbers. **a** $Re = 3320$, **b** $Re = 4980$, **c** $Re = 6640$

Table 2.3 Comparison of air distributions of VWAV, mixing ventilation, and displacement ventilation

Ventilation mode		Mixing ventilation	Displacement ventilation	Vertical wall attachment ventilation (VWAV)	Column attachment ventilation (CAV)
Schematic diagram					
					
Objectives and control zone		<ul style="list-style-type: none"> Eliminate whole room heat load Uniform temperature and humidity in the whole room 	<ul style="list-style-type: none"> Eliminate part of the room heat load, i.e., eliminate the heat load of the occupied zone (control zone) Temperature gradients exist at room height 		
Airflow characteristic	Air movement mechanism	<ul style="list-style-type: none"> Inertial force dominates Mechanical forces are opposite to thermal buoyancy Thermal buoyancy exerts an inhibiting effect on airflow 	<ul style="list-style-type: none"> Thermally buoyant force dominates Mechanical forces are in the same direction as thermal buoyancy The buoyancy force contributes to the airflow movement 	<ul style="list-style-type: none"> Inertial and thermally buoyant forces jointly dominate the flow Mechanical forces are in the same direction as thermal buoyancy Buoyancy force contributes to the airflow movement 	
Airflow feature		<ul style="list-style-type: none"> Strong airflow mixing 	<ul style="list-style-type: none"> Airflow momentum diffusion, thermal plume induction 		
Air supply parameters		<ul style="list-style-type: none"> Large temperature difference, high supply air velocity 	<ul style="list-style-type: none"> Small temperature difference, low supply air velocity 	<ul style="list-style-type: none"> Medium temperature difference and supply air velocity 	
Space occupancy		Utilize upper space	Occupation of the lower space or occupied zone	Upper space	Upper column space

(continued)

Table 2.3 (continued)

Ventilation mode	Mixing ventilation	Displacement ventilation	Vertical wall attachment ventilation (VWAV)	Column attachment ventilation (CAV)
Engineering cost	Medium	High	Medium	Medium
Ventilation effectiveness	Uniform temperature and concentration distribution	Temperature and concentration stratification		
Air quality	Close to return and exhaust air region	Close to air supply region		
Ventilation efficiency	≈ 50%	50–100%		
Temperature efficiency	≈ 1.0	1.2–1.5 (office building)	1.1–1.4 (office building), relate to room height, higher for large spaces	1.1–1.3 (office building), relate to space height, higher for large spaces

References

- ASHRAE (2008) ASHRAE handbook: system and equipment. In: Chapter 19, Room air distribution equipment. American Society of Heating, Refrigeration and Air-Conditioning Engineers, Inc., Atlanta
- ASHRAE (2017) ASHRAE handbook: fundamentals. American Society of Heating, Refrigeration and Air-Conditioning Engineers Inc., Atlanta
- Awbi HB (2003) Ventilation of buildings, 2nd edn. Taylor and Francis, USA
- Awbi HB (2008) Ventilation systems: design and performance. Taylor and Francis, USA
- Awbi HB (2011) Ventilation of buildings (trans: Li XT, Zhao B, Shao XL, Cai H). China Machine Press, Beijing (in Chinese)
- Bauman FS (2003) Underfloor air distribution (UFAD) design guide. American Society of Heating Refrigerating and Air-Conditioning Engineers Inc., Atlanta
- Cao XD, Liu JJ, Jiang N, Chen QY (2014) Particle image velocimetry measurement of indoor airflow field: a review of the technologies and applications. *Energy Build* 69:367–380
- Cho YG, Awbi HB, Karimipناه T (2008) Theoretical and experimental investigation of wall confluent jets ventilation and comparison with wall displacement ventilation. *Build Environ* 43(6):1091–1100
- Coanda H (1936) Device for deflecting a stream of elastic fluid projected into another elastic fluid. US Patent 2052869 A 1 Sept 1936
- Coanda H (1938) Propelling device. US Patent 2108652 A 15 Feb. 1938
- Coanda H (1964) Lifting apparatus. US Patent 3261162 A 20 May 1964
- Cui WF (2010) A new type of ventilation-2DPDV studies of air curtain ventilation in a slot-ventilated outlet: volumetric heat source condition. Xi'an University of Architecture and Technology, Xi'an (in Chinese)
- Etheridge DW, Sandberg M (1996) Building ventilation: theory and measurement. Wiley, Chichester
- Fan JC (2002) Modern flow visualization. National Defense Industry Press, Beijing (in Chinese)
- Hosni MH, Jones BW (2002) Development of a particle image velocimetry for measuring air velocity in large-scale room airflow applications/discussion. *ASHRAE Trans* 108:1164
- JGJ/T 177-2009 (2009) Standard for energy efficiency test of public buildings. China Architecture & Building Press, Beijing (in Chinese)
- Li XP (1993) An analysis on the characteristics of the limited sticking jet. *J Xi'an Inst Metall Cons Eng* 25(4):413–416 (in Chinese)
- Li QM (2000) Displacement ventilation: principles, design and applications. *J HV&AC* 30(5):41–46 (in Chinese)
- Li AG (2019) Extended Coanda effect and attachment ventilation. *Indoor Built Environ* 28(4):437–442
- Li AG, Tao PF, Zhao YJ, Yin HG (2010) Air supply method with circular column surface attached-jet. Chinese patent ZL201010548896.9 (in Chinese)
- Li AG, Yin HG, Wang GD (2012a) Experimental investigation of air distribution in the occupied zones of an air curtain ventilated enclosure. *Int J Vent* 11(2):171–182
- Li AG, Yin HG, Zhang WD (2012b) A novel air distribution method—principles of air curtain ventilation. *Int J Vent* 10(4):383–390
- Liu ZY (2016) Study on air distribution characteristics and design procedures of square column-attached air curtain ventilation. Xi'an University of Architecture and Technology, Xi'an (in Chinese)
- Liu CP, Li AG, Yang CQ, Zhang WR (2017) Simulating air distribution and occupants' thermal comfort of three ventilation schemes for subway platform. *Build Environ* 125:15–25
- Ma RM (1997) Displacement ventilation effectiveness and evaluation of the micro thermal environment. *J HV & AC* 27(4):1–6+65 (in Chinese)
- Panitz T, Wasan DT (1972) Flow attachment to solid surfaces: the Coanda effect. *AIChE J* 18(1):51–57

- Qin EW, Liu W, Bao X, Li AG (2009) Discussion of two important problem of PIV experiment. *Build Energy Environ* 28(2):83–85 (in Chinese)
- Qiu SH (2008) A new type of ventilation-2DPIV study of downward directed vertical wall jets formed by slot inlet. Xi'an University of Architecture and Technology, Xi'an (in Chinese)
- Qiu SH, Li AG (2010) Downward directed vertical wall jet formed by slot inlet: impact of air velocity. *J HV & AC* 40(1):101–105 (in Chinese)
- Song GJ (2005) Visualization of the airflow patterns of 12 typical diffusers and experimental investigation on the turbulence coefficient. Xi'an University of Architecture and Technology, Xi'an (in Chinese)
- Sun YX (2017) Study on air distribution characteristics and ventilation effect of circular column attached ventilation. Xi'an University of Architecture and Technology, Xi'an (in Chinese)
- Wang GD (2009) A new type of ventilation-2DPIV studies of air curtain ventilation in a slot-ventilated enclosure: non-isothermal condition. Xi'an University of Architecture and Technology, Xi'an (in Chinese)
- Wang X (2010) Experimental study on airflow performance of floor based air distribution using novel mushroom diffuser by 2D PIV: isothermal conditions. Xi'an University of Architecture and Technology, Xi'an (in Chinese)
- Wen JX (1982) Distribution mechanism of airflow attached to planar surface. Xi'an University of Architecture and Technology (former Xi'an Institute of Metallurgy and Construction Engineering) (in Chinese)
- Yin HG (2012) Study on design procedures of air distribution by air curtain ventilation with a linear slot diffuser. Xi'an University of Architecture and Technology, Xi'an (in Chinese)
- Yin HG, Li AG (2012) Airflow characteristics by air curtain jets in full-scale room. *J Cent South Univ* 19(3):675–681
- Yin HG, Li AG (2013) Mixing ventilation VS, displacement ventilation-principles and design cases of vertical wall attachment ventilation. In: *Proceedings of 2013 National conference on ventilation technology*, 2013:16–22 (in Chinese)
- Yin HG, Li AG (2014) Design principle of air curtain ventilation. *Lecture notes in electrical engineering*, vol 262, pp 307–315
- Yin HG, Li AG (2015) Study on airflow characteristics of attached air curtain ventilation model. *J Xi'an Uni Arch Tech (Natural Science Edition)* 47(6):879–884 (in Chinese)
- Yin HG, Li AG, Liu ZY, Sun YX, Wang RL (2015) An “□shaped” plenum with constant cross section for square column attached air supply. Chinese patent ZL201510260706.6 (in Chinese)
- Yin HG, Chen T, Liu ZY et al (2016a) Air distribution characteristics of air curtain ventilation mode based on square column attached. *J HV & AC* 46(9):128–134+140 (in Chinese)
- Yin HG, Li AG, Liu ZY, Sun YX, Chen T (2016b) Analysis on influence factors of square column attached displacement ventilation mode. *J Xi'an Univ Arch Tech (Natural Science Edition)* 48(4):593–600 (in Chinese)
- Yin HG, Li AG, Liu ZY, Sun YX, Chen T (2016c) Experimental study on airflow characteristics of a square column attached ventilation mode. *Build Environ* 109:112–120
- Zhang WD (2005) Prediction and visualizing validation of downward directed vertical wall jets and air lake phenomenon. Xi'an University of Architecture and Technology, Xi'an (in Chinese)
- Zhao Y (2004) Study on the tracer particle properties of PIV test. Dalian University of Technology, Dalian (in Chinese)
- Zheng K, Han WS, Pan YG, Zhang J, Jin CH, Guo R, Zhao G, Guo SY, Wang WL (2019) Analysis on key energy-saving technologies of HVAC of a government office building in Beijing. *Constr Sci Technol* 379:75–80 (in Chinese)
- Zhu JY (1984) Study on nonisothermal horizontal plane confined attached jet. Xi'an University of Architecture and Technology (former Xi'an Institute of Metallurgy and Construction Engineering), Xi'an (in Chinese)

Open Access This chapter is licensed under the terms of the Creative Commons Attribution-NonCommercial-NoDerivatives 4.0 International License (<http://creativecommons.org/licenses/by-nc-nd/4.0/>), which permits any noncommercial use, sharing, distribution and reproduction in any medium or format, as long as you give appropriate credit to the original author(s) and the source, provide a link to the Creative Commons license and indicate if you modified the licensed material. You do not have permission under this license to share adapted material derived from this chapter or parts of it.

The images or other third party material in this chapter are included in the chapter’s Creative Commons license, unless indicated otherwise in a credit line to the material. If material is not included in the chapter’s Creative Commons license and your intended use is not permitted by statutory regulation or exceeds the permitted use, you will need to obtain permission directly from the copyright holder.



Chapter 3

Isothermal Attachment Ventilation Mechanisms



Abstract This chapter expounds on the airflow mechanisms of isothermal vertical wall attachment ventilation, rectangular column attachment ventilation, and circular column attachment ventilation. This chapter presents the characteristic parameters of the isothermal attachment ventilation and the airflow characteristics in the vertical attachment, jet impingement, and horizontal air reservoir regions. The parameter correlations of velocity distribution (maximum velocity or centerline velocity decay and cross-sectional velocity profiles), jet thickness, cross-sectional airflow rate of attachment ventilation, etc., have been established.

Keywords Isothermal jet · Attachment ventilation · Attached ventilation · Attached jet · Velocity distribution · Centerline velocity · Jet thickness

This chapter elaborates on the air distribution mechanisms of isothermal attachment turbulent jets, mainly including the air velocity distributions in the vertical attachment and horizontal air reservoir regions. There is a significant difference between the motion characteristics of the wall-attached jet and the free jet. This chapter presents the characteristic parameters of the isothermal wall-attached jet and the airflow movement feature in the vertical attachment, jet impinging, and horizontal air reservoir regions for VWAV and CAV. The interaction between the wall-attached jet and the vertical wall and floor is determined (region I–III). The parameter correlations of velocity distribution (maximum velocity or centerline velocity decay and cross-sectional velocity profiles), jet thickness, cross-sectional airflow rate of attachment ventilation, etc., have been established.

In solving the problems of design ventilation, it is necessary to take the following factors into account:

1. airflow rate supplied to and extracted from the room;
2. characteristic parameters of the incoming air and the treatment of the air, including heating, cooling, etc.;
3. layout and geometric parameters of the inlets and outlets;
4. geometric shape and size of the room;
5. location and capacity of sources that change air composition and state, in particular, sources of heat and pollution;

6. air currents created by these sources, human behaviors, and industrial production activities.

3.1 Wall-Attached Jet Parameters

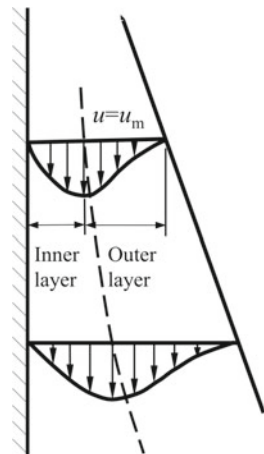
When the air supply opening is located in the upper part of the vertical wall (or its vicinity, not exceeding the maximum attachment distance), the supply air jet forms a confined wall-attached jet caused by the Coanda effect and extended Coanda effect (Li 2019). Generally, this wall jet can be divided into a boundary layer closing to the wall surface and a free-shear flow away from the wall.

The turbulent wall-attached jet can also be divided into inner and outer layers. In the inner layer (near the wall surface), the flow field is similar to that of the flat plate or plane boundary layer; in the outer region, the flow field is similar to that of a free jet. The inner layer and outer region are bounded by $u = u_m$, as shown in Fig. 3.1.

From the perspective of ventilation and air-conditioning, the whole room can be divided into a jet-dominating zone (including an inner layer and outer layer) and an air-diffusing zone ($u \leq 0.3$ m/s for environment allowable velocity, which can be extended to 0.8 m/s for the temporary staying zone, such as subway stations, industrial plants, occupied zone of hydropower plants). ASHRAE 55-2017 specifies that the maximum acceptable velocity is 0.8 m/s when the operating temperature is 26 °C.

Concerning the wall-attached jet parameters, the fundamental characteristic parameters are assumed as follows. For wall-attached jets entering a steady-state environment, the fundamental parameters are centerline velocity u_m (i.e., maximum velocity), jet thickness, the width of slot b , and velocity at the slot inlet u_0 . The inner layer thickness δ_m is the normal distance between the wall and the point where the attached jet velocity is equal to u_m ; characteristic thickness $\delta_{0.5}$ is the normal distance

Fig. 3.1 Inner and outer layers of a turbulent wall-attached jet (bounded by $u = u_m$)



between the wall and the point where the attached jet velocity is equal to $0.5u_m$ in the outer layer of the wall-attached jet; total thickness δ_0 is the normal distance between the wall and the outer layer boundary, as illustrated in Fig. 3.2a. These parameters of the wall-attached jet can be normalized as dimensionless characteristic parameters. The wall-attached jet features are mainly related to the supply air velocity (u_0), supply and exhaust air temperature (t_0, t_e), indoor load (Q), and supply and exhaust opening positions (h, S), etc. For a jet attached to a smooth wall, the dimensionless characteristic parameters mainly include:

- Centerline velocity of the wall-attached jet $\frac{u_m}{u_0}$;
- Velocity profile of the jet main section $\frac{u}{u_m}$;
- Characteristic thickness of the jet $\delta_{0.5}$;
- Cross-section airflow rate along the jet direction $\frac{Q}{Q_0}$;
- The dimensionless excess temperature of the jet centerline $\frac{t_m - t_n}{t_0 - t_n}$ (for a nonisothermal jet).

In addition, for deflected wall-attached jets, the position of the attachment point (see Fig. 3.2a) should also be taken into account.

The parameters characterizing the jet's fundamental features are jet centerline velocity $u_m(x, y)$, section thickness $\delta(x, y)$, and cross-sectional velocity $u(x, y)$.

For the sake of discussion, the origin of the coordinate system used in this book is located at the intersection of the jet-attached wall surface and the floor, as shown in Fig. 3.2a.

It should be noted that for flow-field analysis of the wall-attached jet, two Cartesian coordinate systems are adopted, namely x - y and x - y^* . The z -axis is perpendicular

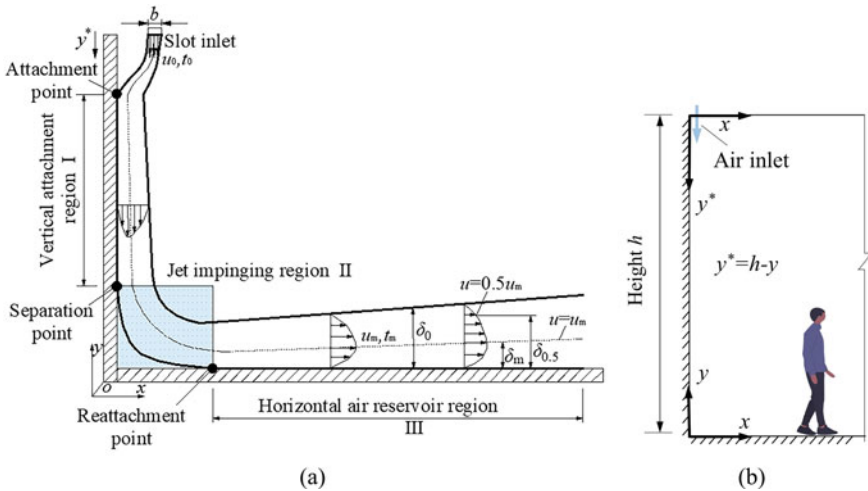


Fig. 3.2 **a** Theoretical analysis of the wall-attached jet, **b** coordinate system used for wall-attached jets analysis. *Note* The centerline velocity in this book is defined as the maximum velocity of the jet

Table 3.1 Dimensionless characteristic parameters of the wall-attached jet

Parameters	Vertical attachment region	Horizontal air reservoir region
(1) Centerline velocity of the wall-attached jet	$\frac{u_m}{u_0} = f\left(\frac{y^*}{b}\right)$	$\frac{u_m}{u_0} = f\left(\frac{x}{b}\right)$
(2) Velocity profile of the main section	$\frac{u}{u_m} = f\left(\frac{x}{\delta_{0.5}}\right)$	$\frac{u}{u_m} = f\left(\frac{y}{\delta_{0.5}}\right)$
(3) Characteristic thickness	$\delta_{0.5} = f(y^*)$	$\delta_{0.5} = f(x)$
(4) Section flow rate	$\frac{Q}{Q_0} = f\left(\frac{y^*}{b}\right)$	$\frac{Q}{Q_0} = f\left(\frac{x}{b}\right)$
(5) Excess temperature of jet centerline (for a nonisothermal jet)	$\frac{t_m - t_n}{t_0 - t_n} = f\left(\frac{y^*}{b}\right)$	$\frac{t_m - t_n}{t_0 - t_n} = f\left(\frac{x}{b}\right)$
(6) Interval between the slot and the jet-attached wall surface	$S/b, s/b$	—

to the coordinate plane, as shown in Fig. 3.2b. The difference between these two coordinate systems lies in that y and y^* are in opposite directions, i.e., $y^* = h - y$, where h is the slot's installation height. In this book, the x - y^* coordinate system is mainly used in the theoretical analysis of the wall-attached jet (see Fig. 3.2b).

The characteristic parameters of the wall-attached jet are shown in Table 3.1.

3.2 Jet Impinging Region

The jet impinging region is defined as the region where the jet velocity and pressure, etc., are affected by impinging within the scope of HVAC. This region is usually 0.5–1.0 m away from the vertical wall and horizontal floor, respectively (see Fig. 3.2a). In the jet impinging region, it can be found that the adverse pressure gradient increases as the jet approaches the floor. As illustrated in Fig. 3.3a, it can be observed there are the vortical structures in the jet impinging region, where a large-scale vortex is generated, and secondary vortexes at the corner are induced. The direction of vortex recirculation is approximately opposite to that of mainstream movement. The separation point and reattachment point could characterize the location of the large-scale vortex in the jet impinging region. The separation point ($\partial u_y / \partial x|_{x=0} = 0$) is located at the end of the vertical attachment region, which is also treated as the start of the jet impinging region. Likewise, the reattachment point ($\partial u_x / \partial y|_{y=0} = 0$) lies at the end of the jet impinging region and the start of the horizontal air reservoir region. The separation point and reattachment point are expounded in more detail as follows.

For an isothermal wall-attached jet, it can be expressed in a dimensionless form based on experimental and numerical results. In the range of $0.5 \leq (h/b)^{2/3} Re^{-1/3} \leq 1.2$ (see Fig. 3.3c), the separation point can be determined by the Eq. (3.1a)

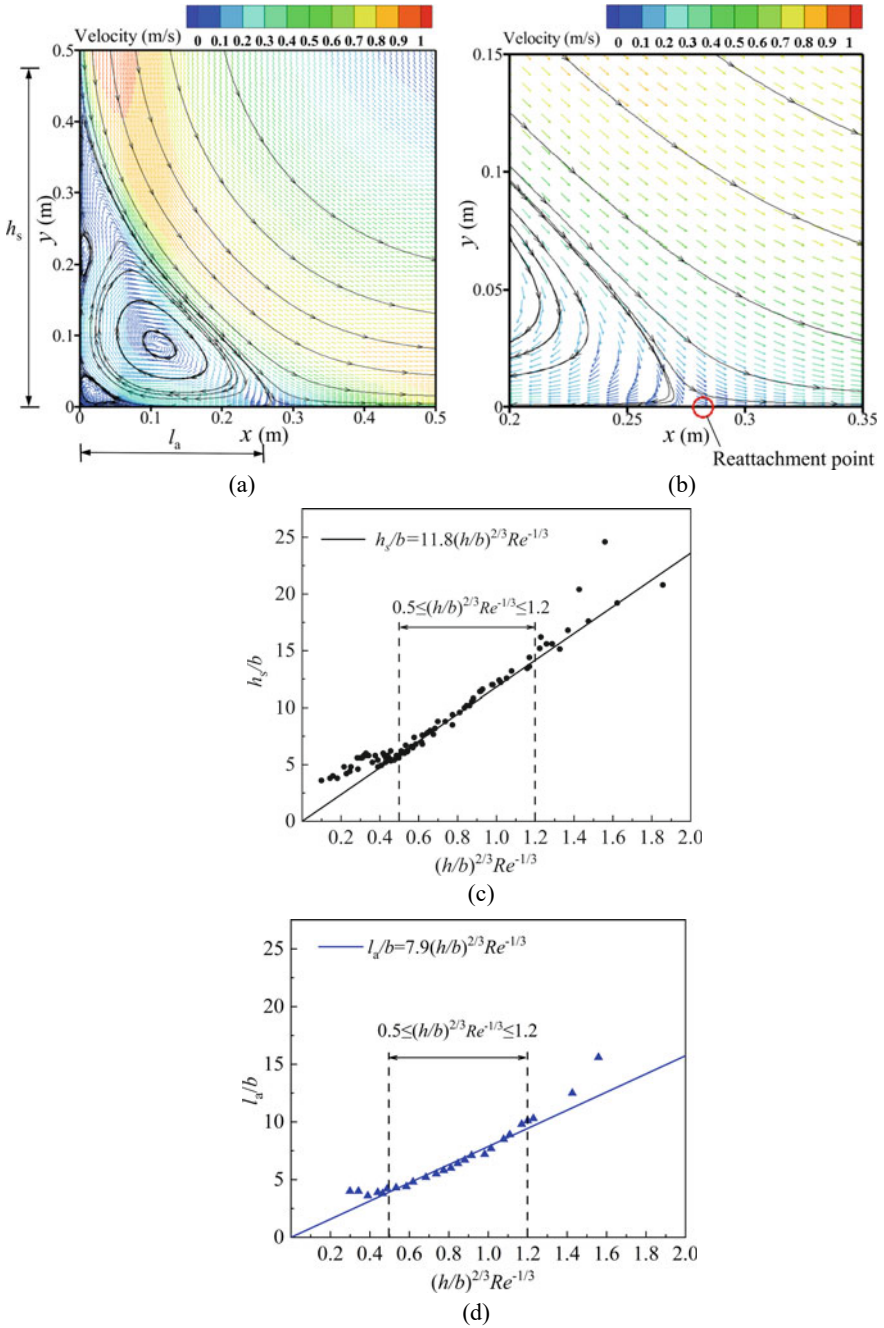


Fig. 3.3 **a** Velocity-vector field with streamlines in the jet impinging region, **b** reattachment point location, **c** separation point h_s/b as a function of $(h/b)^{2/3} Re^{-1/3}$, **d** reattachment point l_a/b as a function of $(h/b)^{2/3} Re^{-1/3}$

$$\frac{h_s}{b} = 11.8 \left(\frac{h}{b} \right)^{\frac{2}{3}} Re^{-\frac{1}{3}} \quad (3.1a)$$

where h_s is the normal distance between the floor and the separation point, see Fig. 3.3a. It could be regarded as a function of jet discharge velocity u_0 , opening height h , opening width b , air density ρ , and air kinetic viscosity μ , etc.

Similarly, the reattachment point (see Fig. 3.3b, d) is presented by Eq. (3.1b)

$$\frac{l_a}{b} = 7.9 \left(\frac{h}{b} \right)^{\frac{2}{3}} Re^{-\frac{1}{3}} \quad (3.1b)$$

where l_a is the normal distance between the attached wall and the reattachment point, see Fig. 3.3a, b. In the range discussed above, it can be concluded that $\frac{l_a}{h_s} \approx 0.67$.

Figure 3.4 shows the velocity contours corresponding to different air supply velocities in the jet impinging and horizontal air reservoir regions. With the enhancement of u_0 , from 1.0 m/s to 2.0 m/s, it can be observed that the clockwise vortex in the corner diminishes. For the increment of velocity, the jet impinging on the floor is further enhanced, and the air around the corner gets more squeezed, which narrowly the circumfluence vortex correspondingly. The comparison results of the corner regions of Fig. 3.4a, c, d, f further support this argument. These findings provide insights into the role of the wall-attached jet impinging region.

It can be obtained from Fig. 3.4g, that the jet centerline velocity profile shows similarity in the horizontal region (region III), except the jet impinging region (region II). In region II, the air “initial velocity” (maximum centerline velocity in region II) grows with the supply air velocity increasing (dynamic pressure regaining). For a given velocity $u_0 = 1.5$ m/s, 3.0 m/s and 5.0 m/s, the “initial velocity” reaches 0.6 m/s, 1.3 m/s and 2.25 m/s, respectively. It is also observed that the centerline velocity in the jet impinging region is approximately symmetrical along the bisector of 90° .

The angle between two adjacent walls also influences the flow field. When the jet opening is located in a room’s intersection area (concave corner), the jet’s boundary changes significantly with the air velocity. Figure 3.5 demonstrates the forms of the boundary layer at the angle area of 60° between two walls (dihedral angle). If expressed in polar coordinates, it can be seen that there is an interface point between laminar flow and turbulent flow at the angular bisector to the apex of the angle (Sun 1992). The wall-attached jet flow is related to the angle’s sharpness degree and Reynolds number Re (i.e., velocity) of supply air. When Re increases, the laminar flow area in the angle area will become smaller (Sun 1992). The sharper angle is in response to the larger viscous sublayer.

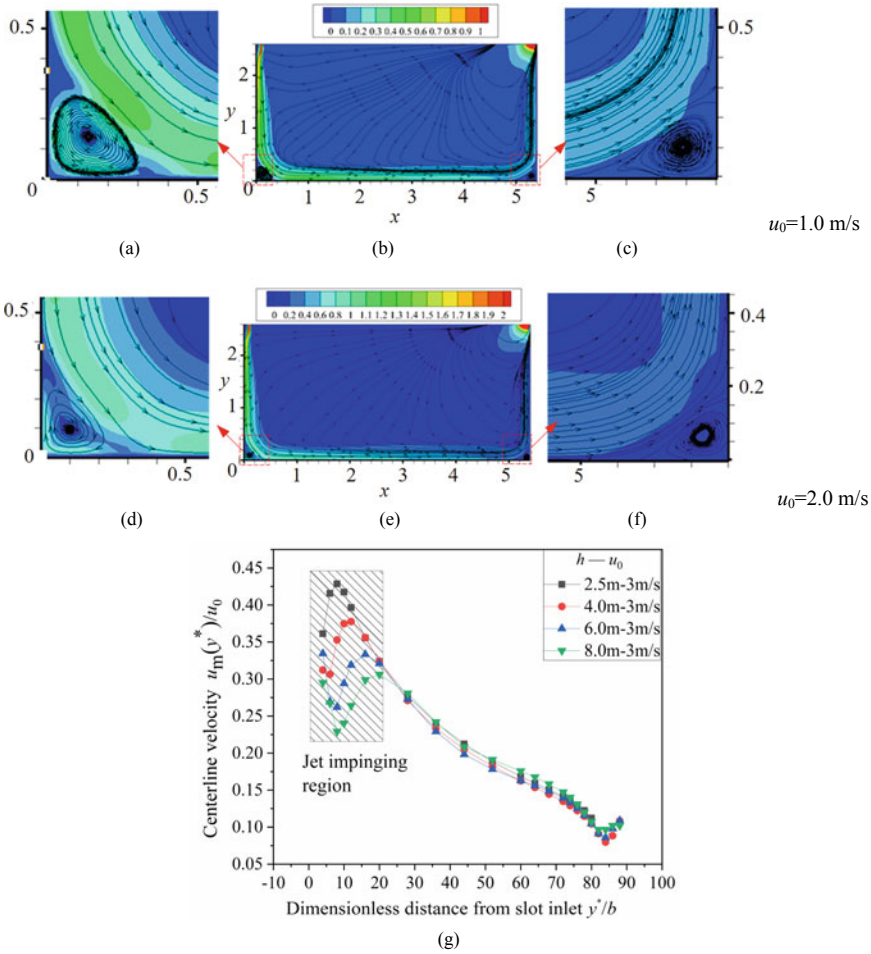


Fig. 3.4 Indoor air velocity distributions with different air supply velocities, **a–f** airflow patterns of the impinging region or corner, **g** dimensionless centerline velocity of the horizontal region as a function of distance x/b

3.3 Isothermal Vertical Wall Attachment Ventilation Parameter Correlations

The air movement of a ventilated room depends on the time-averaged flow and turbulence characteristics of the air jet and thermal plume. Air distribution in ventilated spaces only the steady-state flow situation is considered. To achieve a well-designed room air distribution, it is necessary to understand the mechanisms and prediction method of airflow. This section presents mathematical models and semi-empirical expressions for predicting wall-attached jet flow.

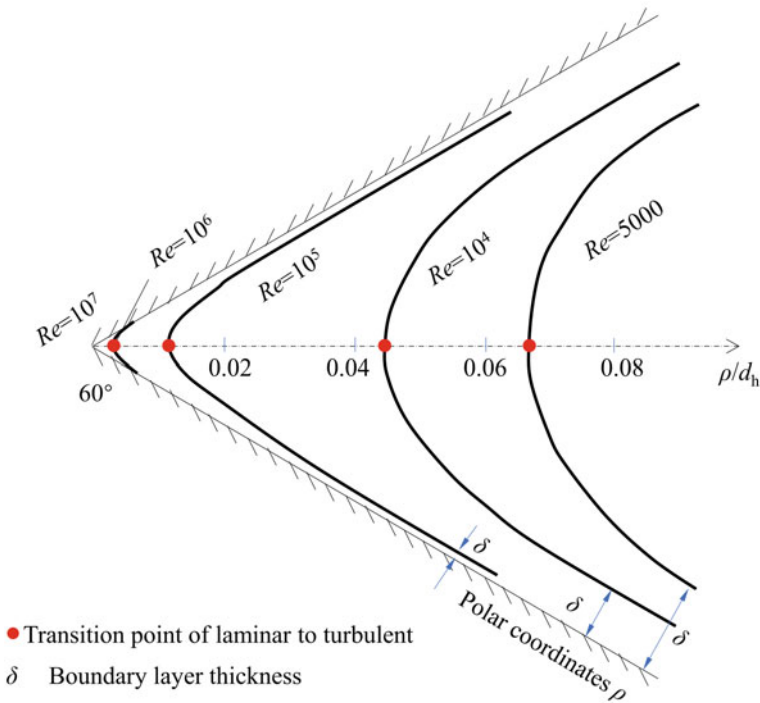


Fig. 3.5 Boundary layer of the concave corner (Sun 1992)

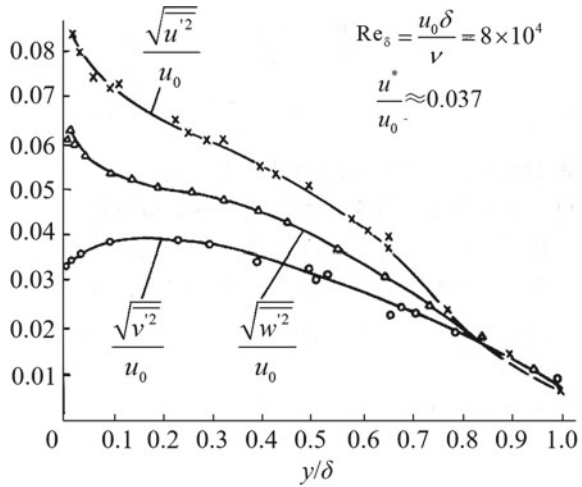
Generally, the velocity components of a turbulent wall-attached jet can be decomposed into a time-averaged u_m and fluctuating components u' , v' , w' . Eckert once investigated the fluctuating velocity components u' , v' , w' in the jet boundary layer of the smooth wall. Results indicate that the fluctuating velocities u' , v' , w' are about 4–8% of the time-averaged velocity u_m for the wall-attached jet boundary layer in the mainstream (see Fig. 3.6) (Eckert and Drake 1972). Hence, the time-averaged velocity distributions, in the vertical attachment region and the horizontal air reservoir region have proved to be satisfactory in reflecting the fundamental features of the attachment ventilation.

This section presents the time-averaged velocity distribution and corresponding expressions or correlations under isothermal conditions in detail.

3.3.1 Centerline Velocity in Vertical Attachment Region

So far, the theoretical calculation of the turbulent boundary layer of the incompressible flow has not developed enough to get rid of the semi-empirical theory. In this book, the author attempts to establish semi-empirical theoretical expressions of the

Fig. 3.6 Fluctuating velocity components in the boundary layer of a wall jet (Eckert and Drake 1972)



centerline velocity distributions of attachment ventilation. For the wall-attached jet, the following conclusions can be obtained from the visualization investigation in the previous chapters:

1. In the fully developed region, there is a similarity of the time-averaged velocity distributions (e.g., centerline velocity and cross-sectional velocity) of the wall-attached jet, which can be described by $f(\frac{u}{u_0}, \frac{y^*}{b}, \frac{x}{b}) = 0$ (see Fig. 3.2b).
2. For the centerline velocity of the two-dimensional wall-attached jet, the function can be simplified as $f(\frac{u_m}{u_0}, \frac{y^*}{b}) = 0$ and $f(\frac{u_m}{u_0}, \frac{x}{b}) = 0$ in the vertical attachment region and horizontal air reservoir region, respectively.

The centerline velocity’s semi-empirical expression has been derived theoretically and experimentally, using the hypothesis for free turbulent flow due to Prandtl (1942). The air movement in the wall-attached jet is a self-similar flow with a universal flow profile. That is to say, for different distances y^* , the velocity profiles derived is shown to be identical as long as the scale factors of velocity and width are appropriately selected.

The equations governing a turbulent wall-attached jet are considered here. On the boundary layer approximation, the pressure is uniform everywhere, and the eddy viscosity ϵ is introduced. The momentum and continuity equations are given by Eqs. (3.2a) and (3.2b), respectively

$$u \frac{\partial u}{\partial y^*} + v \frac{\partial u}{\partial x} = \frac{\partial}{\partial x} \left(\epsilon \frac{\partial u}{\partial x} \right) \tag{3.2a}$$

$$\frac{\partial u}{\partial y^*} + \frac{\partial v}{\partial x} = 0 \tag{3.2b}$$

The boundary conditions are

$$u = v = 0 \text{ at } x = 0;$$

$$u \rightarrow 0 \text{ as } x \rightarrow \infty (\text{ambient fluid velocity is } 0)$$

where

- y^* distance along the wall measured from the slot opening, m;
- x distance normal to the wall, m;
- u velocity component along the y^* direction, m/s;
- v velocity component along the x -direction, m/s;
- ϵ eddy viscosity.

Assumptions regarding the eddy viscosity ϵ are made according to Prandtl's hypothesis for free turbulent flow (Prandtl 1942). The eddy viscosity is constant across the breadth of the jet, and is proportional to the product of the maximum difference between time-averaged velocity and width of the layer

$$\epsilon = \rho k \delta (\bar{u}_{\max} - \bar{u}_{\min})$$

where

- ρ density, kg/m^3 ;
- k a universal constant;
- δ a typical measure of the boundary layer width, m;
- $\bar{u}_{\max} - \bar{u}_{\min}$ the maximum difference of the time-average velocity in the fluid micro-cluster, m/s. It is obtained from a lot of measured data of free turbulent jets by Prandtl.

Consider the possibility that there shall be a similarity solution of Eq. (3.2a) (Glauert 1956)

$$u \sim y^{*p}, \delta \sim y^{*q}, \epsilon \sim y^{*p+q}$$

$$\frac{\partial u}{\partial y^*} \sim p - 1, u \frac{\partial u}{\partial y^*} \sim 2p - 1$$

According to the boundary layer theory, x is the distance normal to the wall and thus has the same magnitude with δ , i.e., $x \sim \delta$, we obtain

$$\frac{\partial}{\partial x} \left(\epsilon \frac{\partial u}{\partial x} \right) \sim 2p - q$$

The two sides of Eq. (3.2a) should vary with y in the same manner, thus

$$2p - 1 = 2p - q, q = 1 \tag{3.3}$$

Introduce (external) momentum flux F below. Multiply Eq. (3.2a) by y^* and integrate with respect to x between the limits x and ∞ , we have

$$\int_x^\infty y^* u \frac{\partial u}{\partial y^*} dx + \int_x^\infty y^* v \frac{\partial u}{\partial y^*} dx = \int_x^\infty y^* \in \frac{\partial^2 u}{\partial x^2} dx \quad (3.4)$$

Considering $u \rightarrow 0$ as $x \rightarrow \infty$, Eq. (3.4) is simplified as

$$\frac{\partial}{\partial y^*} \int_x^\infty y^* u^2 dx - y^* v u + y^* \in \frac{\partial u}{\partial x} = 0 \quad (3.5)$$

Multiplying by $y^* u$, and integrating with respect to x between the limits 0 and ∞ , we then have

$$\begin{aligned} & \frac{\partial}{\partial y^*} \int_x^\infty y^* u \left\{ \int_x^\infty y^* u^2 dx \right\} dx - \int_x^\infty \frac{\partial(y^* u)}{\partial y^*} \left\{ \int_x^\infty y^* u^2 dx \right\} dx \\ & - \int_0^\infty y^{*2} v u^2 dx + \left[\frac{1}{2} \in y^{*2} u^2 \right]_0^\infty = 0 \end{aligned} \quad (3.6)$$

From the continuity equation, the second term of Eq. (3.6) is

$$- \left[y^* v \int_x^\infty y^* u^2 dx \right]_0^\infty + \int_0^\infty y^{*2} v u^2 dx$$

At $x = 0$, $u = v = 0$; at $x \rightarrow \infty$, $u \rightarrow 0$, so Eq. (3.6) reduces to

$$\frac{\partial}{\partial y^*} \int_0^\infty y^* u \left\{ \int_x^\infty y^* u^2 dx \right\} dx = 0$$

or

$$F = \int_0^\infty y^* u \left\{ \int_x^\infty y^* u^2 dx \right\} dx = \text{constant} \quad (3.7)$$

The physical significance of Eq. (3.7) is that the external momentum flux is conserved. In the case of a similarity solution, $x^2 \sim \delta^2 \sim y^{*2q}$, and $u \sim y^{*p}$, so Eq. (3.7) shows that

$$3p + 2q + 2 = 0 \quad (3.8)$$

Equations (3.3) and (3.8) now show that,

$$p = -\frac{4}{3}, q = 1 \quad (3.9)$$

Thus

$$u \sim (y^*)^{-\frac{4}{3}}, \delta \sim (y^*)^1$$

If

$$\frac{u}{u_m} = g\left(\frac{x}{\delta}\right) \quad (3.10)$$

Considering the dimensional consistency, we have

$$u_m \sim (y^*)^{-\frac{4}{3}}$$

Therefore, the centerline velocity u_m of the wall-attached jets is represented by

$$\frac{u_m(y^*)}{u_0} \sim \left(\frac{y^*}{b}\right)^{-\frac{4}{3}} \quad (3.11a)$$

or

$$\frac{u_0}{u_m(y^*)} \sim \left(\frac{y^*}{b}\right)^{\frac{4}{3}} \quad (3.11b)$$

Equation (3.11a, 3.11b) is derived based on Prandtl's hypothesis, i.e., the eddy viscosity is constant across the breadth of the jet, which is drawn from measured data of free turbulent jets. Therefore, it is understandable that there shall be some differences when the expression is used for the wall-attached jet. It can be assumed that the centerline velocity of the wall-attached jet in the vertical attachment region (main region) has a negative γ power function relation with y^* , which is expressed as Eq. (3.12)

$$\frac{u_0}{u_m(y^*)} \sim \left(\frac{y^*}{b}\right)^{\frac{4}{3}}, \quad \gamma > 0 \quad (3.12)$$

where γ is determined by experimental data, which indicates the momentum decay rate of the wall-attached jets.

Figure 3.7 shows the characteristic parameters and the centerline velocity decay in the vertical attachment region for vertical wall attachment ventilation. The parameters are shown in Fig. 3.7a, and Fig. 3.7b presents centerline velocity decay under different slot heights h , and air supply velocities u_0 in the vertical attachment region. The

centerline velocity decay shown in Fig. 3.7b agrees well with the above theoretical analysis.

Based on the theoretical analysis and experimental data of attachment ventilation, the semi-empirical correlations Eq. (3.13) of the centerline velocity decay in the vertical attachment region is proposed for engineering applications.

$$\frac{u_m(y^*)}{u_0} = \frac{1}{0.01\left(\frac{y^*}{b}\right)^{1.11} + 1} \quad (3.13)$$

It can be seen that the factors affecting the centerline velocity distribution are as follows: air supply velocity u_0 , vertical distance along the vertical wall measured from the slot opening y^* ($y^* = h - y$, reflecting the effect of room height h), characteristic dimension b of the slot, and exhaust outlet (the exhaust outlet is also called as the air inlet in ANSI/ASHRAE Standard 113 (2013) and ASHRAE Handbook: Fundamentals (2017)) forms, etc. As illustrated in Fig. 3.7, the centerline velocity decay shows similarity in the vertical attachment region with different air supply heights h and air supply velocities u_0 . In the range of $0 \leq y^*/b \leq 40$, the centerline velocity of the jet decays rapidly (a large curve slope). When the jet continues to move downward along the vertical wall, the centerline velocity declines slowly till it reaches the separation point, $\partial u_y / \partial x |_{x=0} = 0$, where the jet turns out to be separated from the vertical wall.

The free jet's centerline velocity decay is simultaneously shown in Fig. 3.7. It can be observed that the curve slope of the wall-attached jet is much less than that of the free jet. That is to say, the centerline velocity of the vertical wall-attached jet decays more slowly. For the same discharge velocity, it means that the wall-attached jet can reach a much further distance. For instance, at $y^*/b = 40$, the centerline velocity of the free jet is only approximately 20% of the wall-attached jet.

3.3.2 Centerline Velocity in Horizontal Air Reservoir Region

As mentioned above, when separating from the vertical wall, the wall-attached jet impinges on the floor, then expands in a radial pattern and moves along the floor, forming an air reservoir at the horizontal floor. The air reservoir is directly related to the conditioned environment of the occupied zone, so it is vital to establish the centerline velocity distributions in the horizontal air reservoir region. Figure 3.8 illustrates the dimensionless centerline velocity decay in the horizontal air reservoir region. Likewise, it can be drawn that the dimensionless centerline velocity demonstrates similarity. The decay rate of the centerline velocity is relatively lower in the horizontal air reservoir region than in the vertical attachment region.

According to the dimensional analysis, the centerline velocity u_m in the horizontal air reservoir region is primarily related to the air inlet types, the air supply velocity u_0 , the distance normal to the wall x , the characteristic dimension b of the inlet, and

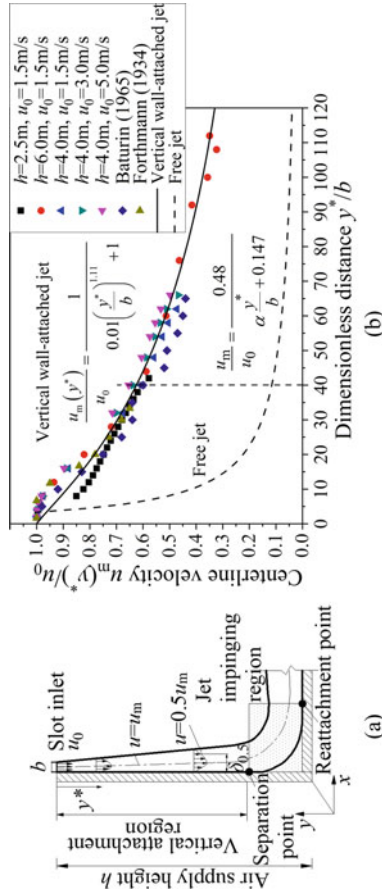


Fig. 3.7 Semi-empirical correlation of centerline velocity in the vertical attachment region and compared with a free jet. **a** Characteristic parameters, **b** centerline velocity distribution in the vertical attachment region

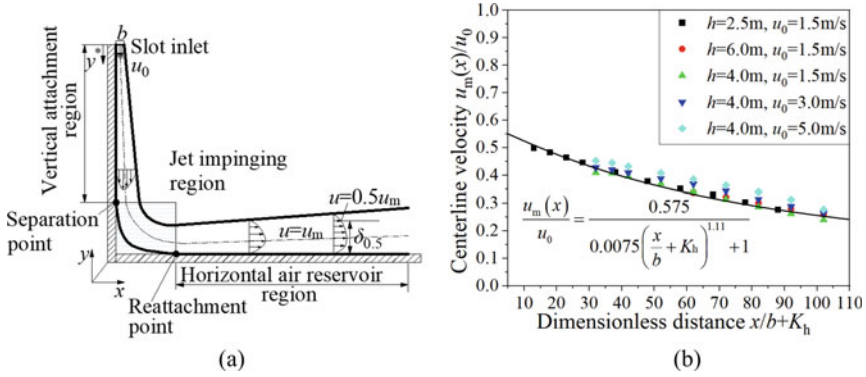


Fig. 3.8 Characteristic parameters and centerline velocity decay in the horizontal air reservoir region ($S/b = 0$). **a** Characteristic parameters, **b** centerline velocity decay in the horizontal air reservoir region

the air supply height h , which can be expressed as

$$f\left(\frac{u_m(x)}{u_0}, \frac{x}{b}, \frac{h}{b}\right) = 0 \tag{3.14}$$

Figure 3.8b represents plots of dimensionless centerline velocity $u_m(x)/u_0$ versus dimensionless distance $x/b + K_h$ in the horizontal air reservoir region. It can be observed that the dimensionless curve of centerline velocity decay is identical for different air supply heights h and air supply velocities u_0 . Although the centerline velocity is different for different positions of the horizontal air reservoir region, centerline velocity similarity still exists in this region.

Similarly, in the horizontal air reservoir region (see Fig. 3.8b), the centerline velocity of the wall-attached jet has negative α and β power function relations with the distance from the vertical wall x and the slot installation height h , respectively.

According to the experimental results, we have

$$\begin{aligned} \frac{u_m(x)}{u_0} &\sim \left(\frac{x}{b}\right)^{-\alpha}, \quad \frac{u_m(x)}{u_0} \sim \left(\frac{h}{b}\right)^{-\beta} \\ \frac{u_m(x)}{u_0} &= \frac{0.575}{0.0075\left(\frac{x}{b} + K_h\right)^{1.11} + 1} \end{aligned} \tag{3.15}$$

where

h air supply height, m,

K_h correction factor, $K_h = \frac{1}{2} \frac{h-2.5}{b}$. A reference height of 2.5 m for ordinary offices is adopted according to the Chinese standard JGJ67-2006 “Code for Design of Office Buildings”.

3.3.3 Cross-Sectional Velocity Profile

The flow of the wall-attached jet's inner layer can be simplified according to the boundary layer theory. The governing equations are

$$\frac{\partial u}{\partial y^*} + \frac{\partial v}{\partial x} = 0 \quad (3.16)$$

$$u \frac{\partial u}{\partial y^*} + v \frac{\partial u}{\partial x} = -\frac{1}{\rho} \frac{\partial p}{\partial y^*} + v \frac{\partial^2 u}{\partial x^2} + \frac{1}{\rho} \frac{\partial \tau_t}{\partial x} \quad (3.17)$$

where τ_t denotes turbulent shear stress.

The self-similarity exists for the wall-attached jet on the smooth wall surface. u_m is adopted as characteristic velocity, and the distance between the wall and the point where $u = 0.5u_m$ in the outer layer of the wall-attached jet is regarded as characteristic thickness $\delta_{0.5}$ (for the sake of discussion, it may be expressed as δ). The cross-sectional velocity profile can be expressed as Eq. (3.18) (Zhang 2011)

$$\frac{u}{u_m} = f\left(\frac{x}{\delta}\right) = f(\eta) \quad (3.18)$$

If we write $\frac{\tau_t}{\rho u_m^2} = g(\eta)$, and let $u_m \propto y^{*p}$, $\delta \propto y^{*q}$, the values of the exponents p, q can be obtained from the governing equations and similarity relation.

According to $u = u_m f(\eta)$ in Eq. (3.18), we obtain

$$\begin{aligned} \frac{\partial u}{\partial y^*} &= \frac{\partial}{\partial y^*}(u_m f) = u_m \frac{df}{d\eta} \frac{d\eta}{d\delta} \frac{d\delta}{dy^*} \\ &+ f \frac{du_m}{dy^*} = -u_m f' \frac{x}{\delta^2} \delta' + f u_m' \end{aligned} \quad (3.19)$$

$$u \frac{\partial u}{\partial y^*} = u_m u_m' f^2 - \frac{u_m^2 \delta'}{\delta} \eta f f' \quad (3.20)$$

According to Eq. (3.16), we have

$$\begin{aligned} v &= \int_0^x \frac{\partial v}{\partial x} dx = - \int_0^x \frac{\partial u}{\partial y} dx = \int_0^x \left(\frac{u_m \delta'}{\delta} \eta f' - u_m' f \right) dx \\ &= u_m \delta' \int_0^x \eta f' d\eta - u_m' \delta \int_0^x f dx \end{aligned} \quad (3.21)$$

$$\frac{\partial u}{\partial x} = \frac{\partial}{\partial x}(u_m f) = u_m f' \frac{\partial \eta}{\partial x} = \frac{u_m}{\delta} f' \quad (3.22)$$

$$v \frac{\partial u}{\partial x} = \frac{u_m^2 \delta'}{\delta} f' \int_0^\eta \eta f' d\eta - u_m u_m' f' \int_0^\eta f d\eta \quad (3.23)$$

$$\frac{1}{\rho} \frac{\partial \tau_t}{\partial x} = \frac{1}{\rho} \frac{\partial}{\partial x} (\rho u_m^2 g) = \frac{u_m^2}{\delta} \frac{\partial g}{\partial \eta} = \frac{u_m^2}{\delta} g' \quad (3.24)$$

where $\delta' = \frac{d\delta}{dy}$, $u_m' = \frac{du_m}{dy}$, $f' = \frac{df}{d\eta}$, $g' = \frac{dg}{d\eta}$

In most cases, the Reynolds number $\frac{u_m \delta}{\nu}$ is large, thus the viscosity term in Eq. (3.17) can be ignored. Considering $\frac{\partial p}{\partial y^*} = 0$, Eqs. (3.20), (3.23) and (3.24) now show that

$$g' = \frac{\delta u_m'}{u_m} \left(f^2 - f' \int_0^\eta f d\eta \right) - \delta' \left(\eta f f' - f' \int_0^\eta \eta f' d\eta \right) \quad (3.25)$$

Since g' is a function of η only, the right side of Eq. (3.25) should also be a function of η , then $\frac{\delta u_m'}{u_m}$ and δ' should be independent of y , thus

$$\frac{\delta u_m'}{u_m} \sim y^0, \delta' \sim y^0$$

Thus $q = 1$, i.e., $\delta \sim y$.

According to the conservation of momentum, we have

$$\frac{d}{dy} \int_0^\infty \rho u^2 dx = 0 \quad (3.26)$$

Equations (3.18) and (3.26) show that

$$\frac{d}{dy} \rho u_m^2 \int_0^\infty f^2 d\eta = 0 \quad (3.27)$$

and hence $u_m^2 \delta \sim y^0$, $2p + q = 0$.

Since $q = 1$, then we have $p = -0.5$. Thus, $\delta_{0.5} \sim y^*$, $\frac{u_m}{u_0} \sim 1/\sqrt{y^*/b}$.

For the turbulent wall-attached jet, the cross-sectional velocity profile obtained from experiments agrees well with the results from Glauert (1956), Verhoff (1963), Schwarz and Cosart (1961), etc., see Eq. (3.28).

As shown in Fig. 3.9, there are similarities in the cross-sectional velocity profile. In the near-wall region, the velocity increases sharply from the wall and reaches the maximum value at $\eta = 0.25$. However, for $0.25 < \eta \leq 2.0$, the cross-sectional velocity decreases gradually until the jet peripheral velocity tends to be consistent

with the ambient air velocity. The cross-sectional velocity profile can be expressed by Eq. (3.28)

$$\frac{u}{u_m} = -0.83 + 2.03 \times e^{-0.42\eta} \quad (0.25 \leq \eta \leq 2) \quad R^2 = 0.995 \quad (3.28)$$

where η is the dimensionless distance; $\eta = \frac{x}{\delta_{0.5}}$ for the vertical attachment region, $\eta = \frac{y}{\delta_{0.5}}$ for the horizontal air reservoir region.

For the wall-attached jet, according to experimental data, it is found that the cross-sectional velocity profile can also be described by semi-empirical equation Eq. (3.29) obtained by Verhoff (1963).

$$\frac{u}{u_m} = 1.48\eta^{1/7}[1 - \text{erf}(0.68\eta)] \quad (3.29)$$

This expression is in good agreement with the measured data, as shown in Fig. 3.9.

When $\frac{u}{u_m} = 1$, the path or trajectory of the centerline velocity (maximum velocity) can be calculated. In the vertical attachment region, the x coordinate of the wall-attached jet centerline position can be expressed by Eq. (3.30).

$$x = 0.247\delta_{0.5} = 0.247a(y^* + c) \quad (3.30)$$

This expression shows agreement with the above analysis result that $\delta_{0.5} \sim y^*$.

Similarly, in the horizontal air reservoir region, the y coordinate of the centerline position can be expressed by Eq. (3.31).

$$y^* = 0.247\delta_{0.5} = 0.247a(x + c) \quad (3.31)$$

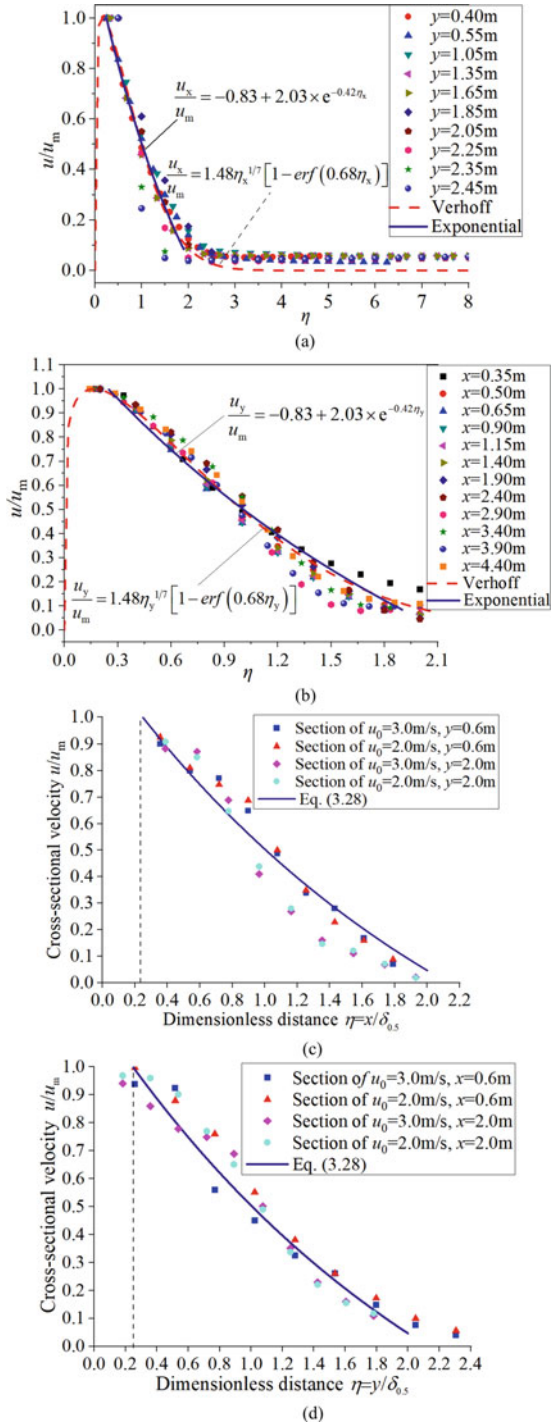
Thus, the inner layer thickness of the wall-attached jet is determined, $\delta_m = 0.247\delta_{0.5}$.

where a and c are constants obtained from experiments data, and the values of a and c of wall-attached jets will be provided in Sect. 3.3.4.

3.3.4 Characteristic Thickness of a Wall-Attached Jet

The free side of the wall-attached jet continuously entrains ambient air, accordingly the jet thickness increases gradually (see Fig. 2.10). It can be found in Fig. 3.10a, although the parameters are different, S/b and h varied, the characteristic thickness $\delta_{0.5}$ of the wall-attached jet increases in a linear approximation. It suggests that the slot opening be better installed close to the vertical wall. Comparing $S/b = 0$ (wholly attached to the wall) and $S/b = 1.5$, it is found that the former's jet thickness is correspondingly smaller under the same supply air velocity, which means there is lower entrainment and momentum decay of the wall-attached jet for the same jet

Fig. 3.9 Cross-sectional velocity profile of vertical wall-attached jet. **a** Vertical attachment region, **b** horizontal air reservoir region, **c** vertical attachment region (field test data), **d** horizontal air reservoir region (field test data)



throw. For different slot installation heights (i.e., $h = 2.5$ m, 4.0 m, and 6.0 m), the characteristic jet thickness also presents self-similarity in the attachment region.

In the theoretical analysis of wall-attached jets and attachment ventilation, the characteristic thickness $\delta_{0.5}$ in the vertical attachment region is related to air inlet types (shape factor C), and the vertical distance along the vertical wall from the slot opening y^* . The relationship can be written as

$$f(\delta_{0.5}, y^*, C) = 0 \tag{3.32}$$

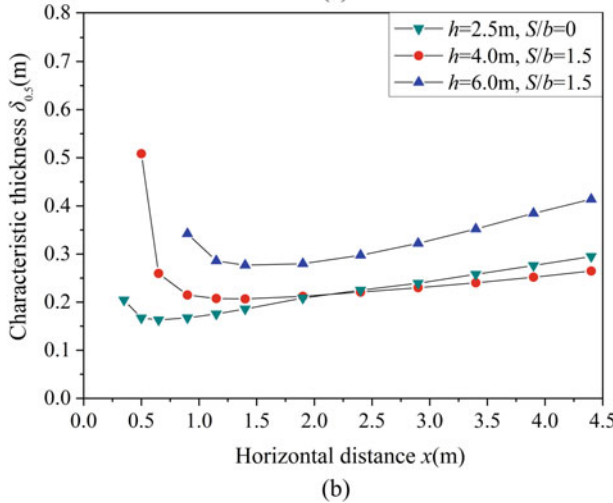
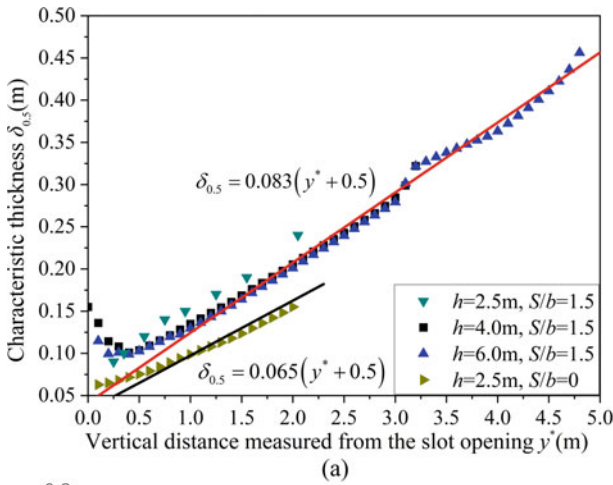


Fig. 3.10 Characteristic thickness of wall-attached jets with different deflection distances. **a** Vertical attachment region, **b** horizontal air reservoir region

The centerline velocity profiles are illustrated in Fig. 3.10a. The characteristic thickness $\delta_{0.5}$ in the vertical attachment region is directly proportional to the distance y^* , which shows agreement with the previous theoretical analysis, and given by Eq. (3.33)

$$\delta_{0.5} = a(y^* + c) \quad (3.33)$$

where a and c are constants obtained from experiments data, which depend on S . $a = 0.065$, $c = 0.5$ for $S/b = 0$; $a = 0.083$, $c = 0.5$ for $S/b = 1.5$. Note that this expression only applies to the vertical attachment region.

As shown in Fig. 3.10b, there is an adverse pressure gradient in the jet impinging region where the jet changes its original airflow direction. After impinging, the jet is reattached to the floor and remains moving forward, and the jet's thickness gradually expands. The jet thickness variation in the horizontal air reservoir region is consistent with that of the vertical attachment region and is affected by air supply velocity, deflection distance, slot height, etc.

3.3.5 Cross-Sectional Flow Rate

Cross-sectional flow rate can be obtained by integrating jets velocity u

$$Q = \int_0^{\infty} u dx \quad (3.34)$$

where velocity u is characterized by Eq. (3.29)

$$\frac{u}{u_m} = 1.48\eta^{1/7}[1 - \text{erf}(0.68\eta)] \quad (3.29)$$

where $\eta = \frac{x}{\delta_{0.5}}$.

Equations (3.29) and (3.34) show that

$$Q = u_m \delta_{0.5} \int_0^{\infty} f d\eta = u_m \delta_{0.5} \int_0^{\infty} 1.48\eta^{1/7}[1 - \text{erf}(0.68\eta)] d\eta = 1.093 u_m \delta_{0.5} \quad (3.35)$$

where centerline velocity is

$$\frac{u_m(y^*)}{u_0} = \frac{1}{0.01\left(\frac{y^*}{b}\right)^{1.11} + 1} \quad (3.13)$$

The jet characteristic thickness $\delta_{0.5}$ is expressed by Eq. (3.33)

$$\delta_{0.5} = 0.065(y^* + 0.5) \quad (3.33)$$

Equations (3.13), (3.33), and (3.35) now show that

$$Q = u_0 \frac{0.071(y^* + 0.5)}{0.01\left(\frac{y^*}{b}\right)^{1.11} + 1} \quad (3.36)$$

The wall-attached jet discharge flow rate is

$$Q_0 = u_0 b \quad (3.37)$$

Then we obtain

$$\frac{Q}{Q_0} = \frac{0.071(y^* + 0.5)}{b\left(0.01\left(\frac{y^*}{b}\right)^{1.11} + 1\right)} \quad (3.38)$$

where

Q cross-sectional flow rate of a wall-attached jet in the vertical attachment region, m^3/s ;

Q_0 discharge flow rate of a wall-attached jet, i.e., air supply rate, m^3/s .

3.4 Airflow of Column Attachment Ventilation

3.4.1 Rectangular Column-Attached Jet

To some extent, the flow mechanism of RCAV is similar to that of VWAV. The velocity distributions and the corresponding vertical wall attachment ventilation expressions have been described in previous sections.

The airflow characteristics of a rectangular column-attached jet (including square columns and polygonal columns) are essentially similar to the vertical wall-attached jet. The common point is that supply air is delivered from the slot opening and downwards along the wall based on the Coanda effect. Likewise, when the jet reaches the floor, affected by the adverse pressure gradient, the jet separates from the vertical wall. After impinging, it attaches to the floor and spreads over the horizontal surface (extended Coanda effect, ECE). The difference between the two attachment ventilation modes is that the rectangular column aris causes the confluence and superposition of supply air from two adjacent surfaces after impinging on the floor. The

jet momentum is further consumed. Under the same supply air velocity, the airflow velocity of the rectangular column-attached jet is lower than that of the vertical wall-attached jet in the horizontal air reservoir region.

1. Centerline velocity in the vertical attachment region

In a physical sense, if the column width $l \gg b$, the rectangular column can be regarded as an infinite vertical flat, and the jet features shall be the same as the vertical wall-attached jet. In a mathematical sense, the rectangular column-attached jet can also be simplified to a two-dimensional jet due to its symmetry. The governing equations are identical to those of the vertical wall-attached jets. However, in engineering applications, the length-to-width ratio of the column cross-section is usually slight, generally $l/b \leq 5$, and the column arris influence the jet flow. That means the vertical wall-attached jet flow and rectangular column-attached jet flow are not precisely the same. On the other hand, according to the cyclotomic method, there is a similarity between the rectangular column-attached jet and a circular column-attached jet.

Figure 3.11a shows the vertical attachment region's characteristic parameters. Figure 3.11b demonstrates the dimensionless centerline velocity decay under different slot heights ($h = 2.5$ m, 4.0 m, 6.0 m, and 8.0 m). In the vertical attachment region, it can be observed that the centerline velocity exhibits a declining trend with increasing y^*/b . Likewise, the centerline velocity distribution in the vertical attachment region can be obtained and expressed as Eq. (3.39)

$$\frac{u_m(y^*)}{u_0} = \frac{0.83}{0.01\left(\frac{y^*}{b}\right)^{1.11} + 1} \quad (3.39)$$

2. Centerline velocity in the horizontal air reservoir region

In the horizontal air reservoir region, the characteristic parameters and centerline velocity distribution of the wall-attached jet are shown in Fig. 3.12. Although the slot heights are different, the dimensionless centerline velocity distributions are the same, decreasing with dimensionless distance $x/b + K_h$ increases. Under different slot heights, all the centerline velocities in the horizontal air reservoir region reduce gradually, and the decay rate decreases. Finally, the jet velocity diminishes to the ambient air velocity.

Compared with Figs. 3.11 and 3.12, the velocity in the horizontal air reservoir region decays slower than that of the vertical attachment region. The centerline velocity decay in the horizontal air reservoir region is given by

$$\frac{u_m(x)}{u_0} = \frac{0.575}{0.018\left(\frac{x}{b} + K_h\right)^{1.11} + 1} \quad (3.40)$$

where K_h is the height correction factor, $K_h = \frac{1}{2} \frac{h-2.5}{b}$, the Cartesian coordinate system is shown in Fig. 3.11a.

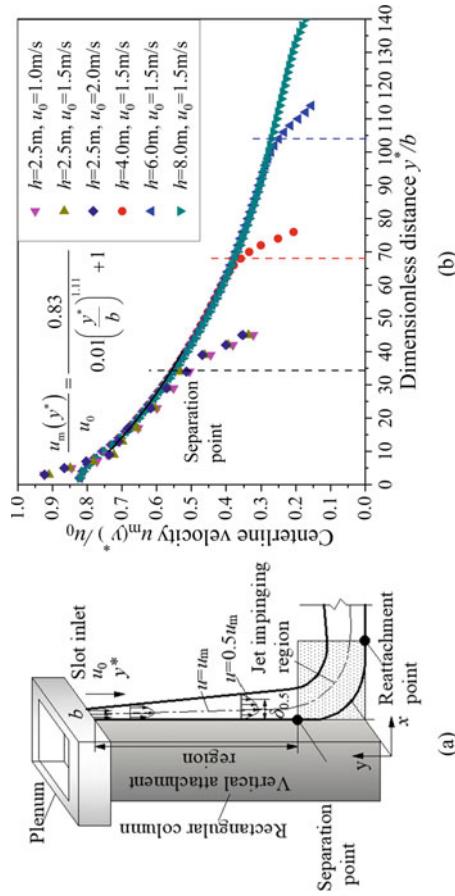
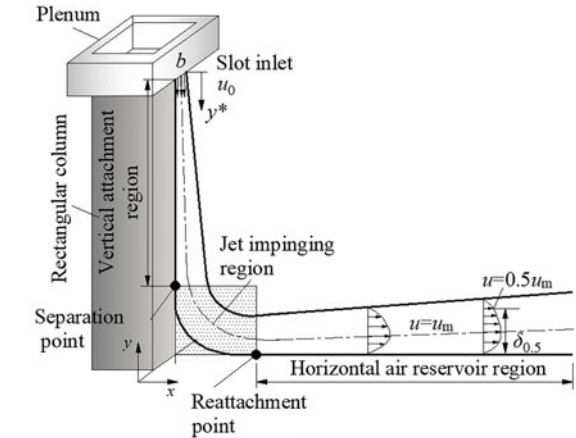
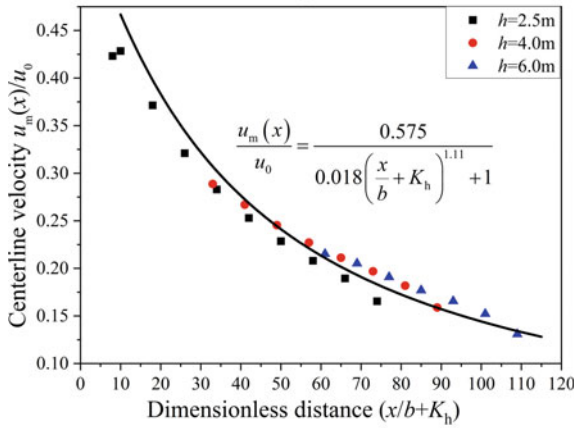


Fig. 3.11 Centerline velocity decay in the vertical attachment region of RCAV. **a** Characteristic parameters, **b** dimensionless centerline velocity

Fig. 3.12 Centerline velocity decay in the horizontal air reservoir region of RCAV. **a** Characteristic parameters, **b** dimensionless centerline velocity



(a)



(b)

3.4.2 Circular Column-Attached Jet

As mentioned above, circular column’s attachment ventilation is similar to rectangular column’s. The main difference between these two types of attachment ventilation is the circular column’s curvature effect. In the horizontal direction, the jet flow varies along the radial direction.

Eckert (2015) once pointed out that when the thickness of the fluid boundary layer δ is greater than or equal to the radius r of the circular column, the curvature effect should be taken into account. Nevertheless, for $\delta/r < 0.1$, the curvature effect can be ignored. Mostly, $\delta/r < 0.1$ in the practical engineering application, thus, the circular column-attached jet could be treated as a rectangular column or vertical wall-attached jet in the vertical attachment region.

1. Centerline velocity in the vertical attachment region

For circular column attachment ventilation, the jet parameters in the vertical attachment region are shown in Fig. 3.13a. Figure 3.13b illustrates the dimensionless centerline velocity distribution under different slot heights, i.e., $h = 2.5$ m, 4.0 m, 6.0 m, and 8.0 m in the vertical attachment region. It can be seen from Fig. 3.13b that, in the range of $0 < y^*/b \leq 45$, the centerline velocity of the column-attached jet decays rapidly (decreasing almost linearly); while for $y^*/b > 45$, the centerline velocity decays relatively slow. Similar to the rectangular column attachment ventilation, the centerline velocity in the vertical attachment region can be expressed as Eq. (3.41)

$$\frac{u_m(y^*)}{u_0} = \frac{0.83}{0.01\left(\frac{y^*}{b}\right)^{1.11} + 1} \quad (3.41)$$

It should be noted that the column-attached jet will separate from the vertical wall when it is close to the floor. The separation point position is related to the slot height h . As h increases, the wall-attached jet will separate from the wall at a higher position. For $h \leq 4.0$ m, such as ordinary office rooms, the height of the separation point is about 0.5 m; as h increases to 6.0 m, the position rises to about 1.0 m away from the floor.

Centerline velocity in the horizontal air reservoir region

For a circular column with a large curvature radius, the velocity decay in the horizontal air reservoir region is similar to that of the rectangular column, as shown in Fig. 3.14. The dimensionless centerline velocity decay also exhibits similarities, decreasing with the increase of x/b . The dimensionless centerline velocity distribution can be expressed by Eq. (3.42)

$$\frac{u_m(x)}{u_0} = \frac{0.575}{0.035\left(\frac{x}{b} + K_h\right)^{1.11} + 1} \quad (3.42)$$

where K_h is the height correction factor, $K_h = \frac{1}{6} \frac{h-2.5}{b}$.

It should be pointed out that Eq. (3.42) is only applicable to the horizontal air reservoir region.

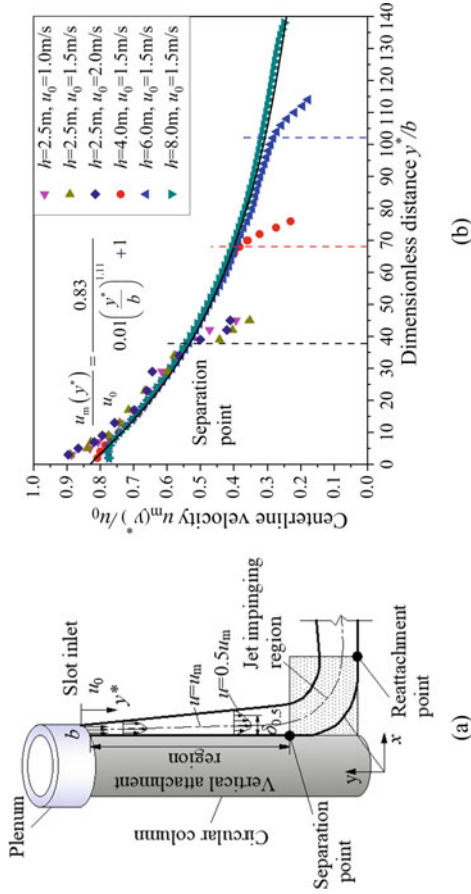


Fig. 3.13 Centerline velocity in the vertical attachment region of CCAV. **a** Characteristic parameters, **b** dimensionless centerline velocity

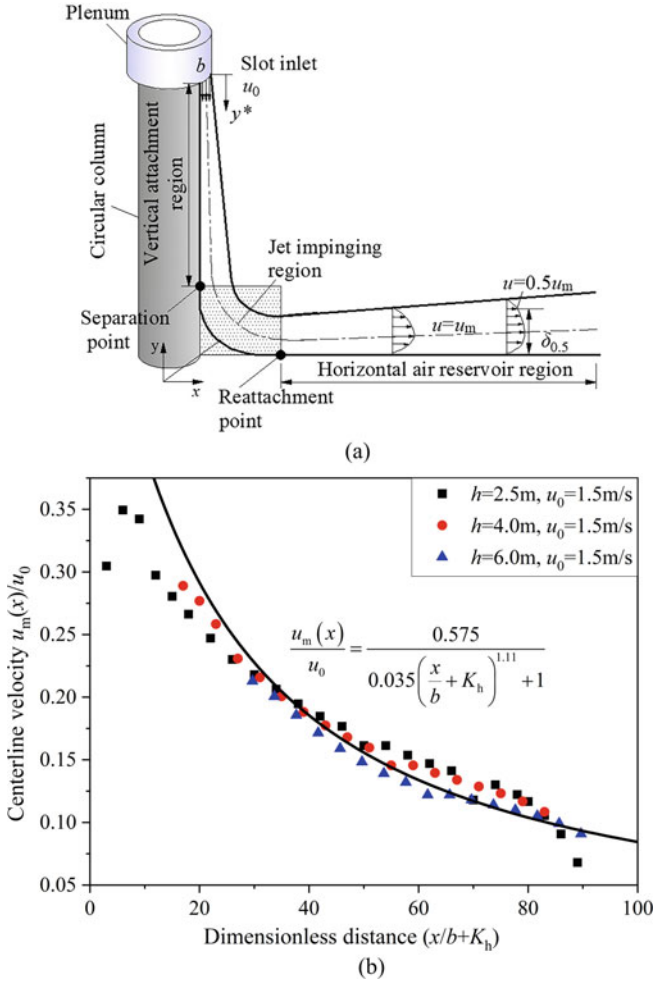


Fig. 3.14 Dimensionless centerline velocity decay in the horizontal air reservoir region of CCAV. **a** Characteristic parameters, **b** dimensionless centerline velocity

3.5 Velocity Distributions with Different Attachment Ventilation Modes

In order to have a deeper understanding of the similarities and differences between the VWAV, RCAV, and CCAV in nature, this section compares the centerline velocity distributions among those attachment ventilation modes.

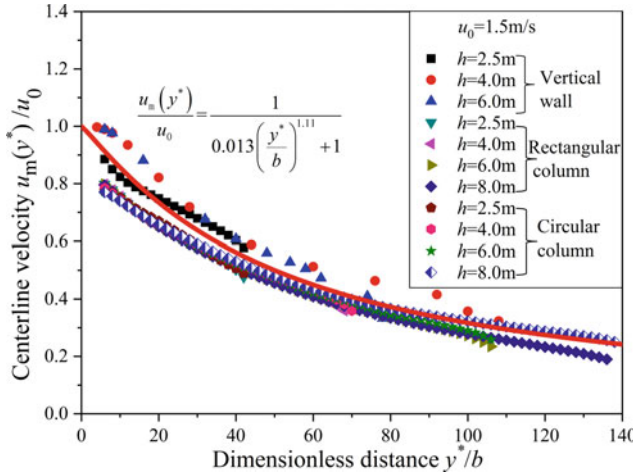


Fig. 3.15 Comparison of dimensionless centerline velocities in the vertical attachment region

3.5.1 Comparison of Centerline Velocity in Vertical Attachment Region

As shown in Fig. 3.15, in the vertical attachment region, there are similarities among the centerline velocity profiles of vertical wall-attached, rectangular column-attached, and circular column-attached jets. The dimensionless centerline velocities decrease exponentially as the distance y^*/b increases. The centerline velocity in the vertical attachment region can be expressed as a unified Eq. (3.43) with a relative error of less than 10%. For most ventilation engineering applications, Eq. (3.43) provides sufficient accuracy.

$$\frac{u_m(y^*)}{u_0} = \frac{1}{0.013\left(\frac{y^*}{b}\right)^{1.11} + 1} \tag{3.43}$$

3.5.2 Comparison of Centerline Velocity in Horizontal Air Reservoir Region

In the horizontal air reservoir region, there are significant differences among the three attachment ventilation’s centerline velocity distributions. As shown in Fig. 3.16, the velocity profiles reflect the influence of the attached wall on the velocity decay. When $x/b + K_h \leq 40$, the VWAV’s centerline velocity decays slowest, followed by the RCAV, and the quickest for the CCAV. For $x/b + K_h > 40$, the velocity decay becomes slower than it would be in the range of $x/b + K_h \leq 40$. In this range, the

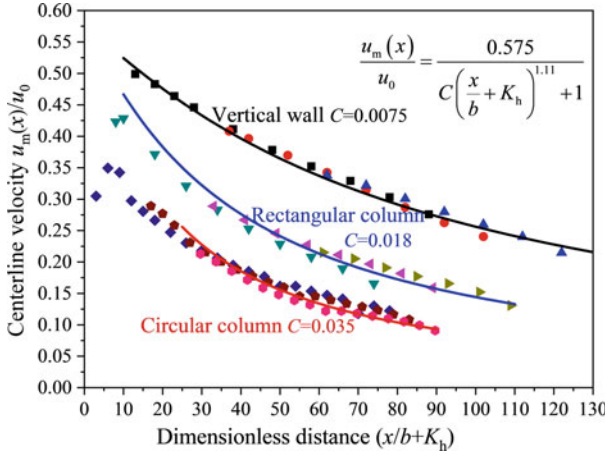


Fig. 3.16 Comparison of dimensionless centerline velocities in the horizontal air reservoir region

VWAV’s centerline velocity maintains the highest, the middle for the RCAV, and the lowest for the CCAV. The primary reason is that, for a rectangular column, the aris edges lead to the merging and superposition of airflow, which causes further momentum decay. Accordingly, for circular columns, particularly those with smaller diameters, the curvature effect exerts a remarkable influence on velocity decay.

We can conclude that the centerline velocity decays of all three attachment ventilations depend upon the shape factor C of the wall-attached jet and determined semi-empirical equations for the horizontal air reservoir region, which can be generally expressed as Eq. (3.44)

$$\frac{u_m(x)}{u_0} = \frac{0.575}{C \left(\frac{x}{b} + K_h\right)^{1.11} + 1} \tag{3.44}$$

where C is shape factor, $C = 0.0075$ for VWAV, $C = 0.0180$ for RCAV, and $C = 0.0350$ for CCAV. K_h is the height correction factor, see Sects. 3.3 and 3.4.

The parameter correlations of vertical wall, rectangular column, and circular column attachment ventilation are summarized in Table 3.2.

Table 3.2 Correlations of various characteristic parameters of attachment ventilation air distribution

Characteristic parameters		Vertical wall attachment ventilation	Rectangular column attachment ventilation	Circular column attachment ventilation	Unified correlation equations for attachment ventilation
Centerline velocity	Vertical	$\frac{u_m(y^*)}{u_0} = \frac{1}{0.01 \left(\frac{y^*}{b}\right)^{1.11} + 1}$	$\frac{u_m(y^*)}{u_0} = \frac{0.83}{0.01 \left(\frac{y^*}{b}\right)^{1.11} + 1}$		$\frac{u_m(y^*)}{u_0} = \frac{1}{0.013 \left(\frac{y^*}{b}\right)^{1.11} + 1}$
	Horizontal	$\frac{u_m(x)}{u_0} = \frac{0.575}{0.0075 \left(\frac{x}{b} + K_h\right)^{1.11} + 1}$	$\frac{u_m(x)}{u_0} = \frac{0.575}{0.018 \left(\frac{x}{b} + K_h\right)^{1.11} + 1}$	$\frac{u_m(x)}{u_0} = \frac{0.575}{0.035 \left(\frac{x}{b} + K_h\right)^{1.11} + 1}$	$\frac{u_m(x)}{u_0} = \frac{0.575}{C \left(\frac{x}{b} + K_h\right)^{1.11} + 1}$ C is the shape factor: C = 0.0075 for the vertical wall, C = 0.018 for the rectangular column, C = 0.035 for the circular column K_h is the height correction factor, $K_h = \frac{1}{2} \frac{h-2.5}{b}$ for the vertical wall and the rectangular column, $K_h = \frac{1}{6} \frac{h-2.5}{b}$ for the circular column
Cross-sectional velocity	Vertical /Horizontal	$\frac{u}{u_m} = 1.48 \eta^{1/7} [1 - erf(0.68\eta)]$			
		or $\frac{u}{u_m} = -0.83 + 2.03 \times e^{-0.42\eta} (0.2 \leq \eta \leq 2.0)$			

References

- ANSI/ASHRAE Standard 113-2013 (2013) Method of testing for room air distribution. American Society of Heating, Refrigeration and Air-Conditioning Engineers Inc., Atlanta
- ASHRAE (2017) ASHRAE handbook: fundamentals. American Society of Heating, Refrigeration and Air-Conditioning Engineers Inc., Atlanta
- Eckert HU (2015) Simplified treatment of the turbulent boundary layer along a cylinder in compressible flow. *J Aeronaut Sci* 19(1):23–28
- Eckert ERG, Drake RM Jr (1972) Analysis of heat and mass transfer. McGraw Hill, New York
- Glauert MB (1956) The wall jet. *J Fluid Mech* 1(6):625–643
- Li AG (2019) Extended Coanda effect and attachment ventilation. *Indoor Built Environ* 28(4):437–442
- Prandtl L (1942) Bemerkungen zur Theorie der freien Tubulenz. *J Appl Math Mech* 22:241–243
- Schwarz WH, Cosart WP (1961) The two-dimensional turbulent wall jet. *J Fluid Mech* 10(4):481–495
- Sun DX (1992) Theoretical analysis of turbulent flow frictional resistance inside ducts of arbitrary angular cross sections. *J Hydrodynam B* 1:35–45
- Verhoff A (1963) The two-dimensional turbulent wall jet without an external free stream. Princeton University
- Zhang H (2011) Theoretical analysis and solution on flow field of indoor confined jet ventilation. Xi'an University of Architecture and Technology, Xi'an (in Chinese)

Open Access This chapter is licensed under the terms of the Creative Commons Attribution-NonCommercial-NoDerivatives 4.0 International License (<http://creativecommons.org/licenses/by-nc-nd/4.0/>), which permits any noncommercial use, sharing, distribution and reproduction in any medium or format, as long as you give appropriate credit to the original author(s) and the source, provide a link to the Creative Commons license and indicate if you modified the licensed material. You do not have permission under this license to share adapted material derived from this chapter or parts of it.

The images or other third party material in this chapter are included in the chapter's Creative Commons license, unless indicated otherwise in a credit line to the material. If material is not included in the chapter's Creative Commons license and your intended use is not permitted by statutory regulation or exceeds the permitted use, you will need to obtain permission directly from the copyright holder.



Chapter 4

Nonisothermal Attachment Ventilation Mechanisms



Abstract Under nonisothermal conditions, the heated or cooled supply air jet interacts with indoor convection of heat sources, producing a specific temperature field, velocity field, and concentration field. This chapter deals with the airflow mechanisms of nonisothermal attachment ventilation. It discusses the air movement of nonisothermal attached jets, which provides a theoretical basis for the design of the air distribution system for attachment ventilation. The parameter correlations of temperature and velocity distribution of attachment ventilation, etc., are obtained. The influencing factors of human movement and wall roughness elements on the airflow field have also been discussed.

Keywords Nonisothermal jet · Attachment ventilation · Attached ventilation · Heat source · Temperature distribution · Human motion · Wall roughness

Under nonisothermal conditions, the heated or cooled supply air jet interacts with the indoor convection of heat sources, producing a specific temperature field, velocity field, and concentration field. This chapter mainly discusses the indoor air movement of nonisothermal attachment ventilation, including VWAV, RCAV, CCAV, etc., which provides a theoretical basis for designing attachment ventilation. The parameter correlations of temperature and velocity distribution of attachment ventilation are established. The influencing factors of human movement and wall roughness elements on the airflow field have also been discussed.

4.1 Nonisothermal Vertical Wall Attachment Ventilation

The jet flow can be divided into thermal plumes, momentum jets, and buoyant jets. The thermal plume refers to the air currents rising from a hot body or descending from a cold body, and buoyancy usually promotes its further movement and diffusion after entering the environment. The momentum jet refers to fluid flows produced by a pressure drop through an orifice or opening. The buoyant jet, also called a forced plume, refers to the flow whose motion is transitioning from a plume to a momentum jet. In fact, it is a kind of modified plume or momentum jet.

Considering the influence of thermal buoyancy caused by the density or temperature difference, the continuity equation, and momentum equation can be expressed in the following forms (see Fig. 3.2b for the coordinate system)

$$\frac{\partial u}{\partial y^*} + \frac{\partial v}{\partial x} = 0 \quad (4.1)$$

$$u \frac{\partial u}{\partial y^*} + v \frac{\partial u}{\partial x} = g - \frac{1}{\rho} \frac{\partial p}{\partial y^*} + \frac{\partial}{\partial x} \left(\epsilon \frac{\partial u}{\partial x} \right) \quad (4.2)$$

Let ρ_n denote the density of the surrounding fluid, and assume the pressure of the surrounding fluid is the static pressure distribution in the vertical direction, so

$$\frac{\partial p}{\partial y^*} = \rho_n g \quad (4.3)$$

Since the air density difference is slight, the Boussinesq approximation can be adopted. The Boussinesq model neglects density differences except in the gravity term of the momentum equation. In Eq. (4.2), ρ of the pressure gradient term is replaced by ρ_n (except for the natural convection with high temperature difference, the simplification is reasonable), and Eq. (4.2) is written as

$$u \frac{\partial u}{\partial y^*} + v \frac{\partial u}{\partial x} = \frac{\rho - \rho_n}{\rho_n} g + \frac{\partial}{\partial x} \left(\epsilon \frac{\partial u}{\partial x} \right) \quad (4.4)$$

For buoyant jets, the specific momentum flux M and the specific buoyancy flux B are two parameters of great significance, which can be used to describe the characteristics of buoyant jets.

In a specific cross-section, the total momentum of the buoyant jet is

$$m = \int_0^{\infty} \rho u^2 dx \quad (4.5)$$

Specific momentum flux is

$$M = \frac{m}{\rho} = \int_0^{\infty} u^2 dx \quad (4.6)$$

The specific buoyancy flux B reflects the initial density gradient between the mixture injection fluid and ambient fluid.

According to the principle of mass conservation, the flux conservation relationship of the density difference $\rho - \rho_n$ can be obtained

$$\int_0^{\infty} u \frac{\rho - \rho_n}{\rho_n} g \, dx = \text{Constant} \quad (4.7)$$

The specific buoyancy flux is

$$B = \int_0^{\infty} u \frac{\rho - \rho_n}{\rho_n} g \, dx \quad (4.8)$$

Here, the dimensional analysis method is applied to determine the maximum velocity and temperature decay rate.

First, the plume in steady state is considered. Ignore the initial flow rate and initial momentum of the plume, and consider the time-averaged characteristics of the plume as a function of specific buoyancy flux B , axial distance y^* , kinematic viscosity ν , and diffusion coefficient k , thus (Rodi 1982)

$$u_m = f(B, y^*, \nu, k) \quad (4.9)$$

The dimension of B is $L^3 S^{-3}$. According to dimensional analysis, u_m is given by

$$u_m = B^{\frac{1}{3}} f\left(\frac{B^{\frac{1}{3}} y^*}{\nu}, \frac{\nu}{k}\right) \quad (4.10)$$

where

$\frac{B^{\frac{1}{3}} y^*}{\nu}$ local Reynolds number;
 $\frac{\nu}{k}$ Prandtl number.

For the fully developed turbulent plume, it can be assumed that the flow is self-similarity with respect to the local Reynolds number (this hypothesis is reasonable and validated by Pera et al. 1971 and Mollendorf and Gebhart 1973), and the molecular characteristics of the fluid are not of great importance, then $f\left(\frac{B^{\frac{1}{3}} y^*}{\nu}, \frac{\nu}{k}\right)$ tends to a non-zero limit constant K_p . The final formulation of u_m thus reads

$$u_m = K_p B^{\frac{1}{3}} \quad (4.11)$$

For the buoyant jet, a characteristic length scale $l_M = \frac{M_0}{B_0^{\frac{1}{3}}}$ is defined. Here, M_0 is the initial specific momentum flux, and B_0 is the initial specific buoyancy flux. This scale can determine the relative magnitude of momentum and buoyancy. It can be considered that the time-averaged features of the buoyant jet is a function of the initial specific momentum flux M_0 , the initial specific buoyancy flux B_0 , and the axial distance y^* , thus

$$u_m = f(M_0, B_0, y^*) \quad (4.12)$$

where the dimension of M_0 is L^3S^{-2} , dimension of B_0 is L^3S^{-3} . According to dimensional analysis, u_m is given by

$$u_m = \left(\frac{M_0}{y^*}\right)^{\frac{1}{2}} f\left(\frac{y^* B_0^{\frac{2}{3}}}{M_0}\right) \quad (4.13)$$

When $\frac{x B_0^{\frac{2}{3}}}{M_0} \rightarrow \infty$, the buoyancy dominates flow, the buoyant jet changes into a plume. According to the previous analysis, we can see that $u_m \sim y^{*0}$, and thus $f\left(\frac{y^* B_0^{\frac{2}{3}}}{M_0}\right) \rightarrow \left(\frac{y^* B_0^{\frac{2}{3}}}{M_0}\right)^{\frac{1}{2}}$.

If $\frac{x B_0^{\frac{2}{3}}}{M_0} \rightarrow 0$, the buoyancy effect can be neglected, the buoyant jet changes into a momentum jet. From the analysis in the previous chapters, we can see that $u_m \sim y^{*-\frac{4}{3}}$, and thus $f\left(\frac{y^* B_0^{\frac{2}{3}}}{M_0}\right) \rightarrow \left(\frac{y^* B_0^{\frac{2}{3}}}{M_0}\right)^{-\frac{5}{6}}$.

From the above analysis, it can be concluded that the exponent of axial distance y^* should be in the range of $-\frac{4}{3} \sim 0$ as a function of centerline velocity u_m of the nonisothermal attached jet, and the specific expression depends on the relative magnitude of $y^* \cdot B_0^{\frac{2}{3}}$ and M_0 . Since $B_0 \ll M_0$ is common in actual conditions, the exponent should be closer to $-\frac{4}{3}$, which is also illustrated in the empirical curve obtained from the experiment, see Fig. 4.1a.

When Eq. (4.13) is used for nonisothermal attached jets, the exponent functional relationship of the centerline velocity u_m with respect to the axial distance y^* can be determined experimentally.

In engineering applications, the heat load distribution can be considered evenly distributed on the floor with a constant heat flux intensity, as the indoor heat distribution of ordinary offices or residential buildings is scattered, and human movement enhances indoor air uniformity. Taking ordinary office buildings as an example, the influence of supply air temperature t_0 and heat load q (heat flux intensity) is investigated, and detailed information is shown in Table 4.1.

The jet centerline velocity and excess temperature decay for the vertical attachment region are shown in Fig. 4.1. As shown in Fig. 4.1a, it is found that for different heat flux intensities and supply air temperatures, there is the similarity of the centerline velocity distributions.

In the condition of $0 \leq y^*/b \leq 7.5$, the centerline velocity remains unchanged in the initial attachment region, and then the jet enters the main region with the fully developed turbulence. With the increase of supply air throw, the centerline velocity decreases exponentially, which can be regarded as linear decay within a certain distance. When $y^*/b > 47.5$, in the jet terminal, the centerline velocity decays sharply due to impinging effect. Since the fluid micro-cluster with low momentum in the

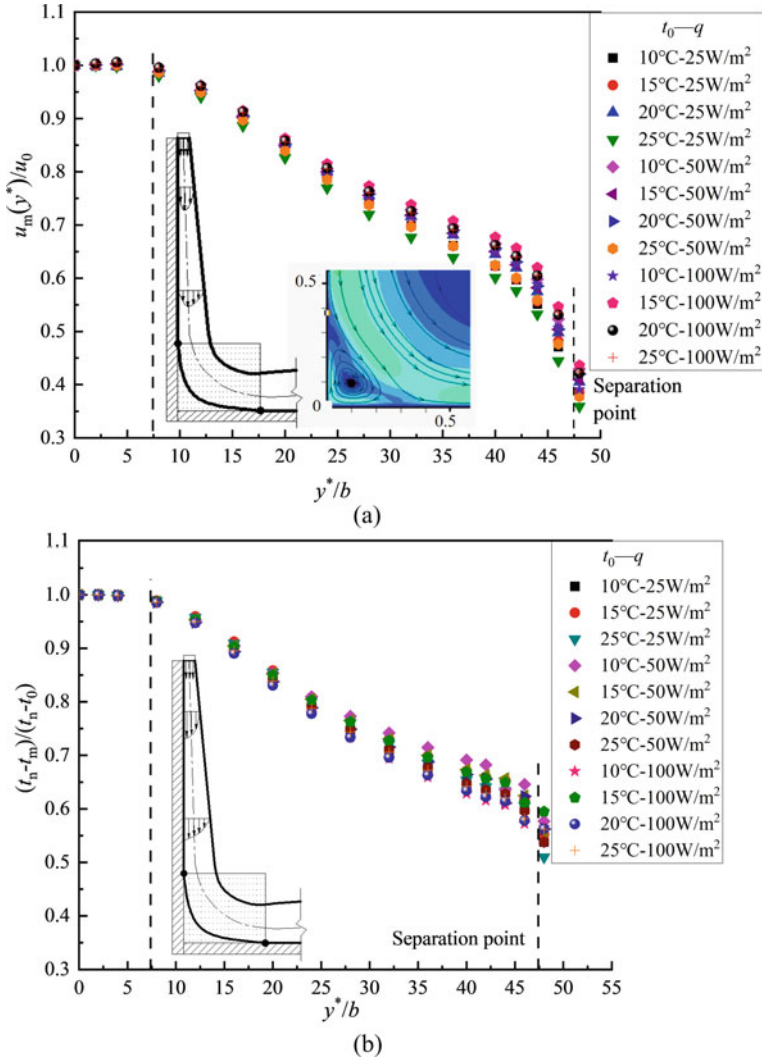


Fig. 4.1 Influence of supply air temperature t_0 and heat flux intensity q on the centerline velocity and temperature in the vertical attachment region ($h = 2.5$ m, $u_0 = 3.0$ m/s). **a** Dimensionless centerline velocity, **b** excess temperature decay

Table 4.1 Cases with different air supply temperature t_0 and heat flux intensity q ($h = 2.5$ m, $u_0 = 3.0$ m/s)

Supply air temperature t_0 ($^\circ\text{C}$)	10			15			20			25		
Heat flux intensity q (W/m^2)	25	50	100	25	50	100	25	50	100	25	50	100

viscous fluid boundary layer is not enough to resist the increased pressure caused by impinging, the jet separates from the wall (see Fig. 4.1a).

The consistency of the distribution of centerline velocity u_m and centerline temperature t_m is discussed below. The momentum equation and enthalpy difference equation are listed

$$\int_0^{\infty} \rho u^2 dx = \rho_0 u_0^2 b \quad (4.14)$$

$$\int_0^{\infty} \rho u c_p (t - t_a) dx = \rho_0 u_0 c_p (t_0 - t_n) b \quad (4.15)$$

where t_n is the temperature of surrounding air and c_p is the specific heat at constant pressure.

Equations (4.14) and (4.15) lead to the following approximate relationship

$$\frac{u_m}{u_0} \sim \frac{t_m - t_n}{t_0 - t_n} \quad (4.16)$$

Some studies have also presented the following empirical correlations of nonisothermal turbulent jets (Ping 1995)

$$\frac{t_0 - t_n}{t_m - t_n} \approx \left(\frac{u}{u_m} \right)^{\text{Pr}} \quad (4.17)$$

For any position y , the temperature profile is wider than the velocity profile. This is because the exponent $\text{Pr} \approx 0.7$ for air, and $\frac{u}{u_m}$ is always less than 1.

Thus, as a simplification, it can be approximated that the centerline velocity decay and the excess temperature decay have almost the same form, and the experimental data also support this argument (see Fig. 4.1).

In the horizontal air reservoir region, the centerline velocity profile is almost consistent with excess temperature, as shown in Fig. 4.2. It can be found from experimental results that the jet presents an “elastic effect” in the jet impinging region. The centerline velocity in the horizontal region first rises ($x/b \leq 10$ in the jet impinging region) and then falls. The jet centerline temperature almost decreases linearly due to the mixing with the surrounding air. However, outside the range of $x/b \geq 90-100$, the centerline velocity and temperature drop rapidly. It should be noted that in summer conditions, the cold air jet may be heated by floor ($t_m \geq t_n$), so the excess temperature is negative in the flow terminal.

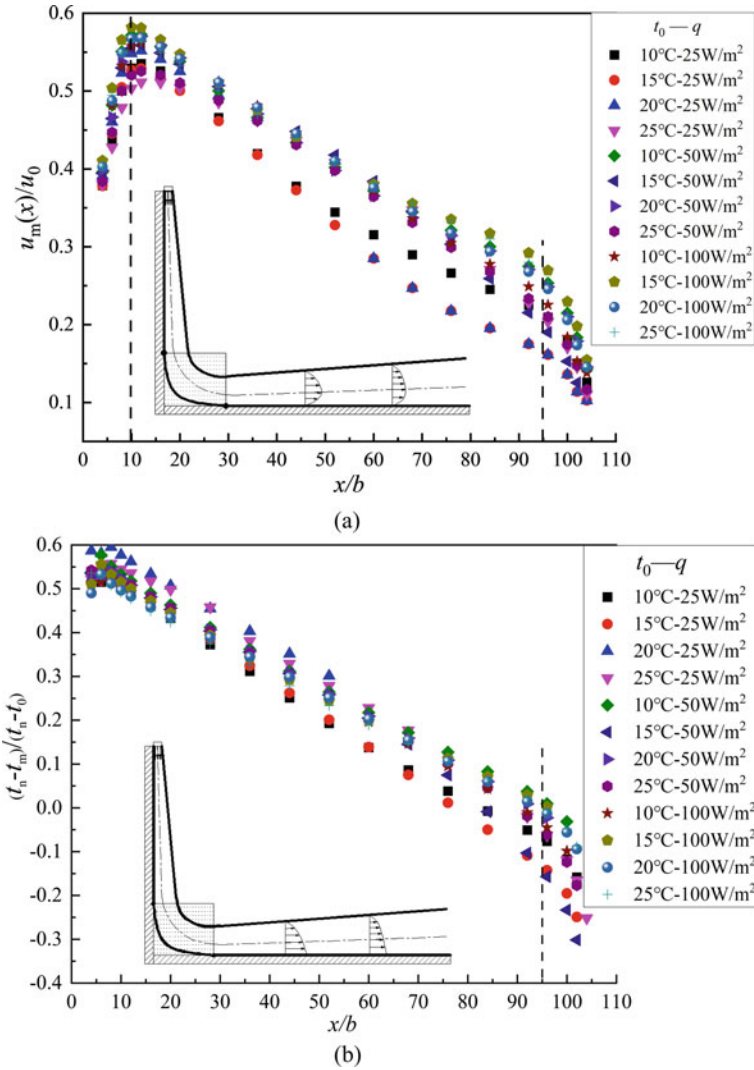


Fig. 4.2 Influence of t_0 and q on the centerline velocity and temperature in the horizontal air reservoir region of attachment ventilation. **a** Centerline velocity distribution, **b** excess temperature distribution

4.2 Nonisothermal Column Attachment Ventilation

In the vertical attachment region, as shown in Fig. 4.3, the decay of centerline velocity and excess temperature show good similarity. In RCAV, the ambulatory-shaped “ \square ” air inlet is usually adopted. The mixing properties of the airflow resulting from the interaction of flow due to the rectangular column’s aris is investigated. Researches

show that the RCAV's velocity and temperature decay more quickly than that of VWAV.

Generally, for CCAV, the curvature radius r of the circular column is large enough than the magnitude boundary layer thickness δ , the influence of column curvature can be ignored. In this condition, the experimental study shows that the flow feature of CCAV is similar to that of RCAV.

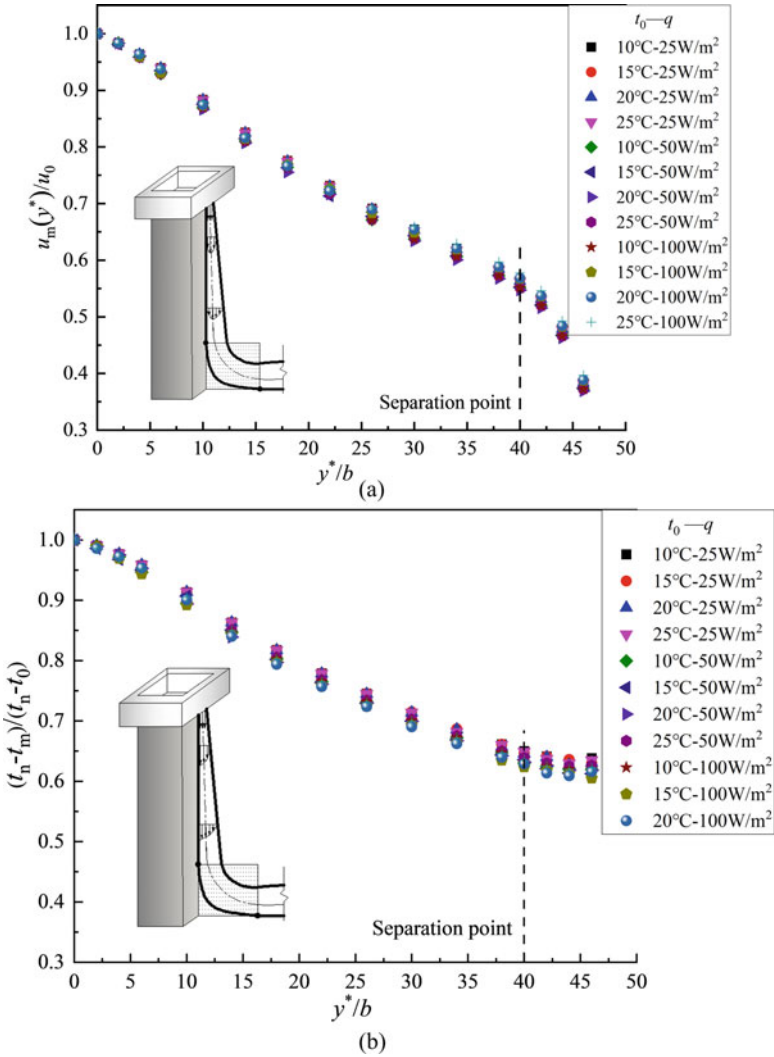


Fig. 4.3 Influence of t_0 and q on the centerline parameters in the vertical attachment region of RCAV. **a** Centerline velocity distribution, **b** excess temperature decay

In the horizontal air reservoir region, the decay of centerline velocity and excess temperature is shown in Fig. 4.4. The dimensionless centerline velocity and temperature distribution in the main regions are self-similarities. However, due to the “arris effect” of rectangular columns, the intersection and superposition of two adjacent attached jets further consume the jet momentum. Compared RCAV and VWAV, the former’s centerline velocity is slightly lower.

As discussed in Chap. 3, the time-averaged velocity distributions have proved to be sufficient in reflecting the fundamental features of attachment ventilation. The time-averaged centerline velocity distribution in the horizontal air reservoir region of CCAV is consistent with that of the RCAV, as shown in Fig. 4.5. That is to say, the centerline velocity increases at the initial stage and then decreases, and the excess temperature decreases exponentially.

4.3 Characteristic Parameter Correlations of Nonisothermal Attachment Ventilation

The thermal jet flows of different attachment ventilation modes (including VWAV, RCAV, CCAV, etc.) indicate dissimilarities and similarities. The characteristics of the jet flow field of three types of nonisothermal attachment ventilation under different parameters, including supply air height h and velocity u_0 are compared as follows.

4.3.1 Vertical Attachment Region

The centerline velocity and temperature distribution in the vertical attachment region under different air supply heights ($h = 2.5, 6.0, \text{ and } 8.0 \text{ m}$) are illustrated in Figs. 4.6, 4.7, and 4.8. y_{\max}^* is defined as the maximum attaching length, and it can be expressed by Eq. (4.18).

$$y_{\max}^* = 0.92h - 0.43 \quad (4.18)$$

Equation 4.18 is applicable when $h \geq 0.5 \text{ m}$.

With regard to the building space size, noise limitation, and economy, in the range of $0 < y^*/b \leq 70$ of VWAV, Eq. (4.18) would possess better accuracy, and the error is generally no more than 5%. When the air supply height increases from 2.5 to 8.0 m, the separation point rises slightly and lies in the range of 0.5–1.0 m.

The equations shown in Table 4.2 characterize the decay profile of centerline velocity and excess temperature in the VWAV, RCAV, and CCAV.

For the engineering application, taking the simple and practical as a principle, the centerline velocity and temperature decay in the vertical attachment region of the VWAV, RCAV, and CCAV can be uniformly expressed by Eqs. (4.19) and (4.20). The correlation equations have high accuracy in the range $y^*/b \leq 40$, and the error is no

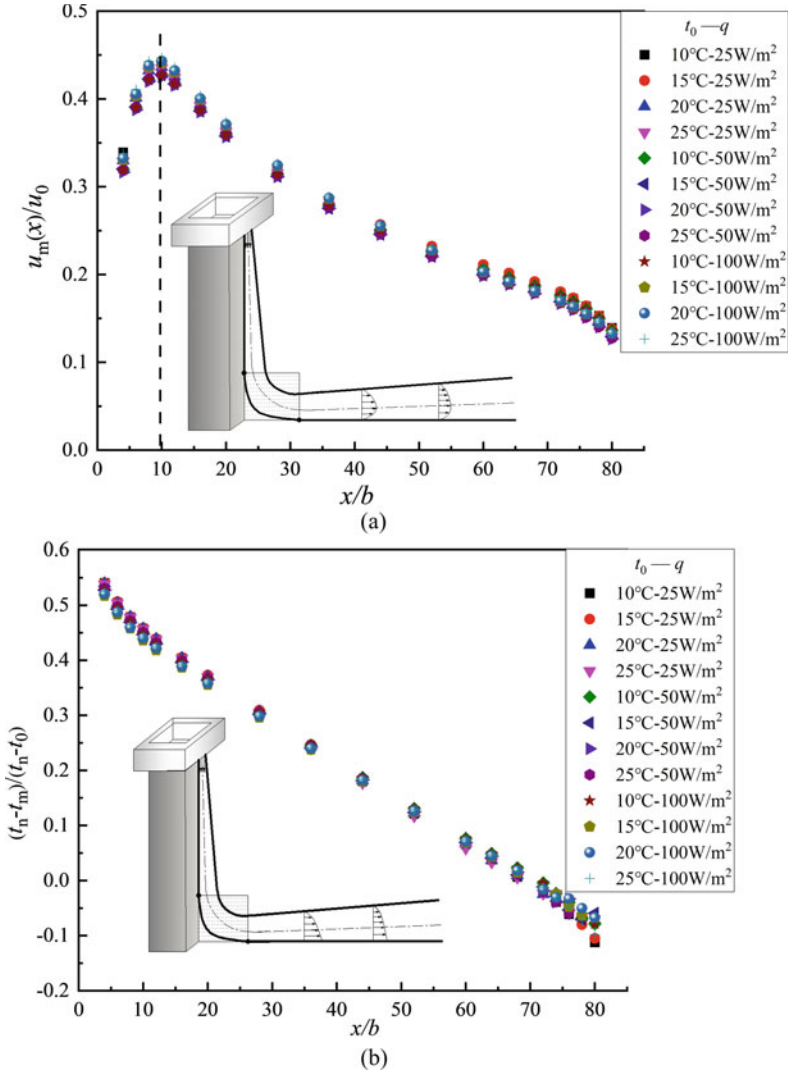


Fig. 4.4 Effect of t_0 and q on characteristics of the horizontal air reservoir region of RCAV. **a** Dimensionless centerline velocity, **b** excess temperature distribution. The reason for the negative value of excess temperature is that the floor heat sources may cause the centerline temperature t_m to be higher than the indoor averaged temperature t_n , $\frac{t_n - t_m}{t_n - t_0} < 0$

more than 5–8% (5% for the vertical attachment region, and 8% for the horizontal air reservoir region, respectively). For nonisothermal attached jets, the arris effect of a rectangular column and the curvature effect of a circular column gradually appear some distance away from the air inlet or opening (see the region of $y^*/b > 40$ in Fig. 4.9).

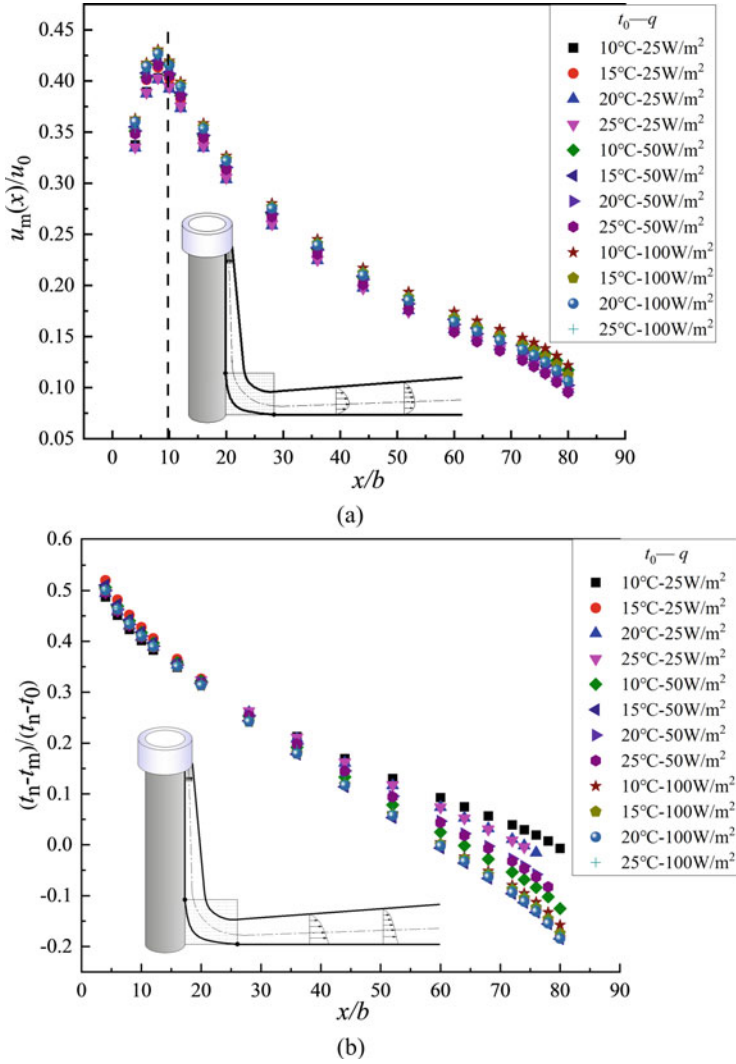


Fig. 4.5 Effect of t_0 and q on characteristics of the horizontal air reservoir region of CCAV. **a** Dimensionless centerline velocity, **b** excess temperature decay

$$\frac{u_m(y^*)}{u_0} = \frac{1}{0.012\left(\frac{y^*}{b}\right)^{1.11} + 0.90} \quad (4.19)$$

$$\frac{t_n - t_m}{t_n - t_0} = \frac{1}{0.01\left(\frac{y^*}{b}\right)^{1.11} + 0.942} \quad (4.20)$$

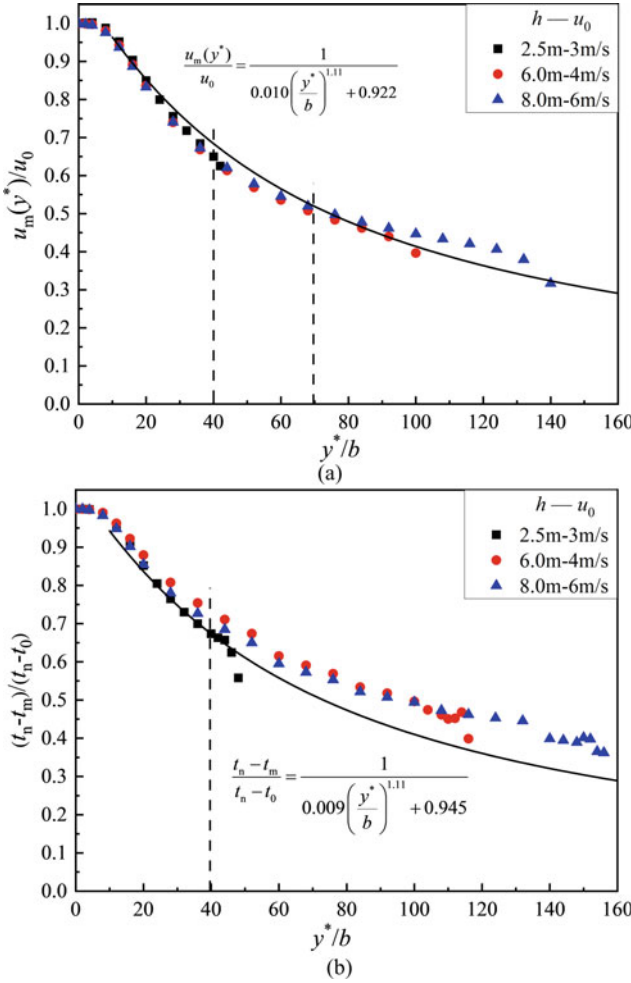


Fig. 4.6 Parameters variations in the vertical attachment region of VWAV. **a** Centerline velocity, **b** excess temperature distribution

The arris effect of a rectangular column and the curvature effect of a circular column will influence the flow field. However, with the increase of the rectangular column’s length-to-width ratio or the circular column’s curvature radius, both the airflow patterns of RCAV and CCAV tend toward that of VWAV. The recommended slot inlet widths of attachment ventilation are shown in Fig. 4.10 (Chen 2018). For example, for a circular column with a diameter of 500 mm, the upper and lower bounds of f/F of slot inlet are 0.05 and 0.7, respectively. It is recommended that the slot inlet width should be selected within 30–150 mm.

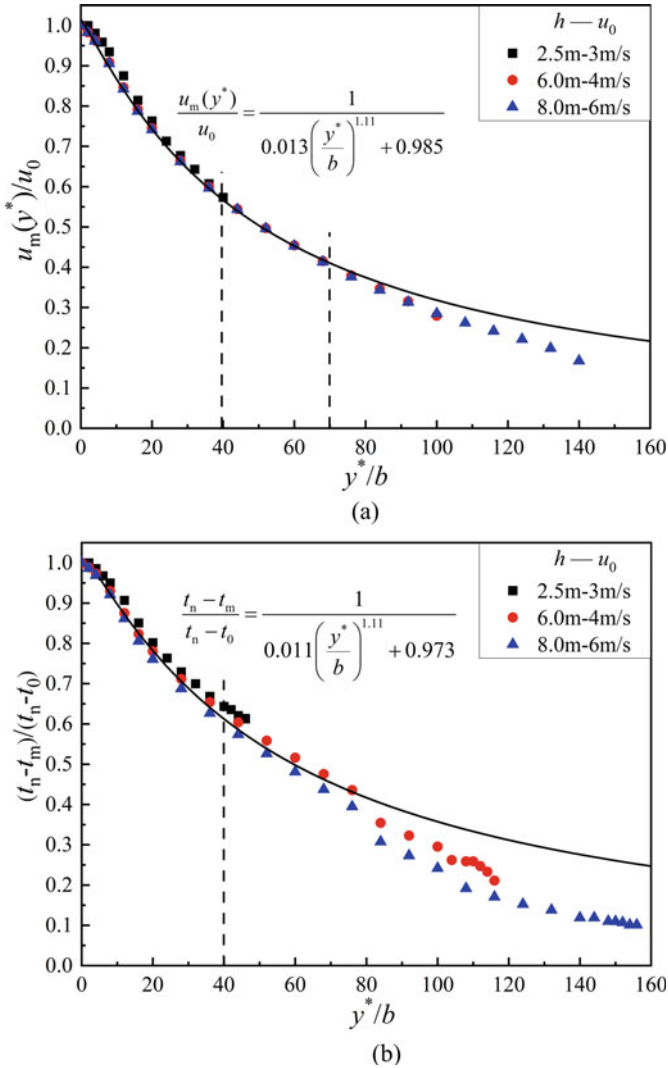


Fig. 4.7 Parameters variation in the vertical attachment region of RCAV. **a** Centerline velocity, **b** excess temperature distribution

4.3.2 Horizontal Air Reservoir Region

The centerline velocity distribution in the horizontal air reservoir region of VWAV, RCAV, and CCAV under different air supply heights are shown in Fig. 4.11. The air supply velocity should be further enhanced for the larger air supply height. The larger air supply height and velocity trigger expanding the impinging region and intensifying the air entrainment rate.

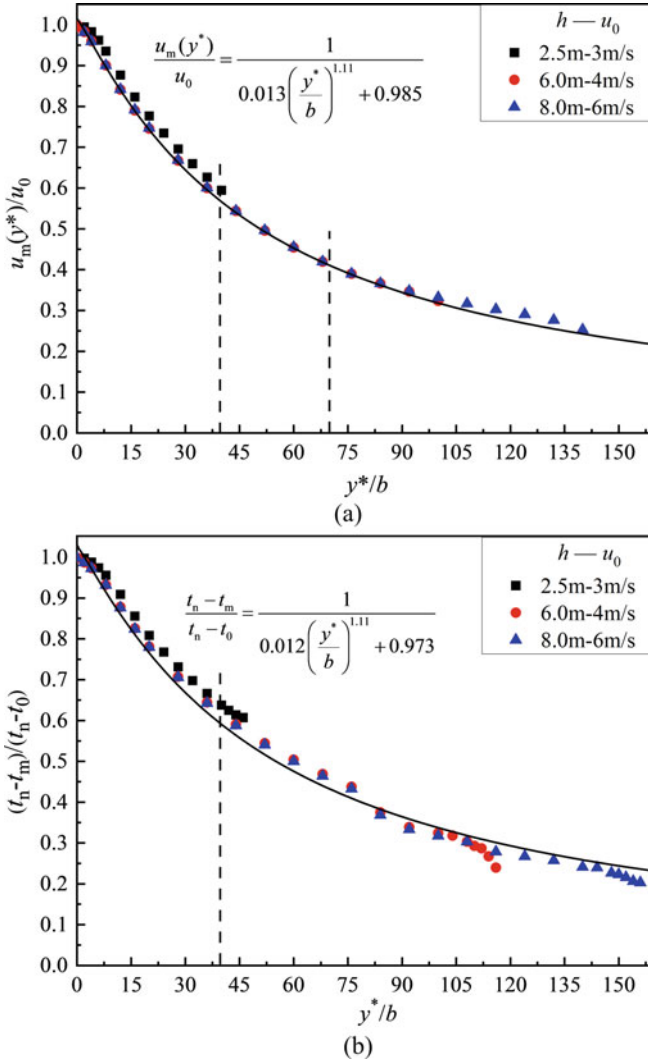


Fig. 4.8 Parameters variation in the vertical attachment region of CCAV. **a** Centerline velocity, **b** excess temperature distribution

The airflow centerline velocity away from the vertical wall of 1.0 m, which is the boundary of the control zone (more information can be found in Chap. 6), can be calculated by Eq. (4.21) (physically “equivalent” to the air supply velocity of displacement ventilation).

$$\frac{u_m(y_{\max}^*)}{u_0} = k_v \frac{u_{m,1.0}}{u_0} + C_v \tag{4.21}$$

Table 4.2 Comparison of centerline velocity and excess temperature in the main section of the vertical attachment region

	Dimensionless centerline velocity $\frac{u_m}{u_0}$	Excess temperature $\frac{t_n - t_m}{t_n - t_0}$
Vertical wall attachment ventilation	$\frac{u_m(y^*)}{u_0} = \frac{1}{0.010\left(\frac{y^*}{b}\right)^{1.11} + 0.922}$	$\frac{t_n - t_m}{t_n - t_0} = \frac{1}{0.009\left(\frac{y^*}{b}\right)^{1.11} + 0.945}$
Rectangular column (circular column) attachment ventilation	$\frac{u_m(y^*)}{u_0} = \frac{1}{0.013\left(\frac{y^*}{b}\right)^{1.11} + 0.985}$	$\frac{t_n - t_m}{t_n - t_0} = \frac{1}{0.011\left(\frac{y^*}{b}\right)^{1.11} + 0.973}$

where

- $u_{m,1.0}$ = air velocity in the control boundary, i.e., the airflow centerline velocity in the air reservoir region at a distance of 1.0 m from the vertical wall, m/s;
- $u_m(y^*_{max})$ = centerline velocity at the separation point of a wall-attached jet, m/s;
- k_v, C_v = empirical coefficient, which are different for different attached walls. $k_v = 1.808, C_v = -0.106$ for VWAV; $k_v = 1.374, C_v = -0.060$ for CAV.

The excess centerline temperature distributions in the horizontal air reservoir region of the VWAV and CAV are shown in Fig. 4.12. The excess centerline temperature decreases linearly in most areas of the horizontal air reservoir region. It can be observed that there is a negative excess temperature. The centerline temperature t_m will increase due to the floor heat sources and is higher than the indoor temperature t_n , so the excess temperature $\frac{t_n - t_m}{t_n - t_0} < 0$.

The correlations of jet characteristic parameters of attachment ventilation under isothermal and nonisothermal conditions are summarized in Table 4.3.

In summary, there are self-similarities for the centerline velocity and excess temperature in the jet’s main regions (regions I and III). The centerline velocity can be uniformly expressed as

$$\frac{u_m(\gamma)}{u_0} = \frac{1}{a_i\left(\frac{\gamma}{b} + b_i\right)^m + c_i} \tag{4.22}$$

The excess temperature in the vertical attachment region can be uniformly expressed as

$$\frac{t_n - t_m}{t_n - t_0} = \frac{1}{a_j\left(\frac{\gamma}{b} + b_j\right)^n + c_j} \tag{4.23}$$

where $\gamma = y^*$ for the vertical attachment region, $\gamma = x$ for the horizontal air reservoir region. y^* is the vertical distance from the jet entrance along the flow direction of the vertical wall to a given point, x is the horizontal distance from a given point in the horizontal air reservoir region to the vertical attached-wall surface, and b is the characteristic width scale of the air inlet or opening. In addition, the coefficients $a_i,$

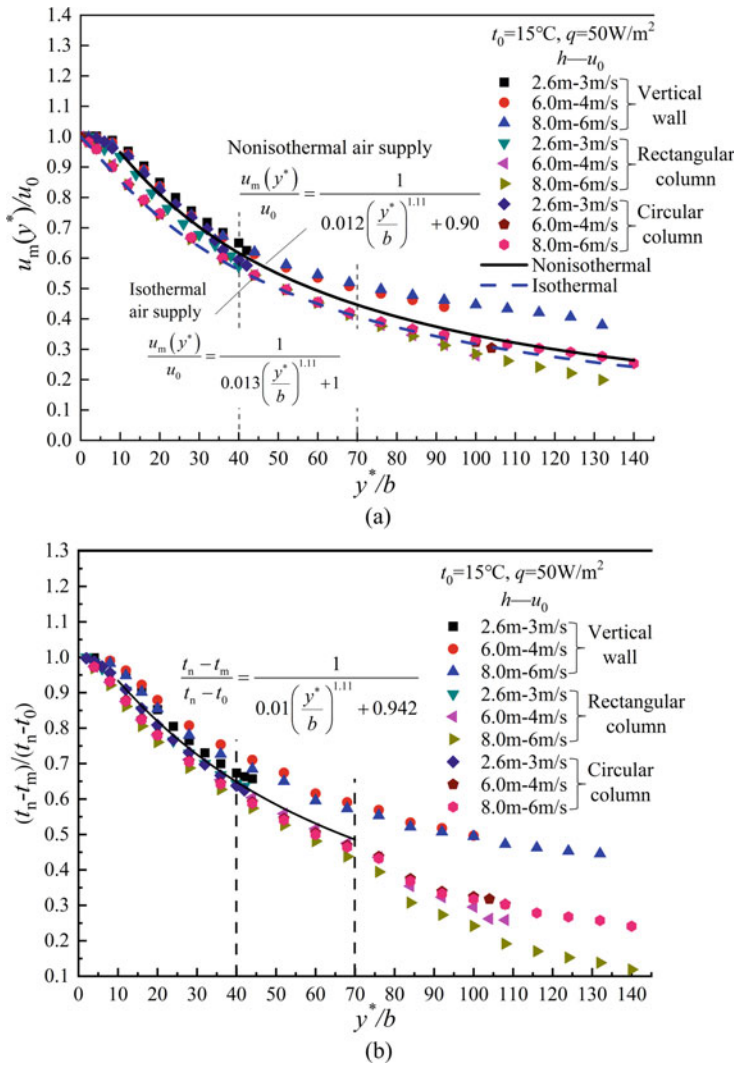


Fig. 4.9 Unified correlations of centerline velocity and excess temperature distributions in the vertical attachment region of three attachment ventilation modes. **a** Centerline velocity distribution, **b** excess temperature decay

b_i , c_i , and a_j , b_j , c_j are related to the air inlet structures (turbulence coefficient), the air inlet position, etc.

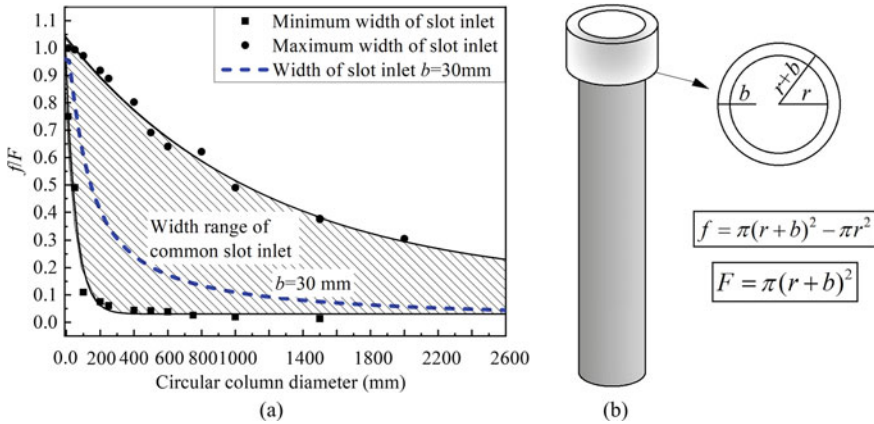


Fig. 4.10 Slot inlets or air inlets width range of attachment ventilation. **a** Recommended slot inlet width for CCAV, **b** geometric parameters of the circular column

4.4 Air Opening and Control Zone in Rooms

The main elements affecting room air environmental parameters include the air supply velocity and temperature difference. The following factors should also be taken into account.

- (a) form of air openings, such as geometry and location of air inlets, and exhaust outlets;
- (b) interior geometry and room occupied zone;
- (c) heat source’s location, distribution, and heat dissipation, including room surface temperature;
- (d) internal disturbances (such as human activities, industrial production, etc.);

This section analyzes factors such as the shapes of the air opening, the control zone, etc.

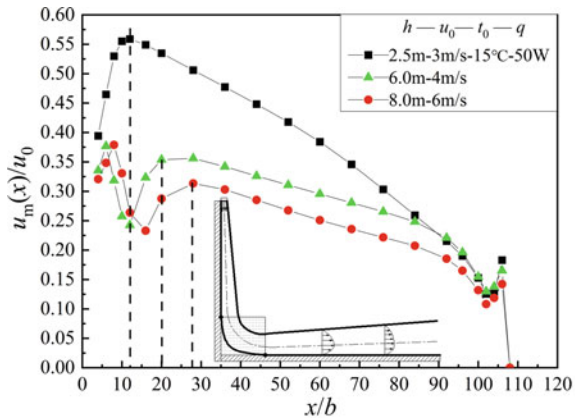
4.4.1 Influence of Air Opening Types

In this section, taking the slot inlet used in the RCAV and CCAV as examples, the effects of the circular column diameter and the rectangular column dimension on the attachment ventilation performance are analyzed, respectively.

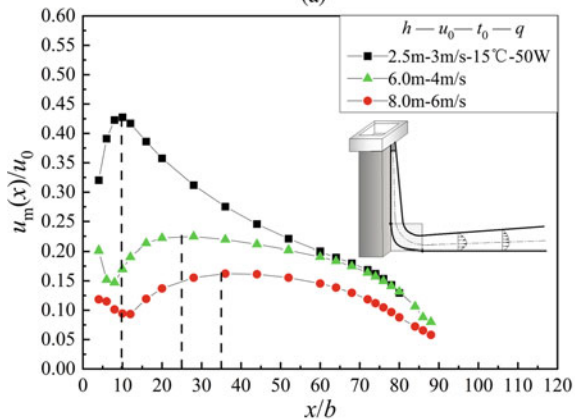
1. Circular column diameter

The velocity distributions under different column diameters are shown in Fig. 4.13. The velocity decay of the attached jet becomes slower as the column diameter d increases from 0.25 to 1.50 m. With the increase of the column diameter, the air

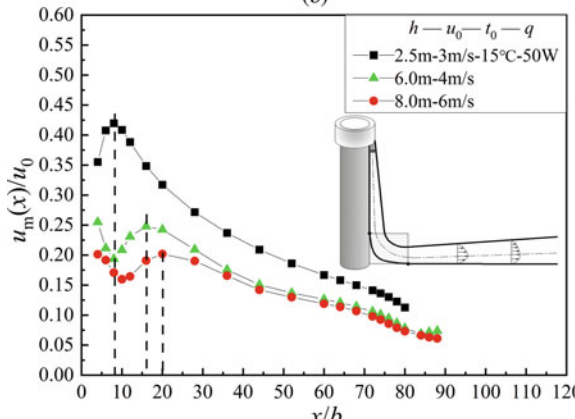
Fig. 4.11 Comparison of centerline velocities in horizontal air reservoir region of three attachment ventilation modes. **a** Vertical wall, **b** rectangular column, **c** circular column



(a)



(b)



(c)

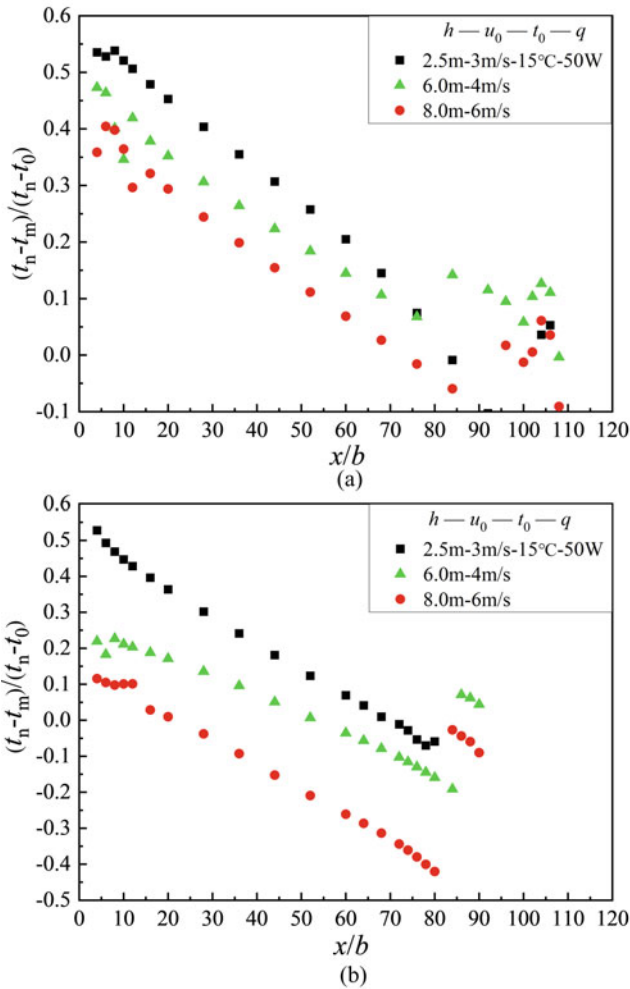


Fig. 4.12 Effect of air supply heights on centerline temperature in the horizontal air reservoir region. **a** Vertical wall, **b** rectangular column

inlet area and air supply rate are correspondingly enlarged, the thickness of the air reservoir is increased, and the horizontal jet throw is enhanced. Therefore, large-size columns are required for larger spaces.

2. Rectangular column side length

Taking the square column as an example, the velocity in the horizontal air reservoir region increases by about 0.1 m/s as the column side length increases from 0.6 to 1.0 m when the air supply velocity is 1.5 m/s, as shown in Fig. 4.14. In the horizontal reservoir zone, the smaller the column's side length a , the more significant impact of

Table 4.3 Correlations of characteristic parameters of attachment ventilation under isothermal and nonisothermal conditions

Characteristic parameters		Vertical wall attachment ventilation	Rectangular column attachment ventilation	Circular column attachment ventilation	Unified correlation equations for attachment ventilation
Isothermal	Velocity in the vertical attachment region	$\frac{u_m(y^*)}{u_0} = \frac{1}{0.01 \left(\frac{y^*}{b}\right)^{1.11}} + 1$	$\frac{u_m(y^*)}{u_0} = \frac{0.83}{0.01 \left(\frac{y^*}{b}\right)^{1.11}} + 1$		$\frac{u_m(y^*)}{u_0} = \frac{1}{0.013 \left(\frac{y^*}{b}\right)^{1.11}} + 1$
	Velocity in the horizontal air reservoir region	$\frac{u_m(x)}{u_0} = \frac{0.575}{0.0075 \left(\frac{x}{\beta} + K_h\right)^{1.11}} + 1$	$\frac{u_m(x)}{u_0} = \frac{0.575}{0.018 \left(\frac{x}{\beta} + K_h\right)^{1.11}} + 1$	$\frac{u_m(x)}{u_0} = \frac{0.575}{0.035 \left(\frac{x}{\beta} + K_h\right)^{1.11}} + 1$	$\frac{u_m(x)}{u_0} = \frac{0.575}{C \left(\frac{x}{\beta} + K_h\right)^{1.11}} + 1$ C is shape factor, C = 0.0075 for the vertical wall, C = 0.018 for the rectangular column, C = 0.035 for the circular column K_h is the height correction factor, $K_h = \frac{1}{2} \frac{h-2.5}{b}$ for the vertical wall and rectangular column, $K_h = \frac{1}{6} \frac{h-2.5}{b}$ for the circular column
Nonisothermal	Velocity in the vertical attachment region	$\frac{u_m(y^*)}{u_0} = \frac{1}{0.01 \left(\frac{y^*}{b}\right)^{1.11}} + 0.922$	$\frac{u_m(y^*)}{u_0} = \frac{1}{0.013 \left(\frac{y^*}{b}\right)^{1.11}} + 0.985$		$\frac{u_m(y^*)}{u_0} = \frac{1}{0.012 \left(\frac{y^*}{b}\right)^{1.11}} + 0.90$
	Temperature in the vertical attachment region	$\frac{t_n - t_m}{t_n - t_0} = \frac{1}{0.009 \left(\frac{y^*}{b}\right)^{1.11}} + 0.945$	$\frac{t_n - t_m}{t_n - t_0} = \frac{1}{0.011 \left(\frac{y^*}{b}\right)^{1.11}} + 0.973$		$\frac{t_n - t_m}{t_n - t_0} = \frac{1}{0.01 \left(\frac{y^*}{b}\right)^{1.11}} + 0.942$

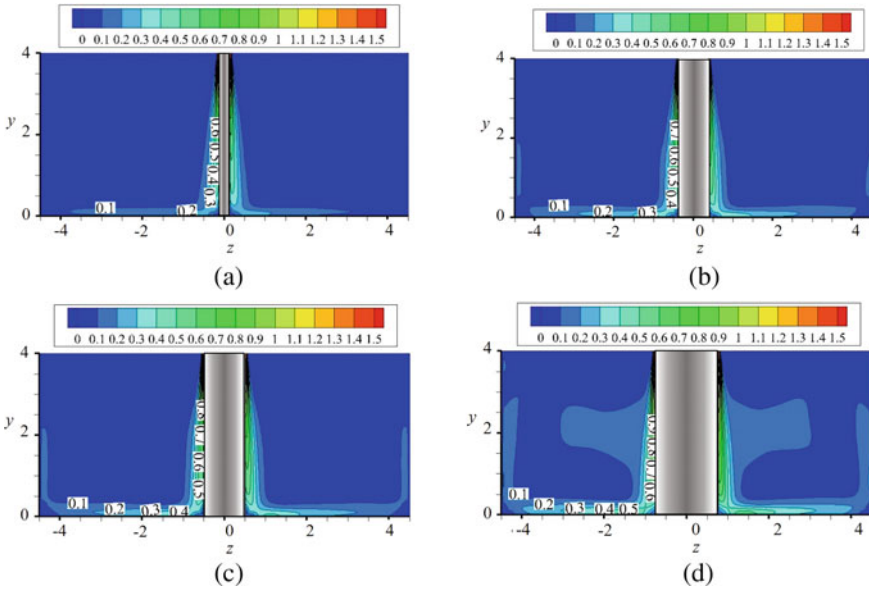


Fig. 4.13 Velocity distributions of room longitudinal section with different column diameters. **a** $d = 0.25$ m, **b** $d = 0.75$ m, **c** $d = 1.00$ m, **d** $d = 1.50$ m

the arris effect on the air movement. The increase of the column’s side length a means the augment of the air supply rate, and decrease of the occupied zone temperature.

3. Plenum

The plenum is a device that converts dynamic pressure into static pressure, and it is used to stabilize the opening airflow, and reduce the airflow turbulence and noise to ensure the slots’ air supply uniformity. The uniformed or low turbulence intensity airflow is the goal of the plenum design. So, the appropriate plenum can improve ventilation or temperature efficiency (Li et al. 2010; Hanzawa et al. 1987).

Here, plenums used for CCAV are presented as examples, which have been installed in Zhengzhou subway station, as shown in Fig. 4.15.

As illustrated in Fig. 4.15, the plenum design parameters for CCAV are as follows:

- Plenum: inner diameter $\Phi_1 = 1.26$ m, outer diameter $\Phi_2 = 2.10$ m, plenum thickness 0.60 m.
- Grille opening on the bottom of the plenum: inner diameter $\varphi_1 = 1.50$ m, outer diameter $\varphi_2 = 1.59$ m, net area $A = 0.16$ m².

In this plenum, two pieces of perforated plates with variable aperture sizes are fixed inside the plenum. For instance, when the measured airflow rate is 2000 m³/h, the plenum overall velocity non-uniformity coefficient is 6.8%, with excellent air supply uniformity, as shown in Fig. 4.15e.

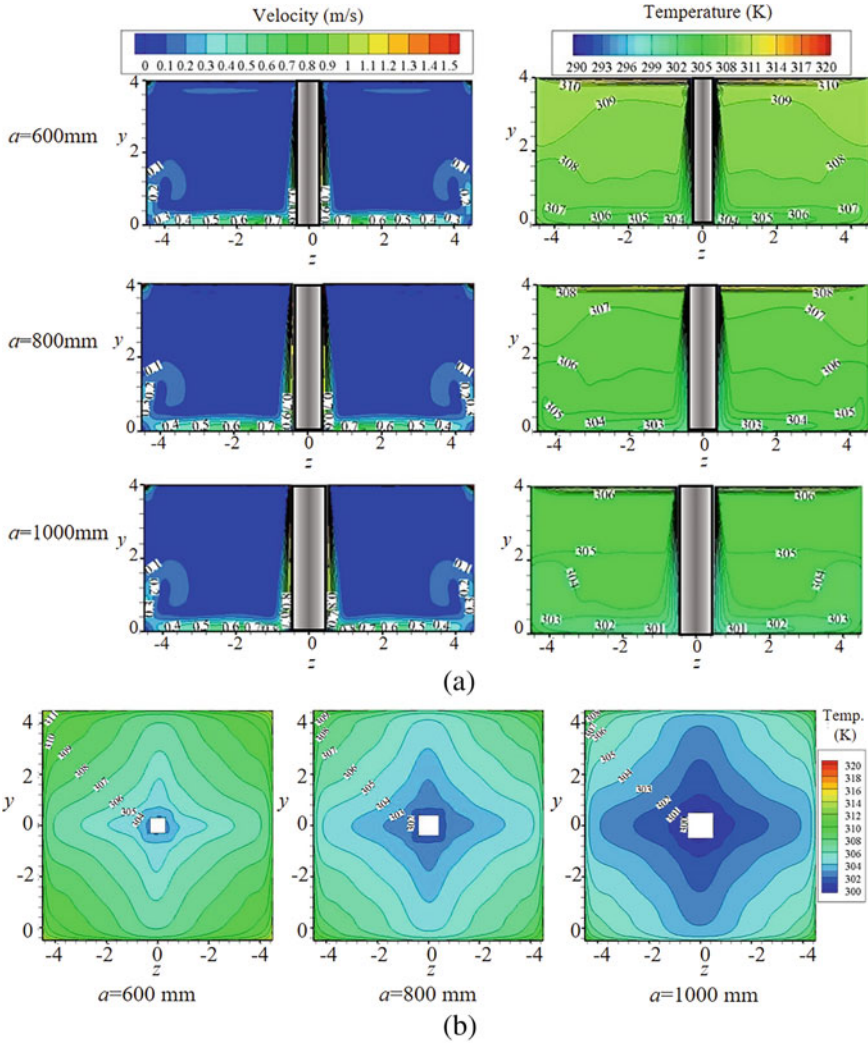


Fig. 4.14 Influence of side length of the square column. **a** Velocity and temperature field in the longitudinal section, **b** temperature field in the ankle plane

4.4.2 Control Zone and Column Spacing

From the view of human comfort, the control zone (occupied zone) is generally within 2.0 m from the floor. While for the industrial environment, the scope of the control zone is related to the service objects.

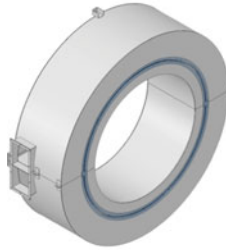
The jet effective diffusion radius and the jet envelope surface are defined as follows.

Fig. 4.15 Plenums used for CCAV. **a** Prototype, **b** installed in Zhengzhou subway station, **c** 3-dimensional structure, **d** plan view of the plenum, **e** structure and test points, **f** air velocity testing at the plenum opening

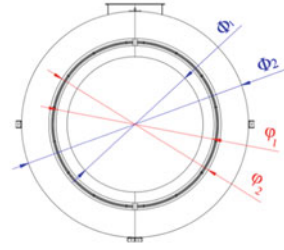


(a)

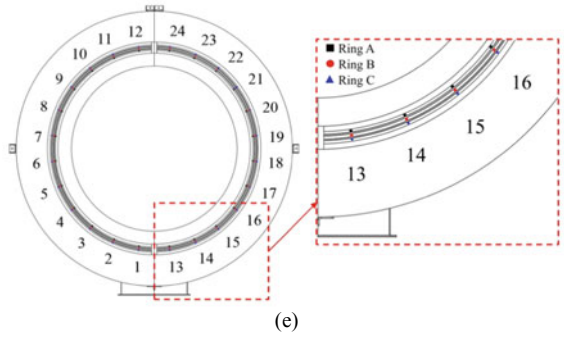
(b)



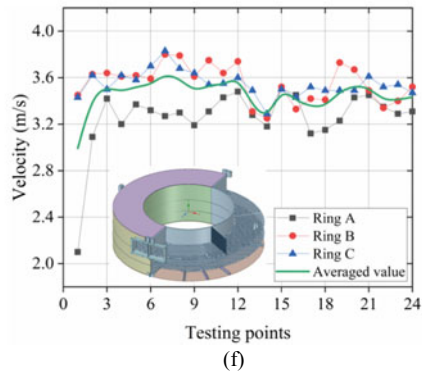
(c)



(d)



(e)



(f)

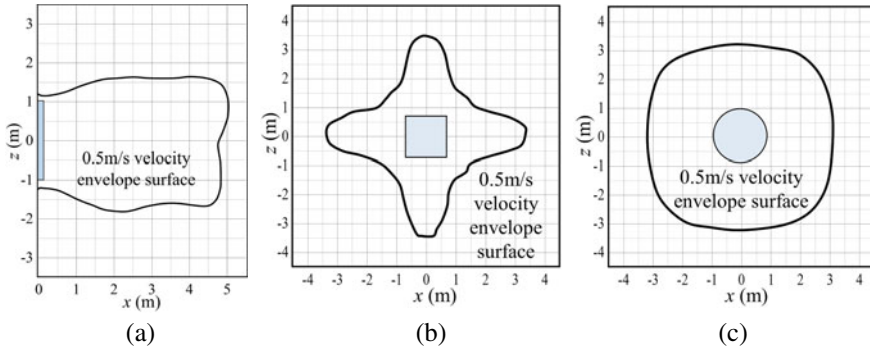


Fig. 4.16 Airflow envelope surfaces of several attachment ventilation modes. **a** VWAV, **b** RCAV, **c** CCAV

- (1) **Jet effective diffusion radius for CAV.** The horizontal distance from the attached wall to the point where the jet speed decays to 0.25 m/s (allowed air speed). For temporary staying zones, such as airport terminals, subways stations, and other temporary stops of traffic places, the allowed air speed can be taken as 0.5–0.8 m/s. For multiple columns arranged uniformly on the ground, the effective diffusion radius is $(l - d)/2$, where l is the column center spacing, and d is the column hydraulic diameter.
- (2) **Airflow envelope surface.** The interface formed by the constant velocity points, where the air velocity is specified by ventilation design. The velocity of the airflow envelope surface can be taken as 0.25–0.5 m/s (JG/T 20-1999). As shown in Fig. 4.16, there are three airflow envelope surfaces with a velocity of 0.5 m/s for different attachment ventilation modes.

1. Control zone

Figure 4.17 presents the velocity field distribution for different occupied zone lengths. The occupied zone lengths are 5.4 m (size ratio, i.e., length/height ratio $L/h = 2.1$) and 2.5 m ($L/h = 1.0$), respectively, with the same jet inlet height and location. When the length of occupied zone L changes from 5.4 to 2.6 m, the control zone shrinks, the jet flow field “thickens”, and the wall-normal velocity gradient decreases. When $L/h = 1.0$, the inducing effect of the upper exhaust outlet is more significant, which may cause a short circuit of the airflow path. When the air supply velocity increases from 1.0 to 2.0 m/s, the vortex at the far end of the horizontal air reservoir region becomes remarkably larger. It is recommended that h/L should not exceed 1:1.5.

2. Column spacing

In HVAC engineering applications, there are usually multiple columns in large spaces. When column attachment ventilation is used, those columns will lead to confluence flow in the air reservoir region (Wu 2019). As shown in Fig. 4.18, the double-column and four-column attached air supply form a “—” shaped and a “+” shaped airflow

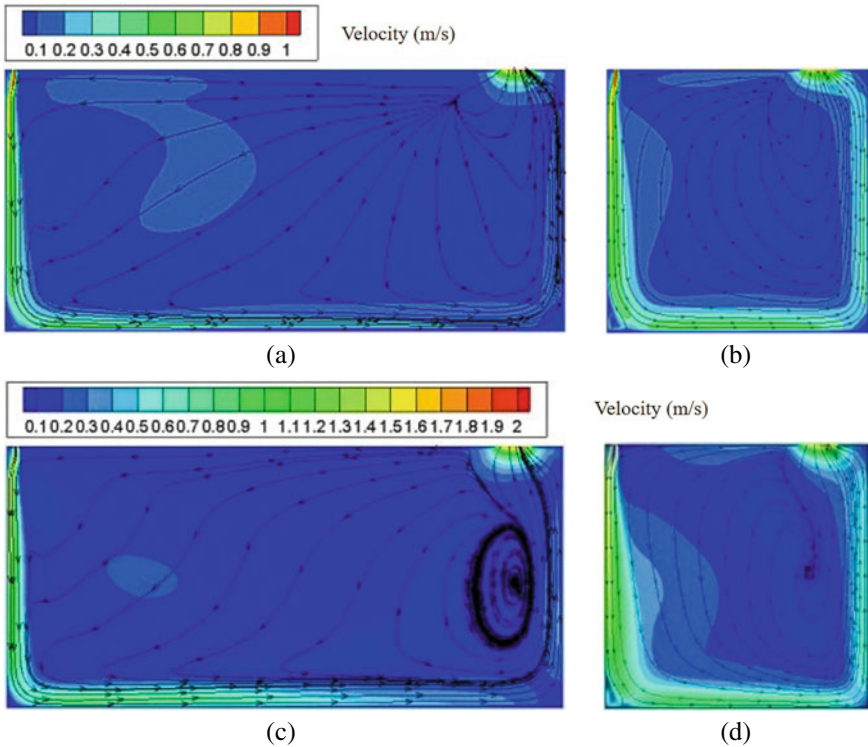


Fig. 4.17 Influence of size ratios L/h on the flow field. **a** $u_0 = 1.0$ m/s, $L/h = 2.1$, **b** $u_0 = 1.0$ m/s, $L/h = 1.0$, **c** $u_0 = 2.0$ m/s, $L/h = 2.1$, **d** $u_0 = 2.0$ m/s, $L/h = 1.0$

pattern, respectively. There seems to be an “invisible air wall” between the two columns; thus, the flow field of multi-columns can be regarded as the confined single-column attached airflow. The design of multi-column attachment ventilation can refer to the single-column attachment ventilation design method. However, their throw may be different.

The effective diffusion radius of the RCAV airflow on the horizontal floor is related to the control zone length (column spacing), indicated by the symbol l . The velocity and temperature distribution of the longitudinal section (vertical section) and human ankle cross-section ($y = 0.1$ m) are shown in Figs. 4.19 and 4.20, respectively, in the conditions of the air supply velocity $u_0 = 1.50$ m/s, air supply temperature $t_0 = 15$ °C, and floor cooling load $q = 100$ W/m². Although l is different, from 6 to 12 m, there is all apparent vertical temperature stratification, and the temperature gradient in the occupied zone (within 2.0 m above the floor) is approximately 2 °C.

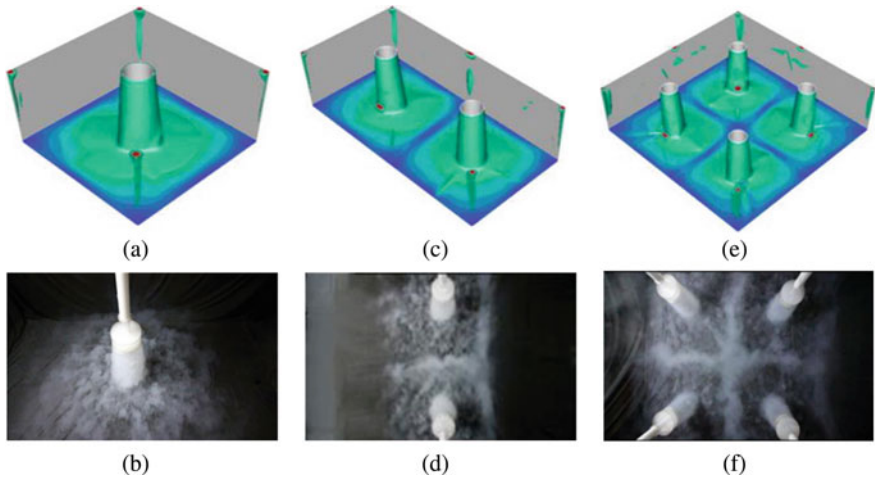


Fig. 4.18 CFD simulation and flow visualization of multi-column attachment ventilation. **a, c, e** CFD simulation, **b, d, f** flow visualization

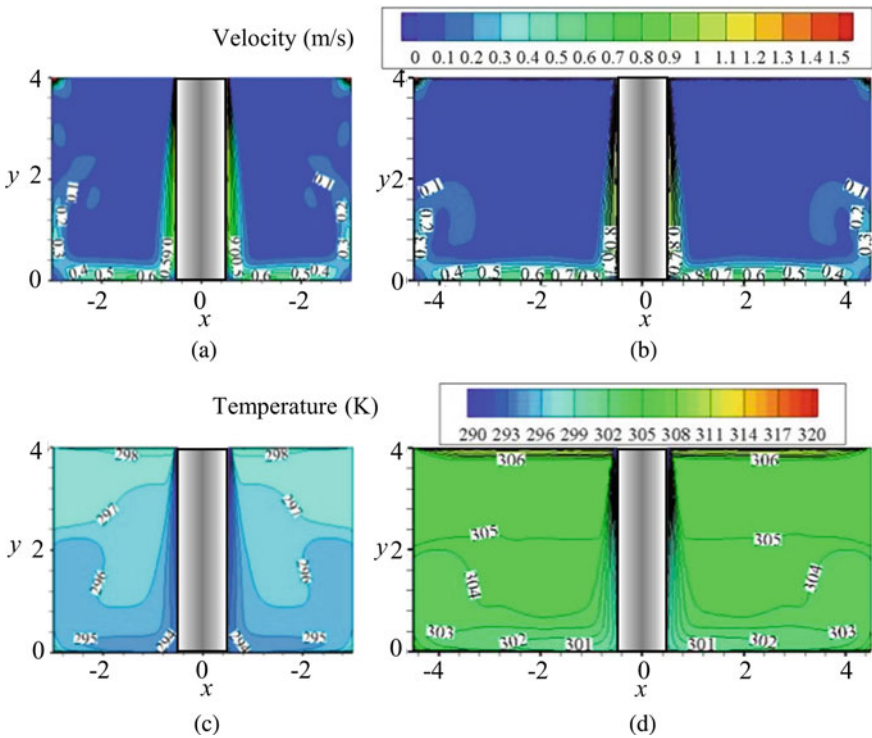


Fig. 4.19 Velocity and temperature contours of RCAV in the central longitudinal section. **a** $l = 6$ m, velocity contour, **b** $l = 9$ m, velocity contour, **c** $l = 6$ m, temperature contour, **d** $l = 9$ m, temperature contour

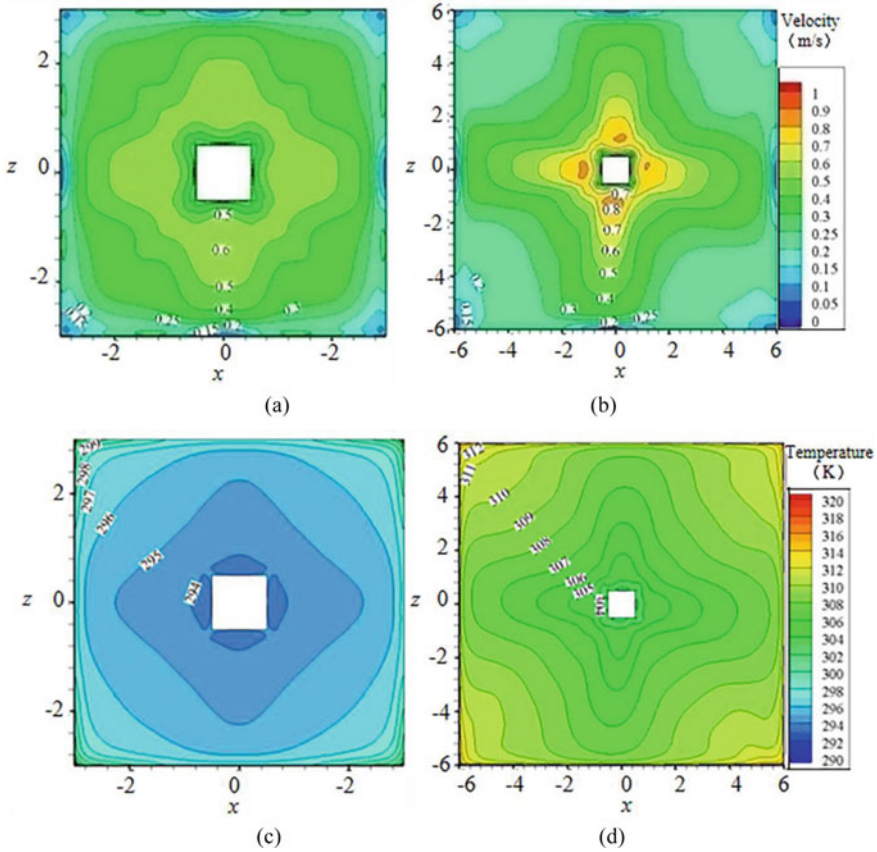


Fig. 4.20 Velocity and temperature contours of RCAV in the ankle plane ($y = 0.1$ m) of rectangular column attached air supply. **a** $l = 6$ m, velocity contour, **b** $l = 12$ m, velocity contour, **c** $l = 6$ m, temperature contour, **d** $l = 12$ m, temperature contour

4.4.3 Airflow at the Exhaust Outlet

The room airflow distribution is mainly determined by the air jet discharged from the air inlet. The exhaust outlet (suction outlet) has a limited influence due to the rapid decay of airflow velocity near the outlet. For a spherical suction outlet, the radial velocity is approximately inversely proportional to the square of the distance from the air outlet. For the long and narrow slots, the velocity is inversely proportional to their width.

Generally, the width-length ratio of the exhaust outlet is greater than 0.2, and $0.2 \leq \frac{x}{d}$ (or $\frac{x}{1.13\sqrt{F_0}} \leq 1.5$), the exhaust outlet velocity decay can be estimated by Eq. (4.24)

$$\frac{u}{u_0} = \frac{1}{9.55\left(\frac{x}{d}\right)^2 + 0.75} \quad (4.24)$$

The airflow velocity decays to about 5% of the center velocity at double diameters away from the exhaust outlet. For attachment ventilation, the exhaust outlet can be located at the upper sidewall or the center of the ceiling.

4.5 Effect of Heat Sources on Indoor Airflow

One of the ventilation tasks is eliminating the excessive heat generated by indoor heat sources. The indoor air temperature distribution mainly depends on the heat source distribution form and heat dissipation conditions. The heat sources for different industrial and civil buildings can be classified into the following modes: evenly distributed heat sources on the floor, concentrated plane heat sources, and volumetric heat sources. This section mainly introduces the effects of these three typical heat sources on the wall-attached jet movement.

4.5.1 Evenly Distributed Heat Sources on the Floor

Studies have shown that for the air supplied downwards and exhausted upwards systems with evenly distributed heat sources on the floor, such as the floor radiant heating system, the indoor vertical temperature distribution is a nearly linear profile (except for the air temperature near the floor). It can be deduced that if the full-plane heat source moves upward from $y = 0$ to a higher position of $y + \Delta y$, the vertical linear temperature profile will exist above the position of $y + \Delta y$.

Taking the CCAV as an example, the effect of evenly distributed heat sources on ventilation performance and thermal comfort is analyzed (Yin et al. 2017). Figure 4.21a shows a library reading room with a dimension of 6.0 m \times 6.0 m \times 4.0 m (length \times width \times height), in which 8 human models with a height of 1.7 m are evenly arranged. Detailed information can be found in Table 4.4. The vertical temperature gradients of the occupied zone within 2 m and the draft sensation at ankle plane $y = 0.1$ m are presented in Fig. 4.21b, c, respectively.

For a certain supply air rate and temperature, the averaged air speed in the occupied zone increases slightly with the increasing heat source intensity. The main reason is that the momentum of the thermal plume is smaller than that of the mechanical air supply. When the heat source intensity q increases from 80 to 150 W/m², the averaged flow speed in the occupied zone only increases by 0.035 m/s. However, the temperature gradient in the occupied zone remains almost unchanged at 0.45 °C. The temperature gradient gradually increases above the occupied zone due to the rise of

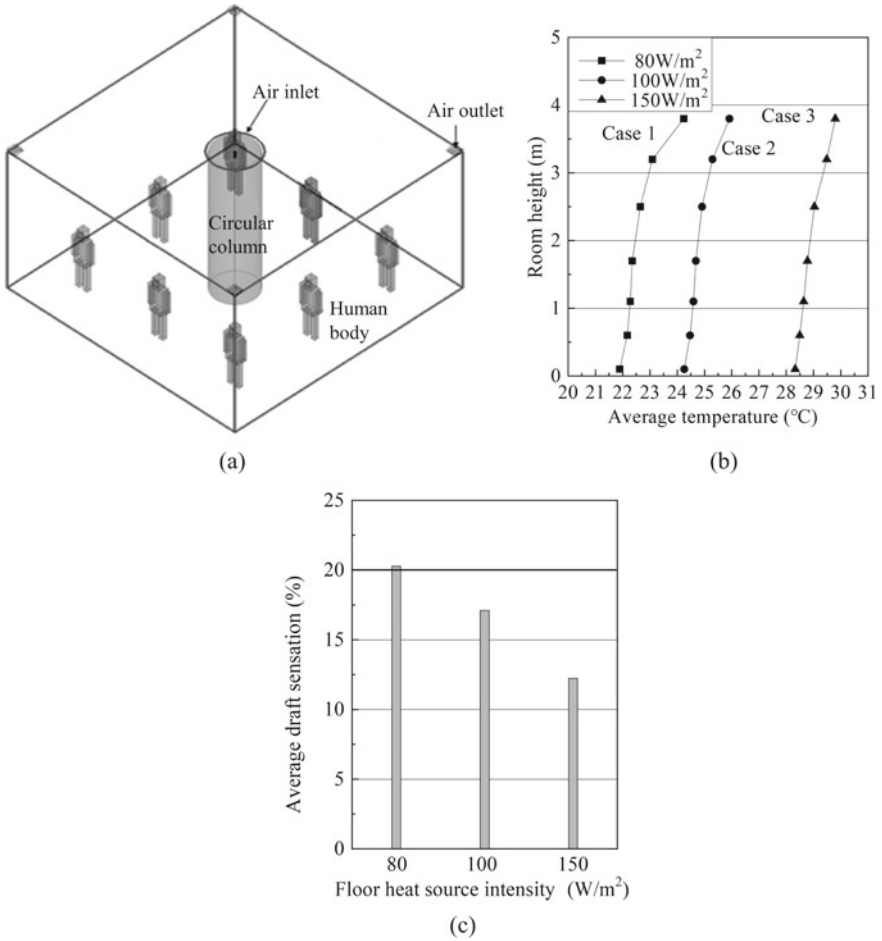


Fig. 4.21 Effect of heat sources on indoor thermal environment parameters. **a** Physical model, **b** vertical temperature gradient, **c** draft sensation at ankle plane ($y = 0.1$ m)

Table 4.4 Parameters of heat sources and circular column attachment ventilation

Case	Column diameter D (m)	Air supply height h (m)	Slot inlet width b (m)	Room size (m ³)	Supply air velocity (m/s)	Supply air temperature (°C)	Heat flux intensity (W/m ²)	Body heat dissipation (W/person)
1	1.0	4.0	0.05	6.0 × 6.0 × 4.0	2.0	17	80	161
2							100	
3							150	

the body's thermal buoyancy effect, reflecting the temperature distribution effect of the evenly distributed heat sources (Fig. 4.21b).

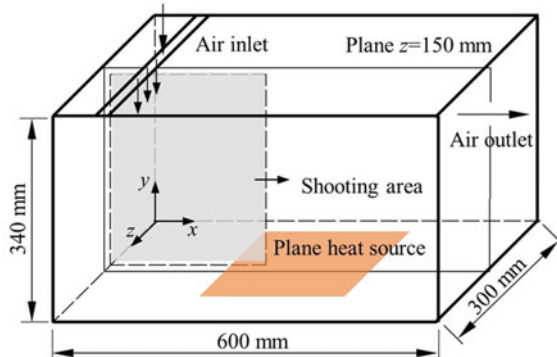
The intensity of heat sources influences indoor temperature and air speed, affecting human thermal comfort. The draft sensation at the ankle position $y = 0.1$ m decreases from 20.3 to 12.2% with the heat flux increasing (Fig. 4.21c).

4.5.2 Concentrated Plane Heat Sources

The effect of the plane heat source plume on the attached ventilation flow field is investigated by the 2D-PIV laser test method (Wang 2009). The dimension of the test chamber is $600 \text{ mm} \times 300 \text{ mm} \times 340 \text{ mm}$. The plane heat source is simulated by the electric heating wires evenly coiled on a mica plate, $160 \text{ mm} \times 160 \text{ mm}$, as shown in Fig. 4.22. During the tests, keep the indoor ambient temperature $t_n = 24$ °C, and the width of the slot inlet $b = 10$ mm. Figure 4.23 shows the velocity vector at $z = 150$ mm under $S = 45$ mm ($S/b = 4.5$), and the experimental cases are shown in Table 4.5.

Figure 4.23 clearly shows that as the intensity of the plane heat source increases from 1.0 to 3.0 W, the airflow momentum above the heat sources increases significantly, resulting in a flow velocity increase in the horizontal air reservoir region. The mechanical air supply, thermal plume, and the return air work together to produce a "large-recirculation" airflow pattern at a certain height above the floor, which grows larger with increasing heat source intensity.

Fig. 4.22 Scheme of the attachment ventilation 2D-PIV test with a plane heat source



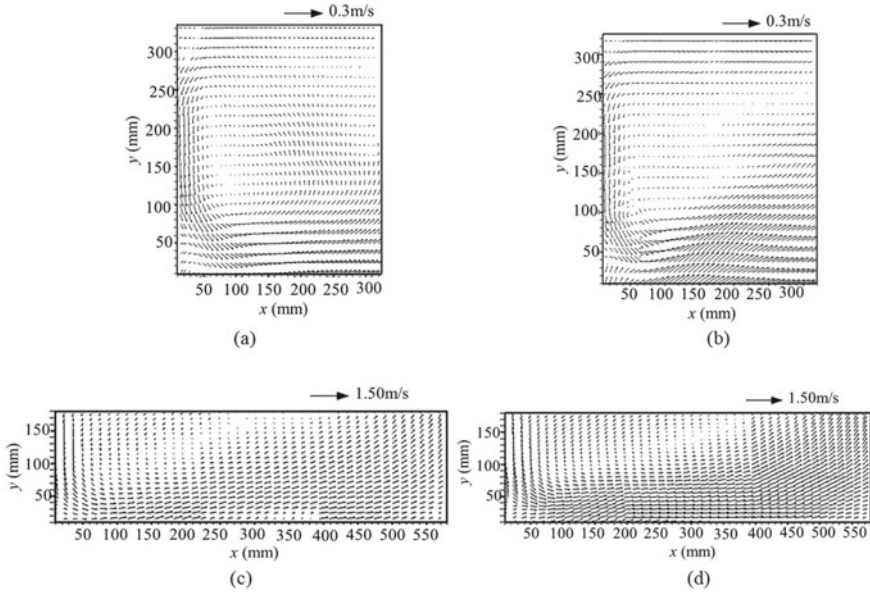


Fig. 4.23 Effect of plane heat sources on VWAV, 2D-PIV velocity vector diagram in plane $z = 150$ mm. **a** Longitudinal section, $u_0 = 0.3$ m/s, $Q = 1.0$ W, **b** longitudinal section, $u_0 = 0.3$ m/s, $Q = 3.0$ W, **c** horizontal air reservoir region, $u_0 = 1.5$ m/s, $Q = 1.0$ W, **d** horizontal air reservoir region, $u_0 = 1.5$ m/s, $Q = 3.0$ W

Table 4.5 Experimental cases of 2D-PIV of attachment ventilation with a plane heat source

Case	Heat source intensity Q (W)	Supply air temperature t_0 (°C)	Supply air temperature difference Δt (°C)	Supply air velocity u_0 (m/s)	Ar
1	1.0	28.8	4.8	0.3	0.0177
2		27.6	3.6	1.0	0.0012
3		27.2	3.2	1.5	0.0005
4	2.0	33.3	9.3	0.3	0.0339
5		31.2	7.2	1.0	0.0024
6		30.6	6.6	1.5	0.0010
7	3.0	37.7	13.7	0.3	0.0493
8		35.1	11.1	1.0	0.0036
9		33.6	9.6	1.5	0.0014

4.5.3 Volumetric Heat Sources

Volumetric heat sources, such as industrial workshops, ordinary household appliances, and modern electronic equipment, are common in buildings. The thermal plumes generated by these heat sources will affect the air distribution of attachment ventilation (Cui 2010).

1. Influence of volumetric heat source intensity on the air reservoir

The influence of volumetric heat source intensity on the air reservoir is investigated by 2D-PIV. The test chamber used has been introduced in Sect. 4.5.2. A volumetric heat source is arranged in the center of the test chamber with a size of $80 \text{ mm} \times 80 \text{ mm} \times 90 \text{ mm}$, as shown in Fig. 4.24. Details of the experiment cases are shown in Table 4.6.

In view of the symmetry of the chamber, half of the flow velocity field ($x = 0\text{--}335 \text{ mm}$) is measured by 2D-PIV, as shown in Fig. 4.25. A continuous thermal plume is produced by the buoyancy above the heat source, which has a significant induction effect on the horizontal airflow reservoir. Figure 4.25c, d show a clearly horizontal piston flow similar to the displacement ventilation in the occupied zone. As the heat source intensity increased from 1.0 to 10 W, the induction effect of thermal convection on the upward movement of horizontal piston flow is further strengthened, and a “large-recirculation” flow field is formed in the upper-middle part of the space (Fig. 4.25d).

Fig. 4.24 2D-PIV test chamber of attachment ventilation with a volumetric heat source

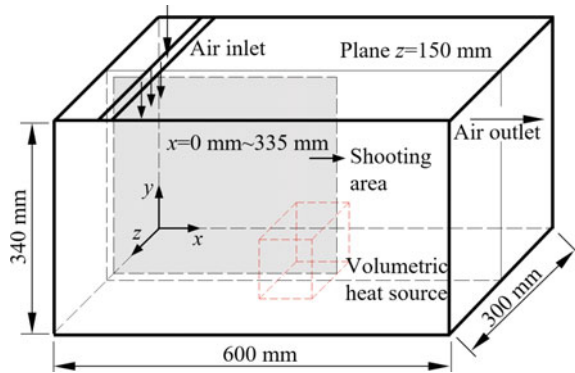


Table 4.6 Experiment cases of 2D-PIV of attachment ventilation (volumetric heat source)

Case	Volumetric heat source intensity (W)	Air inlet location S/b	Supply air velocity u_0 (m/s)
1	1	4.5	0.3, 1.0, 1.5
2	5		
3	10		

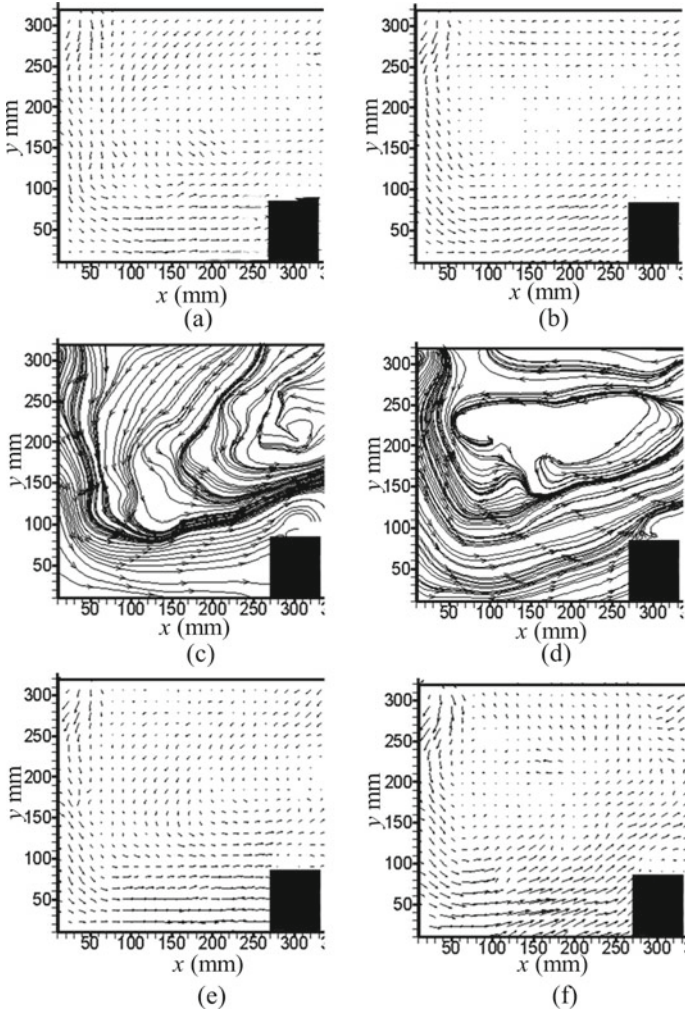


Fig. 4.25 Velocity vector and streamline diagram, effect of volumetric heat sources on attachment ventilation flow field. **a** $u_0 = 1.0$ m/s, $Q = 1.0$ W, velocity vector, **b** $u_0 = 1.0$ m/s, $Q = 10$ W, velocity vector, **c** $u_0 = 1.0$ m/s, $Q = 1.0$ W, streamline, **d** $u_0 = 1.0$ m/s, $Q = 10$ W, streamline, **e** $u_0 = 1.5$ m/s, $Q = 1.0$ W, velocity vector, **f** $u_0 = 1.5$ m/s, $Q = 10$ W, velocity vector

2. Effect of heat source intensity on the vertical attachment region

The influence of volumetric heat source intensity on the airflow in the vertical attachment region is investigated in this section. The decay of the dimensionless centerline velocity u_m/u_0 with dimensionless distance y^*/b is shown in Fig. 4.26 for wall-attached jets under various volumetric heat source intensities. In the vertical attachment region, when $u_0 = 1.5$ m/s, the centerline velocity distribution of the vertical

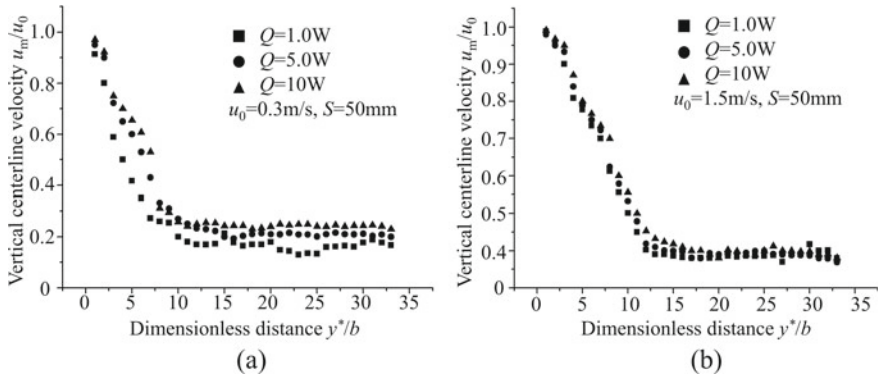


Fig. 4.26 Jet time-averaged velocity as a function of volumetric heat sources in the vertical attachment region. **a** $u_0 = 0.3\text{ m/s}$, **b** $u_0 = 1.5\text{ m/s}$

attachment region presents strong self-similarity under different heat source intensities (Fig. 4.26b). The inertial forces mainly drive the airflow in this region, and the influence of the thermal plume can be negligible. However, the thermal plume affects the centerline velocity when the air supply velocity is lower ($u_0 = 0.3\text{ m/s}$ or less). It can be observed that the centerline velocity increases very slowly with a high heat source intensity enhancement. In fact, the jet velocity of $u_0 = 0.3\text{ m/s}$ has the same order of magnitude as the velocity of the thermal plume. Therefore, for the air supply velocity of 1–5 m/s, the influence of heat sources on the airflow velocity can be ignored in the vertical attachment region.

3. Heat sources off the floor

In a built environment, most of heat sources are usually placed at a certain distance away from the floor, such as office electronics, household electrical equipment, and heat transfer in windows, etc. The normal distance between the heat source bottom and the floor is represented by y ($y > 0$). With the increase of y , the influence of the heat source is further weakened on the flow field close to the floor, and the thermal stratification interface height will also rise (Zhao 2010; Yin et al. 2017; Yang 2019) (see Figs. 4.27 and 4.28).

Figure 4.27 shows the effect of y on the indoor air velocity distribution. The air movement path is as follows.

Jet inlet (air inlet) \rightarrow vertical wall-attached flow \rightarrow impinging on the floor \rightarrow horizontal air reservoir \rightarrow upward movement together with thermal plumes \rightarrow jet entraining air and moves to the ceiling (exhausted by the return air outlet or air outlet).

The influence of y on the indoor temperature distribution is shown in Fig. 4.28. With the heat source's elevation, the thermal plume's induction effect on the lower occupied zone's airflow gradually decreases. However, the induction effect on the upper room zone's airflow is gradually increased. The thermal stratification is quite remarkable, and the ventilation efficiency is improved to some extent. We can

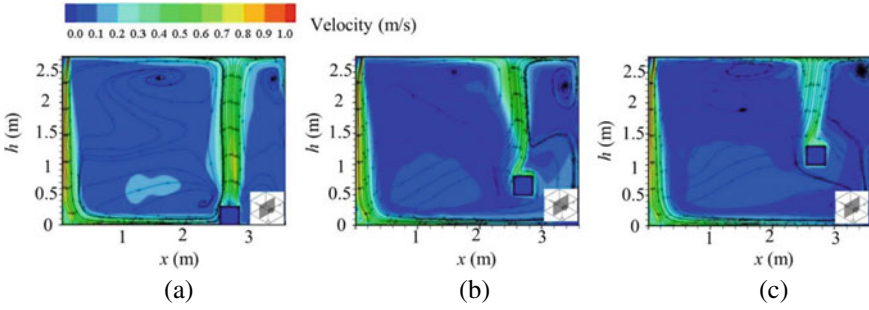


Fig. 4.27 Flow field of AWAV affected by heat sources above the floor. **a** $y = 0$ m, **b** $y = 0.5$ m, **c** $y = 1.0$ m

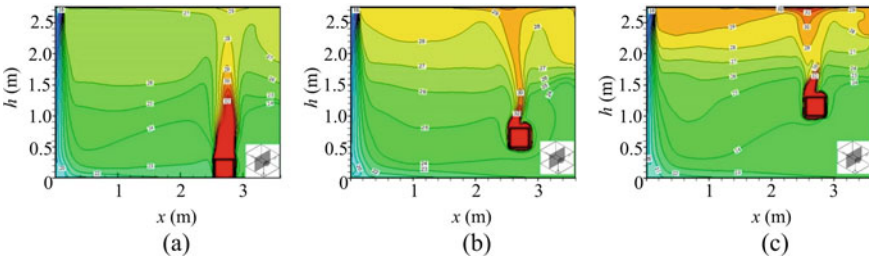


Fig. 4.28 Temperature field of AWAV affected by heat sources above the floor. **a** $y = 0$ m, **b** $y = 0.5$ m, **c** $y = 1.0$ m

conclude that it is beneficial to the thermal environment control in the occupied zone to place equipment with high heat intensity at a high position above the floor in a workshop.

4.6 Human Movement Effect on Airflow Field of Attachment Ventilation

Airflow affects the thermal comfort of the human body. Conversely, human activities will also directly impact indoor airflow. This section discusses the effect of human movement on the indoor flow field for VWAV (Cao 2016).

The influence of human movement speeds on the indoor flow field is investigated. The room dimension is $4.0\text{ m} \times 4.0\text{ m} \times 2.5\text{ m}$, the slot inlet size is $1.0\text{ m} \times 0.05\text{ m}$, and the exhaust outlet size is $0.2\text{ m} \times 0.5\text{ m}$, as shown in Fig. 4.29. The human body is simplified as a cuboid of $1.7\text{ m} \times 0.3\text{ m} \times 0.2\text{ m}$ (height \times width \times thickness) (Zhang and Gu 2009; GB/T 13547-1992). The dynamic grid technique is used to simulate human movement.

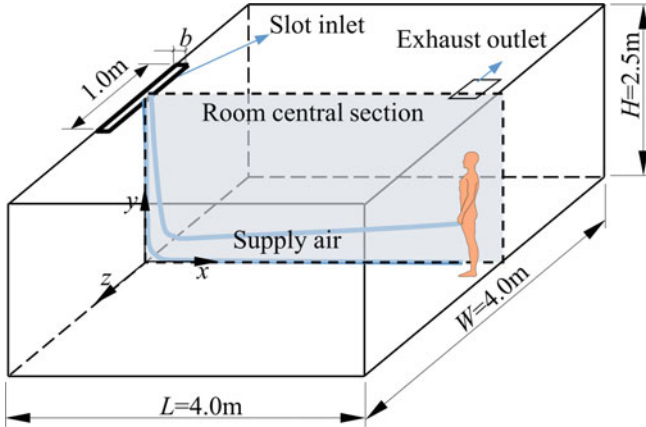


Fig. 4.29 Physical model and CFD calculation domain

The walking speeds are taken as 0.9 m/s (slow speed), 1.2 m/s (normal speed), and 1.8 m/s (fast speed) (Han and Wang 2011), and the corresponding human body heat loss is 115 W/m², 150 W/m², and 220 W/m², respectively (Fanger et al. 1988). The floor heat flux intensity is 30 W/m² (Zhao 2010). The detailed information is listed in Table 4.7. For the sake of discussion, the coordinate origin is located in the central section (see Fig. 4.29).

When the human body is stationary ($t = 0$), the indoor flow field is shown in Fig. 4.30a. The jet velocity decay in the vertical attachment region is almost independent of the human body, and the mean air velocity in the horizontal air reservoir region is about 0.2 m/s. To some extent, the human body is equivalent to a stationary heat source, and the thermal plume with a velocity of 0.3 m/s is formed above the human body.

The indoor flow field changes continuously during human movement. When VWAV air supply velocity is 1.0 m/s, walking speed is 1.2 m/s, and the initial position is $x = 3.5$ m, the flow fields corresponding to different human movement positions ($x = 0.9, 2.6, 1.7, 0.8$ m) are shown in Fig. 4.30. In the initial stage of the movement, a large induced wake velocity is formed in the far area behind the human body, reaching 2.0 m/s or more, which is about twice than the speed of human movement. The airflow velocity near the body (3–5 cm) is about 1.2 m/s, the same as the

Table 4.7 Human movement speed and relevant parameters

Movement path	Movement speed (m/s)	Human heat dissipation (W/m ²)	Supply air velocity u_0 (m/s)	Supply air temperature t_0 (°C)
$x = 3.5$ m ↓ $x = 0.9$ m	0.9 (slow speed)	115	1.0 (ACH = 4.5)	17
	1.2 (normal speed)	150		
	1.8 (fast speed)	220		

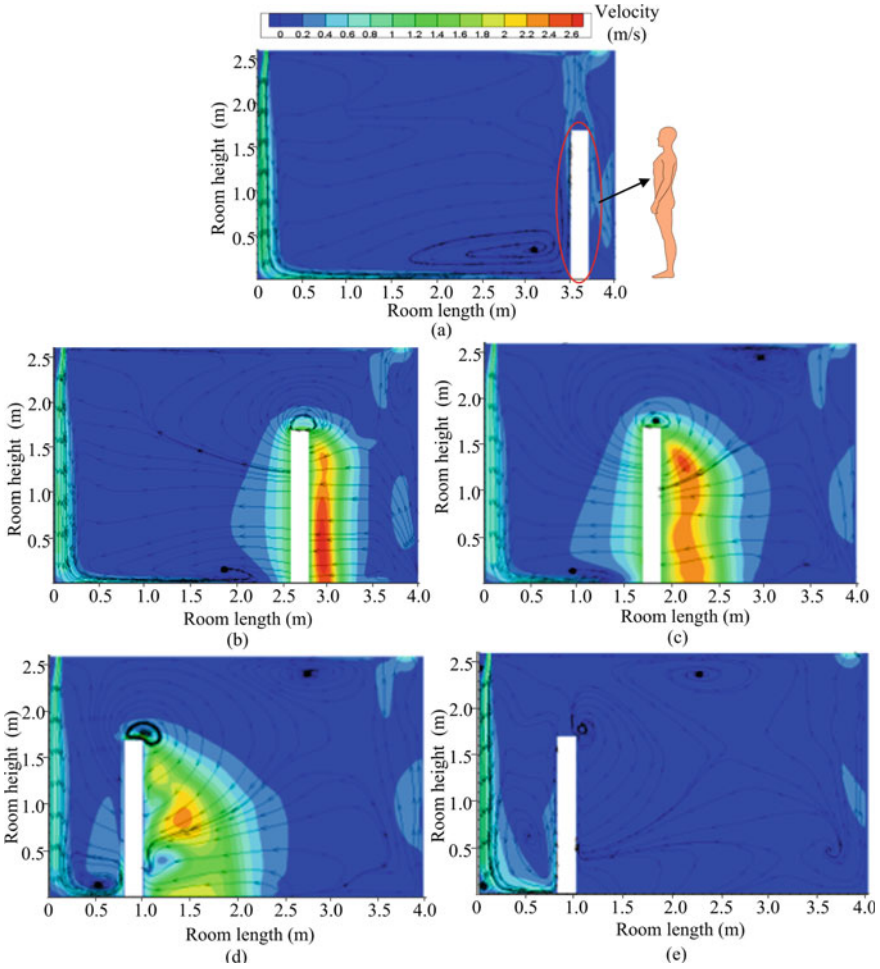


Fig. 4.30 Influence of human movement on flow field, at room central section, windward walking speed 1.2 m/s. **a** $x = 3.5$ m (starting point), stationary, 0 m/s, **b** $x = 2.6$ m, **c** $x = 1.7$ m, **d** $x = 0.8$ m, **e** $x = 0.8$ m, 4.0 s after pausing

human movement speed. The wake influence further expands when walking close to the air supply side. In the vertical direction, human movement only influences the air velocity in the occupied zone (within 2.0 m above the floor). In the horizontal direction, the influence occurs in front of the human body within 0.6 m.

There is a spherical vortex overhead during human walking. Once the human movement stops, the airflow speed in the occupied zone quickly diminishes to 0.2 m/s (ambient air speed) within 1.0 s. In fact, the influence of human movement on indoor airflow only lasts for a short time, about 1.0–4.0 s. The higher the air change rate, the shorter the recovery time of the flow field.

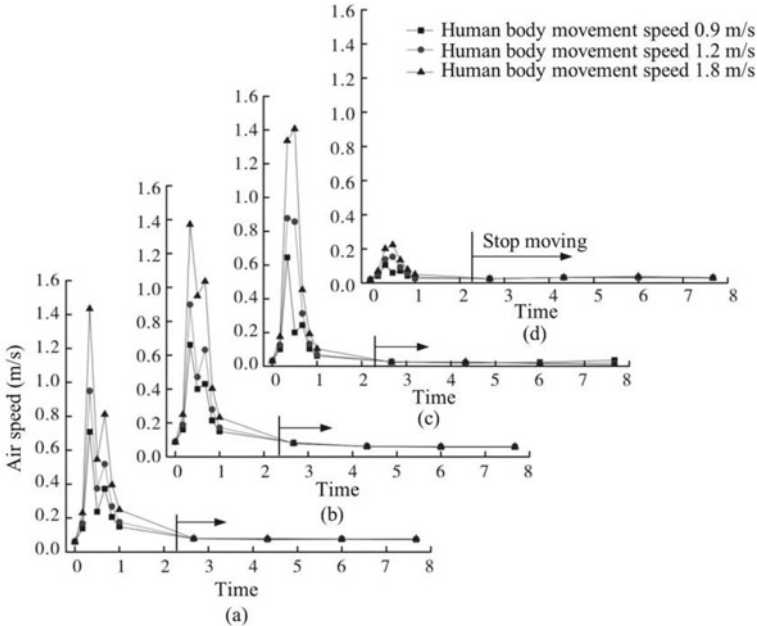


Fig. 4.31 Influence of human movement on indoor air speed with different heights. **a** 0.5 m height, **b** 1.0 m height, **c** 1.5 m height, **d** 2.0 m height. *Note* See Fig. 4.29, central longitudinal section $z = 0$ m, height $y = 0.5, 1.0, 1.5$ and 2.0 m

It is found that there is no significant difference in air speed within the range of human height in the occupied zone, regardless of whether the movement speed is 0.9 m/s or 1.8 m/s. However, outside the occupied zone, a very low air speed exists, approximately 0.2 m/s. Figure 4.31 shows the indoor air velocities under different human motion speeds. It can be concluded that when the human body moves slowly, the affected zone is merely within the scope of the occupied zone, and the flow field can quickly recover once the movement stops. The most important factor affecting the indoor flow field is jet momentum.

4.7 Effect of Wall Temperature

The thermal conditions at the jet attached-wall surface are usually approximated with reasonable accuracy to be constant surface temperature or constant surface heat flux. Natural convection heat transfer occurs at the vertical jet-attached surface due to the temperature difference between the wall and the jet. The flow regime in natural convection is governed by the dimensionless Grashof number Gr , which represents the ratio of the buoyancy force to the viscous force acting on the airflow.

$$Gr = \frac{g\beta(T_s - T_\infty)L_c^3}{\nu^2} \quad (4.25)$$

where

- g = gravitational acceleration, m/s²;
- β = coefficient of volume expansion, 1/K;
- T_s = temperature of the surface, °C;
- T_∞ = indoor air temperature, air far from the surface, °C;
- L_c = characteristic length of the wall, m;
- ν = kinematic viscosity of the fluid, m²/s.

In comparison, the role played by the Reynolds number in forced convection is played by the Grashof number in natural convection. As such, the Grashof number provides the main criterion in determining whether the flow is turbulent or not in natural convection. For vertical walls, the plume is observed to become turbulent at Grashof numbers greater than 3×10^8 .

When the vertical wall surface is subjected to the attached jet, this issue involves both natural and forced convection. The relative importance of each mode of heat transfer can be determined by Gr/Re^2 . Natural convection effects can be negligible if $Gr/Re^2 \ll 1$, free convection dominates and the forced convection effects can be negligible if $Gr/Re^2 \gg 1$, and both effects are significant and should be considered if $0.1 \leq Gr/Re^2 \leq 10$.

When the wall temperature is higher than the indoor air temperature ($t_w > t_n$), a convective flow along the vertical wall is generated (Fig. 4.32a); when the wall temperature is lower ($t_w < t_n$), the airflow will move downward due to cooling (Fig. 4.32b). If the thermal convection takes the same direction as the mechanical force, assisting mixed convection is formed; otherwise, opposing mixed convection is generated (Zhang et al. 2001; Rohsenow et al. 1992), as shown in Fig. 4.32c–d.

Here is an example of the wall temperature's influence on attachment ventilation. The air supply temperature $t_0 = 15$ °C, the air supply height $h = 4.0$ m, and the air inlet size is $2.0 \text{ m} \times 0.05 \text{ m}$. More information is shown in Table 4.8.

Figures 4.33 and 4.34 show the indoor velocity and temperature field under different wall temperatures. With the increase in wall temperature, the indoor air velocity field does not change significantly, whereas the indoor air temperature does increase to a certain extent. It is observed that the temperature stratification takes place obviously in the entire room.

Figure 4.35 shows the influence of wall temperature on the jet centerline velocity and temperature. When $Gr/Re^2 \leq 0.1$, due to the larger momentum of mechanical ventilation, the effect of natural convection generated by the nonadiabatic wall can be ignored. The jet velocity in the vertical attachment region is almost identical to that of the adiabatic wall, see Fig. 4.35. It means that if the wall-attached jet flows along the interior wall, the wall temperature's effect on the supply flow field may be ignored. Otherwise, the wall convective heat transfer should be taken into account.

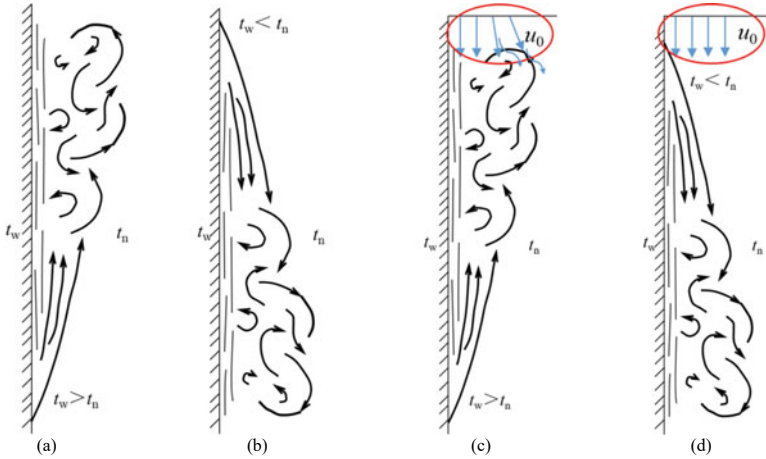


Fig. 4.32 Natural and mixed convection resulting from the wall temperature difference. **a** $t_w > t_n$, **b** $t_w < t_n$, **c** opposing mixed convection, **d** assisting mixed convection

Table 4.8 Room wall temperature t_w and air supply parameters of attachment ventilation

Supply air velocity u_0 (m/s)	Room wall temperature t_w (°C)	Gr/Re^2	Note
1.5	15	0.00	$t_w = t_0$, each wall's temperature is t_w
	20	0.23	When $0.1 \leq Gr/Re^2 \leq 10$, the effect of natural convection heat transfer on the wall cannot be ignored
	25	0.45	
	30	0.66	
	35	0.88	
3.2	25	0.11	$Gr/Re^2 < 0.1$, mechanical ventilation
4.0		0.06	

4.8 Effect of Wall Roughness

In practical attachment ventilation applications, rough elements or protruding objects may be on the wall surface, so the wall cannot be considered smooth. The relative roughness is represented by k/δ , where δ and k denote the boundary-layer thickness and height of the roughness elements, respectively. The critical point of the flow through a rough wall surface is that the relative roughness k/δ decreases along the wall when k remains constant because δ increases downstream. This circumstance causes the front of the wall to behave differently from its rearward portion as far as the influence of roughness on drag is concerned (Schlichting 1995).

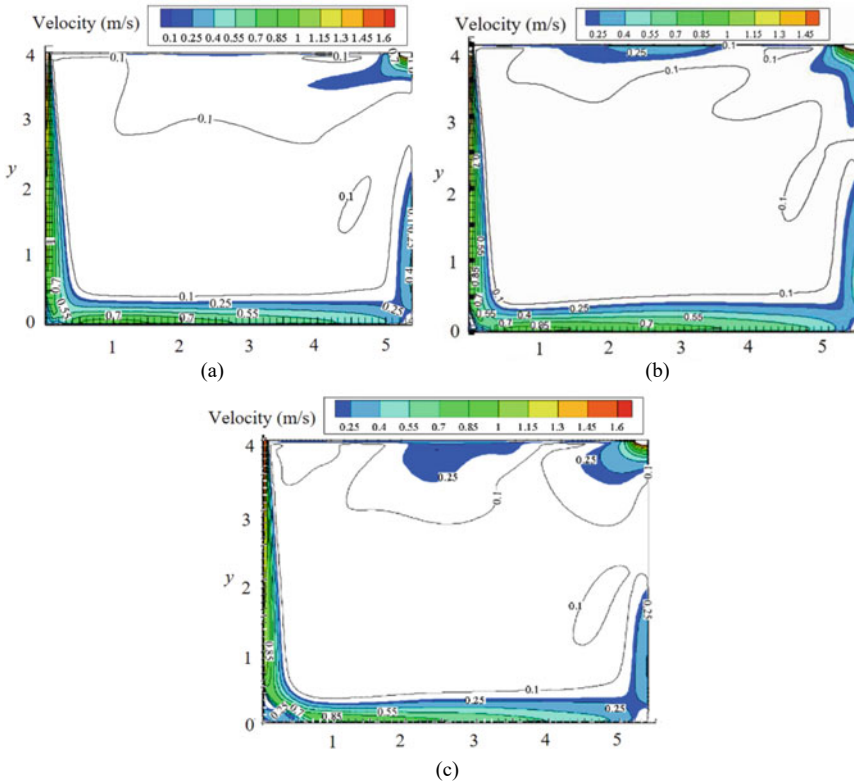


Fig. 4.33 Influence of wall temperature on indoor flow field with $u_0 = 1.5$ m/s. **a** $t_w = 15$ °C, **b** $t_w = 20$ °C, **c** $t_w = 30$ °C

The amount of roughness which is considered “admissible” in engineering applications is that maximum height of individual roughness elements which causes no increase in drag compared with a smooth wall (Schlichting 1995). Turbulent boundary layer roughness has no effect if all protruding objects are contained within the sublayer. However, from the view of ventilation, it seems more convenient to specify a value of relative roughness k/b . We can obtain the allowed value of k/b from the experiments.

Here, a case study about the attachment length and centerline velocity under different roughness heights is presented by the 2D-PIV laser velocity measurement technique. The experimental apparatus is shown in Fig. 4.36 (photo shooting area: $x = 10\text{--}250$ mm, $y = 12\text{--}330$ mm), the test chamber dimension is 600 mm \times 300 mm \times 340 mm, and the slot inlet width $b = 10$ mm. The roughness elements are arranged evenly, and the absolute roughness heights k are 0.5 mm, 1.0 mm, and 2.0 mm, respectively. Detailed information can be found in Table 4.9.

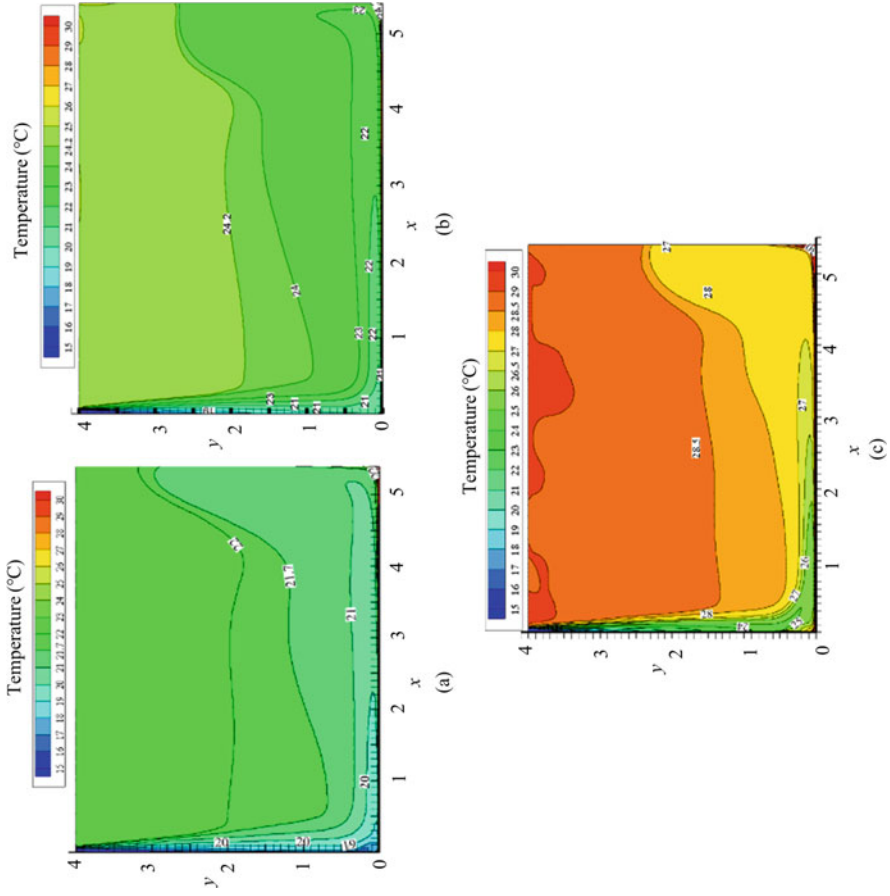


Fig. 4.34 Influence of wall temperature on temperature stratification with $u_0 = 1.5$ m/s. **a** $t_w = 15^\circ\text{C}$, **b** $t_w = 20^\circ\text{C}$, **c** $t_w = 30^\circ\text{C}$

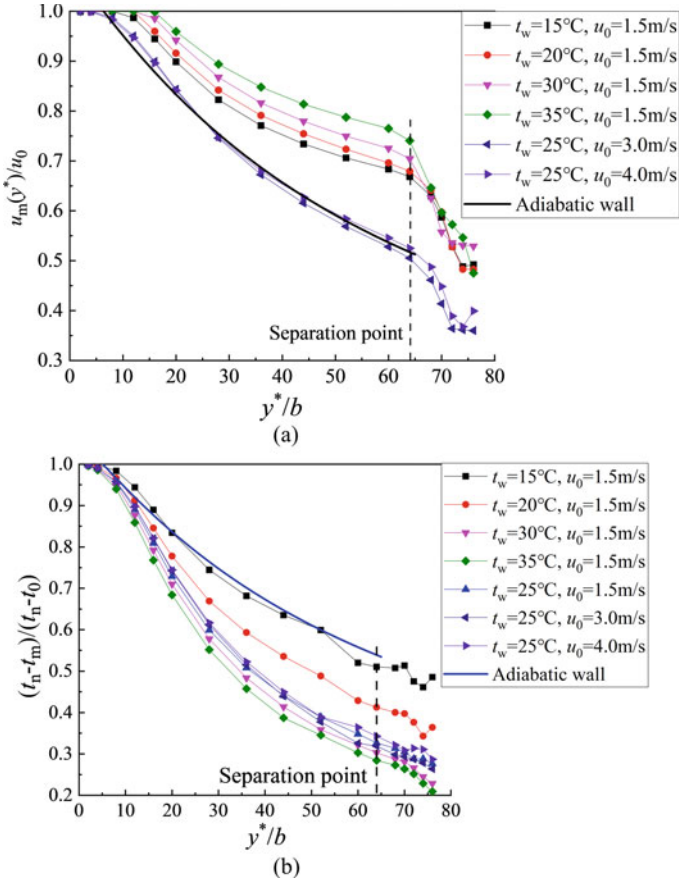


Fig. 4.35 Effect of wall temperature on the flow field of attachment ventilation ($t_0 = 15^\circ\text{C}$). **a** Centerline velocity, and **b** excess temperature in the vertical attachment region

Fig. 4.36 Experimental diagram of the room with a rough surface

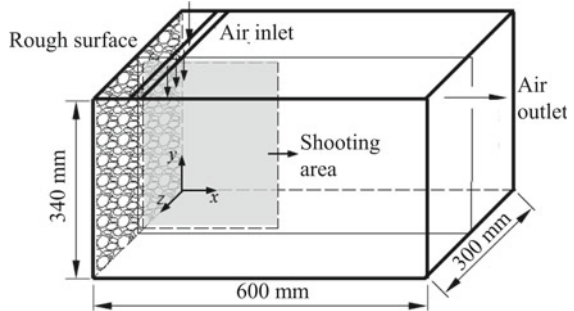


Table 4.9 Experimental cases for studying the effect of roughness on vertical wall attachment ventilation

Relative roughness, k/b	Location of the air inlet, S/b	Supply air velocity, u_0 (m/s)	Supply air temperature, t_0 /indoor air temperature, t_n ($^{\circ}\text{C}$)
0	7.5	0.3, 1.0, 1.5	24 (isothermal conditions)
0.05			
0.1			
0.2			

1. Effect of roughness on attachment length

The attachment length is defined as the distance between the initial jet attachment point y_1 and the separation point y_2 . The airflow velocity vector graphs under different roughness heights measured by 2D-PIV are shown in Figs. 4.37 and 4.38. It can be found that with the increase of the roughness height, the attachment point location is little altered, and the separation point moves slightly downwards closer to the floor (see Fig. 4.39). It means that the roughness elements may hinder the Coanda effect. In fact, the stronger the Coanda effect, the longer the vertical attachment region. The experiment shows that the central position of the “recirculating vortex”, in the upper left corner area (at $y = 265$ mm, see Fig. 4.37; at $y = 290$ mm, see Fig. 4.38) between the air supply jet and the vertical sidewall, is not significantly affected by the roughness. However, the separation point location y_2 moves further downwards (see Fig. 4.38).

From the flow field measured by 2D-PIV (Fig. 4.39), we can find that with the increase of air velocity, the roughness elements’ influence on the attachment length will gradually decrease. When u_0 increases to 1.5 m/s, the attachment length is almost irrelevant to the roughness.

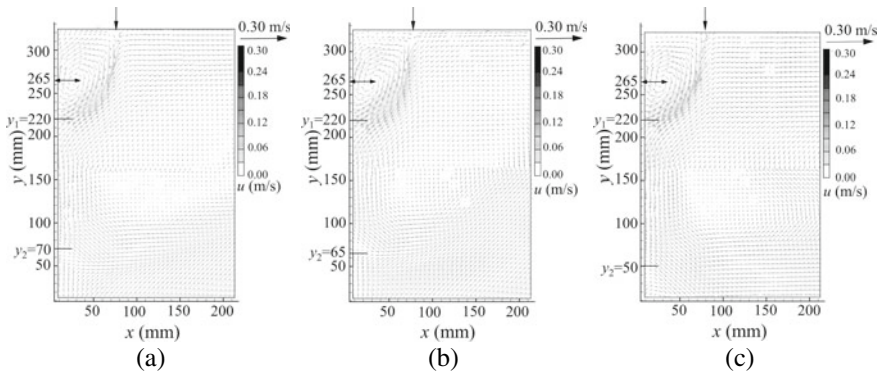


Fig. 4.37 Effect of sidewall roughness on attachment length, $u_0 = 0.3$ m/s. **a** $k/b = 0.05$, **b** $k/b = 0.1$, **c** $k/b = 0.2$

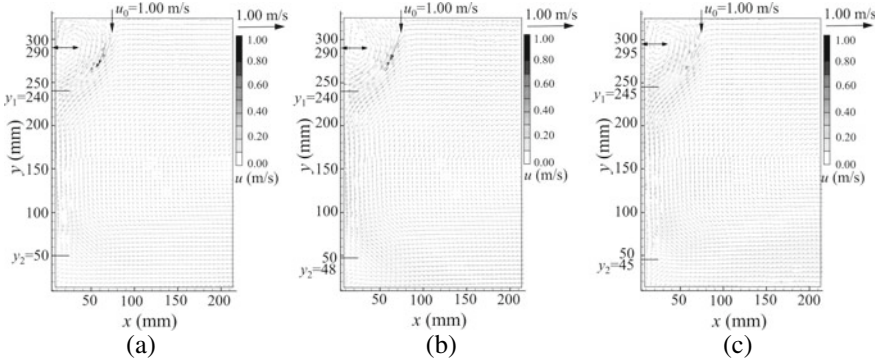
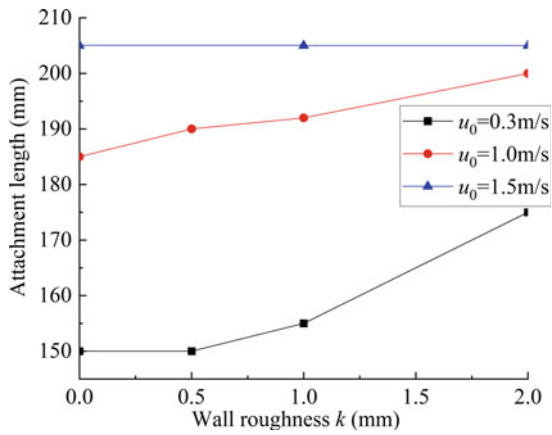


Fig. 4.38 Effect of sidewall roughness on attachment length, $u_0 = 1.0$ m/s. **a** $k/b = 0.05$, **b** $k/b = 0.1$, **c** $k/b = 0.2$

Fig. 4.39 Attachment length as a function of roughness and air supply velocities



2. Effect of roughness on centerline velocity

The jet centerline velocities under different k/b are shown in Fig. 4.40. It can be seen that in the range of $0 \leq k/b \leq 0.2$, the centerline velocity decays of the wall-attached jet are basically identical. The roughness does not significantly influence the centerline velocity.

For the deflected wall-attached jet, taking $S/b = 7.5$ as an example, the centerline velocity decay is shown in Fig. 4.40. In the range of $y^*/b < 12$, the supply air jet has not yet attached to the sidewall, the centerline velocity decays almost as fast as that of the free jet. When the S/b exceeds the extreme attachment distance S_{max} , the jet fails to attach to the sidewall, leading to poor attachment ventilation performance. Hence, it is recommended that the air supply opening be installed as close as possible to the adjacent wall to ensure the attachment ventilation effectiveness.

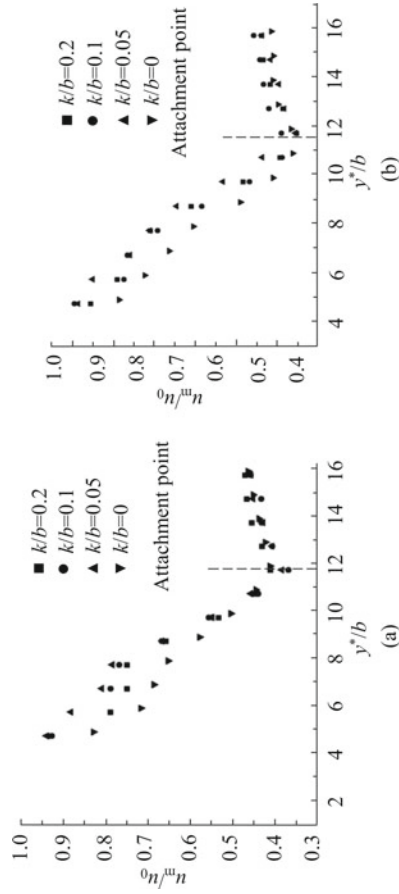


Fig. 4.40 Centerline velocity measured by 2D-PIV as a function of roughness ($S/b = 7.5$). **a** $u_0 = 1.0$ m/s, **b** $u_0 = 1.5$ m/s

References

- Cao YR (2016) Numerical simulation and evaluation for influence of human motion on indoor air distribution under the condition of air curtain ventilation. Xi'an University of Architecture and Technology, Xi'an (in Chinese)
- Chen T (2018) Study on influence of curvature effect on air distribution of circular column attachment ventilation. Xi'an University of Architecture and Technology, Xi'an (in Chinese)
- Cui WF (2010) A new type of ventilation-2DPIV studies of air curtain ventilation in a slot-ventilated outlet: volumetric heat source condition. Xi'an University of Architecture and Technology, Xi'an (in Chinese)
- Fanger PO, Melikov AK, Hanzawa H, Ring J (1988) Air turbulence and sensation of draught. *Energy Build* 12:21–39
- GB/T 13547-1992 (1992) Human dimension in workspace. China Quality and Standards Publishing & Media Co., Ltd, Beijing (in Chinese)
- Han YL, Wang XS (2011) The biomechanical study of lower limb during human walking. *Sci China Tech Sci* 54:983–991 (in Chinese)
- Hanzawa H, Melikov AK, Fanger PO (1987) Airflow characteristics in the occupied zone of ventilated spaces. *ASHRAE Trans* 93(1):524–539
- JG/T 20-1999 (1999) Method of testing for rating air distributor performance. China Quality and Standards Publishing & Media Co., Ltd, Beijing (in Chinese)
- Li AG, Yin HG, Tao PF, Li X (2010) A plenum with uniform air discharge and adjustable opening. Chinese patent ZL201010549210.8 (in Chinese)
- Liu WX (2016) Study on the effects of indoor heat source and the obstacle by air curtain ventilation. Xi'an University of Architecture and Technology, Xi'an (in Chinese)
- Mollendorf JC, Gebhart B (1973) An experimental and numerical study of the viscous stability of a round laminar vertical jet with and without thermal buoyancy for symmetric and asymmetric disturbances. *J Fluid Mech* 61(02):367–399
- Pera L, Gebhart B (1971) On the stability of laminar plumes: some numerical solutions and experiments. *Int J Heat Mass Transf* 14(7):975–984
- Ping J (1995) Jet theory and application. China Astronautic Publishing House, Beijing (in Chinese)
- Rodi W (1982) Turbulent buoyant jets and plumes. Pergamon Press, New York
- Rohsenow WM, Hartnett JP, Cho YI (1992) Handbook of heat transfer fundamentals, vol 1 (trans: Qi X). China Science Publishing & Media Ltd. (in Chinese)
- Schlichting H (1995) Boundary-layer theory. McGraw-Hill, Inc.
- Wang GD (2009) A new type of ventilation-2DPIV studies of air curtain ventilation in a slot-ventilated enclosure: non-isothermal condition. Xi'an University of Architecture and Technology, Xi'an (in Chinese)
- Wu R (2019) Study on air distribution characteristics of circular column attached ventilation under different column layout modes. Xi'an University of Architecture and Technology, Xi'an (in Chinese)
- Yang CQ (2019) Study on thermal natural ventilation based on different combination patterns of heat sources and thermal stratification. Xi'an University of Architecture and Technology, Xi'an (in Chinese)
- Yin HG, Wu R, Chen T, Sun YX, Li AG (2017) Study on ventilation effectiveness of circular column attached displacement ventilation mode. *Procedia Eng* 205:3511–3518
- Zhang Q, Gu L (2009) Ergonomics. Beijing Institute of Technology Press, Beijing (in Chinese)
- Zhang XM, Ren ZP, Mei FM (2001) Heat Transfer, 4th edn. China Architecture & Building Press, Beijing (in Chinese)
- Zhao HZ (2010) Indoor heat convection and ventilation. China Architecture & Building Press, Beijing (in Chinese)

Open Access This chapter is licensed under the terms of the Creative Commons Attribution-NonCommercial-NoDerivatives 4.0 International License (<http://creativecommons.org/licenses/by-nc-nd/4.0/>), which permits any noncommercial use, sharing, distribution and reproduction in any medium or format, as long as you give appropriate credit to the original author(s) and the source, provide a link to the Creative Commons license and indicate if you modified the licensed material. You do not have permission under this license to share adapted material derived from this chapter or parts of it.

The images or other third party material in this chapter are included in the chapter's Creative Commons license, unless indicated otherwise in a credit line to the material. If material is not included in the chapter's Creative Commons license and your intended use is not permitted by statutory regulation or exceeds the permitted use, you will need to obtain permission directly from the copyright holder.



Chapter 5

Adaptive Attachment Ventilation with Deflectors



Abstract This chapter mainly expounds on the principle of adaptive attachment ventilation (AAV), which is beneficial for directionally delivering fresh air or cold/warm air to the breathing zone or occupied zone with a deflector. The appropriate setting of deflectors can effectively improve ventilation efficiency. The deflector forms and installation height are analyzed, which directly influences ventilation effectiveness. In contemporary architectural engineering, especially in some symbolic modern architectural styles, the wall structure often adopts circular arc, elliptical and inclined wall forms. Hence, curved surface attachment ventilation is proposed, and its airflow patterns are discussed. Moreover, the attachment ventilation modes applied to some particular spaces, such as the concave corner attachment ventilation, are briefly introduced.

Keyword Attachment ventilation · Attached ventilation · Deflector · Curved surface · Velocity distribution · Temperature field · Large space

The point of departure for designing attachment ventilation airflow distribution is to ensure that the air temperature and velocity, etc., in the occupied zone or control zone with excessive heat meet the requirements of hygiene and human comfort. In most cases, the control zone occupies only a tiny portion of the room volume and height. The percentage of zones of control in residential and office buildings is 40–60%, while the percentage of zones of control in industrial workshops is only 10–30%. The appropriate air distribution created by attachment ventilation can allow the entire room space to divide into the control zone and the noncontrolled adjacent zone. By removal of the excessive heat in the occupied zone, the total energy consumption of the built environment control system is reduced accordingly.

This chapter mainly expounds on the principle of adaptive attachment ventilation (AAV). AAV denotes the ventilation mode in which the discharge jet moves downwards to the deflector and is then directionally distributed or injected into the target control zone by a deflector or a guide plate. By AAV, cooling air can be directly delivered to the human breathing zone or the conditioned zone. The deflector forms and installation height are analyzed, which directly influences ventilation effectiveness.

In contemporary architectural engineering, especially in some symbolic modern architectural styles, the wall structure often adopts circular arc, elliptical and inclined

wall forms. Hence, curved surface attachment ventilation is proposed, and its airflow patterns are discussed. Moreover, the attachment ventilation modes applied to some particular spaces, such as the concave corner attachment ventilation, are briefly introduced.

5.1 Adaptive Attachment Ventilation for Breathing Zone

As mentioned earlier, the indoor occupied zone (control zone) is only a part of the whole internal space, which are usually the zone people live in or industrial manufacture. In some instances, those control zones need to be adjusted frequently according to different scenarios. Variable control zone refers to the zone where the control zone can be adjusted when industrial and agricultural production activities changes. AAV for the breathing zone or target zone is an effective air supply mode applicable to the control zone (Li et al. 2019), see Fig. 5.1.

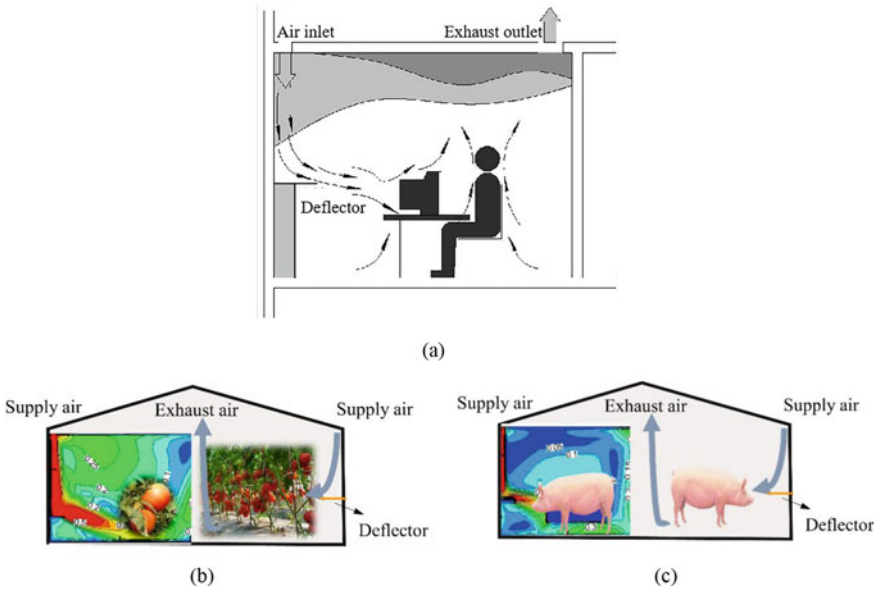


Fig. 5.1 Schematic diagram for AAV with deflectors. **a** Air supply for human's occupied zone (breathing zone), **b** air supply for facility agriculture plant growth zone, **c** air supply for animal's breathing zone

5.1.1 Deflector Forms

Generally, deflectors' shape, width, installation height, etc., will directly impact the airflow movement in the occupied zone. Taking an operation room in a hospital as a case study, we analyze the influence of deflector forms on AAV (Li et al. 2016). As indicated in *REHVA Guidebook—Displacement Ventilation*, the breathing zone refers to the zone within 1.1 m (sedentary occupant) or 1.7 m (standing occupant) away from the floor. As shown in Fig. 5.2, the room size is 3.6 m × 4.2 m × 2.75 m, and the slotted tuyere size is 1.2 m × 0.05 m, with a desk and staff inside. As a case study, two deflectors, i.e., horizontal deflector and circular arc deflector, are applied, see Fig. 5.2. See Table 5.1 for detailed parameters.

The deflector structure, such as the deflector width b_0 , will have a direct impact on air jet motion. The airflow movement velocity and temperature distribution in the room's central cross-section ($z = 2.1$ m) are shown in Figs. 5.3 and 5.4.

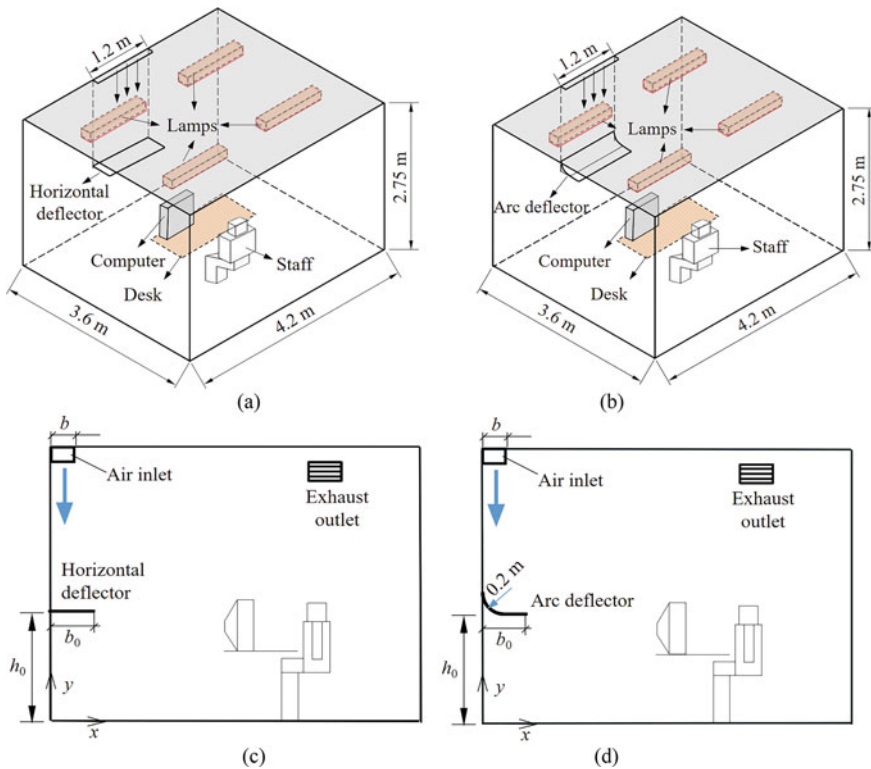


Fig. 5.2 Forms and layouts of two types of deflectors. **a** Horizontal deflector, **b** circular arc deflector, **c** front view of the horizontal deflector, **d** front view of the circular arc deflector

Table 5.1 Structural forms and air supply parameters of deflectors

Case	Air supply velocity (m/s)	Air supply temperature (°C)	Deflector shape	Deflector width b_0 (m)	Deflector installation height h_0 (m)	Heat source (convection heat load)
1	1.5	16.0	Horizontal plate	0.4	1.1	Human body 134 W, lamps 60 W × 4
2			Horizontal plate	0.2		
3			Arc plate	Horizontal projection, 0.4 (Arc radius 0.2)		

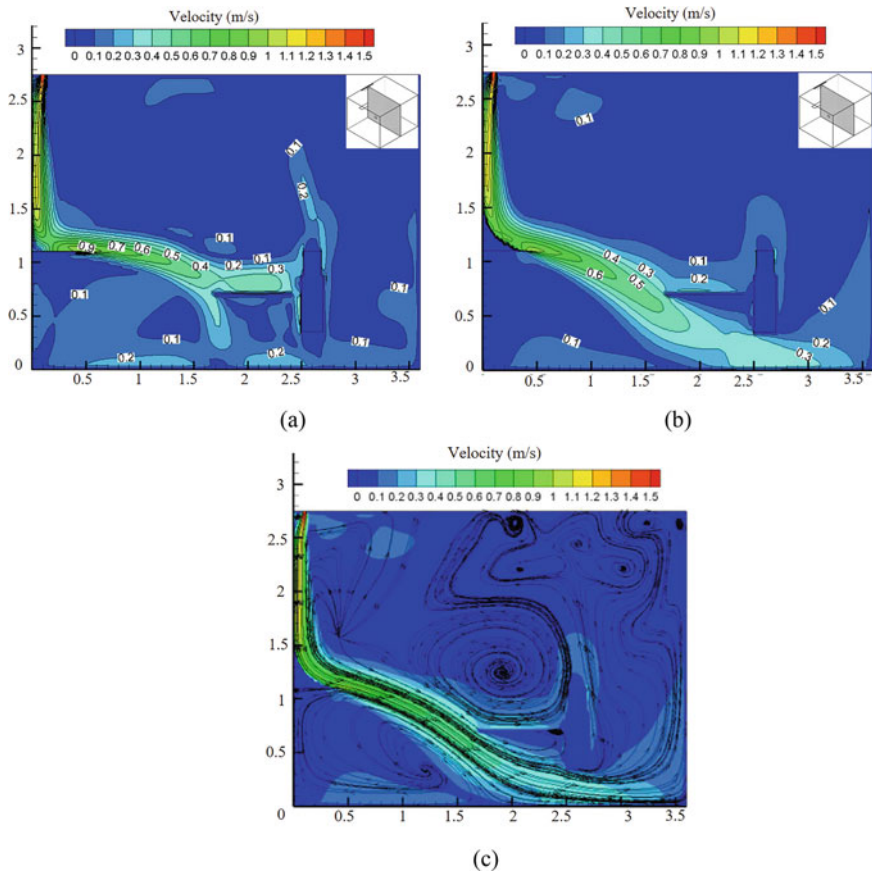


Fig. 5.3 Velocity and streamline distribution created by AAV with different deflector forms. **a** Horizontal deflector, **b** circular arc deflector, **c** velocity field with streamline of circular arc deflector

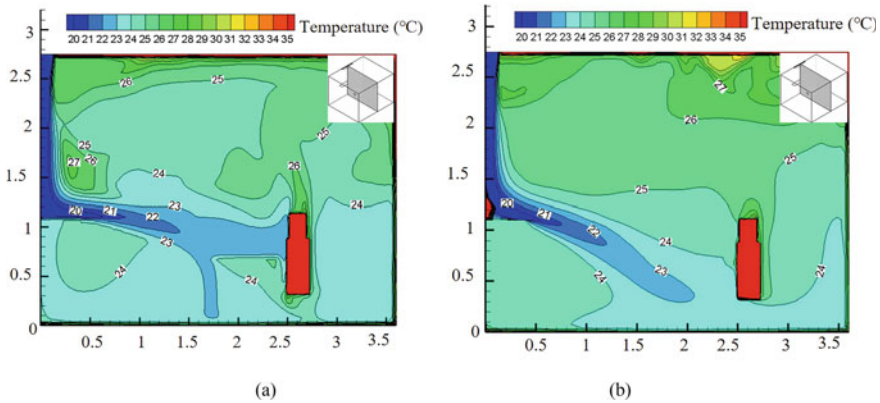


Fig. 5.4 Indoor temperature field affected by deflectors (air supply temperature is 16 °C). **a** Horizontal deflector, **b** circular arc deflector

Horizontal deflector

As shown in Fig. 5.3, the horizontal deflector is located in the middle of the left-side wall, 1.1 m away from the floor. The discharged jet moves downward along the vertical wall surface, impinges on the deflector, and turns its direction. So, the air jet dominated by the horizontal deflector can remain inertial motion in the horizontal direction. The desk, as an obstacle, affects the airflow movement, causing some airflow to flow obliquely downward; the other part of the horizontal flow is induced by the thermal plume generated by the human body, showing upward movement with a velocity of approximately 0.2 m/s.

Circular arc deflector (radius 0.2 m, 1/4 circular arc)

Similarly, the circular arc deflector can directionally deliver the airflow to the occupied zone or control zone. As we can see from the velocity field and airflow pattern of Fig. 5.3b, c, the airflow approaches the human body’s vicinity through inertial motion, resulting in large vortex recirculation in the upper space of the room. The airflow velocity around the human body and ankle ($y = 0.1$ m) is about 0.3 m/s.

Figure 5.4 shows the room temperature field distribution of two deflector forms. Comparing horizontal and circular arc deflectors, the former’s airflow temperature in the human breathing zone is 1.0–2.0 °C lower than that of the latter, which is attributed to different deflectors’ inertia effects. For a horizontal deflector, the breathing zone of a human is located within the air supply jet zone. Under the same air supply conditions, the horizontal deflector can achieve a longer horizontal jet throw.

Deflector width

The deflector width b_0 will directly affect the flow field. As noted in Sect. 5.1.1, while the deflector width increases, the inertial momentum retention is enhanced for the airflow moving along the horizontal direction after impinging the deflector. The

velocity and temperature fields in the room's central cross-section ($z = 2.1$ m) with different deflectors' widths (0.2, 0.4, and 0.6 m) are presented in Figs. 5.5 and 5.6.

When the deflector width becomes narrower (such as 0.2 m), the airflow can drop down at the edge of the deflector earlier, as shown in Fig. 5.5a. With the increase of the deflector width from 0.4 to 0.6 m, the inertial motion retention of the airflow along the horizontal direction is further enhanced. The air age reflects the freshness of indoor air to some extent, see Fig. 5.5d.

More details can be derived in Fig. 5.6. Comparing the temperature field with different deflector widths from 0.2 to 0.6 m, it is found that the air temperature in the breathing zone decreases by about 1.0–2.0 °C successively. The wider the deflectors, the more inclined the airflow stratification to a certain extent (Zou et al. 1983).

In engineering applications, it is recommended to utilize a horizontal deflector with width $b_0 = 0.4\text{--}0.6$ m to achieve better supply airflow distribution in the

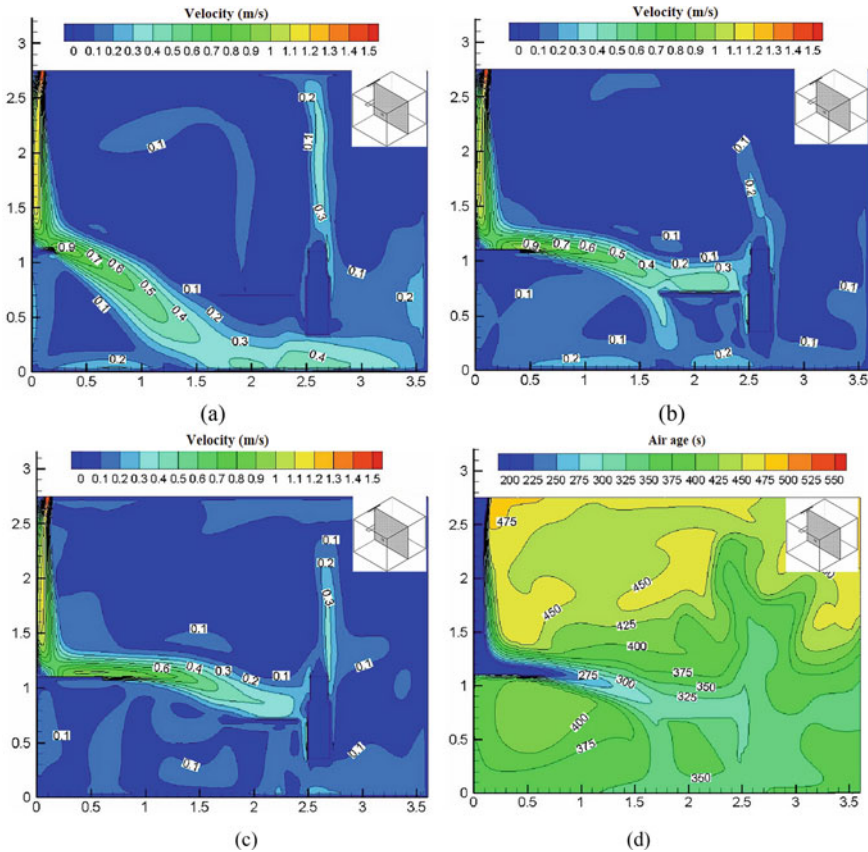


Fig. 5.5 Air age and indoor flow field under different deflector-width b_0 . **a** $b_0 = 0.2$ m, **b** $b_0 = 0.4$ m, **c** $b_0 = 0.6$ m, **d** air age ($b_0 = 0.4$ m)

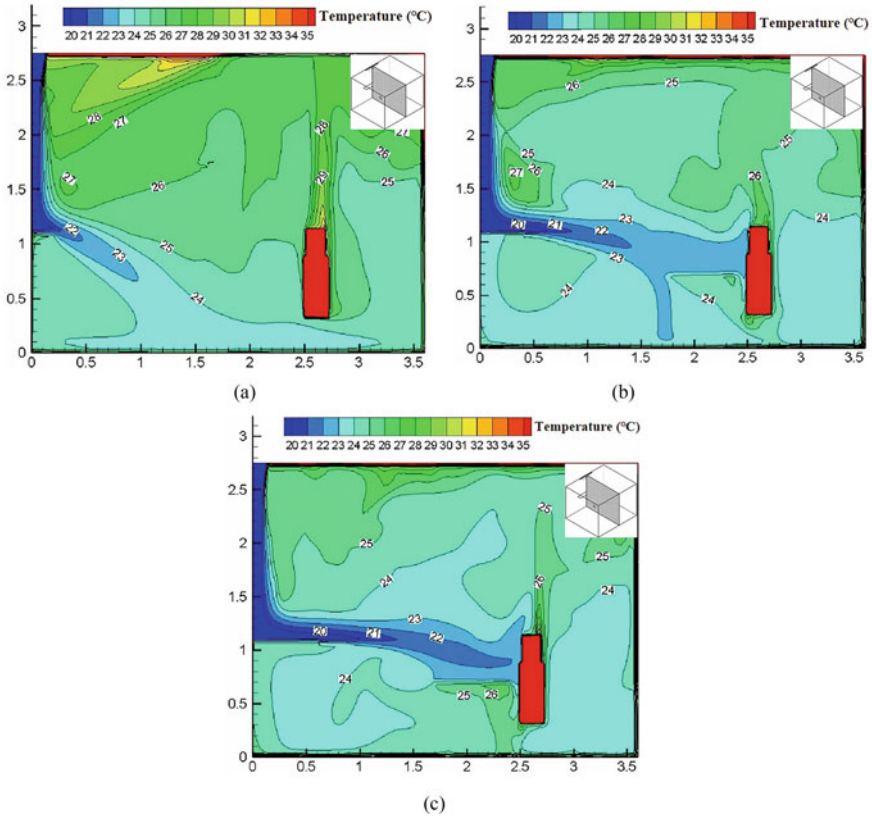


Fig. 5.6 Indoor airflow temperature field with different deflector-width. **a** $b_0 = 0.2$ m, **b** $b_0 = 0.4$ m, **c** $b_0 = 0.6$ m

breathing zone. When the deflector width exceeds 0.6 m, it may occupy a larger room space. In this case, the deflector can be made folding to occupy less space.

5.1.2 Installation Height of Deflectors

First of all, the orientation of the deflector relative to the direction of incoming jet flow has a significant influence on the control zone’s flow field. Figure 5.7 shows the indoor velocity field distribution corresponding to the heights of three different deflectors (1.1, 1.3, and 1.5 m). Similar to the air reservoir flow field created by the VWAV, Fig. 5.8 demonstrates the indoor temperature stratification phenomena. For the breathing zone, it is recommended that the installation height of deflectors be in the range of 1.1–1.7 m from the floor. It should be pointed out that a deflector

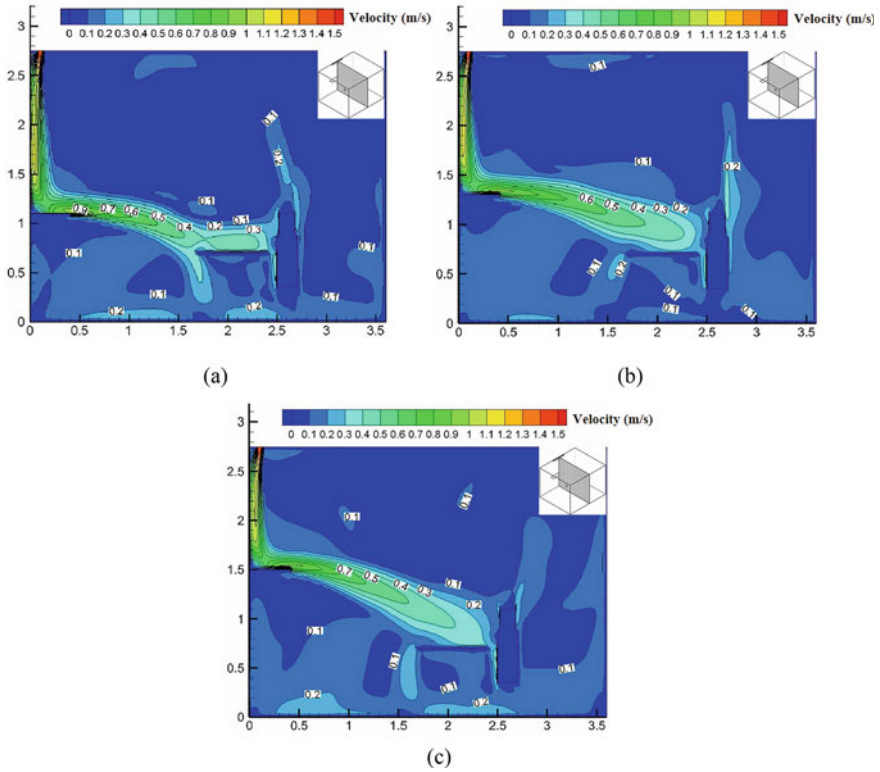


Fig. 5.7 Heights of deflectors influencing indoor airflow movement (deflector width 0.4 m). **a** $h_0 = 1.1$ m, **b** $h_0 = 1.3$ m, **c** $h_0 = 1.5$ m

can also be installed or fixed at any location as required. In this scenario, the airflow pattern may be different from the above-mentioned.

5.1.3 Deflector Application

Adaptive attachment ventilation (AAV) with deflectors is used in office buildings, industrial fields, facility agriculture, animal husbandry, and other occasions. Taking the ordinary train compartment as an example ($3.1 \text{ m} \times 3.0 \text{ m} \times 2.5 \text{ m}$), the attachment air distribution can be utilized, and air slots are located at both sides of the compartment ceiling, with the slot size of $3.0 \text{ m} \times 0.1 \text{ m}$. The deflectors are installed 2.0 m away from the floor, at an angle of 30° with the sidewalls. The exhaust outlets are located on the lower parts of two sidewalls, with a size of $0.4 \text{ m} \times 0.2 \text{ m}$, as shown in Fig. 5.9.

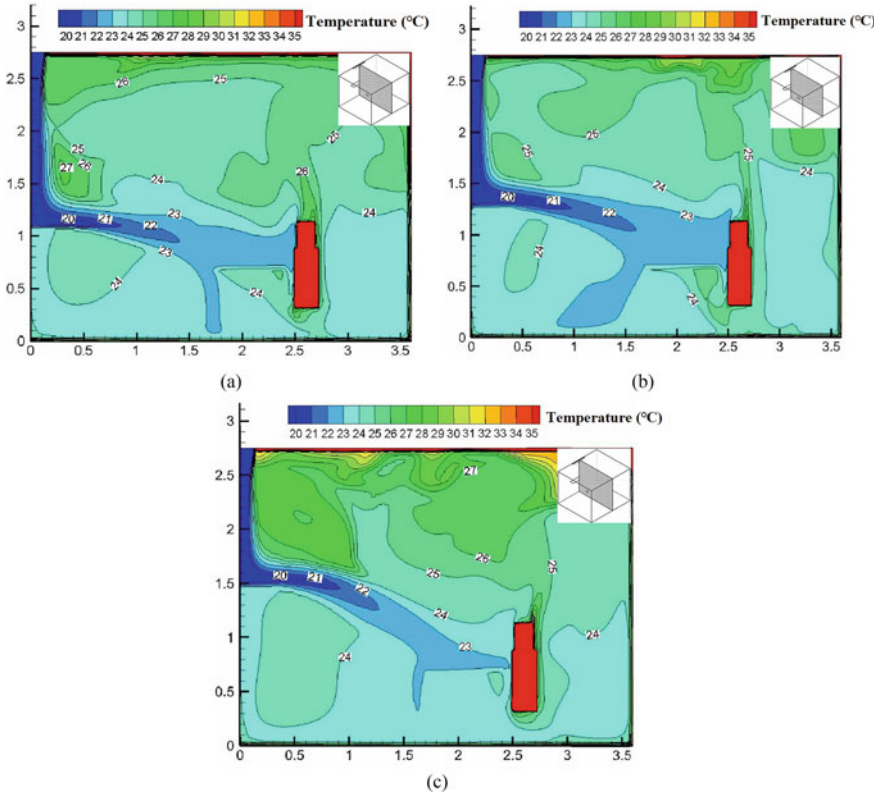


Fig. 5.8 Temperature field with different deflector heights (deflector width 0.4 m). **a** $h_0 = 1.1$ m, **b** $h_0 = 1.3$ m, **c** $h_0 = 1.5$ m

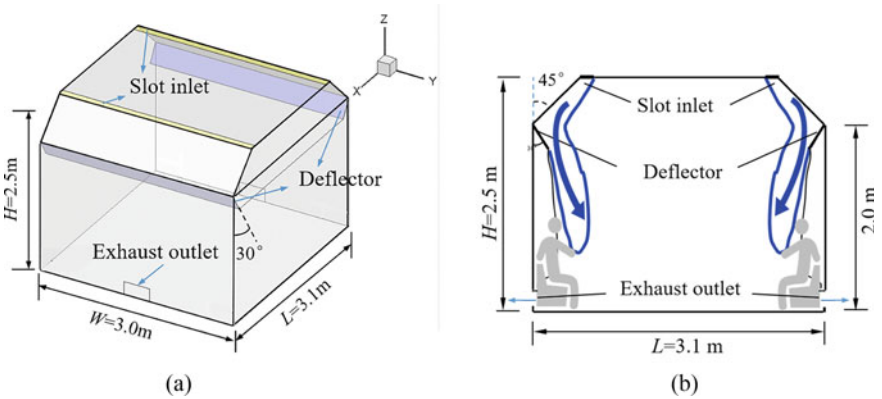


Fig. 5.9 AAV compartment deflectors. **a** Compartment physical model, **b** schematic diagram of AAV in the compartment

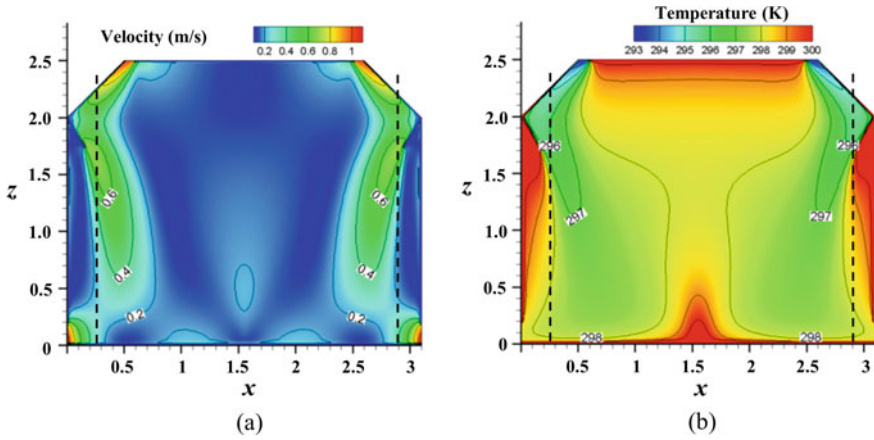


Fig. 5.10 Airflow velocity and temperature distribution in the compartment ($t_0 = 20\text{ }^\circ\text{C}$, $u_0 = 1.0\text{ m/s}$). **a** Velocity distribution, **b** temperature distribution

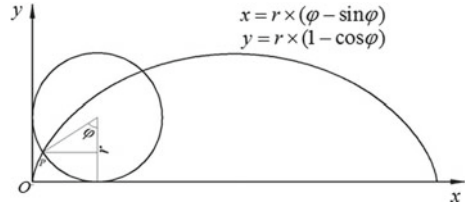
For AAV with deflectors, the air supply at a temperature of $20\text{ }^\circ\text{C}$, a velocity of 1.0 m/s , the floor and wall loads are 120 W/m^2 and 80 W/m^2 , respectively. The air velocity and temperature contours are shown in Fig. 5.10. In compartments with air distribution, the concern about thermal comfort mainly focuses on draught at the neck and discomfort due to the directly blowing airflow. The ceiling corner-mounted slots could be regarded as two wall-attached air supply modes with regard to the length of the control zone. The deflectors make the discharge flow deflected from the sidewalls to avoid draught risk at the neck of the human body, see Fig. 5.10.

5.2 Curved Surface Attachment Ventilation

Normally, a building has two duties to fulfill: protecting man from adverse elements and providing a comfortable environment for him to work and live in. John Ruskin once asked the question: “Can anything be beautiful as well as functional?”. It is suggested a building performing its duties should also enhance its aesthetic quality (Croome and Roberts 1981). In modern architecture, there are a number of curved and inclined-wall structures. These special-shaped structural forms combine architects’ inspiration, aesthetics, environment, function, structure, and other factors. However, regarding the built environments with these special-shaped structural forms, creating a comfortable environment is a challenging task for HVAC engineers. This section deals with the problems of curved or inclined surface attachment ventilation airflow movement.

The functionally curved surfaces of various buildings could be described by mathematical functions such as spherical, ellipsoidal, cylindrical, conical, and other regular surfaces. For instance, among the curved surfaces, the fastest descent curve

Fig. 5.11 Coordinates representation of brachistochrone



surface is the brachistochrone surface, i.e., the curved cycloid surface proposed by Galileo, as shown in Fig. 5.11. Newton and Leibniz first presented their analytical Eq. (5.1)

$$x = r \times (\varphi - \sin\varphi); \quad y = r \times (1 - \cos\varphi) \tag{5.1}$$

where r indicates the radius of a circle, m ; φ indicates the radian (rolling angle) of the radius of a circle, rad .

In this section, we take the curved surface of brachistochrone as a case study (Yang 2017; Li et al. 2019). As shown in Fig. 5.12, the room area is $5.4 \text{ m} \times 7.0 \text{ m}$, and the height is 2.5 m . The slot size is $2.0 \text{ m} \times 0.05 \text{ m}$, and an air inlet of $0.3 \text{ m} \times 0.3 \text{ m}$ is used. The centerline velocity and temperature distribution of curved surface attachment ventilation are illustrated below under isothermal or nonisothermal air supply conditions with different curvatures ($0.236\text{--}0.436 \text{ m}^{-1}$).

5.2.1 Isothermal Curved Surface Attachment Ventilation

With regarding to the brachistochrone curved surface, the indoor air flow fields with different curvatures and air supply velocities are investigated. See Table 5.2 for different cases, the velocity field distribution is shown in Fig. 5.13.

Although the curvatures of the three cases are quite different, the airflow patterns in the curved surface attachment region behave similarly. All three cases can form air reservoir distribution in the occupied zone, as shown in Fig. 5.13. It is found that the air reservoir thickness is about 0.4 m , which can effectively deliver fresh air or cool/warm air to the occupied zone without causing drafts to people. It is worth noting that, compared to a vertical wall attached jet, the airflow attached to the curved surface may move forward more smoothly along the floor than that attached to a vertical wall, without resulting in the large vortex from the jet impinging on the floor. Hence, the curved surface attachment ventilation can achieve a minor momentum loss, a greater centerline velocity, and a larger energy efficiency, as shown in Fig. 5.14b.

The influence of curvatures on the air supply centerline velocity is shown in Fig. 5.14. The centerline velocity distributions demonstrate a consistent attenuation tendency along the curved surface attachment region. With curvature further

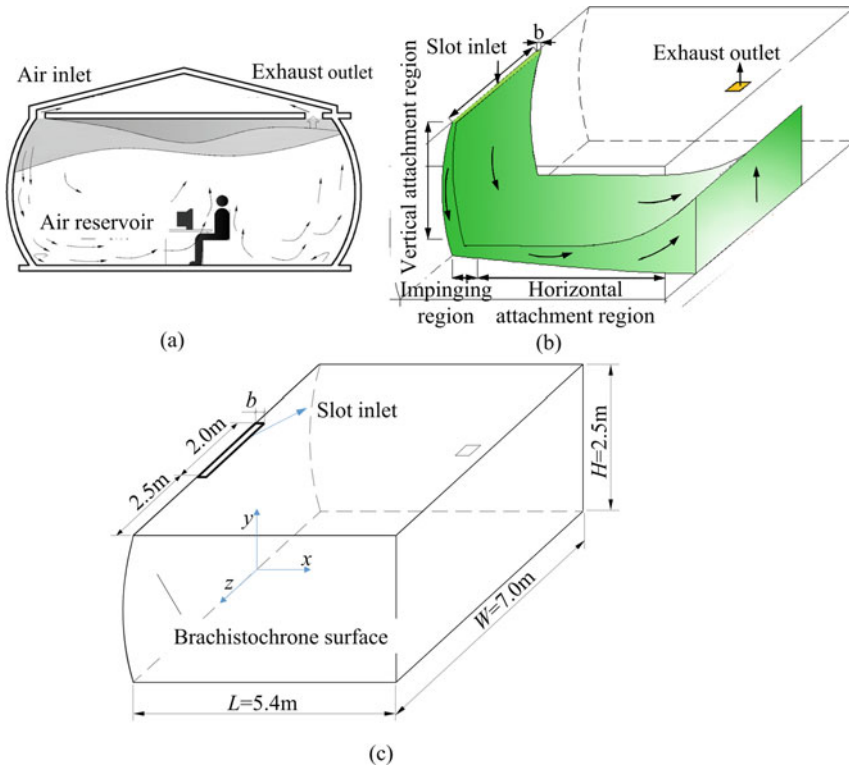


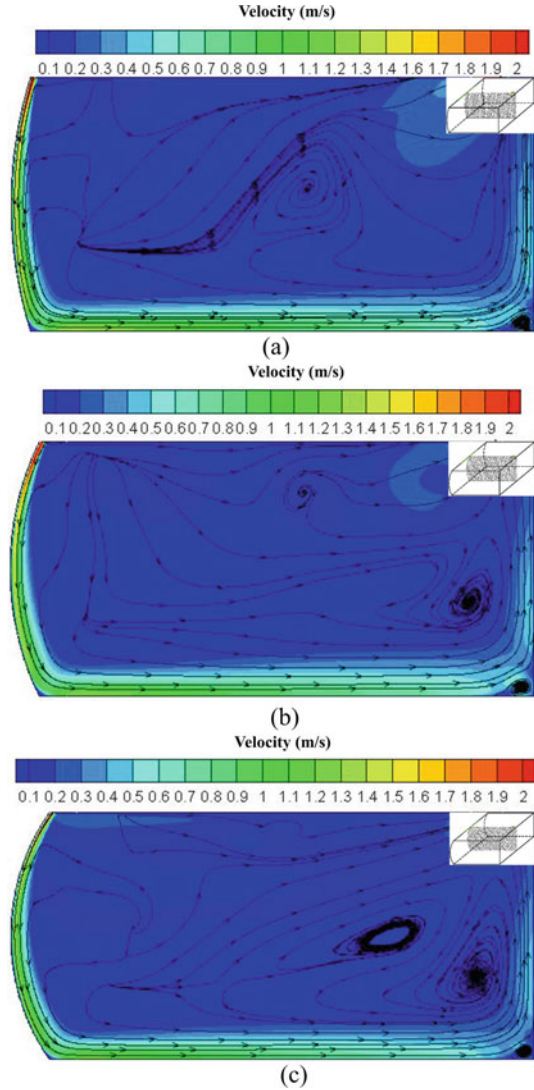
Fig. 5.12 Curved surface attachment ventilation. **a** Schematic diagram of curved surface attachment airflow distribution, **b** airflow patterns, **c** room structure and slot layout

Table 5.2 Parameters of isothermal curved surface attachment ventilation

Curvature	Approximation curvature (m^{-1})	Inlet cut angle ($^\circ$)	Air supply velocity (m/s)	Air opening ($\text{m} \times \text{m}$)
Mild	0.236	72	1.0, 1.5, 2.0	2×0.05
Moderate	0.336	63		
Severe	0.436	52		

increasing, the centerline velocity attenuation of both vertical and horizontal attachment regions increases slightly, and the amplitude of variation is less than 10% in the range of $0.236\text{--}0.436 \text{ m}^{-1}$ of curvature.

Fig. 5.13 Curved surface attachment ventilation velocity field with different curvatures ($u_0 = 2.0$ m/s). **a** Curvature 0.236, **b** curvature 0.336, **c** curvature 0.436



5.2.2 Nonisothermal Curved Surface Attachment Ventilation

The work carried out in a curved surface attachment ventilation room has been compared the patterns of air movement and temperature distribution resulting from different surface curvatures. Detailed parameters can be found in Table 5.3. Taking the curve surface of brachistochrone with curvature of 0.336 m^{-1} as an example, the indoor temperature distribution of nonisothermal curved surface attachment ventilation is shown in Fig. 5.15.

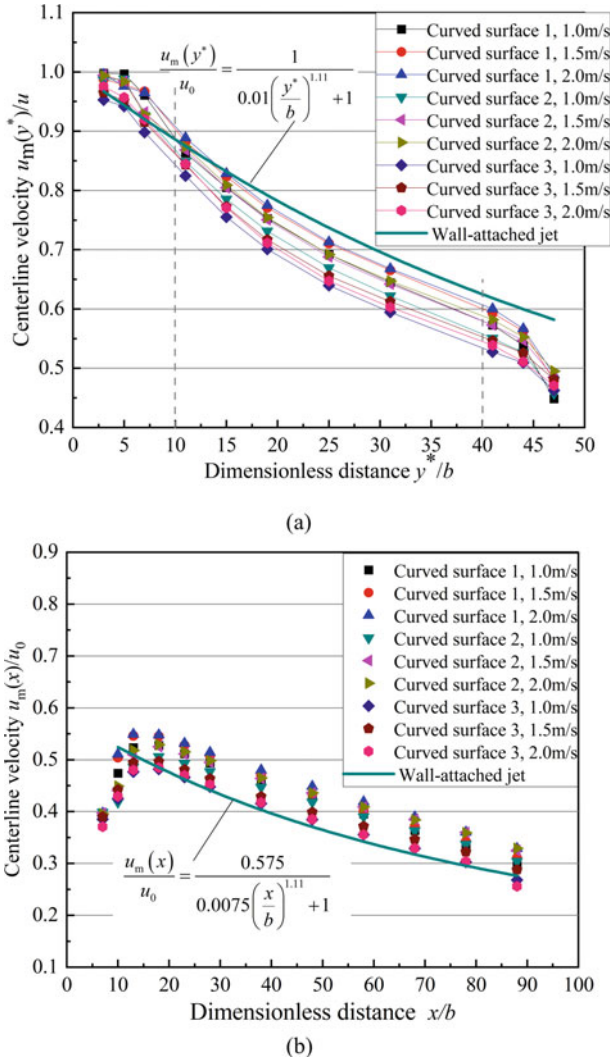


Fig. 5.14 Centerline velocity of curved surface attachment ventilation with different curvatures (curved surface 1: curvature 0.236; curved surface 2: curvature 0.336; curved surface 3: curvature 0.436). **a** Centerline velocity in the wall attachment region, **b** centerline velocity in the air reservoir region

1. Indoor temperature field

When the indoor cooling load remains constant, the room temperature fields formed by different air supply temperatures and velocities are shown in Fig. 5.15. There is a significant vertical temperature stratification in the ventilation room, whereas the temperature remains almost uniform over the entire occupied zone. In addition, the

Table 5.3 Nonisothermal curved surface attachment ventilation parameters

Curvature	Approximation curvature (m^{-1})	Supply air velocity (m/s)	Supply air temperature ($^{\circ}C$)	Heat flux q (W/m^2)
Mild	0.236	1.0, 1.5, 2.0	17	50
Moderate	0.336		19	
Severe	0.436		21	

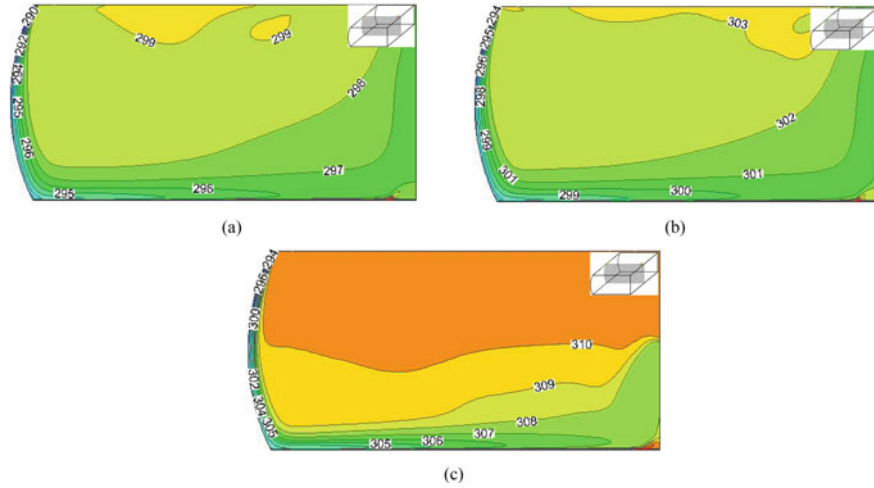


Fig. 5.15 Indoor temperature distribution, nonisothermal curved surface attachment air supply (curvature $0.336 m^{-1}$). **a** $t_0 = 17^{\circ}C$, $u_0 = 2.0 m/s$, **b** $t_0 = 21^{\circ}C$, $u_0 = 2.0 m/s$, **c** $t_0 = 21^{\circ}C$, $u_0 = 1.0 m/s$

maximum temperature gradient does not exceed $3.0^{\circ}C$, which meets the comfort requirements of the temperature gradient between the head and ankle levels.

When the air supply temperature further rises (Fig. 5.15a, b), the indoor air temperature increases correspondingly; in other words, both temperature rises are almost identical.

The jet discharge velocity will significantly affect the indoor vertical temperature stratification. Compared with Fig. 5.15b, c, the smaller the air supply velocity, the more significant the vertical temperature stratification, quite similar to displacement ventilation.

2. Centerline excess temperature distribution

The curvature of a wall has little effect on the centerline temperature distribution, as shown in Fig. 5.16. For the curved surface attachment region, there are no much differences in excess temperature during the initial section, $0 \leq y^*/b \leq 10$. When $y^*/b > 10$, the centerline excess temperature of the curved surface attachment region at a lower air supply velocity is less than that at a higher air supply velocity (such as

$u_0 = 1.5$ and 2.0 m/s). It indicates that more attention should be paid to selecting the appropriate air supply velocity in designing curved surface attachment ventilation.

Similar to VWAV, for the horizontal air reservoir region, the centerline excess temperature attenuates exponentially with the jet throw, which is the distance from the centerline of an air opening perpendicular to a point in the airstream where the velocity has been reduced to a specified terminal velocity (e.g., 0.25 m/s).

The curvature variation has little effect on the air movement in the occupied zone. It should be noted that the conclusion derived from the brachistochrone curved

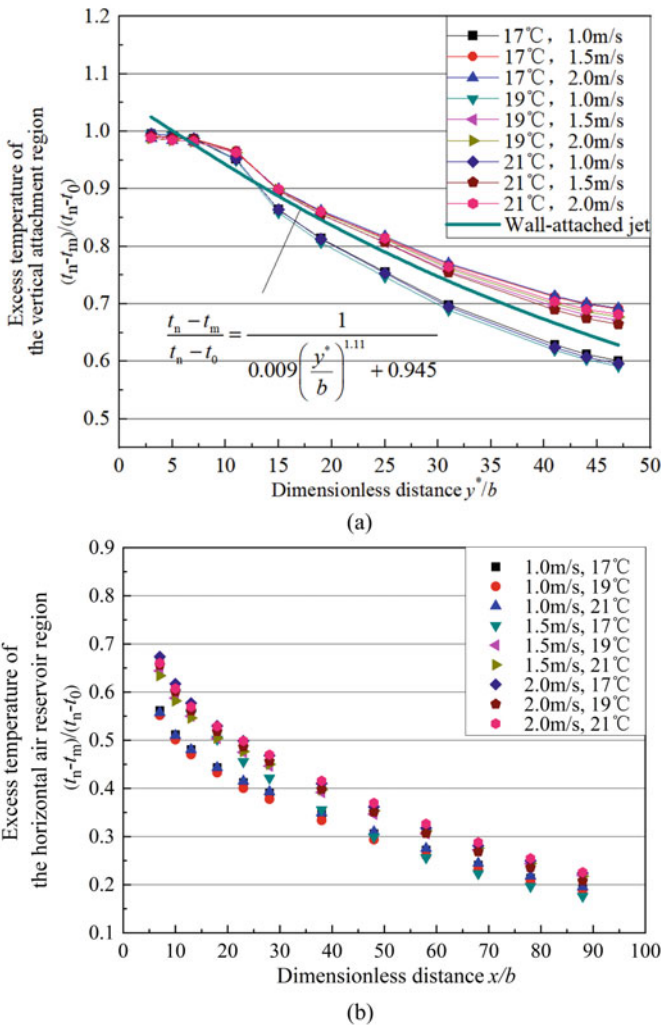
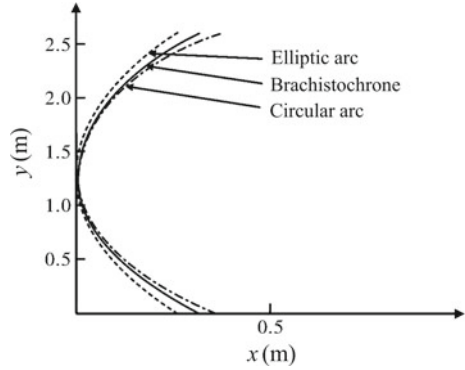


Fig. 5.16 Excess temperature, nonisothermal curved surface attachment air supply (curvature 0.336 m^{-1}). **a** Curved surface attachment region, **b** horizontal air reservoir region

Fig. 5.17 Three kinds of curved surfaces with equal height (curvature 0.336 m^{-1})



surface attachment ventilation with the curvatures of $0.236\text{--}0.436 \text{ m}^{-1}$ might also be applicable to other types of curved surface attachment ventilation. Special-shaped structural forms or curved surfaces are often encountered for commercial or industrial buildings, including circular arc, elliptical arcs, brachistochrone surfaces, etc. For ordinary rooms, at the same height, there is virtually no remarkable curvature difference; see Fig. 5.17.

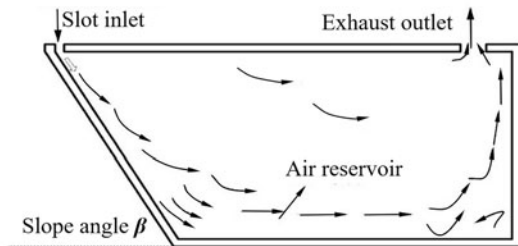
3. Inclined wall attachment ventilation

An inclined wall can be regarded as a particular case of curved surface. See Fig. 5.18 for indoor airflow distribution of inclined wall attachment ventilation. The discharge air moves along the inclined wall and downwards to the floor, then gently turns to a horizontal direction, and spreads forward over the floor, forming an air reservoir in the occupied zone with a vertical temperature stratification.

In the wintertime, it is worth noting that for a thermal wall-attached jet, the smaller the slope angle β , the more unfavorable for the thermal jet to reach the occupied zone, which means more air supply momentum (or jet discharge velocity) could be needed for small β , as shown in Fig. 5.19. For ordinary residential or office rooms, the



(a)



(b)

Fig. 5.18 Diagram for inclined wall attachment ventilation. **a** Slope wall, **b** schematic diagram of inclined wall attachment airflow distribution

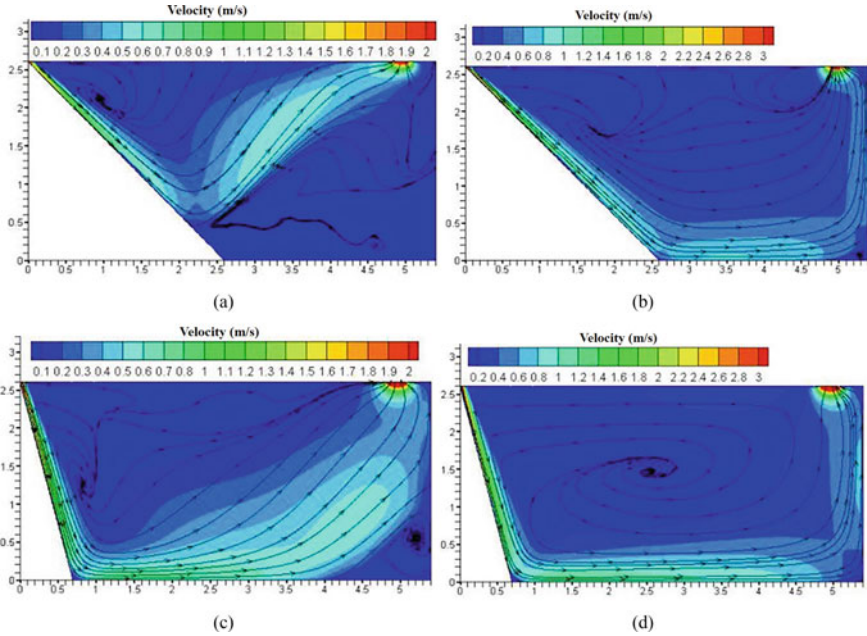


Fig. 5.19 Effect of inclination angle on the indoor velocity field. **a** $\beta = 45^\circ$, $u_0 = 2.0$ m/s, **b** $\beta = 45^\circ$, $u_0 = 3.0$ m/s, **c** $\beta = 75^\circ$, $u_0 = 2.0$ m/s, **d** $\beta = 75^\circ$, $u_0 = 3.0$ m/s

velocity of warm air supply should not be less than 2.0–3.0 m/s so as to ensure that the warm air is supplied to the occupied zone in wintertime.

5.3 Some Applications of Attachment Ventilation

5.3.1 Tiny Interior Spaces

In addition to being used in large spaces, attachment ventilation has also been used more and more in some tiny spaces. Often the cooling systems are installed in particular rooms, such as crane control rooms and subway carriages, to remove excessive heat from the room. The interior spaces are pretty compact and occupied by facilities. An appropriate air distribution design is required to ensure its internal air environment and thermal comfort.

This section briefly discusses several air supply modes suitable for tiny spaces, such as impinging side-wall attachment ventilation (Fig. 5.20a), concave corner attachment ventilation (Fig. 5.20b), and impinging-ceiling attachment ventilation (Fig. 5.20c).

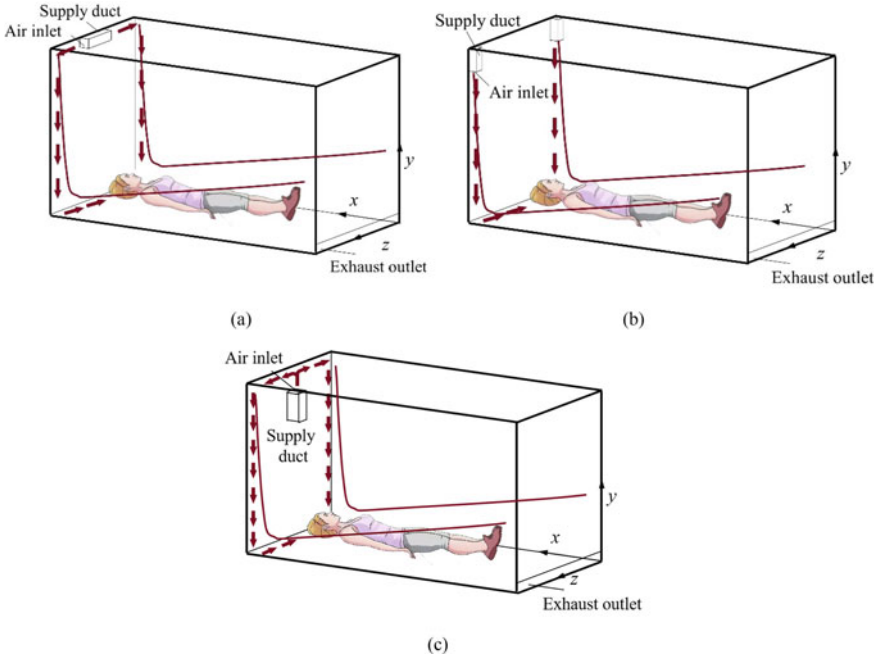


Fig. 5.20 Airflow distribution modes for particular spaces. **a** Impinging side-wall attachment ventilation, **b** concave corner attachment ventilation, **c** impinging-ceiling attachment ventilation

For the air distribution of those particular spaces mentioned above, air supply modes, such as impinging side-wall attachment, concave corner attachment, and impinging-ceiling attachment ventilation, etc., can be used. For impinging side-wall attachment ventilation (Fig. 5.20a), two air openings are mounted at the both sides of the ceiling. The discharge air jet is attached to the ceiling and reaches both sidewalls, then downwards further to the bottom and spreads at a low velocity, creating a uniform thermal environment.

For concave corner attachment ventilation (Fig. 5.20b), its features lie that two air jets are supplied separately from the plenum opening fixed at the ceiling, and move downwards along the intersection line of adjacent sidewalls, impinging on the floor. This mode almost behaves the same air distribution as the impinging side-wall attachment ventilation with a smaller air discharge velocity.

With regard to impinging-ceiling attachment ventilation (Fig. 5.20c), it is characterized by:

Air jet upward impinges on the ceiling → move along the ceiling → impinge on both sidewalls → turn direction and flow downwards to the floor. The indoor velocity and temperature fields of those three kinds of air supply modes are shown in Figs. 5.21 and 5.22.

Comparing the three air supply modes mentioned above, at the same air supply velocity, the averaged velocity in the occupied zone is 0.20 m/s, 0.25 m/s, and

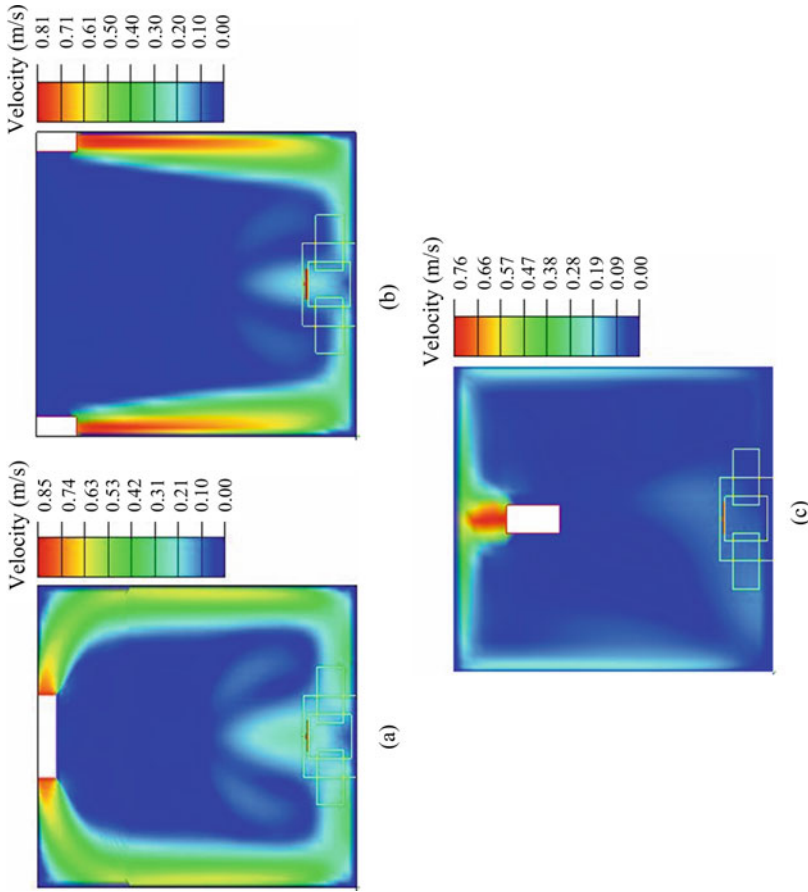


Fig. 5.21 Indoor velocity field of three air supply modes ($u_0 = 1.0$ m/s, $t_0 = 23$ °C). **a** Impinging side-wall attachment, **b** concave corner (internal corner) attachment, **c** impinging-ceiling attachment

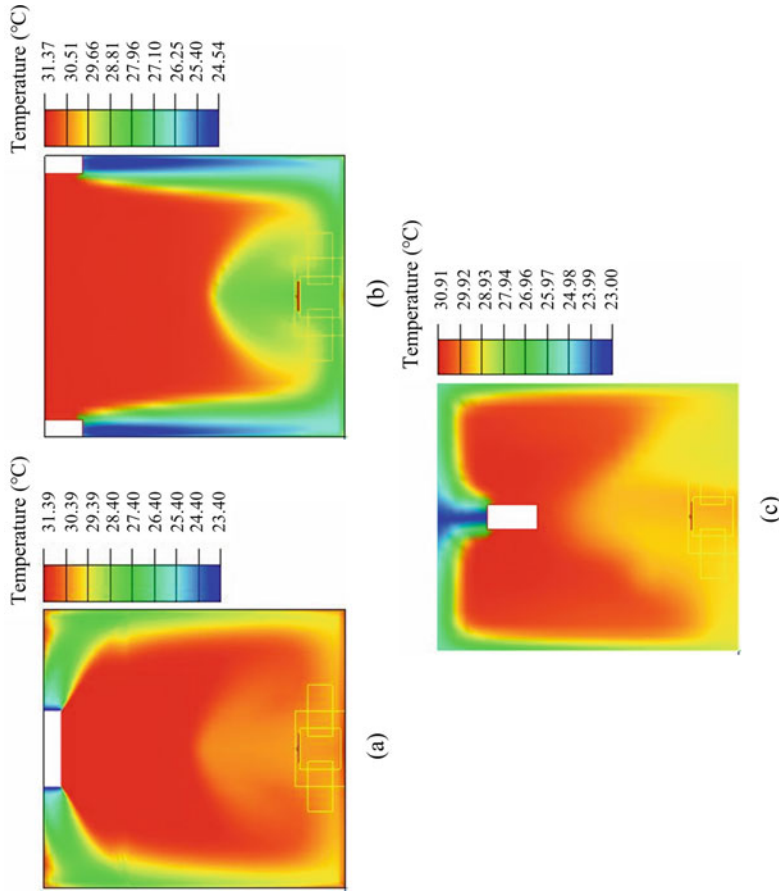


Fig. 5.22 Indoor temperature fields of three air supply modes ($u_0 = 1.0$ m/s, $t_0 = 23$ °C). **a** Impinging side-wall attachment, **b** concave corner (internal corner) attachment, **c** impinging-ceiling attachment

0.10 m/s, respectively, see Fig. 5.22. This indicates that the air opening's installation position significantly affects the air distribution for those particular spaces and others.

5.3.2 *Some Applications to Particular Spaces*

More specialized attachment ventilation modes have been developed, as also shown in Fig. 5.23 (Li and Li 2016; Reese 2005; Li et al. 2011, 2012; Yin et al. 2018). For instance, the floor-based air distribution with a novel mushroom diffuser is presented in Fig. 5.23a. The horizontal airflow with the air velocity of 0.2–0.5 m/s is supplied from the bottom of seats, moves forward along the floor, and alters its direction after impinging on adjacent steps, which is suitable for theaters and conference rooms, etc.

The horizontal-impinging attachment and inclined-impinging attachment modes are shown in Fig. 5.23b, c. They are applicable to indoor air environment control for certain confined spaces. Its typical feature is that the jet from the air ducts at any angle direction “sticks” on the surface and spreads along the wall. At an angle of $\theta = 90^\circ$, the spread of the air jet takes place uniformly in all directions; at an angle of $\theta = 45^\circ$, the majority of the air travels in the direction involving the smallest deviation (i.e., forwards), whereas $\theta = 22.5^\circ$, practically the whole of the jet flows in one direction. The floor-impinging attachment mode created by circular opening arrays is presented in Fig. 5.23d, which is similar to the impinging ventilation studied by Awbi (2008) to some extent.

As shown in Fig. 5.23e, the attachment ventilation columns have been installed for large spaces like Xi'an airport terminal T5 and the waiting halls of Xiong'an high-speed railway station in China. Rotary outlets/globe-type outlets and slot openings are installed in the same ventilation column. The former is used to create mixed air distribution for the far zones, and the latter is used to create attached air distribution for the near zone. Compared to mixing ventilation, this mode can meet the needs of indoor thermal environment and achieve higher energy efficiency. Figure 5.23f shows the schematic diagram of attachment ventilation application in industrial multi-span buildings.

As mentioned before, the ventilation effectiveness of the air distribution mode can be evaluated by ventilation efficiency or temperature efficiency, which reflects the system's ability to remove excessive heat in a room. Take the ducted-type air conditioner as an example, as shown in Fig. 5.23h, its ventilation performance is jointly tested by the manufacturer and author in a standardized laboratory. Compared to the mixing ventilation mode, the temperature efficiency of the attachment ventilation mode increased by 26.9% at the medium air supply speed of the ducted-type air conditioner (Han et al. 2021).

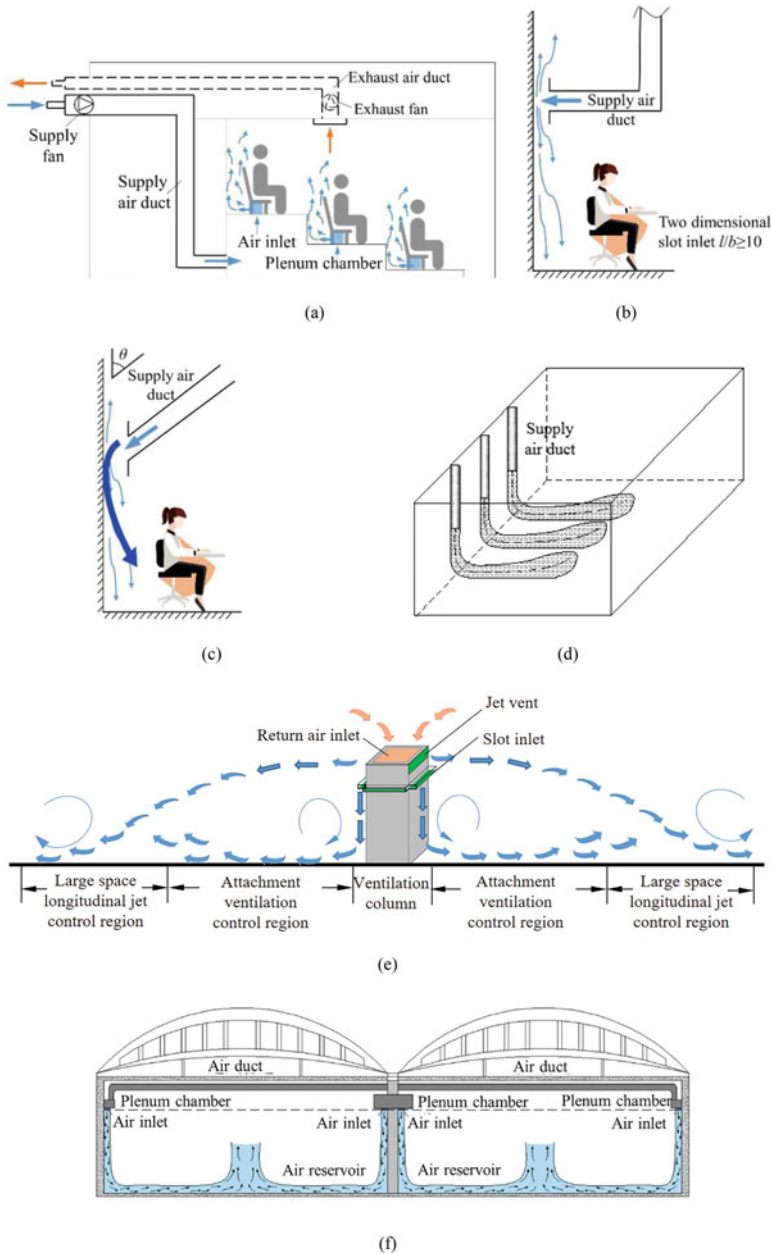
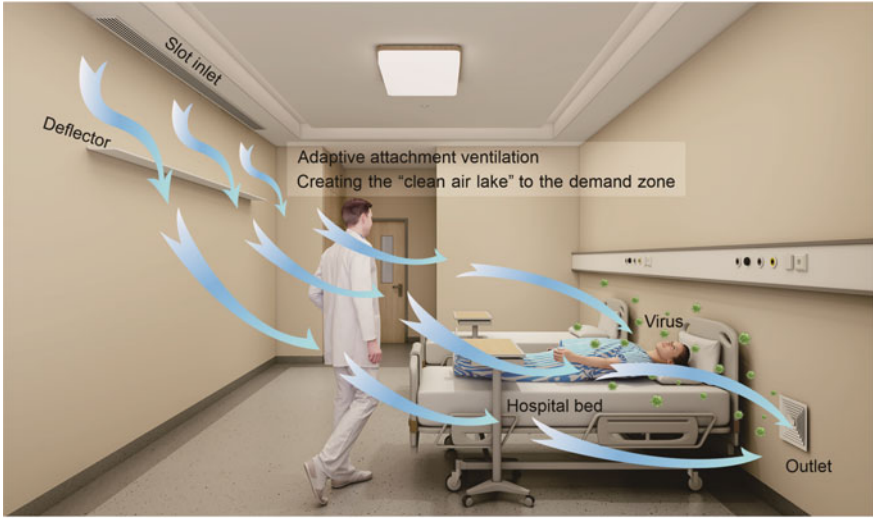
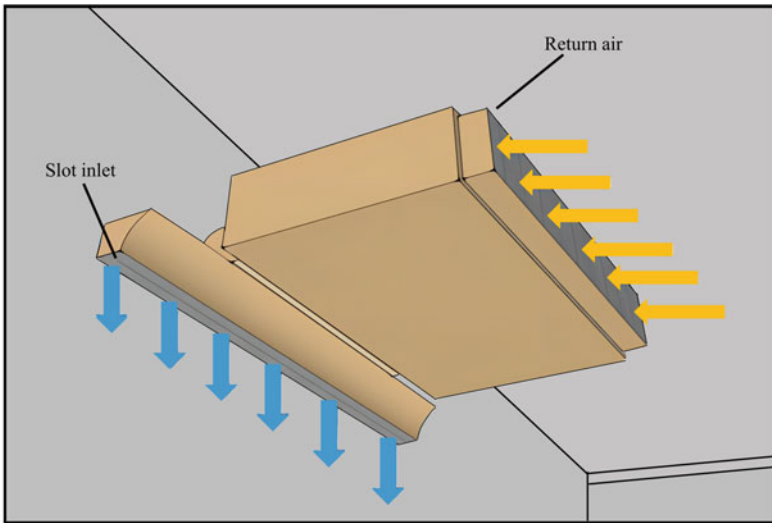


Fig. 5.23 Schematic diagrams for some special attachment ventilation applications. **a** Floor-based air distribution with a novel mushroom diffuser, **b** horizontal-impinging attachment, **c** inclined-impinging attachment, **d** floor-impinging attachment created by circular opening arrays, **e** ventilation columns are set up in a large space to achieve zone control by attachment ventilation for the near zone and longitudinal jet ventilation for the far zone, **f** attachment ventilation for industrial multi-span buildings, **g** adaptive attachment ventilation with a deflector for isolation wards of hospitals, **h** attachment ventilation for ducted-type air conditioner



(g)



(h)

Fig. 5.23 (continued)

References

- Awbi HB (2008) Ventilation systems: design and performance. Taylor and Francis, USA
- Croome DJ, Roberts BM (1981) Air conditioning and ventilation of buildings, vol 10. Pergamon Press
- Han T, Deng HN, Li AG, Liu H, Du H (2021) Measurement and comparison of thermal environment and ventilation performance under different heating air supply modes of wall attached ventilation and mixed ventilation. *J. HV&AC* 51(10):138–144 (in Chinese)
- Li AG, Tao PF, Zhao YJ, Yin HG (2011) A jet impinging air supply mode for capsule hotels. Chinese patent ZL201110121285.0 (in Chinese)
- Li AG, Wang X, Gao R (2010) An adjustable air supply device under seats. Chinese patent ZL201010149577.0 (in Chinese)
- Li AG, Li MM (2016) Research on the effectiveness of air curtain ventilation air distribution for small micro-space. *J Xi'an Univ Arch Tech (Natural Science Edition)* 48(1):115–121 (in Chinese)
- Li AG, Liu WX, Yao CC, Cao YR, Yin HG (2016) CFD and the experimental study of air distribution in the breathing zone based on air curtain ventilation with deflector. *J Xi'an Univ Arch Tech (Natural Science Edition)* 48(5):738–744 (in Chinese)
- Li AG, Hou YC, Yao CC (2017) An environment control method and device for wall attachment air distribution in variable occupied zone. Chinese patent ZL201710698366.4 (in Chinese)
- Li AG, Hou YC, Yang J (2019) Attached ventilation based on a curved surface wall. *Build Simul* 12:505–515
- Reese TA (2005) Crawl space ventilation system. US Patent 6,958,010. 25 Oct 2005
- REHVA (2002) Displacement ventilation-REHVA guidebook No. 1. Brussels, Belgium
- Yang J (2017) Numerical simulation on applicability of attached air curtain ventilation based on the brachistochrone curved wall, inclined wall etc. Xi'an University of Architecture and Technology (in Chinese)
- Yin HG, Li AG, Liu ZY, Sun YX, Chen T (2018) A double-attached combined air supply method and device for soft sleeping compartments of trains. Chinese patent ZL201510795787.X (in Chinese)
- Zou YQ, Wang SB, Peng R, Yang CH (1983) Investigation on cooling load calculation of stratified air conditioning for large space industrial plants. *J Refrigeration* 4:49–56 (in Chinese)

Open Access This chapter is licensed under the terms of the Creative Commons Attribution-NonCommercial-NoDerivatives 4.0 International License (<http://creativecommons.org/licenses/by-nc-nd/4.0/>), which permits any noncommercial use, sharing, distribution and reproduction in any medium or format, as long as you give appropriate credit to the original author(s) and the source, provide a link to the Creative Commons license and indicate if you modified the licensed material. You do not have permission under this license to share adapted material derived from this chapter or parts of it.

The images or other third party material in this chapter are included in the chapter's Creative Commons license, unless indicated otherwise in a credit line to the material. If material is not included in the chapter's Creative Commons license and your intended use is not permitted by statutory regulation or exceeds the permitted use, you will need to obtain permission directly from the copyright holder.



Chapter 6

Design Methods of Attachment Ventilation Systems



Abstract This chapter expounds on a fundamental design principle, design methods, and case studies for attachment ventilation. The design flow charts are provided that describe the primary considerations required and detailed procedures when designing wall-attached air distribution for rooms (spaces) heating or cooling. A comparison of attachment, mixing, and displacement ventilation design methods are also presented. Lastly, the step-by-step design procedures of attachment ventilation systems for typical application scenarios are demonstrated, such as office buildings, exhibition halls, subway stations, and waiting halls of high-speed railway stations.

Keywords Design method · Control zone · Attachment ventilation · Attached ventilation · Case study · Subway station · Air distribution

The primary goal of building ventilation is to provide occupants with clean air for breathing. Creating an appropriate indoor environment is vital for building designers, especially HVAC engineers. The essence of the attachment ventilation design is to clarify the airflow movement path for a given space and determine the air supply parameters (e.g., u_0 , Δt_0 , etc.). Based on the established correlations of characteristic parameters of attachment ventilation in Chaps. 3 and 4, we are able to design attachment ventilation to remove “excessive” heat or pollutants efficiently to meet the demand of parameters in the control zone, which is the scientific connotation of ventilation.

This chapter expounds on fundamental design principles, design methods, and case studies for attachment ventilation. A comparison of attachment, mixing, and displacement ventilation design methods are also presented. Lastly, the step-by-step design procedures of attachment ventilation systems for typical application scenarios are demonstrated, such as office buildings, exhibition halls, subway stations, and waiting halls of high-speed railway stations.

6.1 Scope of Application of Attachment Ventilation Systems

6.1.1 *Distinguishing Features of Attachment Ventilation Systems*

As described in Sect. 4.4.2, the control zone is the volume of the room with a height of 2.0 m above the floor for human-oriented comfort air conditioning, while for industrial air conditioning, the control zone denotes the room-conditioned zone of the equipment or facilities. Distinguishing features of the attachment ventilation system are as follows.

1. Reduce primary investment and operating costs of ventilation and air conditioning systems. Attachment ventilation divides the indoor space into two significant parts: the control zone and the noncontrolled zone, aiming to ensure the control zone environment. In fact, the removed load for the control zone merely occupies part of the whole room load; hence it can remarkably reduce the indoor cooling/heating load and improves the ventilation efficiency. Correspondingly, it also reduces the energy consumption and costs of HVAC systems compared with mixing ventilation.
2. Solve the problem that displacement ventilation is not used to supply warm air to the occupied zone in the wintertime. For large spaces, like airport terminals, attachment ventilation can effectively supply a warm jet to the control zone in wintertime, overcoming the inherent defect that displacement ventilation is normally used for occasions where there is a cooling load.
3. Improve indoor air quality. The fresh air can reach the occupied zone first, so it delivers better air to the target control zone and benefits the building occupants' health and well-being.
4. Save valuable workspace or occupied space. The attachment ventilation system is a kind of less-duct air supply system and is usually installed in the upper part of a room, avoiding occupying lower space or raising the floor (for the installation of displacement ventilation static pressure plenums and piping systems).

Therefore, to some extent, attachment ventilation has the merit of both traditional mixing and displacement ventilation by offering a lowering cooling or heating load on the demand side.

As every coin has two sides, if there are protruding obstacles on the wall surface or equipment nearby the jet-attached wall, attachment ventilation performance will be influenced by those existing obstacles.

6.1.2 *Occupied Zone*

As summarized above, attachment ventilation aims to eliminate the occupied zone's cooling/heating load and provides an intended environment for the conditioned zone, the control zone, or the occupied zone. The occupied zone is between 0.1 and 2.0 m

Table 6.1 Occupied zones

Building envelope	The boundary of the occupied zone (m)		
	Displacement ventilation	Attachment ventilation	Mixing ventilation
Wall/column surface where diffusers are located	0.5–1.5	1.0	1.0
Exterior walls, doors, windows	0.5–1.5	1.0	1.0
Interior walls, column surfaces without inlets or openings	0.25–0.75	0.5	0.5
Floor	0.0–0.2	0.1	0.0
Distance from floor to top	1.1*–2.0**	2.0	1.8

Note The values in the table with * are taken when sitting is the primary posture, and with ** are taken when standing is the primary posture

above the floor and more than 1.0 m from the attached wall, exterior walls/windows or fixed heating, ventilating, or air-conditioning equipment, and 0.5 m from the interior walls. The European Heating, Ventilation and Air Conditioning Association (REHVA) defines the scope of the occupied zone (REHVA 2002), see Table 6.1. The detailed boundaries of the occupied zone are defined as follows.

1. 1.0 m from the wall or column where air inlets or openings are contained.
2. 1.0 m from exterior walls, doors, and windows.
3. 0.5 m from the interior walls.
4. 0.1–2.0 m above the floor.

Figure 6.1 presents the occupied zone of the VWAV, RCAV, and CCAV, see the shaded area. It should be noted that the occupied zone can be changed according to the actual requirements.

6.1.3 Airflow Parameters and Diffusers in the Occupied Zone

According to related standards (GB/T 50155-2015, BS EN ISO 7730-2005, ANSI/ASHRAE Standard 55-2020, etc.), the following airflow parameters are derived for designing attachment ventilation.

- ① Occupied zone temperature difference $t_{0.1} - t_{1.7} \leq 4.0$ °C for standing occupants, $t_{0.1} - t_{1.1} \leq 3.0$ °C for sedentary occupants.
- ② Minimum air temperature at 0.1 m above the floor in the occupied zone $t_{0.1,\min} \geq 19$ °C for winter, $t_{0.1,\min} \geq 21$ °C for summer.
- ③ Air velocity in the occupied zone
 - For ordinary office and residential buildings, $u_n \leq 0.2$ m/s for winter, $u_n \leq 0.3$ m/s for summer.

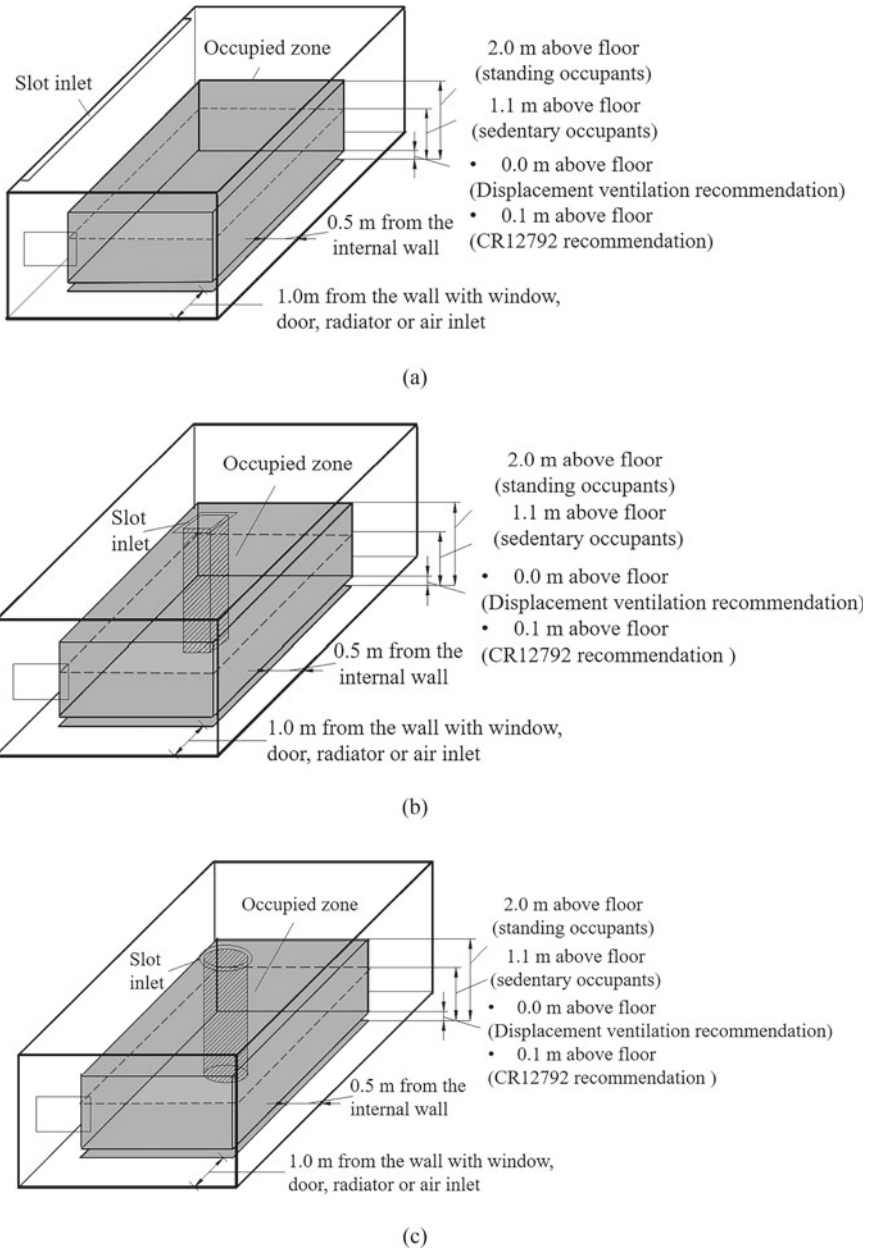


Fig. 6.1 Occupied zone of attachment ventilation. **a** AWAV, **b** RCAV, **c** CCAV

- Regard to temporary staying zones, e.g., railway stations, subway stations and airport terminals, etc., $u_n \leq 0.3\text{--}0.8$ m/s; for industrial buildings, e.g., underground power plants, etc., $u_n \leq 0.2\text{--}0.8$ m/s.
- Air velocity in the control zone can also be determined according to the needs of production processes.

④ Control zone boundary jet velocity $u_{m,1.0}$

- For ordinary offices, residential buildings, etc., $u_{m,1.0} \leq 0.5$ m/s.
- For temporary staying zones, $u_{m,1.0} \leq 1.0$ m/s.
- For industrial workshops, according to the needs of the industrial manufacture process.

In addition, the following principles should be abided by when installing inlets and outlets of attachment ventilation:

- The inlets or openings should not be laid on the exterior wall or the wall with a window.
- There should not be protruding obstacles on the jet-attached wall.

6.2 Attachment Ventilation Design Procedure

The design process of attachment ventilation is to provide appropriate air supply parameters, such as air velocity, temperature, and air opening size, etc., on the premise of meeting the thermal comfort in the occupied zone or industrial processing requirements. The related design parameters are given in Fig. 6.2.

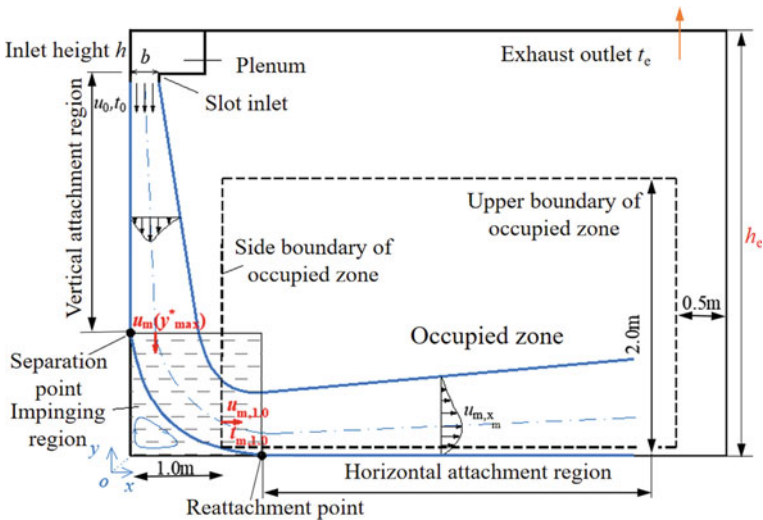


Fig. 6.2 Design parameters related to attachment ventilation

Based on the correlations established in Chaps. 3 and 4, a design method of attachment ventilation has been developed. The design procedure is as follows.

1. Design parameters

- ① Determine air temperature $t_{d,1.1}$

Since t_n in the occupied zone depends mainly on the temperature at the height of 1.1 m above the floor, $t_{d,1.1}$ and t_n can be regarded as identical (Hu 2010).

- ② Determine vertical temperature gradient Δt_g in the occupied zone

The experiments and analysis show that the vertical temperature difference in the horizontal air reservoir region of the attachment ventilation is slightly small, and its temperature gradient is generally lower than that of the displacement ventilation (2.0 °C/m). Δt_g is generally taken as 1.0–1.5 °C/m for attachment ventilation.

- ③ Calculate the excessive heat Q_n within the occupied zone

Q_n is the actual excessive heat in the occupied zone, which is obtained by multiplying the whole room's excessive heat Q by the heat distribution coefficient $m = \frac{t_n - t_0}{t_e - t_0}$. Here, m is the ratio of heat in the control zone (or the occupied zone) to the total heat in the whole room, i.e., m can be determined according to the interface height of thermal stratification (Zhao 2010), or from field tests and calculations. For large spaces with interface heights ranging from 5 to 20 m, m is generally taken from 0.50 to 0.85. For ordinary office rooms, when there is a lack of measurement data, m can be approximately taken as 0.70 (Lu 2007; Huang and Li 1999; Zou et al. 1983).

- ④ Determine the height of the slot inlet and outlet h, h_e , referring to the attached wall/column size.

2. Calculate exhaust air temperature t_e

Calculate t_e from Eq. (6.1)

$$t_e = t_{d,1.1} + \Delta t_g(h_e - 1.1) \quad (6.1)$$

3. Determine air supply temperature t_0

Calculate t_0 from Eq. (6.2)

$$t_0 = t_{d,1.1} - \frac{1 + \kappa(h_e - 1.1)}{1 - \kappa} \Delta t_g \quad (6.2)$$

Determine the air supply dimensionless temperature increment near the floor (0.1 m away from the floor) from $\kappa = \frac{t_{0,1} - t_0}{t_e - t_0}$, which is related to indoor heat source types and locations. In general, for rooms with multiple type of heat sources, $\kappa = 0.50$ is recommended; for distributed heat sources, κ can be assumed to be 0.65 (Lu 2007).

For VWAV, κ can be taken as 0.55, and Eq. (6.2) becomes $t_0 = t_{d,1.1} - (0.88 + 1.22h_e)\Delta t_g$.

4. Derive the air supply velocity u_0

Select the slot inlet width b (generally 0.03–0.15 m) and the length l . Hence, the inlet area F can be preliminarily obtained. Then, u_0 can be derived from the energy balance equation. It should be noted that the air supply velocity u_0 of warm air in wintertime should not be less than 2.0 m/s.

$$u_0 = \frac{Q_n}{\rho \cdot c_p(t_n - t_0) \cdot F} \quad (6.3)$$

5. Check the air velocity at 1.0 m away from the vertical wall $u_{m,1.0}$

Establish $u_{m,1.0}$ from Eqs. (6.4), (4.18), and (4.21)

$$\frac{u_m(y_{\max}^*)}{u_0} = \frac{1}{0.012\left(\frac{y_{\max}^*}{b}\right)^{1.11} + 0.90} \quad (6.4)$$

$$y_{\max}^* = 0.92h - 0.43 \quad (4.18)$$

$$\frac{u_m(y_{\max}^*)}{u_0} = k_v \frac{u_{m,1.0}}{u_0} + C_v \quad (4.21)$$

The coefficients k_v and C_v are related to types of attachment ventilation. $k_v = 1.808$, $C_v = -0.106$ for VWAV; $k_v = 1.374$, $C_v = -0.060$ for CAV.

If $u_{m,1.0} \leq 0.5$ m/s for office and residential buildings, or $u_{m,1.0} \leq 1.0$ m/s for temporary staying zones, such as waiting halls of high-speed railway stations, etc., the design requirements can be met. Otherwise, return to step (4) to reselect b and l .

6. Check the centerline air velocity $u_{m,x}$

$u_{m,x}$ at the end of the air reservoir x can be calculated from Eq. (3.44)

$$\frac{u_{m,x}}{u_0} = \frac{0.575}{C\left(\frac{x}{b} + K_h\right)^{1.11} + 1} \quad (3.44)$$

where

C = shape factor, $C = 0.0075$ for vertical walls; $C = 0.0180$ for rectangular columns; $C = 0.0350$ for circular columns.

K_h = Correction factor, $K_h = \frac{1}{2} \frac{h-2.5}{b}$ for vertical walls and rectangular columns; $K_h = \frac{1}{6} \frac{h-2.5}{b}$ for circular columns.

When $u_{m,x} \leq 0.3$ m/s (or $u_n \leq 0.3$ – 0.8 m/s for the temporary staying zone), if the size of the wall or column can meet the demands of the total slot length, then the whole design procedure is completed. Otherwise, return to step (4) to reselect b and l .

The design procedure is summarized in the flow chart shown in Fig. 6.3.

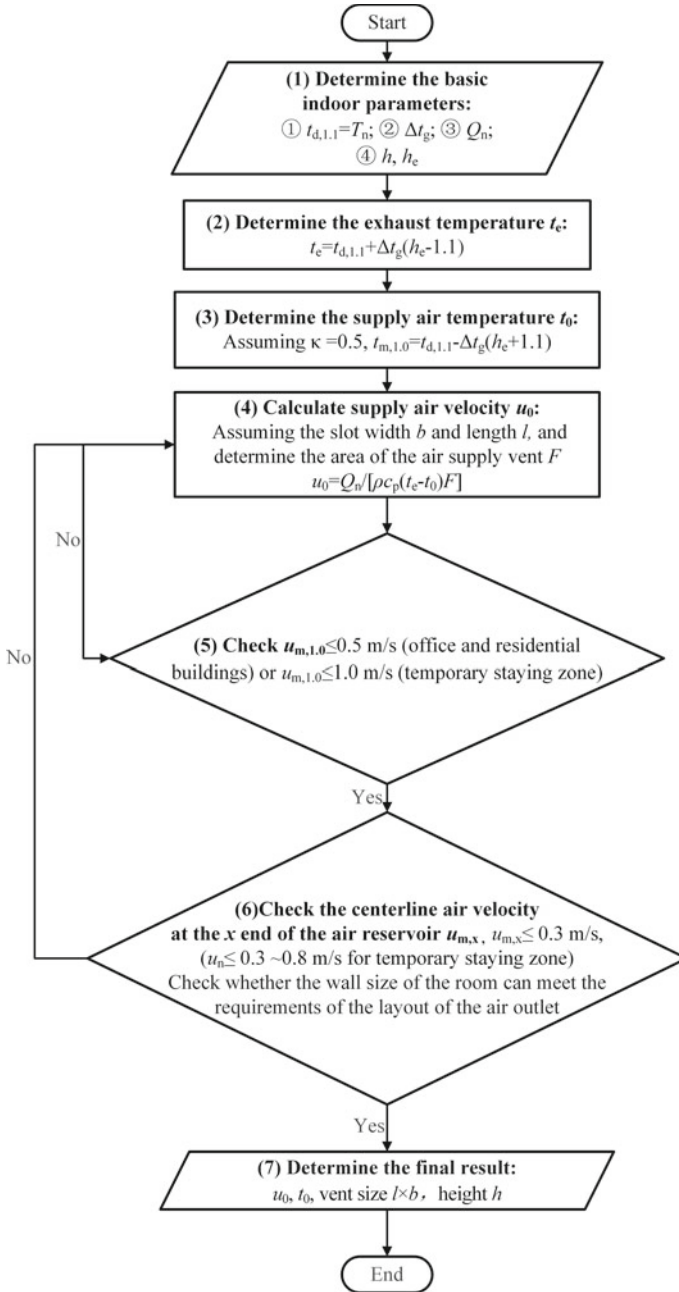


Fig. 6.3 Design procedure flow chart for attachment ventilation

6.3 Adaptive Attachment Ventilation Design Procedure

Adaptive attachment ventilation with deflectors mode (AAV with deflectors) provides us with an “act according to actual circumstances” air distribution method for the scenarios with variable control zones. As described in Chap. 5, it is the deflector that leads the airflow directionally to the breathing zone or the control zone.

For comfort-oriented air conditioning, AAV with deflectors is generally applied to a medium space with a length of 3.0–5.0 m (horizontal jet throw direction). For a large space, the deflector height h_0 can be raised appropriately, see Fig. 6.4. The representative parameters of AAV are shown in Fig. 6.4.

The design procedure of AAV is as follows.

1. Assume the value of b, h_0 . For comfort-oriented air conditioning, $h_0 = 1.1\text{--}1.7\text{ m}$; for industrial process production, h_0 is determined according to the required control zone, and for $b_0 = 0.2\text{--}0.6\text{ m}$ is recommended.
2. Determine the horizontal jet throw $x' = x - b_0 - 0.5$, and the drop $y = h_0 - 0.1$.
3. Establish the Archimedes number Ar of air supply from Eqs. (6.5a, 6.5b) for given values of x' and y .

$$\frac{y}{b} = Ar \left(\frac{x'}{b} \right)^2 \left(0.51 \frac{ax'}{b} + 0.35 \right) \tag{6.5a}$$

or

$$Ar = \frac{\frac{y}{b}}{\left(\frac{x'}{b} \right)^2 \left(0.51 \frac{ax'}{b} + 0.35 \right)} \tag{6.5b}$$

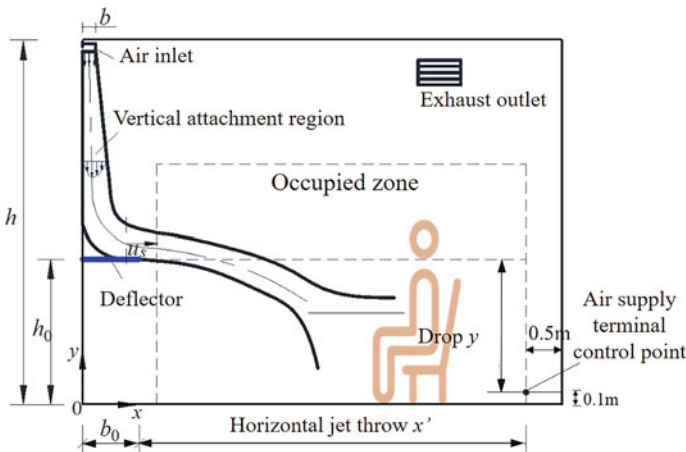


Fig. 6.4 Design parameters of AAV

where

- x' throw, the horizontal distance between the end of the deflector and the side-boundary of the control zone;
 - y drop, the vertical distance between the deflector and the ground of the control zone, 0.1 m above the floor, see Fig. 6.4;
 - a turbulence coefficient of slot inlets, generally, 0.108 is taken for the flat inlet or derived by experiments.
4. Calculate the air supply temperature t_0 by Eq. (6.6).

$$t_0 = t_e - \Delta t_{oz} \quad (6.6)$$

where Δt_{oz} is the temperature difference between supply air and exhaust air, which is ascertained from the related design codes (Δt_{oz} should be less than 10 °C for ordinary rooms with a height of 3.0–5.0 m). For AAV, $t_e = t_n + (2-3 \text{ }^\circ\text{C})$.

5. Determine the air velocity u_s at the deflector by Eq. (6.7).

$$u_s = \sqrt{\frac{gb\Delta t_o}{Ar(t_n + 273)}} \quad (6.7)$$

The temperature difference between air supply and occupied zone $\Delta t_o = t_0 - t_n$, °C;

6. Establish the jet centerline velocity $u_{m,x}$, and jet averaged velocity u_p by Eqs. (6.8a, 6.8b).

$$u_{m,x} = u_s \frac{0.48}{\frac{ax'}{b} + 0.145} \quad (6.8a)$$

$$u_p = 0.5u_{m,x} \quad (6.8b)$$

u_p should meet the following requirements. In the control zone, $u_p \leq 0.2$ m/s for winter, $u_p \leq 0.3$ m/s for summer. Particularly, for the temporary staying zone as mentioned before, or industrial air-conditioning, u_p is determined according to the specific demands. Otherwise, b needs to be reassumed.

7. Calculate the air supply velocity u_0 by Eq. (6.9).

$$\frac{u_s}{u_0} = \frac{1}{0.012\left(\frac{h-h_0}{b}\right)^{1.11} + 0.90} \quad (6.9)$$

8. Derive l from the energy balance Eq. (6.10) for a given value of Q , and check whether the room wall size is satisfied or not. Additionally, the number of inlets can be adjusted according to the room size.

$$l = \frac{mQ}{c_p \rho u_0 b \Delta t_{oz}} \quad (6.10)$$

The above design procedure is summarized in the flow chart shown in Fig. 6.5.

6.4 Comparison of Design Methods of Attachment, Mixing and Displacement Ventilation

Traditional mixing ventilation, displacement ventilation, as well as novel attachment ventilation are discussed and compared in this section.

1. Mixing ventilation

Mixing air distribution aims to dilute room pollutants with cleaner and cooler/warmer fresh air, to promote well mixing and uniform temperature and pollution distribution in the control zone. As shown in Fig. 6.6a, point P_1 , where the flow passes the imaginary horizontal surface that defines the occupied zone (Nielsen 2007), represents the intersection between the jet centerline and the upper boundary line/surface of the occupied zone. To ensure thermal comfort in the occupied zone, the centerline velocity at the boundary should equal $2u_n$, and the air supply temperature difference should be in the range of 5.0–10 °C for $h \leq 5.0$ m for comfort-oriented air conditioning (Zhao 2008; GB50736). The mixing air distribution bears the cooling/heating load of whole rooms.

2. Displacement ventilation

Displacement ventilation has been used in industrial premises for many years, and it has also been used more extensively in non-industrial premises. To reach the same air quality in the occupied zone, displacement ventilation typically requires a lower airflow rate than mixing ventilation. As shown in Fig. 6.6b, point P_2 demonstrates the intersection point between the piston flow centerline and the lateral boundary line/surface of the occupied zone. The thermal comfort can be achieved by controlling the centerline velocity of about 0.25 m/s at P_2 , the air supply temperature to be no less than 18 °C, and the vertical temperature difference to be lower than 3.0 °C (GB50736; Nielsen 2007). Displacement ventilation is used in buildings with large occupancy and internal heat gains where mainly cooling is required (Awbi 2008). The air supply inlets/openings are usually mounted in the occupied zone, occupying the workspace. Unlike mixing ventilation, it only bears part of the cooling load of rooms.

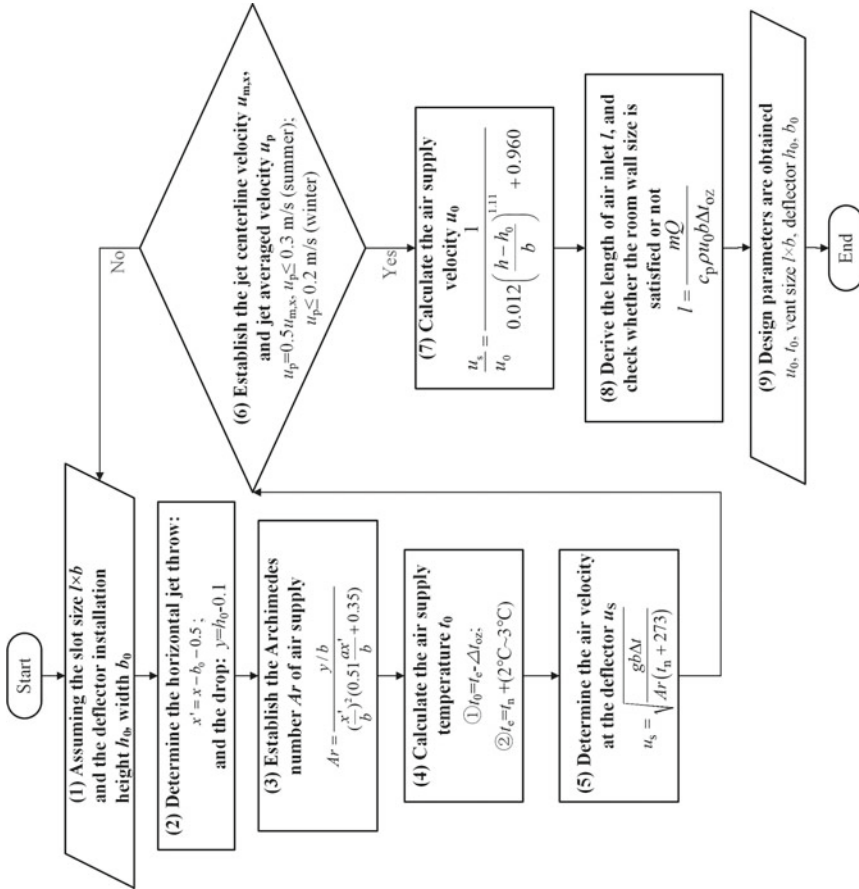


Fig. 6.5 Design procedure flow chart for AAV with deflectors

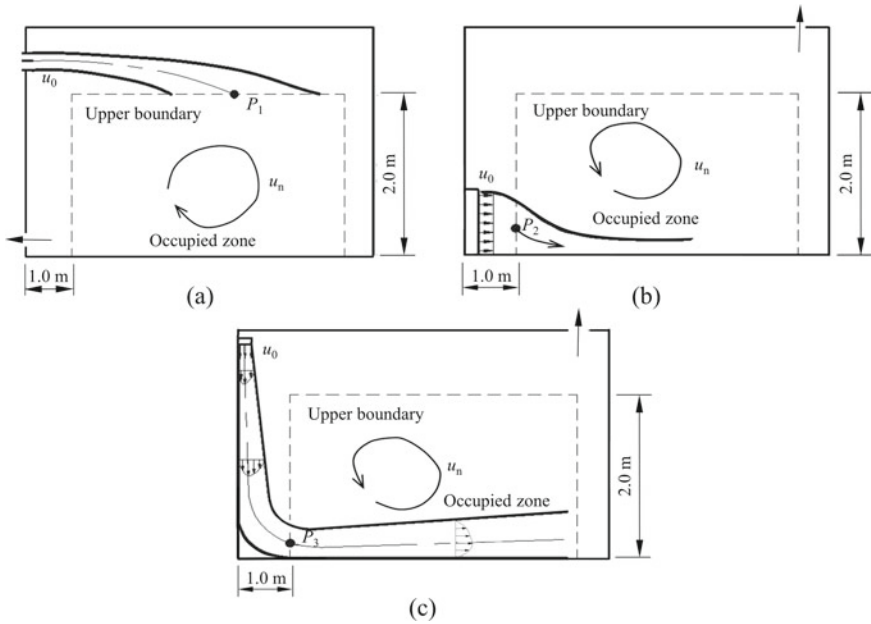


Fig. 6.6 Comparison of air distribution design scheme of **a** mixing ventilation, **b** displacement ventilation, **c** attachment ventilation

3. Attachment ventilation

To overcome the inadequacy of mixing and displacement ventilation mentioned above, attachment ventilation has been developed. As shown in Fig. 6.6c, similar to points P_1 and P_2 , point P_3 illustrates the intersection point between the wall-attached jet centerline and the boundary line/surface of the occupied zone. The ventilation and air conditioning design requirements can be met by controlling the centerline velocity at the lateral boundary of the occupied zone $u_{m,1.0}$ (1.0 m away from the jet-attached wall surface), and vertical temperature difference to be less than $3.0\text{ }^\circ\text{C}$ in the occupied zone. It is recommended that $u_{m,1.0} \leq 0.5\text{ m/s}$ for office and residential buildings, $u_{m,1.0} \leq 1.0\text{ m/s}$ for temporary staying zones, or $u_{m,1.0}$ be determined according to design requirements. Similar to displacement ventilation, attachment ventilation only bears part of the room cooling/heating loads, so it is a high energy-efficiency ventilation mode.

The design principles and methods of mixing, displacement, and attachment ventilation are listed in Table 6.2.

Table 6.2 Comparison of air distribution design procedure of mixing ventilation, displacement ventilation and attachment ventilation

Type	Mixing ventilation, downward air supply (Zhao 2008)	Displacement ventilation with a wall diffuser (Lu 2007; REHVA 2013)	Attachment ventilation
Design scheme			
Load	Mixing ventilation bears the whole cooling/heating load, while displacement and attachment ventilation only bear part of the load (occupied zone load)		
Known condition	Room size $L \times W \times H$ (length \times width \times height), excessive heat Q , indoor design temperature t_n		

(continued)

Table 6.2 (continued)

Type	Mixing ventilation, downward air supply (Zhao 2008)	Displacement ventilation with a wall diffuser (Lu 2007; REHVA 2013)	Attachment ventilation
Design procedure	<p>① Calculate air supply rate according to indoor excessive heat and air supply temperature difference (generally, $t_n - t_0$ should not be greater than 10 °C for comfort-oriented air conditioning) $q_s = Q / [\rho c_p (t_n - t_0)]$</p> <p>② According to the air supply rate and room size, determine the diffuser form and size, derive the number of diffusers N and spacing r, calculate the single diffuser area F and air supply velocity u_0</p> <p>③ Calculate jet throw x: $x = L - 0.5 + (H - 2.0)$</p> <p>④ Check the jet velocity as it enters the occupied zone $u_{m,x}, u_{m,x} = \frac{u_0 K_{m1} \sqrt{kF}}{x}$ (Zhao 2008)</p> <p>If $u_{m,x} \leq 2u_n$, it meets the design requirements. Otherwise, go back to step ② to rearrange the diffusers</p> <p>⑤ Design parameters, including u_0, t_0, diffuser size and location, number, etc. are obtained</p>	<p>① Determine the basic indoor control parameters $t_{d-1.1}, \Delta t_g$</p> <p>② Assume the dimensionless temperature rise near the floor: $\kappa = \frac{t_{0.1} - t_{m,1.0}}{t_e - t_{m,1.0}} = 0.5$</p> <p>③ Calculate the temperature difference between supply and exhaust air: $t_e - t_0 = 2h_e \Delta t_g$</p> <p>④ Derive air supply rate q_s and air supply temperature t_0 $q_s = Q / [\rho c_p (t_e - t_0)]$</p> <p>$t_0 = t_{d-1.1} - \Delta t_g (h + 1.1)$</p> <p>⑤ Check the temperature at floor level $t_{0.1}$: $t_{0.1} \geq 22$ °C for summer</p> <p>⑥ Obtain the inlet opening area F and determine the number N of diffusers: $F = q_s / (3600 \times u_0 \times N \times k)$</p> <p>⑦ Design parameters, including u_0, t_0, diffuser size and location, number, etc. are proposed</p>	<p>① Determine indoor control parameters: $t_{d,1.1}, \Delta t_g, Q_n, h, h_e$</p> <p>② Assume the dimensionless temperature rise near the floor: $\kappa = \frac{t_{0.1} - t_0}{t_e - t_0} = 0.55$</p> <p>③ Determine the exhaust air temperature t_e: $t_e = t_{d,1.1} + \Delta t_g (h_e - 1.1)$</p> <p>④ Determine the air supply temperature t_0: $t_0 = t_{d,1.1} - (0.88 + 1.22h_e) \Delta t_g$</p> <p>⑤ Calculate air supply velocity u_0: assume diffuser size b, l, preliminary determination of inlet area F, then, $u_0 = Q_n / [\rho c_p (t_n - t_0) F]$</p> <p>⑥ Check the control air velocity at 1.0 m from the vertical wall $u_{m,1.0}$</p> <p>If $u_{m,1.0} \leq 0.5$ (or the specified value), the design requirement can be met. Otherwise, return to step ⑤ to re-assume the diffuser size b, l</p> <p>⑦ Check the air velocity at the end of the jet air reservoir $u_{m,x}$: If $u_{m,x} \leq 0.3$ m/s (or the specified value), the calculation procedure is finished. Otherwise, return to the ⑤ step to re-assume b, l. Note l should be appropriate to meet the wall size</p> <p>⑧ Design parameters, including u_0, t_0, diffuser size $l \times b$, installation height h, etc. are determined</p>

6.5 Case Study and Design of Attachment Ventilation Systems

In previous chapters, the semi-empirical correlations have been established by the author to predict the centerline velocity and temperature distribution, etc., characterizing attachment ventilation, which also helps to explain in a basic way room air movement. The essence of air distribution design is to guarantee the critical parameters in the occupied zone (control zone), such as air velocity, temperature, gradient, etc., to meet the design requirements. If the air distribution is designed inappropriately, there may be a draft sensation, and the air conditioning system's energy consumption will be increased remarkably.

This section presents some typical engineering applications of attachment ventilation, including office buildings, exhibition halls, subways, and high-speed railway stations, and describes the air distribution design procedure.

6.5.1 Office Room

Typically, the air distribution design of office rooms is considered as a kind of comfort-oriented air conditioning design.

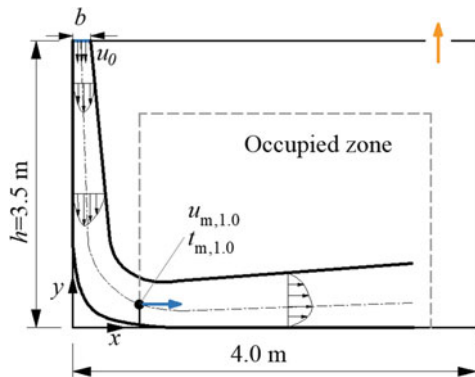
Take an air-conditioned office with dimensions of 4.0 m × 5.0 m × 3.5 m (length × width × height) as an example, the excessive heat Q of this room is 1.56 kW in summer. The schematic diagram of attachment air distribution is shown in Fig. 6.7.

The VWAV design procedure of the office is as follows.

1. Design parameters

- ① Select $t_{d,1.1} = t_n = 26\text{ }^\circ\text{C}$ ($t_{d,1.1}$ depends mainly on t_n);

Fig. 6.7 Schematic diagram of VWAV



- ② Assume vertical temperature gradient $\Delta t_g = 1.3 \text{ }^\circ\text{C/m}$ (1.0–1.5 $^\circ\text{C/m}$ is recommended, where 1.0 $^\circ\text{C/m}$ for low heat dissipation, 1.5 $^\circ\text{C/m}$ for high heat dissipation);
- ③ Calculate excessive heat in the occupied zone by $Q_n = mQ = 0.80 \times 1.56 = 1.25 \text{ kW}$ (Yuan et al. 1999);
- ④ Assume heights of inlet and outlet, $h = h_e = 3.5 \text{ m}$.

2. Calculate the exhaust air temperature t_e

$$t_e = t_{d,1.1} + \Delta t_g(h_e - 1.1) = 26 + 1.3 \times (3.5 - 1.1) = 29.1 \text{ }^\circ\text{C}$$

3. Calculate the air supply temperature t_0

Determine the air supply dimensionless temperature rise near the floor (0.1 m above the floor) from $\kappa = \frac{t_{0.1} - t_0}{t_e - t_0} = 0.55$, then calculate t_0 from $t_0 = t_{d,1.1} - (0.88 + 1.22h_e)\Delta t_g = 26 - (0.88 + 1.22 \times 3.5) \times 1.3 = 19.3 \text{ }^\circ\text{C}$.

4. Calculate the air supply velocity u_0

Assume $b = 0.05 \text{ m}$, $l = 2.0 \text{ m}$, and $F = b \times l$. Then calculate u_0 from $u_0 = \frac{Q_n}{\rho \cdot c_p (t_n - t_0) \cdot F} = 1.55 \text{ m/s}$.

5. Check the air velocity at 1.0 m from the vertical wall $u_{m,1.0}$

$$y_{\max}^* = 0.92h - 0.43 = 0.92 \times 3.5 - 0.43 = 2.79 \text{ m}$$

$$\frac{u_m(y_{\max}^*)}{u_0} = \frac{1}{0.012 \left(\frac{y_{\max}^*}{b} \right)^{1.11} + 0.90} = 0.5$$

$$0.5 = 1.808 \frac{u_{m,1.0}}{u_0} - 0.106$$

$u_{m,1.0} = 0.55 \text{ m/s} > 0.50 \text{ m/s}$, return to step (4) to reselect b and l , and the calculation process is as follows:

Firstly, assume $b = 0.05 \text{ m}$, $l = 3.0 \text{ m}$, so $F = 0.15 \text{ m}^2$. Then, it can be calculated that $u_0 = 1.03 \text{ m/s}$, $u_{m,1.0} = 0.34 \text{ m/s} \leq 0.5 \text{ m/s}$. In addition, $u_{m,x} = 0.3 \text{ m/s}$, which meets the required of air velocity in the occupied zone. In this case, it is finally obtained design parameters including $u_0 = 1.03 \text{ m/s}$, $t_0 = 19.3 \text{ }^\circ\text{C}$, $b = 0.05 \text{ m}$, $l = 3.0 \text{ m}$, as shown in Fig. 6.8. Two slot inlets (1.5 m \times 0.05 m) are evenly arranged along the length of the room.

The air distribution of this office is simulated by CFD, and the results are shown in Fig. 6.9.

Fig. 6.8 Design plan of VWAV of an office room (unit: m)

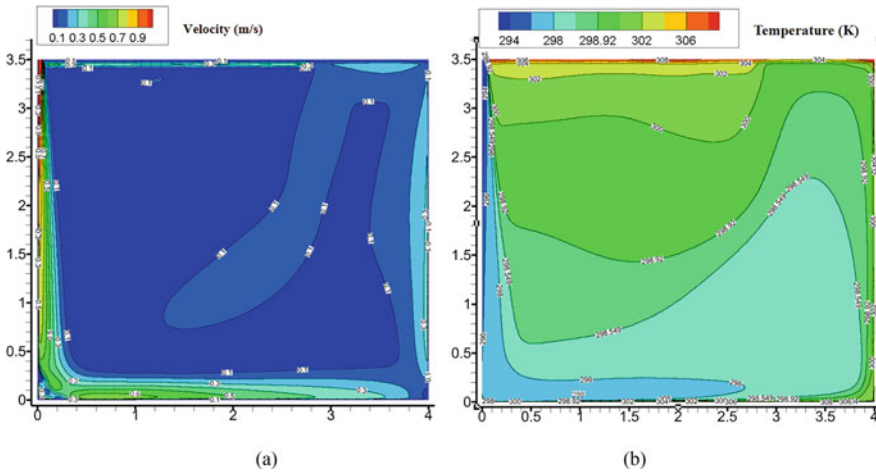
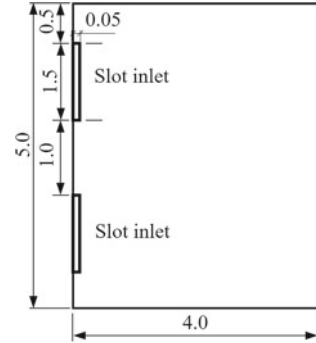


Fig. 6.9 Air distribution for VWAV of the office room. **a** Indoor air velocity contour, **b** indoor air temperature contour

6.5.2 Exhibition Hall

In this section, the VWAV air distribution design of an exhibition hall is conducted.

Take an exhibition hall with dimensions of 24.0 m × 16.0 m × 4.5 m (length × width × height) as an example, the ceiling height of the exhibition hall is 3.5 m. The excessive heat Q of this exhibition hall is 19.2 kW.

In this built space of the exhibition hall, vertical wall attachment air distribution is utilized. The following is the VWAV design procedure for the exhibition hall.

1. Design parameters

- ① Select $t_{d,1.1} = t_n = 26\text{ }^\circ\text{C}$ ($t_{d,1.1}$ depends mainly on t_n);
- ② Assume vertical temperature gradient $\Delta t_g = 1.2\text{ }^\circ\text{C/m}$ (take account of the disturbance of human activities on airflow, Δt_g takes a lower value);

- ③ Calculate excessive heat in the occupied zone by $Q_n = mQ = 0.8 \times 19.2 = 15.36 \text{ kW}$;
- ④ Assume the height of inlet and outlet, $h = h_e = 3.5 \text{ m}$, which are the same as the ceiling height.

2. Calculate the exhaust air temperature t_e

$$t_e = t_{d,1.1} + \Delta t_g (h_e - 1.1) = 26 + 1.2 \times (3.5 - 1.1) = 28.9^\circ\text{C}$$

3. Calculate the air supply temperature t_0

Determine the air supply dimensionless temperature rise near the floor (0.1 m above the floor) from $\kappa = \frac{t_{0.1} - t_0}{t_e - t_0} = 0.55$, then calculate t_0 from $t_0 = t_{d,1.1} - (0.88 + 1.22h_e)\Delta t_g = 26 - (0.88 + 1.22 \times 3.5) \times 1.2 = 19.8^\circ\text{C}$.

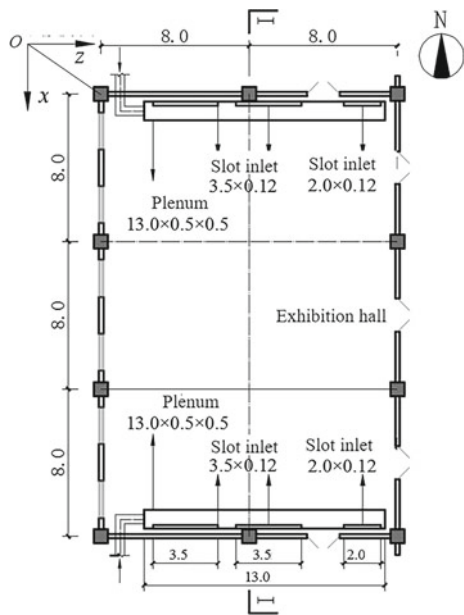
4. Calculate the air supply velocity u_0

Assume $b = 0.12 \text{ m}$, $l = 18 \text{ m}$, and $F = b \times l$. According to the building structure, slot inlets are mounted on the north and south walls, respectively, as shown in Fig. 6.10. Then calculate u_0 from $u_0 = \frac{Q}{\rho \cdot c_p \Delta T \cdot F} = \frac{15.36}{1.2 \times 1.004 \times 6.2 \times 2.16} = 0.95 \text{ m/s}$.

5. Check the air velocity at 1.0 m from the vertical wall $u_{m,1.0}$

$$y_{\max}^* = 0.92h - 0.43 = 0.92 \times 3.5 - 0.43 = 2.8$$

Fig. 6.10 Design plan of VWAV of exhibition hall (unit: m)



$$\frac{u_m(y_{\max}^*)}{u_0} = \frac{1}{0.012\left(\frac{y_{\max}^*}{b}\right)^{1.11} + 0.90} = 0.77$$

$$\frac{u_m(y_{\max}^*)}{u_0} = 1.808 \frac{u_{m,1.0}}{u_0} - 0.106$$

$u_{m,1.0} = 0.46 \text{ m/s} < 0.50 \text{ m/s}$, which satisfied the requirements.

6. Check the centerline velocity $u_{m,x}$ at the end of the air reservoir $x = 12 \text{ m}$

$$\begin{aligned} u_{m,x} &= \frac{0.575u_0}{0.0075\left(\frac{x}{b} + \frac{1}{2}\frac{h-2.5}{b}\right)^{1.11} + 1} \\ &= 0.24 \text{ m/s} < 0.3 \text{ m/s} \end{aligned}$$

Considering that a number of doors and windows are set on the east and west walls of this exhibition hall, so the inlets are arranged on the north and south walls. However, there are fire safety doors on the top of north and south walls; consequently, the length of the slot inlets is not exactly equal. Finally, the outcome is as follows: four slot inlets of $3.5 \text{ m} \times 0.12 \text{ m}$, and two slot inlets of $2.0 \text{ m} \times 0.12 \text{ m}$, $u_0 = 0.95 \text{ m/s}$, $t_0 = 19.8 \text{ }^\circ\text{C}$, as shown in Fig. 6.10.

Both the velocity and temperature contours of the exhibition hall are simulated, and the results are shown in Fig. 6.11.

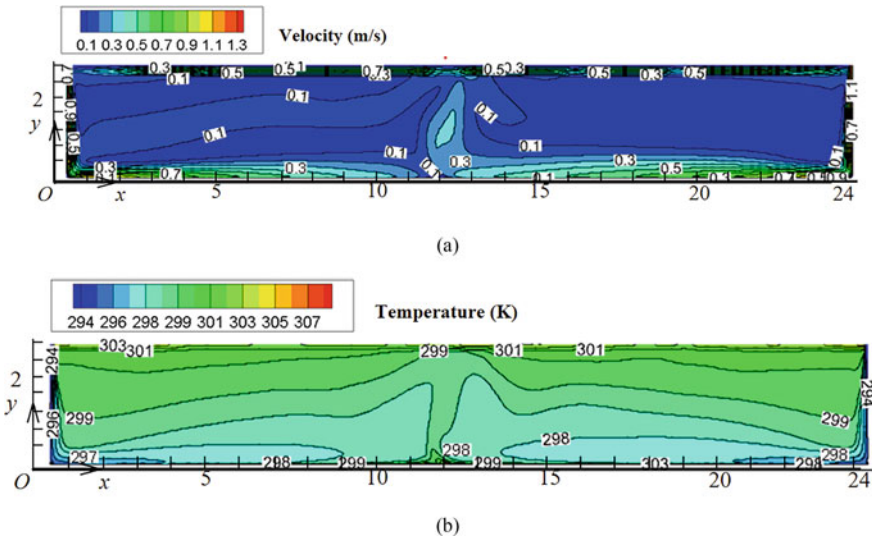


Fig. 6.11 Air distribution of exhibition hall from CFD simulation. **a** Velocity contour of I-I section, **b** temperature contour of I-I section

6.5.3 Subway Station

Different from airflow patterns in office rooms or exhibition halls mentioned in Sects. 6.5.1 and 6.5.2, for the platform and concourse of a subway station, there is a distinguishing feature that passengers usually stay temporarily in the platform and concourse for no more than 10 min. The acceptable air velocity for a temporary staying zone is no more than 0.5 m/s.

Take a subway station with dimensions of 105.0 m × 12.0 m × 6.35 m (length × width × height) as an example, as shown in Fig. 6.11, there are 10 rectangular structural columns uniformly spaced, and the distance between two adjacent columns $l = 9.0$ m. The RCAV is used, and the height of the slot inlets is 4.0 m. The excessive heat Q is 112 kW. As the station is symmetrical along the length direction, the half-width of the station hall is taken into account for the ventilation design, as shown in Fig. 6.12.

The RCAV design procedure of the subway station is as follows.

1. Design parameters

- ① Select $t_{d,1.1} = t_n = 26$ °C ($t_{d,1.1}$ depends mainly on t_n);
- ② Assume vertical temperature gradient $\Delta t_g = 1.3$ °C/m;
- ③ Calculate excessive heat in the occupied zone by $Q_n = mQ = 0.75 \times 56 = 42$ kW;
- ④ Assume heights of inlet and outlet, $h = h_e = 4.0$ m;
- ⑤ The size of rectangular columns is 1.5 m × 1.1 m (length × width), 5 in total.

2. Calculate the exhaust air temperature t_e

$$t_e = t_{d,1.1} + \Delta t_g(h_e - 1.1) = 26 + 1.3 \times (4.0 - 1.1) = 29.8$$
 °C

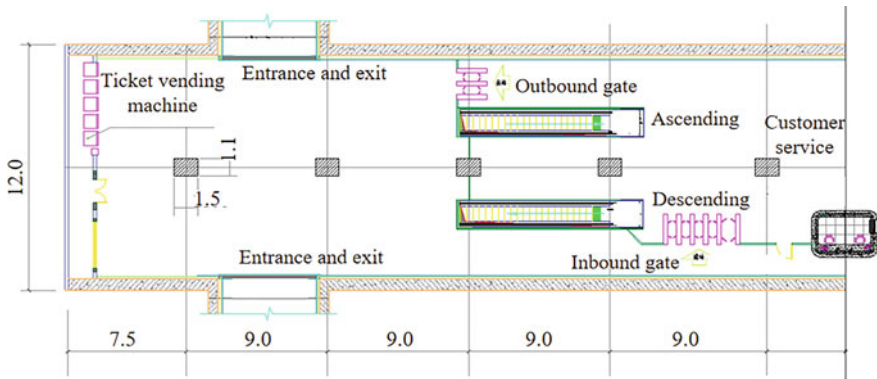


Fig. 6.12 Plan of the subway station (unit: m)

3. Calculate the air supply temperature t_0

Determine the air supply dimensionless temperature rise near the floor (0.1 m above the floor) from $\kappa = \frac{t_{0.1}-t_0}{t_e-t_0} = 0.55$, then calculate t_0 from $t_0 = t_{d,1.1} - (0.88 + 1.22h_e)\Delta t_g = 26 - (0.88 + 1.22 \times 4.0) \times 1.3 = 18.5^\circ\text{C}$.

4. Calculate the air supply velocity u_0

Assume $b = 0.03$ m, the number of columns is 5, and the total area of inlet $F = 0.80$ m². Then calculate u_0 from $u_0 = \frac{Q}{\rho \cdot c_p (t_n - t_0) \cdot F} = \frac{42}{1.2 \times 1.004 \times 7.5 \times 0.8} = 5.81$ m/s.

5. Check the air velocity at 1.0 m from the vertical wall $u_{m,1.0}$

$$y_{\max}^* = 0.92h - 0.43 = 0.92 \times 4 - 0.43 = 3.25 \text{ m}$$

$$\begin{aligned} \frac{u_m(y_{\max}^*)}{u_0} &= \frac{1}{0.012 \left(\frac{y_{\max}^*}{b} \right)^{1.11} + 0.90} \\ &= \frac{1}{0.012 \times \left(\frac{3.25}{0.03} \right)^{1.11} + 0.90} = 0.33 \\ \frac{u_m(y_{\max}^*)}{u_0} &= 1.374 \frac{u_{m,1.0}}{u_0} - 0.060 \end{aligned}$$

$u_{m,1.0} = 1.63$ m/s > 1.00 m/s, return to step (4) to reselect b , and the calculation process is as follows:

Assume $b = 0.1$ m, $l = 3.0$ m, so $F = 2.8$ m², $u_0 = 1.67$ m/s. We obtain $u_{m,1.0} = 0.89$ m/s < 1.00 m/s, which meets the air velocity requirements in the occupied zone.

6. Check the centerline velocity $u_{m,x}$ at the end of the air reservoir $x = 7.5$ m

$$u_{m,x} = \frac{0.575u_0}{0.018 \left(\frac{x}{b} + \frac{1}{2} \frac{h-2.5}{b} \right)^{1.11} + 1} = 0.28 \text{ m/s}$$

$u_{m,x} < 0.8$ m/s, the air velocity at the end of the temporary staying zone of the subway station is satisfied, and the procedure is completed.

In this case, it is finally derived that $u_0 = 1.67$ m/s, $t_0 = 18.5^\circ\text{C}$, $b = 0.10$ m, $F = 2.8$ m², as shown in Figs. 6.13 and 6.14.

6.5.4 Waiting Hall of High-Speed Railway Station

High-speed railway is an important urban infrastructure and transportation hub. Take the waiting hall of a high-speed railway station with dimensions of 200.0 m × 90.0 m × 13.8 m (length × width × height) as an example, the excessive heat Q is 1476 kW.

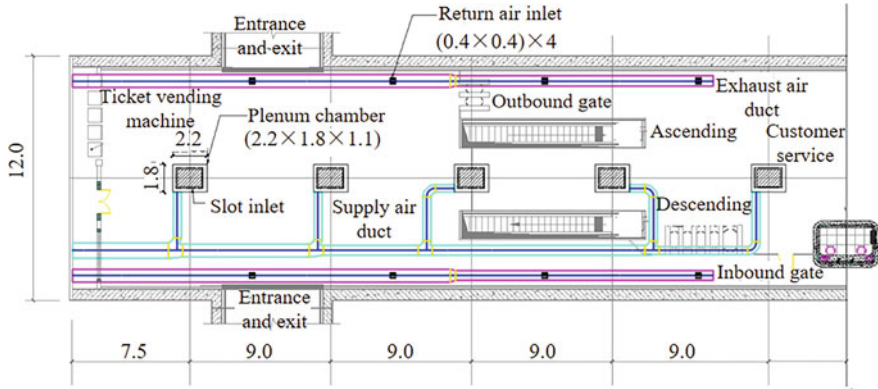


Fig. 6.13 Layout of the air supply system (unit: m)

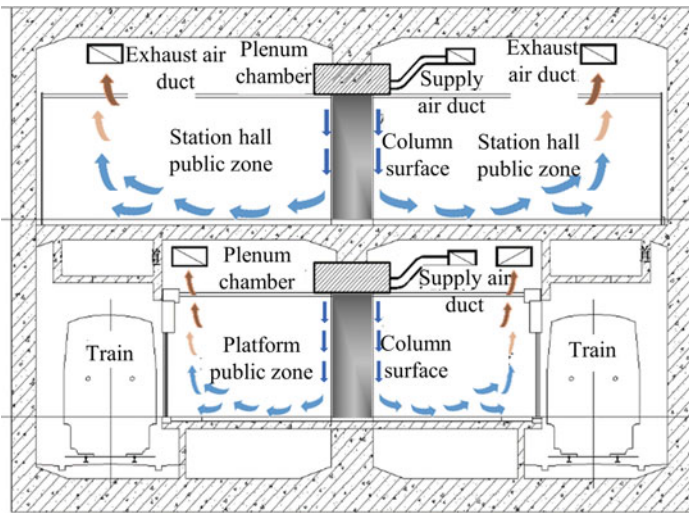


Fig. 6.14 Section of air duct system of RCAV

The RCAV is applied to the waiting hall with 24 ventilation-columns, whose size is 3.0 m × 3.0 m × 4.0 m (length × width × height), and the installation height of slot inlets is 4.0 m from the ground, as shown in Fig. 6.15.

The RCAV design procedure for the high-speed railway station waiting hall is as follows.

1. Design parameters

- ① Select $t_{d,1.1} = t_n = 26\text{ }^\circ\text{C}$ ($t_{d,1.1}$ depends mainly on t_n);
- ② Assume vertical temperature gradient $\Delta t_g = 1.3\text{ }^\circ\text{C/m}$;

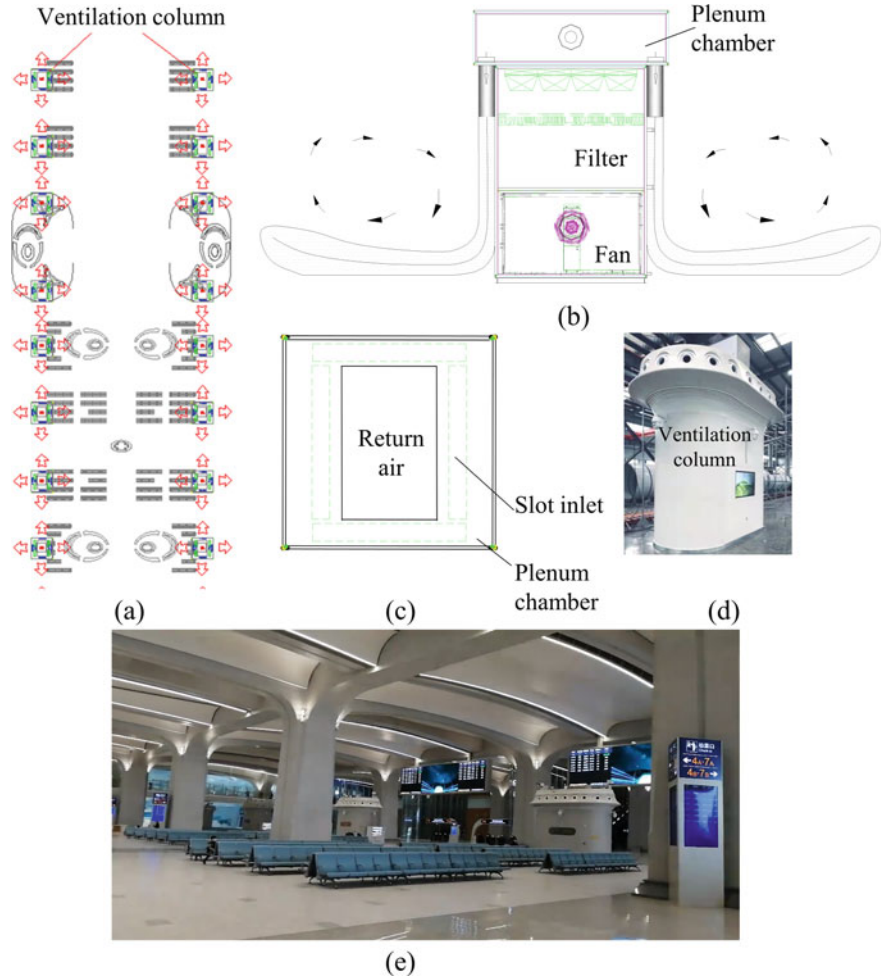


Fig. 6.15 Design for attachment ventilation, high-speed railway station waiting hall. **a** Plan of the waiting hall, **b** schematic diagram of the ventilation column, **c** plenum chamber and slot inlet, **d** ventilation column with top circular openings for the far zone, slots for the near zone, **e** application of RCAV in Xiong'an high-speed railway station

- ③ Calculate excessive heat in the occupied zone by $Q_n = mQ = 1476 \times 0.5 = 738 \text{ kW}$;
- ④ Assume heights of inlet and outlet, $h = h_e = 4.0 \text{ m}$;
- ⑤ The size of rectangular columns is $3.0 \text{ m} \times 3.0 \text{ m} \times 4.0 \text{ m}$ (length \times width \times height), 24 in total.

2. Calculate the exhaust air temperature t_e

$$t_e = t_{d,1.1} + \Delta t_g(h_e - 1.1) = 26 + 1.3 \times (4.0 - 1.1) = 29.8^\circ\text{C}$$

3. Calculate the air supply temperature t_0

Determine the air supply dimensionless temperature rise near the floor (0.1 m above the floor) from, $\kappa = \frac{t_{0.1}-t_0}{t_e-t_0} = 0.55$, then calculate t_0 by $t_0 = t_{d,1.1} - (0.88 + 1.22h_e)\Delta t_g = 26 - (0.88 + 1.22 \times 4.0) \times 1.3 = 18.5 \text{ }^\circ\text{C}$.

4. Calculate the air supply velocity u_0

Assume $b = 0.18 \text{ m}$, the number of columns is 24, and the total area of inlet $F = 54.95 \text{ m}^2$. Then calculate u_0 from $u_0 = \frac{Q}{\rho \cdot c_p (t_n - t_0) \cdot F} = \frac{738}{1.2 \times 1.004 \times 7.5 \times 54.95} = 1.49 \text{ m/s}$.

5. Check the air velocity at 1.0 m from the vertical wall $u_{m,1.0}$

$$y_{\max}^* = 0.92h - 0.43 = 0.92 \times 4.0 - 0.43 = 3.25 \text{ m}$$

$$\begin{aligned} \frac{u_m(y_{\max}^*)}{u_0} &= \frac{1}{0.012 \left(\frac{y_{\max}^*}{b} \right)^{1.11} + 0.90} \\ &= \frac{1}{0.012 \times \left(\frac{3.25}{0.10} \right)^{1.11} + 0.90} = 0.83 \\ \frac{u_m(y_{\max}^*)}{u_0} &= 1.374 \frac{u_{m,1.0}}{u_0} - 0.060 \end{aligned}$$

$u_{m,1.0} = 0.97 \text{ m/s} < 1.00 \text{ m/s}$, which satisfies the requirement.

6. Check the centerline velocity $u_{m,x}$ at the end of the air reservoir $x = 25 \text{ m}$

$$u_{m,x} = \frac{0.575u_0}{0.018 \left(\frac{x}{b} + \frac{1}{2} \frac{h-2.5}{b} \right)^{1.11} + 1} = 0.16 \text{ m/s}$$

$u_{m,x} < 0.8 \text{ m/s}$, the air velocity at the end of the temporary staying zone of the high-speed railway station waiting hall is satisfied, and the procedure is completed.

In this case, it is finally determined that $u_0 = 1.49 \text{ m/s}$, $t_0 = 18.5 \text{ }^\circ\text{C}$, $b = 0.18 \text{ m}$, $F = 54.95 \text{ m}^2$.

The air distribution of this waiting hall of high-speed railway station is simulated by CFD, and the results are shown in Fig. 6.16.

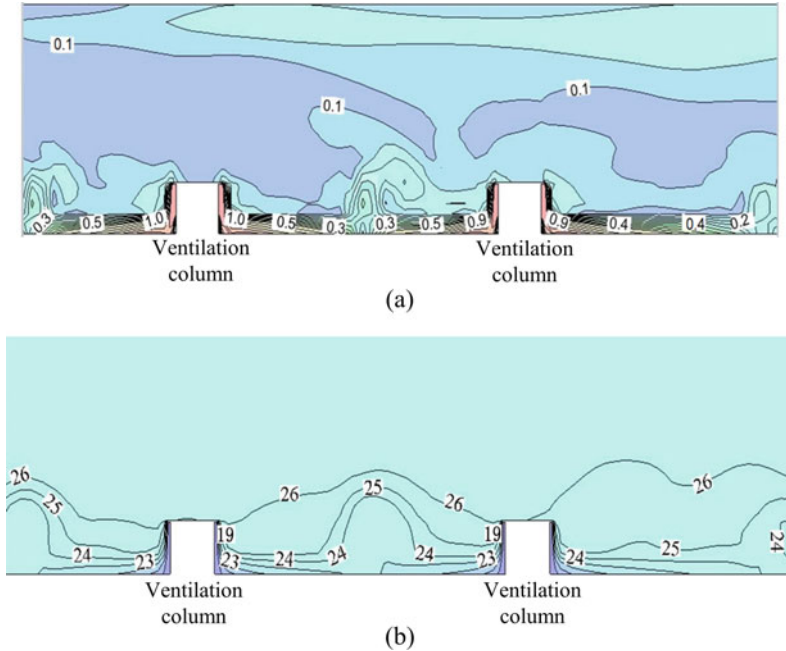


Fig. 6.16 Air distribution of high-speed railway station waiting hall. **a** Air velocity distribution, **b** temperature distribution

References

- Awbi HB (2008) Ventilation systems: design and performance. Taylor and Francis, London and New York
- GB 50736-2012 (2012) Design code for heating ventilation and air conditioning of civil buildings. China Architecture & Building Press, Beijing (in Chinese)
- Hu PF (2010) New technology and application of building ventilation and air conditioning. China Electric Power Press, Beijing (in Chinese)
- Huang C, Li ML (1999) Research of vertical temperature distribution in large space. *J HV&AC* 29(5):28–33 (in Chinese)
- Lu YQ (2007) Practical heating ventilation and air conditioning design handbook, 2nd edn. China Architecture & Building Press, Beijing (in Chinese)
- Nielsen PV (2007) Analysis and design of room air distribution systems. *HVAC&R Res* 13(6):987–997
- REHVA (2002) Displacement ventilation-REHVA Guidebook No. 23. Federation of European Heating, Ventilation and Air Conditioning Associations, Finland
- REHVA (2013) Mixing ventilation-Guide on mixing ventilation air distribution design-REHVA Guidebook No. 19. Federation of European Heating, Ventilation and Air Conditioning Associations, Finland
- Yuan XX, Chen QY, Glicksman LR (1999) Models for prediction of temperature difference and ventilation effectiveness with displacement ventilation. *ASHRAE Trans* 105:353–367
- Zhao HZ (2010) Indoor heat convection and ventilation. China Architecture & Building Press, Beijing (in Chinese)

- Zhao RY (2008) Air conditioning, 4th edn. China Architecture & Building Press, Beijing (in Chinese)
- Zou YQ, Wang SB, Peng R, Yang CH (1983) Investigation on cooling load calculation of stratified air conditioning for large space industrial plants. J Refrig 4:49–56 (in Chinese)

Open Access This chapter is licensed under the terms of the Creative Commons Attribution-NonCommercial-NoDerivatives 4.0 International License (<http://creativecommons.org/licenses/by-nc-nd/4.0/>), which permits any noncommercial use, sharing, distribution and reproduction in any medium or format, as long as you give appropriate credit to the original author(s) and the source, provide a link to the Creative Commons license and indicate if you modified the licensed material. You do not have permission under this license to share adapted material derived from this chapter or parts of it.

The images or other third party material in this chapter are included in the chapter's Creative Commons license, unless indicated otherwise in a credit line to the material. If material is not included in the chapter's Creative Commons license and your intended use is not permitted by statutory regulation or exceeds the permitted use, you will need to obtain permission directly from the copyright holder.

